UAB
Universitat Autònoma de Barcelona

EXPLORING G PROTEIN-COUPLED RECEPTOR ALLOSTERISM BY IN SILICO METHODS

Óscar Díaz Sanzo

Universitat Autònoma de Barcelona

INc Institut de Neurociències UAB

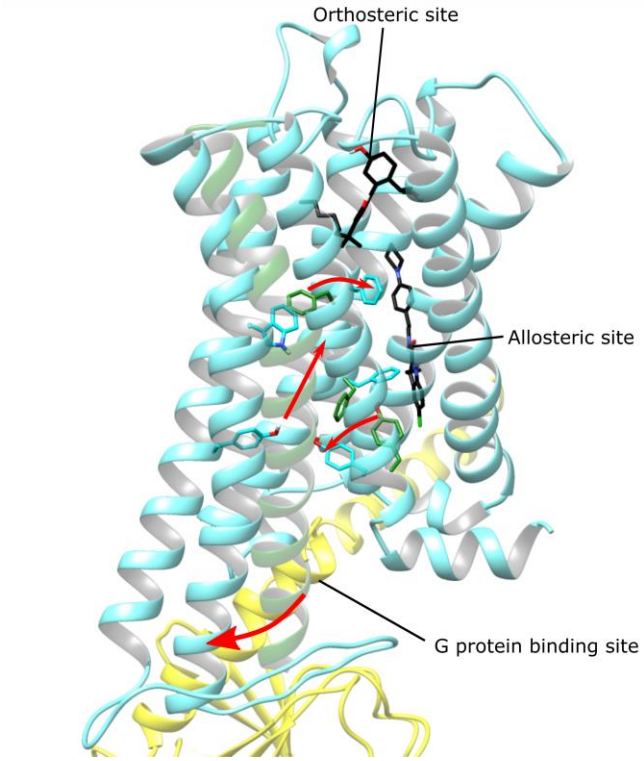

EXPLORING G PROTEIN-COUPLED RECEPTOR ALLOSTERISM BY IN SILICO METHODS

Doctoral Thesis

Student:
Óscar Díaz Sanzo
Director:
Jesús Giraldo

DOCTORAL PROGRAM IN NEUROSCIENCE

Laboratory of Molecular Neuropharmacology and Bioinformatics, Unitat de Bioestadística and Institut de Neurociències, Universitat Autònoma de Barcelona

Unitat de Neurociència Traslacional, Parc Taulí Hospital Universitari, Institut d'Investigació i Innovació Parc Taulí (I3PT), Institut de Neurociències, Universitat Autònoma de Barcelona

Instituto de Salud Carlos III, Centro de Investigación Biomédica en Red de Salud Mental, CIBERSAM

December 2022

Cover legend

The cover figure depicts several superimposed cannabinoid receptor 1 (CB1) structures relevant in this thesis. An active-like conformation generated during Molecular Dynamics simulations presented on Section 5.1 of this thesis is depicted in cyan. This conformation was generated starting from an inactive crystal structure of CB1 (from PDB ID 5U09). For clarity purposes, only transmembrane helix 6 (TM6), and residues F200$^{3.36}$, F237$^{4.46}$ and Y397$^{7.53}$ of the inactive state are depicted in green. Red arrows represent the most relevant conformational changes upon receptor activation as described on Section 5.1, which include outward movement of TM6, upward axial movement of TM3, and conformational shifts of F200$^{3.36}$ and Y397$^{7.53}$. The opening of the intracellular cavity upon activation forms the G protein binding site. A fully active, G protein-bound crystal structure of CB1 (PDB ID 6KPG) is also superimposed, and its co-crystallized G_{α} subunit is depicted in yellow. Superimposed onto these structures, coordinates of co-crystallized ligands CP-55940 and ORG27569 from PDB ID 6KQI are depicted as black sticks, representing the orthosteric binding site and an allosteric binding site, respectively.

Acknowledgements

The work presented in this thesis has been developed in the Laboratory of Molecular Neuropharmacology and Bioinformatics, Institut de Neurociències and Unitat de Bioestadística, Universitat Autònoma de Barcelona. First, I thank Dr. Jesús Giraldo for accepting me within the research group and for providing me the convenience of working from my home in Asturias during and after the COVID-19 pandemic. I also want to thank him for not only directing and guiding the thesis presented here, which he has done with a practical and open mind, but also for caring about my health and wellbeing.

Second, I want to thank Dr. James Dalton and Dr. Pedro Renault for teaching me the structural biology protocols employed in this thesis and fundamental aspects of research. Dr. Jesús Giraldo, Dr. James Dalton and Dr. Pedro Renault have encouraged me to pursue this opportunity and we have participated in discussions not only about my work, but about the field in general, which has helped me understand and focus on the key aspects of G protein-coupled receptors and in the interpretation of results.

Third, to my colleagues in the laboratory, and especially Agustín Bruzzese and Adrià Ricarte, who have been welcoming and supportive, I wish I could have assisted in person to your thesis presentations, and I still cherish the time we spent inside and outside the laboratory.

Fourth, I want to thank the members of my court Dr. Francisco Javier Luque Garriga, Dr. Jordi Ortiz and Dr. Baldo Oliva for being flexible and providing constructive feedback during the evaluation committee sessions.

Finally, I thank my family and my friends for supporting me throughout these years.

Contents

Figure Index

CHAPTER 1.

INTRODUCTION

1.1. G protein-coupled receptors

G protein-coupled receptors (GPCRs) are a family of approximately 800 membrane proteins which are classified into six subfamilies or classes: class A (rhodopsin-like receptors), class B (secretin family), class C (glutamate receptor family), class D (fungal mating pheromone receptors), class E (cyclic AMP receptors) and class F (Frizzled and Smoothened receptors) (Ghosh et al. 2015). In this thesis, we focus on class A GPCRs, which is the most extensively studied family of GPCRs. GPCRs are involved in the signaling process of the cell in response to a wide range of stimuli, including small organic molecules, peptides, proteins or even photons (Lagerström and Schiöth 2008). The signaling function of GPCRs usually results in the binding of transducer molecules, such as G proteins, arrestins and GPCR kinases (GRKs), which modulate downstream signal transduction. The most studied transducers that bind to GPCRs are G proteins, which are heterotrimeric proteins formed by subunits Gα, Gβ and Gγ. Gα subunits can function independently of Gβ and Gγ to regulate key effector signaling pathways such as adenylyl cyclase and phospholipase C (Wootten et al. 2018) and can be classified into 4 families: G_s, $G_{i/o}$, $G_{q/11}$ and $G_{12/13}$. On the other hand, Gβ and Gγ form an obligate heterodimer (Gβγ) that modulates transcription, second messenger molecule generation in organelles, chemotaxis and also regulates Gα signaling (Khan, Sung, and Hébert 2016).

GPCRs are flexible proteins that can adopt multiple conformations. In recent years, technological advances have allowed the optimization of crystallization techniques for GPCRs, including enhancing the expression levels of recombinant GPCRs in host cells, protein engineering and novel purification and crystallization protocols (Ghosh et al. 2015). To date, there are over 700 entries of GPCR crystal structures spanning over 100 GPCRs registered in the Protein Data Bank (PDB) according to GPCRdb (Isberg et al. 2016), most of which are class A GPCR structures in different activation states, and several of them bound to heterotrimeric G protein or G protein mimetic nanobodies. Currently, high resolution structures are usually obtained experimentally from X-ray crystallography or cryo-electron microscopy methods. This has allowed the identification of structural determinants of ligand binding and receptor activation. In general, class A GPRCs share a common structure, formed by seven transmembrane (TM) helices connected by three extracellular loops (ECL1-3) and three intracellular loops (ICL1-3). The N-terminus is located in the extracellular side of the membrane, while the C-terminus extends toward the intracellular region of the membrane, and generally contains an additional helical region (helix 8) that extends parallel to the intracellular leaflet of the membrane. A schematic representation of the structure of cannabinoid receptor 1 (CB1), a class A GPCR, is depicted in Figure 1.

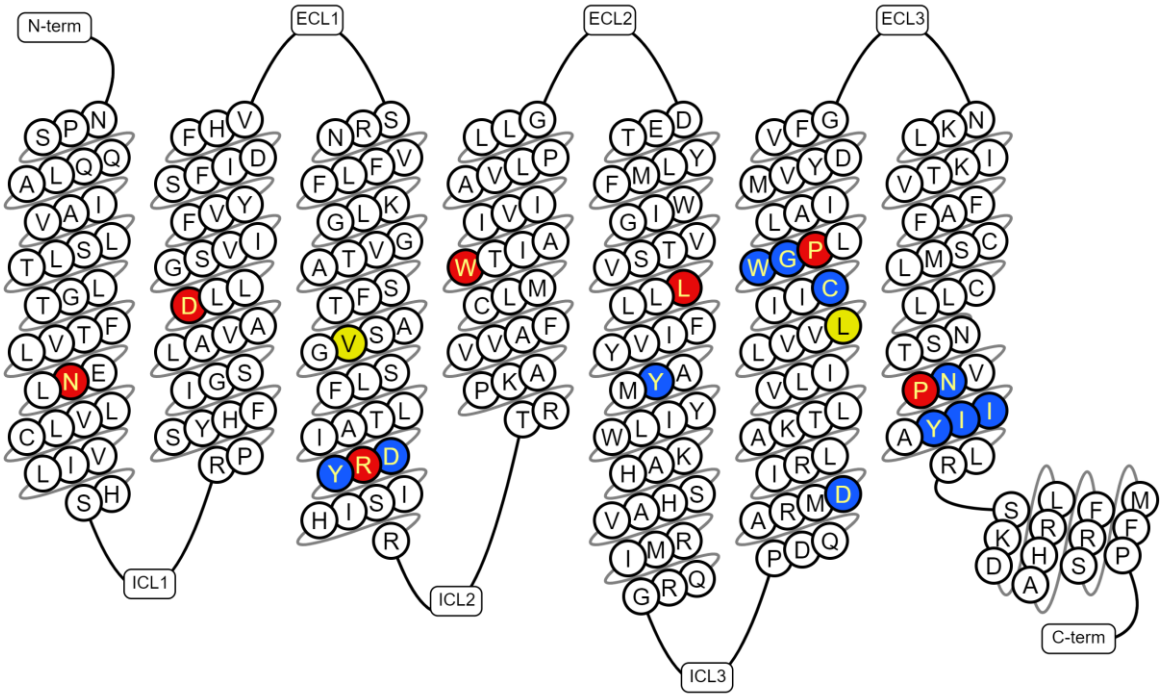

Figure 1. Diagram of the sequence and structure of cannabinoid receptor 1 (CB1), a class A GPCR. Highlighted residues in red: most conserved residues in each TM (x.50); blue: other conserved residues with a well-known role on class A GPCR activation; yellow: residues $V^{3.40}$ and $L^{6.44}$ from the non-conserved "transmission switch" (with $L^{5.50}$ represented in red as it is also the most conserved residue in the helix).

Despite low overall sequence conservation across GPCRs (Isberg et al. 2016), GPCR structure is highly conserved, and contains several highly conserved residues in each of the TMs. For this reason, it is useful to define a particular numeration scheme that allows comparison between different GPCRs. For class A GPCRs, it is common practice to include the Ballesteros-Weinstein numeration scheme (Ballesteros and Weinstein 1995). This numeration scheme consists of two parts x.yy, where x is the number of the TM in which a residue is located, and yy denotes the position of the residue relative to the most conserved residue of the TM. The most conserved residue of each TM is arbitrarily denoted as x.50, and in class A GPCRs, these residues are conserved as follows (sequence identity indicated in brackets): $N^{1.50}$ (98%), $D^{2.50}$ (90%), $R^{3.50}$ (95%), $W^{4.50}$ (97%), $P^{5.50}$ (78%), $P^{6.50}$ (99%) and $P^{7.50}$ (88%) (Isberg et al. 2015). Ballesteros-Weinstein numbering scheme is denoted as a superscript and will be included for all residues located in TMs throughout this thesis. The position of such residues in CB1 are depicted in red in Figure 1. It should be noticed that, given the conservation of GPCR structure, such residues are generally located in similar three-dimensional coordinates. Thus, residues that share the same Ballesteros-Weinstein numbering scheme can be located easily across different class A GPCRs for comparison.

1.2. Class A GPCR activation

The hallmark of class A GPCR activation is a large-scale outward movement of TM6 which is essential in order to open a cavity necessary for the binding of signaling proteins. To a lesser extent, TM6 outward movement is accompanied by TM5, while other conformational changes that shape the binding site of the signaling protein include an upward shift and rotation of TM3, and an inward movement of the intracellular region of TM7 (Katritch, Cherezov, and Stevens 2013). These conformational changes are accompanied by shifts in so-called microswitches, which are highly conserved residues that are commonly associated with receptor activation (Weis and Kobilka 2018; Tehan et al. 2014). These microswitches include the D[E]R$^{3.50}$Y motif in TM3, the NP$^{7.50}$xxY motif in TM7 and the CWxP$^{6.50}$ motif in TM6. Another microswitch is constituted by the P$^{5.50}$ I$^{3.40}$ F$^{6.44}$ residues, which has been denominated the "transmission switch" residues that communicate the orthosteric site with the intracellular region of the receptor to activate the receptor. The location of these well-known microswitches is also depicted in Figure 1 in blue. In Section 5.1 (Article 1) we examine the large-scale conformational changes and the role of these microswitches on the activation mechanism of cannabinoid receptor 1 (CB1), except for the P$^{5.50}$ I$^{3.40}$ F$^{6.44}$ "transmission switch" residues. This is because none of these residues is conserved in CB1, and instead these residues are L$^{5.50}$, V$^{3.40}$ and L$^{6.44}$ in CB1, as shown in yellow (V$^{3.40}$ and L$^{6.44}$) and in red (L$^{5.50}$) in Figure 1.

In crystal structures of G protein-bound class A GPCRs, it can be observed that Gα binds to the intracellular surface of receptor, in a cavity formed mainly by residues in TM3, ICL2, TM5, TM6, TM7 and helix 8 in the active state of the receptor (Carpenter et al. 2017; Rasmussen et al. 2011; Draper-Joyce et al. 2018; Koehl et al. 2018; Krishna Kumar et al. 2019; Hua et al. 2020). However, the specific residues that participate in GPCR-G protein interaction and the orientation of the Gα subunit vary depending on the receptor and the Gα subunit. Consequently, the molecular basis for GPCR-G protein coupling specificity has not been found, although it has been hypothesized that G protein binding specificity is determined at an intermediate state of the formation of the G protein-GPCR complex (Krishna Kumar et al. 2019; Koehl et al. 2018) that may be dependent on the degree of the TM6 outward movement (Gregorio et al. 2017; Rose et al. 2014). Furthermore, although G proteins have been found bound to the active conformation of the receptor in crystal structures, it has been proposed that they may also bind to the inactive receptor conformation to promote receptor activation (Mafi, Kim, and Goddard 2022). Moreover, G proteins may stabilize active-like conformations of the agonist binding site (Renault et al. 2019).

1.3. GPCR modulation by ligands

Due to the variety of stimuli and signaling pathways that they are involved in, GPCRs are important drug targets. Currently, approximately 33% of marketed drugs target GPCRs (Santos et al.

2017). As such, classical approaches in drug design focus on developing small molecules that target the same binding site as the endogenous ligand (orthosteric site), by either mimicking the chemical structure of the endogenous ligand, using substances existing in nature or by synthesizing new compounds. Mathematical models are typically used to fit pharmacological data, and thus allow to obtain parameters that are useful to compare and classify the pharmacological properties of those ligands (Roche, Gil, and Giraldo 2013). As an example, Figure 2 shows the two-state model of agonism (del Castillo and Katz 1957) (reviewed in Leff 1995). This model allows to classify orthosteric GPCR ligands by their affinity for the receptor (K) and their intrinsic efficacy (α). Ligand affinity (K) refers to the equilibrium dissociation constant for the equilibrium between free receptor and ligand-bound receptor, while intrinsic efficacy (α) measures the capability of the ligand to shift the equilibrium of conformations towards the active state, which translates into stimulating a biological response ($\alpha > 1$ in case of an agonist, $\alpha = 1$ in case of a neutral antagonist, $\alpha < 1$ in case of an inverse agonist).

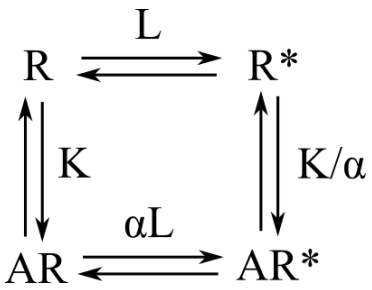

Figure 2. Two-state model of agonism. The receptor is considered in an equilibrium between two states: inactive, R and active, R* that can both bind agonist A. Because of the thermodynamic cycle, equilibrium constants are determined by only three parameters: K (affinity of ligand A to the inactive receptor), L (propensity of the free receptor to form active states, which determines the basal activity of the free receptor) and α (intrinsic efficacy of the ligand). K is the equilibrium dissociation constant, defined as K=[A][R]/[AR], and L=[R*]/[R] measures the constitutive receptor activity.

We can see that the model allows us to examine action of ligand A in two ways: (i) comparing the horizontal arrows, induction model: the ligand bound-receptor has greater ($\alpha > 1$), equal ($\alpha > 1$) or lower ($\alpha < 1$) capability of activating the receptor than the free receptor itself; (ii) comparing the vertical arrows, selection model: the affinity for the receptor active state is greater ($\alpha > 1$), equal ($\alpha > 1$) or lower ($\alpha < 1$) than that for the receptor inactive state. At saturating concentration, full agonists display the maximal response from the receptor, while partial agonists produce a response weaker than the maximal response of the system ($\alpha_{\text{partial agonist}} < \alpha_{\text{full agonist}}$). Neutral antagonists do not affect the activity of the receptor ($\alpha = 1$). Finally, inverse agonists reduce the activity of the receptor below the basal activity ($\alpha < 1$). Concentration-dependent response curves of drugs with different efficacy profiles are depicted in Figure 3. Moreover, although not considered by the two-state model of agonism, some

ligands display signaling bias, meaning they are capable of stimulating only certain signaling pathways (i.e. stimulate G protein binding but not arrestin binding or vice versa), or do so with different efficacy (Weis and Kobilka 2018). See Figure 3 for illustration of examples of different GPCR signaling pathways.

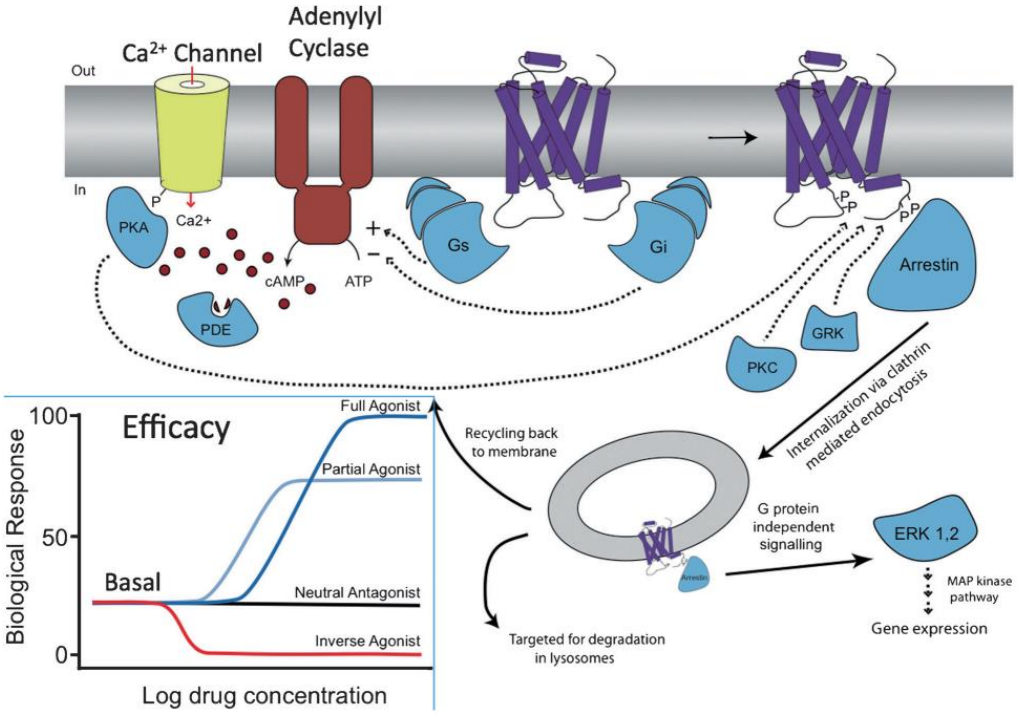

Figure 3. Different signaling pathways of a GPCR and their regulation, including G proteins (G_s and G_i in this case), kinases and arrestins; and drug classification according to their maximal response at saturation (efficacy). Taken and adapted from Kobilka 2013.

The development of drugs that target the orthosteric site has posed several challenges. Due to the evolutionary pressure of binding the same endogenous ligand, orthosteric sites are highly conserved in GPCR subfamilies and thus it can be difficult to discover or design subtype selective orthosteric ligands (Y. Lee, Basith, and Choi 2018; Melancon et al. 2012). Moreover, these ligands do not allow a fine tuning of their effects, meaning their effect is always dose-dependent. These limitations have grown the interest in the development of allosteric modulators, ligands which bind to alternative, less conserved topological binding sites of the receptor (allosteric sites). Allosteric modulators can increase (positive allosteric modulator, PAM) or reduce (negative allosteric modulator, NAM) the affinity and/or efficacy of orthosteric ligands (Christopoulos and Kenakin 2002). Allosteric modulators can also display intrinsic efficacy on their own (ago-allosteric modulators, ago-PAMs) (Schwartz and Holst 2006), or increase agonist affinity while reducing their efficacy (PAM-antagonists) (Kenakin and Strachan 2018). Allosteric modulators can also bias the functional response towards a particular signaling pathway

(biased allosteric modulators, BAMs) (Foster and Conn 2017). Their advantages over orthosteric ligands have attracted research of these compounds, and there are several allosteric modulators in clinical development (Emmitte 2017; Foster and Conn 2017; Lindsley et al. 2016).

Mathematical models of the cooperativity between orthosteric and allosteric ligands have also been published in the literature (Roche, Gil, and Giraldo 2013). Besides the affinity of the allosteric modulator for the free receptor, these models introduce cooperativity factor parameters, which measure the mutual effect of ligand binding on the affinity or efficacy of the other ligand. For example, the binding cooperativity factor (α, do not mistake with intrinsic efficacy from the two-state model of agonism) measures the binding cooperativity between ligands and allow classification between NAMs ($\alpha < 1$), PAMs ($\alpha > 1$) and silent allosteric modulators or SAMs ($\alpha = 1$).

Allosteric modulators may have some advantages over orthosteric ligands (Christopoulos and Kenakin 2002; Melancon et al. 2012). First, because the residues at the allosteric sites are not as conserved as those at the orthosteric sites, the molecular design of allosteric modulators is not so affected by the selectivity limitations between receptor subtypes. Second, allosteric modulators may have intrinsic efficacy or not. In the latter case, the functional dependence of allosteric modulators on the presence of the endogenous ligand may present temporal and spatial activity advantages over orthosteric ligands because they would only affect cells where orthosteric ligands exert their function at a physiologically relevant point in time. Moreover, since no effects would be observed in absence of orthosteric ligand, allosteric modulators may reduce toxicity and avoid cases of overdose (phenomenon known as “ceiling effect”).

1.4. GPCRs can form oligomers

The first evidence of GPCR dimerization was shown for gamma-aminobutyric acid (GABA) receptors, which form heterodimers ($GABA_{B1}$-$GABA_{B2}$) (Kaupmann et al. 1998; Jones et al. 1998). $GABA_B$ receptors belong to the class C GPCRs, and it is well accepted that class C GPCRs form obligate dimers in vivo and are required for receptor function (Kniazeff et al. 2011). On the contrary, class A GPCRs are functional as monomers. Although the presence of class A GPCR oligomers has been under debate (Lambert and Javitch 2014), there is increasing evidence that class A GPCRs are able to form oligomers that display different ligand binding, signaling, trafficking and pharmacological properties compared to the monomeric receptor (Bouvier and Hébert 2014; Gaitonde and Gonza 2017). As an example, conformational changes in one of the protomers can be transmitted to another, which are thus able to modulate ligand affinity and signaling function (Hiller, Kühhorn, and Gmeiner 2013). Although oligomers have not been studied in this thesis at the structural level, it is important to consider

that changes in the conformational space of monomers may affect the propensity of the receptor to form oligomers.

1.5. GPCRs are allosteric proteins

Here, we understand allosteric communication as a mechanism by which GPCRs can transmit a conformational change when a perturbation is introduced in a different site, far from the region where the effect is observed. Allosteric communication between sites can be observed due to the conformational flexibility of GPCRs, which can explore a wide range of states. In fact, allosteric perturbations can alter the dynamical properties of proteins such as the conformational entropy without manifesting structural changes (Tzeng and Kalodimos 2012). In this regard, it has been shown that it is important to consider ensembles of protein conformations when studying allosteric communication, as allosteric perturbations may change the free energy landscape of allosteric proteins. Thus, the effect of allosteric perturbations is a combination of contributions over the full ensemble of conformations of the protein, meaning they can alter the probabilities of visiting the states of the ensemble due to their effect on their free energy (Motlagh et al. 2014).

Many different sites capable of allosteric communication can be found in GPCRs. In the sections above, several cases of allosteric communication have been presented and are summarized in Figure 4. First, an orthosteric ligand can shift the equilibrium of conformations towards particular receptor species, which alter their signaling properties. The orthosteric site and the signaling protein binding site of GPCRs are generally far from each other, and the resulting conformational change upon agonist binding has been observed in crystal structures of class A GPCRs (see Section 1.2). Thus, this constitutes an allosteric perturbation transmitted between orthosteric and signaling protein binding site. Second, an allosteric ligand can modify the orthosteric ligand affinity and/or efficacy, which would ultimately affect the conformational properties of the receptor. Interestingly, native allosteric modulators of GPCRs exist such as cholesterol (McGraw et al. 2019; Nguyen and Taub 2003; Hanson et al. 2008; Bari et al. 2005) and sodium ions (Katritch et al. 2014). Third, receptor can form oligomers that also alter the pharmacological properties of the receptor. Consequently, GPCRs are allosteric proteins by nature. In this regard, GPCRs respond to different molecules such as neurotransmitters and hormones to promote different signaling pathways. This results in a complex picture on the pharmacology of GPCRs, as they can be modulated by orthosteric and allosteric ligands, ions, membrane lipids or other proteins such as G protein or other protomers in a receptor oligomer, as well as receptor mutations that may be present in disease.

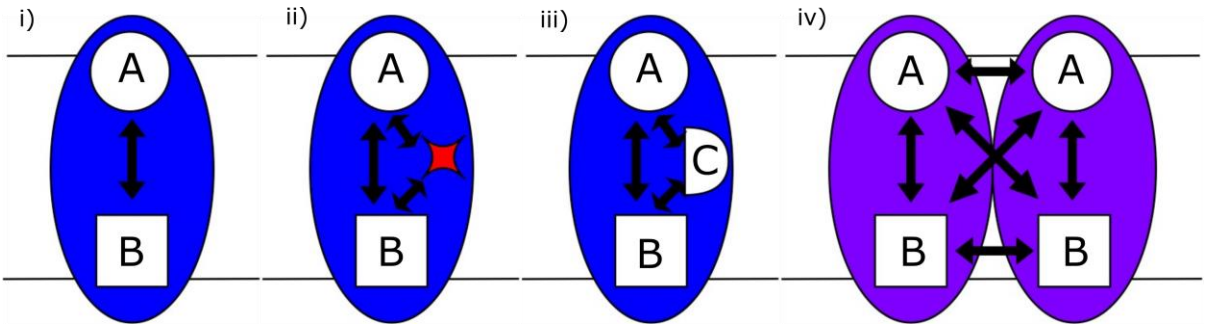

Figure 4. Examples of allosteric communication in GPCRs. Communication between: i) orthosteric site A and G protein binding site B; ii) orthosteric site A, mutation site (red star) and G protein binding site B; iii) orthosteric site A, G protein binding site B and allosteric site C; iv) orthosteric site A and G protein binding site B in a receptor dimer.

1.6. Structural data and Structure-based Drug Design

High-throughput screening has become one of the standard and universal procedures in drug discovery programs since its inception (Pereira and Williams 2007). This approach is based on the assay of large collections of molecules (libraries) against selected drug targets. Molecules identified by this approach ("hits") are then used to develop drug leads and, ultimately, potentially viable drug compounds. As such, this process can be lengthy and expensive, which is often a consequence of low-quality composition of compound libraries (MacArron et al. 2011).

The increasing amount of available structural data has allowed the application of an alternative or complementary approach to high-throughput screening called structure-based drug design (SBDD). SBDD has emerged as a computational tool that can assist drug discovery programs to identify drug candidates using the structural information of the drug target provided by crystal structures and has been successfully applied to several drug targets in the past (Anderson 2003; Wlodawer and Vondrasek 1998; Rutenber and Stroud 1996). The most common methods employed in SBDD consist of molecular docking, virtual screening and molecular dynamics (MD) simulations, which allow to characterize ligand-receptor interactions and predict conformational changes that occur in the drug target upon ligand binding (Batool, Ahmad, and Choi 2019). Collectively, these methods allow the design of ligands that contain desired chemical features for pharmacological function or are used to curate large libraries of compounds for high-throughput screening. They can also be used to provide insights into their mechanisms of function, which then translates into a better understanding when applying SBDD methods. The methods employed in this thesis are described in the following sections.

1.6.1. Molecular docking

Molecular docking is a frequently used method to predict the conformation of a molecule within the binding site of the target when the molecule has not been co-crystallized with the target. This method is based on a scoring system, usually derived from semiempirical parameters and functions. Using this scoring system, docking probes the conformational space of ligand-receptor with the aim to minimize the free energy of binding for a resulting docking pose, although other approaches to obtain docking poses have also been developed (Ferreira et al. 2015; J. Li, Fu, and Zhang 2019). Many docking algorithms are currently available. Among them, commonly used software for docking small drug-like ligands include Autodock (Morris et al. 2009), GOLD (Verdonk et al. 2003) and Glide (Friesner et al. 2006). Molecular docking has the benefit of generally being a fast process. However, it has several weaknesses (Chen 2015): first, algorithms are designed and optimized for different conditions and thus different scores may be found with different algorithms depending on the target; second, the accuracy of docking is highly dependent on the reliability of the structure; third, molecular docking is not able to discriminate the function of the bound molecule by itself; fourth, minimization of the free energy of binding can converge towards a local minimum rather than a global minimum and thus provide a suboptimal docking conformation, although this can be partially overcome by starting the conformational search from different starting points. Moreover, although there is a general agreement between high docking scores and finding drug leads, it should be considered that the highest docking scores do not necessarily provide the best drug leads. Thus, molecular docking requires validation by other approaches, such as binding experiments or MD simulations.

1.6.2. Molecular Dynamics simulations

At high resolution, crystal structures provide an accurate representation of the three-dimensional coordinates of proteins, and thus they can offer insights into their mechanisms of biological function. However, these structures are only snapshots of highly stabilized conformational states and are commonly obtained after modification of the receptor with protein engineering methods. These modifications include the use of fusion proteins (which usually involves the removal of ICL3) and thermostabilizing mutations (Ghosh et al. 2015). Moreover, the experimental conditions of the crystallization process are generally far different from native-like conditions. For this reason, molecular dynamics (MD) simulations have emerged as a complementary tool to experimental findings, as they allow to model the receptor in native-like conditions and to examine many intermediate or metastable conformations, not only low energy conformational states (Torrens-Fontanals et al. 2020). MD simulations is a computational method used to analyze the time-dependent physical movement of atoms and molecules. Currently, the most employed MD simulation methods in GPCRs use atomistic or coarse-grained models, but more detailed Quantum Mechanical (QM) models or more simplified

Continuum Electrostatic models can also be employed (Y. Lee, Basith, and Choi 2018). In this thesis, we focus on the use of atomistic, Molecular Mechanics (MM) models. In MM models, three-dimensional coordinates are represented for each atom and are connected to others by means of a potential energy function called force field. Then, the motion of each atom is calculated according to Newton's laws of movement. Force fields contain the functions and parameters used to model bonded terms (bonds and angles are modeled after a harmonic potential function) and nonbonded terms (including van der Waals and Coulombic interactions), which are fitted to reproduce experimental data. The most commonly used MM force fields for simulating protein dynamics are AMBER (Case et al. 2005), CHARMM (J. Huang and MacKerell 2013) and GROMOS (Schuler, Daura, and van Gunsteren 2001). The potential energy function adopts similar forms in MM force fields. As an example, Equation 1 shows the form of the potential energy function in CHARMM.

Equation 1. Potential energy function in CHARMM22, which includes bonded terms: bond stretches (constants k_b and b_0), angles (constants k_θ and θ_0), dihedrals (constants k_Φ, n and δ), impropers (out of plane bendings, constants k_ω and ω_0), Urey-Bradley (cross-term accounting for angle bending, constants k_u and u_0); and nonbonded terms: van der Waals (calculated by 12-6 Lennard-Jones potential, constant R_{min}) and electrostatic potential (Coulombic potential, constants q_i, q_j and ε). Constants in this function (parameters) are usually derived or adjusted to fit empirical data.

$$V = \sum_{bonds} k_b(b - b_0)^2 + \sum_{angles} k_\theta(\theta - \theta_0)^2 + \sum_{dihedrals} k_\phi[1 + \cos(n\phi - \delta)] + \sum_{impropers} k_\omega(\omega - \omega_0)^2 + \sum_{Urey-Bradley} k_u(u - u_0)^2 + \sum_{nonbonded} \in \left[\left(\frac{R_{min_{ij}}}{r_{ij}}\right)^{12} - \left(\frac{R_{min_{ij}}}{r_{ij}}\right)^{6}\right] + \frac{q_i q_j}{\varepsilon r_{ij}}$$

MM approaches are limited by the simplification of the potential energy function, by how their parameters are derived, and by the atomistic approach itself. The main limitations of the atomistic approach lie in 1) the inability to model chemical reactions because electron potentials are not defined, and 2) achievable timescales. Usually, MM allows to study GPCR systems in MD simulations at the timescale of microseconds at a practical computational speed in current typical workstations. However, GPCR motions can occur at a timescale ranging from fs to ns for side chain movements, μs to ms for large-scale conformational changes such as receptor activation, and seconds to minutes for receptor-G protein complex formation or dimerization (Vilardaga et al. 2003; Y. Wang et al. 2018; Lohse, Maiellaro, and Calebiro 2014). While QM approaches include the definition of electron potentials and thus is possible to observe chemical reactions, they are very computationally demanding (Y. Lee, Basith, and Choi 2018). On the contrary, coarse-grained models allow to study larger timescales by

considering groups of atoms (e.g. all atoms of a residue) as a single unit, increasing the uncertainty (Sengupta et al. 2016). While coarse-grained models are useful in order to study protein-lipid interactions (Sengupta et al. 2018) or protein-protein interactions in GPCRs such as those present in GPCR-G protein complexes (Alhadeff et al. 2018) or predicting GPCR oligomer interfaces (Altwaijry et al. 2017), MM methods are a reasonable compromise between structural accuracy and achievable timescales for studying mechanisms of GPCR function at a monomeric level without including G protein.

One of the main advantages of MD simulations is that they allow to easily control the system conditions in such a way that additional perturbations can be introduced, i.e. ligand or protein binding, receptor mutation or alternative membrane or solute conditions, which might model physiological, pathophysiological or pharmacologically relevant conditions. This allows the examination of mechanisms of conformational change, which can lay a foundation for SBDD methods described above (Y. Lee, Basith, and Choi 2018).

CHAPTER 2. AIMS AND OBJECTIVES

In this thesis we examine examples of allosteric communication between different sites of the receptor, including receptor activation, where the orthosteric site and the intracellular site (binding site of the signaling protein) communicate, the allosteric effects of mutations in the GPCR activation state located at an allosteric modulator binding site, with the aim of understanding the mechanisms of allosteric communication at a structural level in order to provide a general framework to facilitate the use of SBDD approaches in GPCRs. As a model of class A GPCR, we will focus on cannabinoid receptor 1 (CB1). CB1 is a class A GPCR involved in the modulation of pain, mood, behavior and appetite, and as such it has received attention as a drug target (Thakur et al. 2009; Pertwee 2005; Janero and Makriyannis 2009; Seltzman et al. 2016). Despite some cannabinoid medications are currently marketed in the US and EU (Lipnik-Štangelj and Razinger 2020), their development has faced difficulties associated to negative side effects (Giraldo 2010). Moreover, selective drugs towards homologous CB2 have promising application on the treatment of inflammation and neuropathic pain (Lucchesi et al. 2014; Romero-Parra et al. 2016). Thus, understanding the mechanisms of function of cannabinoid ligands can be useful for the design of novel molecules or the modification of currently known drug leads to improve their pharmacology.

Objectives

1. Identify residues involved in agonist-mediated activation of CB1 and key agonist-receptor interactions.
2. Evaluate the structural effects of allosteric perturbations introduced in CB1.
3. Identify key residues involved in the mechanism of allosteric communication between orthosteric and allosteric ligand binding sites in CB1.
4. Examine mathematical models that include ligand cooperativity parameters at the level of the binding kinetics.
5. Offer perspectives on new computational methods applicable to structure-based drug design.

CHAPTER 3. STRUCTURE OF THE THESIS

This thesis is organized as an article compendium, where each article corresponds to at least one of the objectives of the thesis.

First Article: Revealing the mechanism of agonist-mediated cannabinoid receptor 1 (CB1) activation and phospholipid-mediated allosteric modulation

Reference: Díaz, Dalton, and Giraldo 2019b

In this first article, we examine the mechanism of agonist-mediated activation of CB1, in particular, classical cannabinoid AM-11542 and non-classical cannabinoid CP-55940, with the objective of identifying key residues involved in the activation process and critical ligand-receptor interactions. Moreover, we evaluate allosteric modulation exerted by membrane phospholipid 1,2-dioleoyl-*sn*-glycero-3-phosphoglycerol (DOPG), a net negatively charged phospholipid that has been shown to promote β_2 adrenergic receptor both in experiments (Dawaliby et al. 2015) and in MD simulations performed by our research group (Bruzzese et al. 2018).

Second Article: Evaluating allosteric perturbations in cannabinoid receptor 1 by *in silico* single-point mutation

Reference: Díaz, Renault, and Giraldo 2022

Following the previous work on CB1, we introduced an additional allosteric perturbation in the form of F237L mutation. This mutation has been shown to increase CP-55940 affinity for CB1 while $F237^{4.46}$ was proposed to have a role on the activation process (Shao et al. 2019). This residue is located neither at the orthosteric nor G protein binding site, but rather at an allosteric site, where is a contact residue for CB1 PAM-antagonist ORG27569 (Shao et al. 2019) and cholesterol (Hua et al. 2017). Although this mutation has not been associated to diseases in patients, its mechanism of function can provide insights into the mechanism of allosteric modulation by ORG27569, as their proposed effects (increase in CP-55940 binding and decrease in receptor signaling) are seemingly analogous.

Third Article: Allosteric binding cooperativity in a kinetic context

Reference: Díaz et al. 2023

In this article, we examine allosterism of GPCRs using a mathematical model in the context of the equilibrium rate constants, in particular, the allosteric ternary complex model and a heterodimer receptor model. This allowed us to derive a relationship between cooperativity rate constant parameters

that supports many values for these parameters for a single binding cooperativity parameter, which is relevant in order to explain experimental and computational results.

Fourth Article: Artificial Intelligence: A Novel Approach for Drug Discovery

Reference: Díaz, Dalton, and Giraldo 2019a

As seen by the exponential growth of available crystal structures of GPCRs with an increasing variety of co-crystallized ligands with different pharmacological properties, and by the fact that MD simulations can generate very large collections of data about the dynamics of GPCRs, novel machine learning (ML) methods are being developed to identify molecular determinants associated to the pharmacological profile of the bound ligand(s). In this brief spotlight article, we provide an opinion on the use of machine learning techniques in drug discovery programs.

Supporting Information

The supporting information for the research articles is presented in Appendix 1 and 2.

CHAPTER 4. GENERAL METHODS

4.1. Structure preparation

The work presented in this thesis is based on publicly available experimentally determined crystal structures. Receptor coordinates were obtained from Protein Data Bank (PDB) (rcsb.org) (Berman et al. 2000). In general, crystal structures were selected according to their resolution, their activation state or due to the co-crystallization of relevant ligands. Then, a receptor model was generated from these coordinates. In general, this involves the following steps: 1) removal of fusion protein and co-crystallized lipids; 2) reverting mutations in the structure to the *wt* sequence obtained from Uniprot database (The UniProt Consortium 2021); 3) modeling missing regions from the crystal structure. Missing regions of the receptor (in particular, ICL3 is usually replaced by a fusion protein or not solved in crystal structures of GPCRs due to its flexibility) were modeled *ab initio* using MODELLER (Webb and Sali 2014). TM ends were defined according to secondary structure prediction tools PSIPRED (Buchan et al. 2010) and JPRED (Drozdetskiy et al. 2015). N- and C-termini were modeled (*ab initio*) only if a short sequence of residues was missing (<10). Otherwise, a truncated receptor was generated. In the case of single-point mutant receptor models, the mutation was inserted by replacing the *wt* residue with the highest probability score rotamer of the mutant residue according to Dunbrack rotamer library (Shapovalov and Dunbrack 2011). Disulfide bridges, solved in crystal structures of the presented models in this study, were maintained in all cases.

After generating the receptor model, it was energy-minimized in CHIMERA (Pettersen et al. 2004) in the AMBER14SB force field (Case et al. 2005) using steepest descent (1000 steps) and conjugate gradient (100 steps) algorithms (unless otherwise indicated). If co-crystallized ligands were not within the interests of the study, their coordinates were removed, generating a free receptor (apo) model. Then, in order to introduce a ligand of interest, if that ligand was co-crystallized in any crystal structure of the receptor or homologous receptors, they were inserted into the receptor by coordinate superposition in CHIMERA. Otherwise, they were docked into the receptor model using AUTODOCK (Morris et al. 2009). The docking pose was selected according to the docking score and considering experimental data that would indicate critical ligand-receptor interactions, generally in the form of mutational data published in the literature. In any case, the model was further energy-minimized as described above.

4.2. Preparation of Molecular Dynamics simulations systems

The MD simulation systems were built in CHARMM-GUI (Jo et al. 2008). To do this, receptors were oriented according to Orientations of Proteins in Membranes (OPM) database (Lomize et al. 2006) and embedded in homogeneous membranes composed by 1-palmitoyl-2-oleoyl-sn-glycero-3-phosphocholine (POPC) unless otherwise indicated, since POPC is the most widely used membrane phospholipid in MD simulations of GPCRs (Plazinska, Plazinski, and Jozwiak 2015; Niesen,

Bhattacharya, and Vaidehi 2011; Hu et al. 2016; Song et al. 2017; Che et al. 2018; Filipek et al. 2014; Pérez-Benito et al. 2017; Robert B. Laprairie et al. 2016; B. Li et al. 2012; Shim, Bertalovitz, and Kendall 2011; Dalton, Lans, and Giraldo 2015; Bruzzese et al. 2018). The protonation state of the receptor residues at pH 7.4 was predicted using PROPKA (Olsson et al. 2011), but alternative protonation states were also considered due to their potential conformational selection properties (Lans, Dalton, and Giraldo 2015; Bruzzese et al. 2018). MD systems were solvated using the TIP3P model for water molecules and K+ and Cl- ions were used for charge neutralization of the system, generally at a 0.15 M concentration unless otherwise indicated. The use of Na+ ions was avoided due to potential sodium-mediated allosteric modulation (W. Liu et al. 2013; White et al. 2018; Katritch et al. 2014; Tao and Abood 1998).

CHARMM36 force field (or the revised CHARMM36m force field published during the development of this thesis) (J. Huang and MacKerell 2013) was selected for performing MD simulations in this study due to their extensive use (Song et al. 2017; Jaiteh et al. 2020; X. Liu et al. 2017; Koehl et al. 2018; Jung, Cho, and Yu 2018; Mafi, Kim, and Goddard 2022; Krishna Kumar et al. 2019; Shim, Khurana, and Kendall 2016; Miao et al. 2018; Latorraca et al. 2018) and native membrane lipid parameters. Parameters for ligands were generated in ParamChem, which derives parameters from the CHARMM General Forcefield (CGenFF) (Vanommeslaeghe and MacKerell 2012). Before performing MD simulations, energy minimization in the CHARMM36 forcefield was performed with position restraints set for all ligand and receptor heavy atoms, allowing membrane lipids, solvent and protein and ligand hydrogen atoms to optimize their configuration using conjugate gradient minimization algorithm (2000 steps). MD simulations were performed using ACEMD (Harvey, Giupponi, and De Fabritiis 2009) at 300 K and 1 atm and were divided into two main stages: equilibration and production. During equilibration, MD simulation was run on the NPT ensemble with position restraints on protein and ligand heavy atoms progressively released over ~8 ns, after which a ~20ns step was run without restraints. Then, pressure control was released (Harvey, Giupponi, and De Fabritiis 2009) for the production runs. Production runs (at least 2 replicas, but generally 3) were simulated without restraints for 1-3 μs each.

MD trajectories were visually inspected in Visual Molecular Dynamics (VMD) (Humphrey, Dalke, and Schulten 1996). The software used for analysis varied depending on the objective of the measure. In general, properties were measured using VMD and associated plugins, GROMACS (Lindahl, Hess, and van der Spoel 2001) or Bio3D in R (Grant et al. 2006).

Protein-protein docking was performed to validate the capability of G protein binding to assess the presence of active-like receptor conformations. To do this, receptor snapshots were selected and

their ICL3 was removed due to its flexibility. G protein coordinates from available crystal structures were superimposed to receptor coordinates and then translated 5Å in the Z axis (perpendicular to the membrane) away from the receptor to generate a gap. After that, protein-protein docking was performed in Rosie web server (Lyskov et al. 2013). The resulting docking positions with highest docking score and lower RMSD were visually inspected and compared to available crystal structures of receptor-G protein complexes.

CHAPTER 5. RESULTS

5.1. Article 1: Revealing the Mechanism of Agonist-Mediated Cannabinoid Receptor 1 (CB1) Activation and Phospholipid-Mediated Allosteric Modulation

Journal of Medicinal Chemistry

Article

Cite This: J. Med. Chem. 2019, 62, 5638−5654

pubs.acs.org/jmc

Revealing the Mechanism of Agonist-Mediated Cannabinoid Receptor 1 (CB1) Activation and Phospholipid-Mediated Allosteric Modulation

Óscar Díaz,[†,‡,§] James A. R. Dalton,[*,†,‡,§] and Jesús Giraldo[*,†,‡,§]

[†]Laboratory of Molecular Neuropharmacology and Bioinformatics, Unitat de Bioestadística and Institut de Neurociències and [‡]Unitat de Neurociència Traslacional, Parc Taulí Hospital Universitari, Institut d'Investigació i Innovació Parc Taulí (I3PT), Institut de Neurociències, Universitat Autònoma de Barcelona, 08193 Bellaterra, Spain

[§]Instituto de Salud Carlos III, Centro de Investigación Biomédica en Red de Salud Mental, CIBERSAM, 08193 Bellaterra, Spain

Supporting Information

ABSTRACT: Cannabinoid receptor 1 (CB1) mediates the functional responses of Δ^9-tetrahydrocannabinol. Although progress has been made in understanding cannabinoid binding and receptor activation, detailed knowledge of the dynamics involved in the activation mechanism of CB1 is lacking. Here, we use recently determined CB1 crystal structures to analyze its transition from inactive to active state by performing unbiased microsecond-length molecular dynamics (MD) simulations, totaling 32 μs, with and without bound potent cannabinoid agonist CP-55940. CB1 activation is characterized by an upward axial movement of transmembrane (TM) helix 3, inward movement of TM7, and outward movement of TM6. These conformational changes collectively allow G_i protein docking, although fully active states of the receptor occur only transiently during MD simulations. Additionally, positive allosteric modulation of CB1 by anionic phospholipids is found to increase action of the bound agonist. Specifically, this involves protein−lipid interactions at intracellular loop 3, TM6, and ionic lock residue Arg214$^{3.50}$.

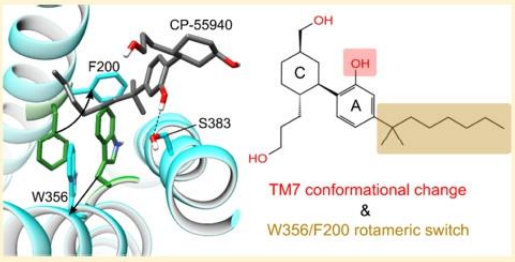

INTRODUCTION

Cannabinoid receptor 1 (CB1) belongs to the class A family of G protein-coupled receptors (GPCRs).[1] It is mainly expressed in the central nervous system and is one of the most abundant GPCRs in the brain, at particularly high levels in the neocortex, hippocampus, basal ganglia, cerebellum, and brainstem,[2,3] controlling both excitatory and inhibitory neurotransmissions.[1,3] In addition, CB1 is also present at lower levels in numerous peripheral organs.[2,4] Downstream signaling pathways mediated by CB1 mainly involve $G_{i/o}$ protein coupling,[5] but the receptor can also activate others such as G_s protein or β-arrestin.[6,7]

CB1 activation is modulated by endogenous lipids (endocannabinoids) and by exogenous molecules with considerably different chemical structures[8−11] including Δ^9-tetrahydrocannabinol (Δ^9-THC), the main psychoactive component of the plant *Cannabis sativa*.[1] Cannabinoid agonists targeting CB1 have shown potential utility in the treatment of pain, glaucoma, depression, gastrointestinal disorders,[8,12] and, more recently, neurodegenerative diseases.[13] Thus, the wide variety of molecules that can bind to CB1 and its multiplicity of signaling pathways make this receptor an excellent drug target.

Understanding the molecular interactions involved in ligand binding and ensuing receptor activation is essential for rational drug design in GPCRs.[14] In this regard, structural comparison between crystallized class A GPCRs in various active and inactive states (including rhodopsin, β_1 and β_2 adrenergic receptors, adenosine receptors A1 and A2A, and muscarinic receptors M1−M4, among others)[15−23] has provided molecular insights into the activation mechanism of GPCRs.[24] Class A GPCRs are composed of an extracellular N-terminal domain, a short helix (H8) parallel to the membrane that contains the intracellular C-terminus, and seven transmembrane (TM) helices interconnected by three intracellular loops (ICLs) and three extracellular loops (ECLs). Thus, all of the residues mentioned in this study include the Ballesteros−Weinstein numbering scheme as a superscript, which aids in the comparison between homologous class A GPCRs.[25] This is an *X.YY* format, where "*X*" indicates the TM number and "*YY*" refers to its location in the TM relative to the most conserved residue in the helix, which is denoted as *X*.50. Rearrangements at the intracellular side of GPCRs upon activation include an outward bend (starting at a conserved Pro$^{6.50}$) of TM6 away from TM3, an outward movement of TM5, and an inward movement of TM7.[26,27] Additionally, a slight rotation and upward movement of TM3 along its axis has been linked to a rearrangement of hydrophobic residues at the core of the

Received: April 9, 2019
Published: May 16, 2019

DOI: 10.1021/acs.jmedchem.9b00612
J. Med. Chem. 2019, 62, 5638−5654

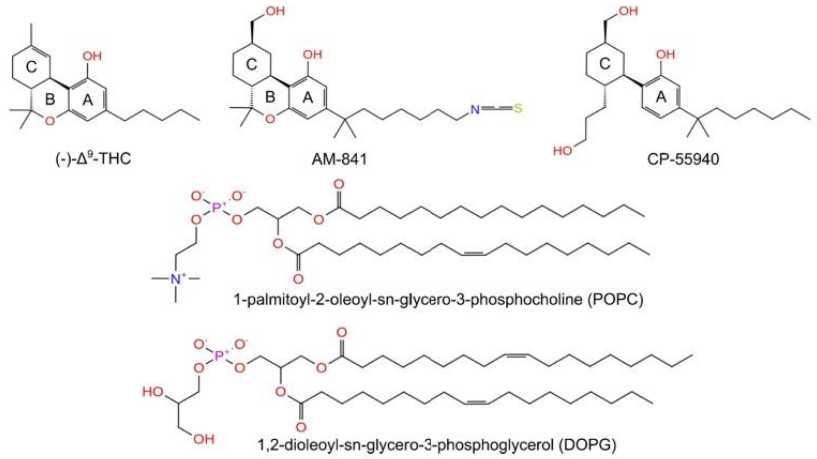

Figure 1. Chemical structures of ABC-tricyclic cannabinoids Δ^9-THC and AM-841, AC-bicyclic cannabinoid CP-55940, and membrane phospholipids POPC and DOPG. POPC is composed of a 16-carbon and an 18-carbon fatty acid chains and a headgroup that includes a choline group, resulting in a net neutral phospholipid. DOPG is composed of two 18-carbon fatty acid chains and a headgroup that includes a glycerol group, resulting in a net negatively charged phospholipid.

receptor.[28] These common conformational changes have been proposed to be triggered by the action of several conserved sequence motifs in their respective TM helices, known as molecular microswitches:[26] the $DR^{3.50}Y$, $NPxxY^{7.53}$ and $CWxP^{6.50}$ motifs and hydrophobic residues in the core of TM3 and TM6. $Arg^{3.50}$ of the $DR^{3.50}Y$ motif on TM3 participates in a salt−bridge interaction with $Asp^{6.30}$ (in TM6) known as the "ionic lock", which has been suggested to maintain the receptor in an inactive state, and is broken in the active state of the receptor.[29] The $Tyr^{7.53}$ residue of the $NPxxY^{7.53}$ motif on TM7 is known to rotate toward the core of the TM helical bundle upon receptor activation, where it has a role in G protein coupling and in blocking TM6 from moving back to its inactive conformation.[14] The $CWxP^{6.50}$ motif on TM6 contains the highly conserved $Trp^{6.48}$ residue, which has been proposed as a link between the orthosteric binding site and the intracellular movement of TM6.[26] In CB1 specifically, McAllister et al.[30] proposed that $Trp356^{6.48}$ undergoes a conformational change consisting of a χ_1 dihedral angle change from gauche(+) to trans, accompanied by a χ_1 dihedral angle change in $Phe200^{3.36}$ from trans to gauche(+), upon receptor activation. Finally, hydrophobic residues in the core of TM6 such as $Phe/Leu^{6.44}$ and $Ile/Val/Leu^{6.40}$ form a cage around $Leu^{3.43}$ that is rearranged in the active state to allow TM3 upward movement.[28] Collectively, these conformational changes lead to the opening of an intracellular cavity that forms the G protein binding site.[14,26,27]

In addition to receptor activation by molecules that bind to the same binding site as the endogenous ligand (i.e., the orthosteric site), CB1 function can also be modulated by molecules that bind to topologically different binding sites (allosteric sites).[31−33] Interestingly, cholesterol enrichment significantly reduces CB1-dependent signaling[34−36] by binding to CB1,[37,38] which highlights the potential role for allosteric modulation of CB1 by membrane lipids. Accordingly, cholesterol also modulates the function of the homologous adenosine A2A receptor,[39] chemokine receptors CXCR4 and CCR5,[40] and β_2 adrenergic receptor.[41] In addition, Dawaliby et al.[42] showed that net negatively charged phospholipids (e.g., 1,2-dioleoyl-*sn*-glycero-3-phosphoglycerol (DOPG), 1,2-dioleoyl-*sn*-glycero-3-[phospho-L-serine], and 1,2-dioleoyl-*sn*-glycero-3-phospho-(1'-myo-inositol)) promote β_2 adrenergic receptor activation and agonist binding, acting as positive allosteric modulators. Moreover, DOPG has been described to stabilize the active conformation of β_2 adrenergic receptor by forming electrostatic interactions with positively charged residues located on ICL3 and the intracellular region of TM6.[43] Since CB1 also contains a large number of positively charged residues in the intracellular regions of TM5, ICL3, and TM6 (9 out of 29 arginine/lysine residues in the receptor, excluding the N- and C-terminus), it is possible that DOPG might also act as an allosteric modulator of CB1.

The binding pocket of CB1 and residues involved in receptor activation have been previously studied by combining mutational analyses, ligand docking, and molecular dynamics (MD) simulations using homology models of CB1.[29,30,44−46] Currently, five crystal structures of CB1 are available: two in an inactive state,[47,48] two in a partially active agonist-bound state,[49] and, most recently, a fully active G_i protein-bound state.[50] Although crystal structures are useful to determine active or inactive states of GPCRs, they only reveal a single snapshot of the receptor in a particular state and are unable to provide information about the mechanism of transition through intermediate states. MD simulations are a suitable method for studying protein function[51] and have been widely used to capture multiple molecular mechanisms in GPCRs, including ligand binding,[52,53] receptor conformational change,[54−56] and allosteric modulation.[43,57,58] However, capturing the transition of class A GPCRs from inactive to active states has proved elusive and has only been fully observed in "enhanced" MD simulations,[59,60] while in unbiased atomistic MD simulations, they have typically been found to spontaneously deactivate when a signaling protein is not included in the system.[43,54,61,62]

In this study, we aim to elucidate the key transition steps from inactive to active state of CB1, starting from its inactive crystal structure, by employing unbiased atomistic microsecond-length MD simulations of CB1 with and without bound potent full-agonist 3-(2-hydroxy-4-(1,1-dimethylheptyl)phenyl)-4-(3-hydroxypropyl)cyclohexanol (CP-55940, Figure 1), which is

DOI: 10.1021/acs.jmedchem.9b00612
J. Med. Chem. 2019, 62, 5638−5654

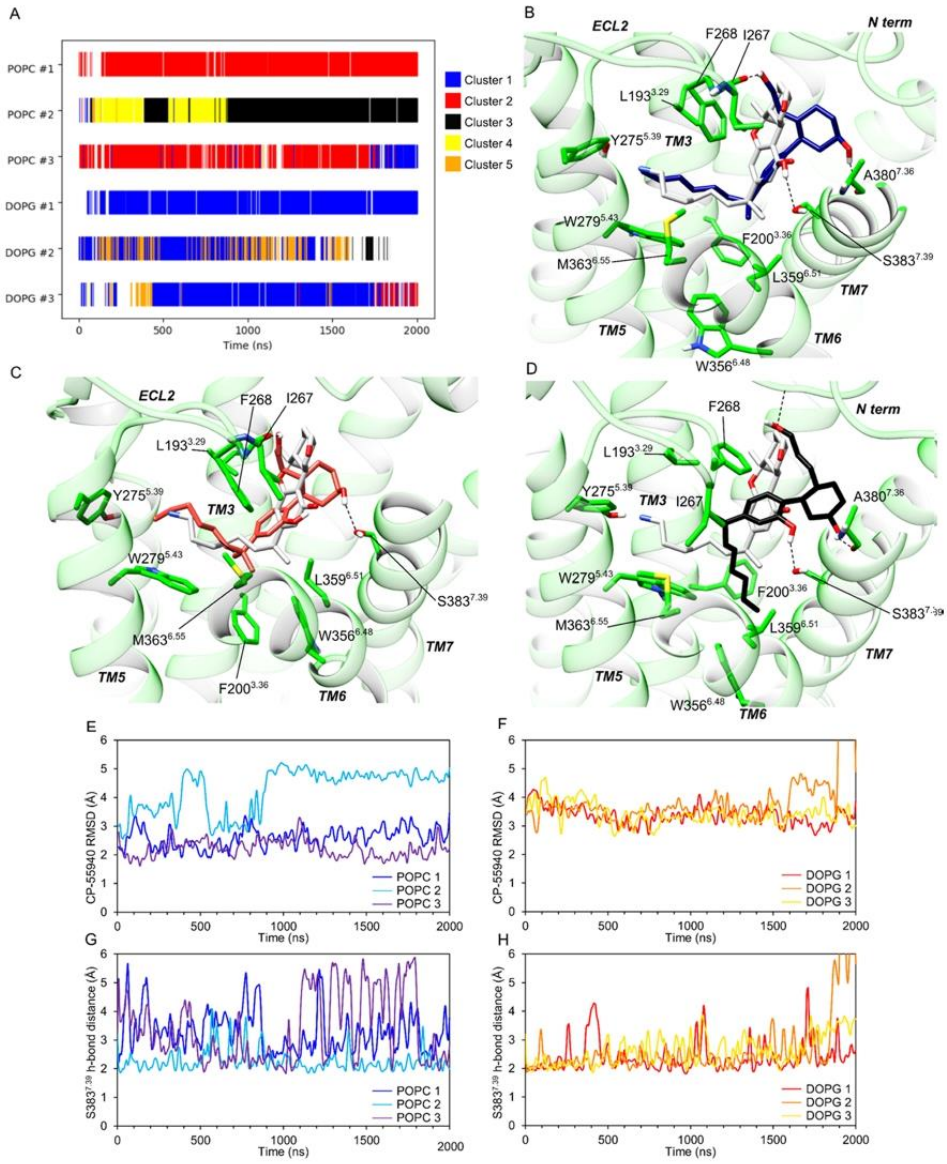

Figure 2. Clustering analysis of CP-55940 conformations along MD trajectories of CP-55940-bound CB1 (A) with representative binding mode of CP-55940 in cluster **1** (B), cluster **2** (C), and cluster **3** (D) compared to the binding mode of co-crystallized AM-841 (white sticks) in the agonist-bound CB1 crystal state (PDB entry 5XR8). (E, F) RMSD of CP-55940 relative to its initial docking position and (G, H) distance of the protein−ligand hydrogen bond between the A-ring hydroxyl group of CP-55940 and Ser383$^{7.39}$ in MD simulations of CB1 in POPC and DOPG membranes, respectively.

of standard use in cannabinoid research as a reference agonist.[63−67] In addition, potential allosteric interactions between phospholipids and CB1 are evaluated by comparison between MD simulations containing homogeneous membranes composed of anionic DOPG or net neutral 1-palmitoyl-2-oleoyl-*sn*-glycero-3-phosphocholine (POPC, Figure 1). These might provide further insight into the key molecular features of CB1 involved in cannabinoid binding, receptor activation, and allosteric modulation.

RESULTS

Docking of Cannabinoid Agonist CP-55940 Is Dependent on CB1 Receptor State. To investigate receptor activation, CP-55940 (see chemical structure in Figure 1) was docked into the inactive CB1 wild-type (WT) crystal structure,[48] yielding a docking score (estimated free energy of binding as calculated by AUTODOCK[68]) of −9.2 kcal/mol. The cyclic core of the agonist comfortably docks into the subpocket formed between TM2, TM3, and TM7, as proposed

DOI: 10.1021/acs.jmedchem.9b00612
J. Med. Chem. 2019, 62, 5638−5654

by Shim et al.[45] In this binding position, the phenolic A-ring of the agonist forms a hydrogen bond with Ser383$^{7.39}$ of the receptor through its hydroxyl group, while also forming $\pi-\pi$ aromatic interactions with Phe268^{ECL2} (Figure S1A, Supporting information). Additionally, the hydrophobic alkyl chain of CP-55940 extends toward TM5, interacting with a second subpocket formed by Leu193$^{3.29}$, Met363$^{6.55}$, Trp279$^{5.43}$, and Leu276$^{5.40}$, while its dimethyl group points toward Trp356$^{6.48}$ and Phe200$^{3.36}$. Both interactions between CP-55940 and Phe268^{ECL2}/Ser383$^{7.39}$, as well as a similar orientation of the ligand alkyl chain pointing toward TM5, are observed in the agonist-bound crystal structure of CB1[49] (Figure S1B, Supporting information), whose co-crystallized agonist AM-841 shares a similar structural scaffold to CP-55940 except for the absence of a B-ring (Figure 1).

To assess the quality of our docking into the inactive receptor state, CP-55940 was also docked into the agonist-bound crystal structure of CB1 (Protein Data Bank (PDB) entry 5XR8),[49] yielding a better docking score of −10.2 kcal/mol and a different orientation of its cyclic core (although with previously described interactions still intact). As such, in the inactive crystal structure, the A- and C-rings are almost perpendicular to TM3, while in the agonist-bound crystal structure, these rings are parallel to TM3, in a similar manner to the co-crystallized agonist AM-841.[49] This results in an increase of interactions with TM7 compared to the docking solution in the inactive state. Due to the inward movement of the extracellular region of TM2 in the agonist-bound crystal, docking of CP-55940 into this structure yields interactions with this helix that are not observed in the docking solution in the inactive state, despite high similarity in its interactions with TM3, TM5, and TM6 (Figure S2A,B, Supporting information). However, Phe170$^{2.57}$Ala/Trp and Phe174$^{2.61}$Ala/Trp mutations do not affect CP-55940 potency,[47] which suggests that CP-55940 does not interact as strongly with TM2. Nevertheless, the A- and C-rings of CP-55940 move toward a binding mode similar to the docking solution in the agonist-bound crystal early in our molecular dynamics (MD) simulations (see below) with the consequent formation of an additional hydrogen bond with Ile267^{ECL2} (Figure S3, Supporting information). Mutational data further support this binding mode, as mutations of residues Phe177$^{2.64}$, Phe189$^{3.25}$, Leu193$^{3.29}$, Phe268^{ECL2}, Pro269^{ECL2}, Ile271^{ECL2}, Tyr275$^{5.39}$, Trp279$^{5.43}$, Met363$^{6.55}$, Phe379$^{7.35}$, and Ser383$^{7.39}$ to Ala all decrease the affinity and/or the potency of CP-55940,[49,69−71] while Phe200$^{3.36}$Ala mutation does not affect CP-55940 binding despite its effect on CB1 function.[30,72] This indicates that our initial binding pose is accurate enough, despite difficulties associated with docking an agonist into the inactive crystal structure.

MD Simulations of CB1 with Bound CP-55940 Reveal Phospholipid-Dependent Binding Mode. MD simulations were performed in triplicate on CB1, starting from its inactive crystal state, with bound CP-55940 in homogeneous membranes composed of two different phospholipids: POPC and DOPG (Figure 1). While POPC forms a membrane of net neutral charge, DOPG instead forms a negatively charged membrane with the potential to form more protein−lipid hydrogen bonds and electrostatic interactions.[43] Here, it is observed that CP-55940 subtly diverts from its initial docking position in all MD simulations (agonist root-mean-square deviation (RMSD) in POPC: 3.0 ± 1.1 Å; in DOPG: 3.5 ± 0.7 Å; Figure 2). To analyze binding mode convergence between replicas, clustering analysis was performed. This shows the presence of three major clusters differentially represented depending on the membrane phospholipid (Figure 2A). CP-55940 adopts an L-shaped conformation in all three major clusters where the A-ring of CP-55940 is almost perpendicular to its alkyl chain (Figure 2). In clusters **1** and **2**, the AC rings of CP-55940 move from the initial docking position and become parallel to TM3 in a similar manner to the co-crystallized agonist AM-841 (Figure 2B,C). This conformation appears to be partially stabilized by the formation of an intermolecular hydrogen bond between the C-ring hydroxypropyl group of CP-55940 and the backbone oxygen atom of Ile267 in extracellular loop 2 (ECL2) of the receptor that is maintained throughout most of our MD simulations (Figure S3, Supporting information). Moreover, cluster **1**, which is over-represented in simulations containing DOPG membranes, shows the most similar set of interactions with TM3, TM5, TM6, TM7, and ECL2 compared to the predicted docking position in the agonist-bound crystal state (Figure S2, Supporting information). On the contrary, cluster **2**, which is over-represented in simulations containing POPC membranes, reveals a lack of interaction between CP-55940 and TM7 compared to the docking position in the agonist-bound crystal state despite its similar interaction with residues in other helices (Figure S2, Supporting information). Finally, cluster **3**, which is only present in replica #2 with a POPC membrane and briefly in replica #2 with a DOPG membrane, represents a different L-shape conformation to clusters **1** and **2**, where the alkyl chain of CP-55940 inserts vertically rather than horizontally between TM3 and TM6 while the AC rings remain perpendicular to TM3 (Figure 2D). This cluster shares similar contacts with TM3 and TM7 compared to the predicted docking position in the agonist-bound crystal while lacking interactions with TM5 and ECL2 (Figure S2, Supporting information). As this unusual movement of the alkyl chain is not necessary to achieve receptor activation (as shown below), this indicates that it may simply be a consequence of inherent system flexibility. The stability of an L-shape ligand conformation is supported by NMR experiments with CP-55940,[67] and its interactions with the receptor are consistent with the agonist-bound crystal structure of CB1, showing the best correlation with cluster **1**[49] (Figure S2, Supporting information). However, as CP-55940 possesses three hydroxyl groups, compared to the two hydroxyl groups of AM-841, an additional transient hydrogen bond with the backbone of Ala380$^{7.36}$ can be formed in CP-55940 clusters **1** and **3**, which is likely stabilized by water molecules in the orthosteric site (Figures S2 and S3, Supporting information). As the formation of hydrogen bonds between agonists and TM7 is a known feature of GPCR agonists,[27] it is possible that this additional interaction favors CB1 activation and CP-55940 stability in the orthosteric site.

Interestingly, CP-55940 function is abolished by a Ser383$^{7.39}$Ala mutation in CB1,[69] which suggests that this residue plays an essential role in agonist binding and function. Supporting this mutational data, the protein−ligand hydrogen bond formed between the A-ring hydroxyl group of the ligand and Ser383$^{7.39}$ of the receptor is observed in clusters **1**−**3** and maintained across all MD simulations (Figure 2G,H) except for one replica (simulation #2 in DOPG), where it destabilizes in the final few nanoseconds. The occupancy of this hydrogen bond is 68.5% (S.D. ± 17.2) in those MD simulations where agonist cluster **1** or **3** is represented and only 22.7% in replica #1 in POPC, where only agonist cluster **2** is represented. Moreover, receptor activation is only observed in replicas where agonist

DOI: 10.1021/acs.jmedchem.9b00612
J. Med. Chem. 2019, 62, 5638−5654

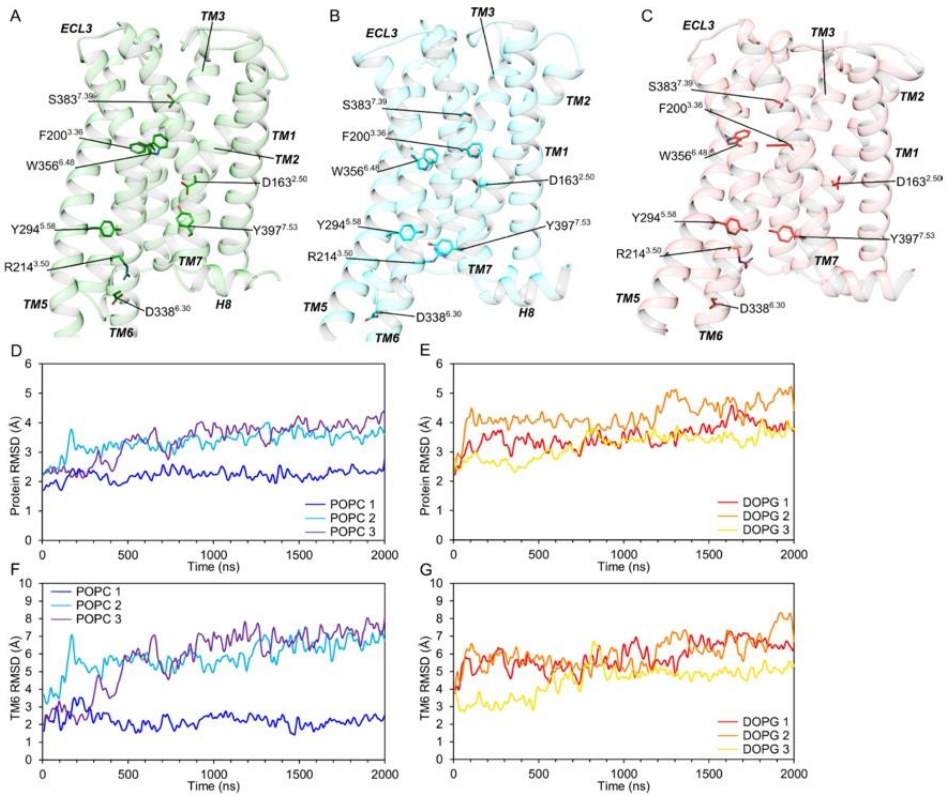

Figure 3. (A) Initial inactive crystal structure of CB1 (PDB entry 5U09). (B) Fully active-like conformation of CB1 after 0.9 μs of MD simulation #2 in POPC with bound CP-55940. (C) Fully active-like conformation of CB1 after 0.6 μs of MD simulation #1 in DOPG with bound CP-55940. RMSD of Cα atoms of CB1 TM helices (D, E) and RMSD of Cα atoms of CB1 TM6 (F, G) from the initial inactive crystal state (PDB entry 5U09) during MD simulations of CB1 with bound CP-55940 in a POPC (blue, cyan, purple) and DOPG (red, orange, yellow) membrane.

clusters **1** or **3** are represented (see below), which highlights the importance of this hydrogen bond. Furthermore, it appears to be more stable in DOPG than in POPC MD simulations, showing an occupancy of 71.5 ± 7.7% in DOPG and 50.1 ± 32.5% in POPC, which suggests that the agonist undergoes less perturbation in the former than the latter (following the same trend observed for ligand RMSD and binding mode convergence; Figure 2). As CP-55940 does not make direct contact with the membrane, it seems the receptor likely mediates this effect.

Bound Agonist CP-55940 Activates CB1 in a POPC Membrane. Receptor activation was observed in two out of three replicas with bound CP-55940 in POPC membranes (receptor RMSD > 3.5 Å; Figure 3), with conformational change most notable in TM6 (RMSD > 5.0 Å; Figure 3F). This increase in RMSD corresponds to an outward movement of TM6 at its intracellular side, which results in the separation of ionic lock residues (Arg214$^{3.50}$ and Asp338$^{6.30}$) whose distance increases from 6.8 to >15.0 Å (Figure 4A; equivalent distance in fully active CB1 crystal structure: 14.9 Å[50]). In addition, at the intracellular side of the receptor, the side-chain oxygen atoms of residues Tyr294$^{5.58}$ and Tyr397$^{7.53}$ approach each other from a distance of 11.6 up to 2.8 Å (Figure 4C; equivalent distance in fully active crystal structure: 3.5 Å[50]), albeit transiently probably due to the lack of a stabilizing G protein in the MD systems. Indeed, in one of these MD simulations (replica #3 in POPC) at the halfway point, the outward movement of TM6 allows the insertion of a single phospholipid molecule into the helical bundle at its intracellular side between TM6 and TM7. This POPC molecule is able to form transient electrostatic interactions between its negatively charged phosphate group and the positively charged Arg214$^{3.50}$ side chain of the ionic lock, as the phospholipid molecule repeatedly moves in and out of the protein (Figure 5). This type of electrostatic protein−lipid interaction has been reported before in MD simulations of the active state of β_2 adrenergic receptor[43,61] and appears to be a specific allosteric interaction favoring the stabilization of TM6 in an outward conformation in CB1 as well. On the contrary, in another replica, where the receptor also undergoes activation with similar conformational changes (replica #2 in POPC), this particular protein−lipid interaction is not observed. This demonstrates that CB1 activation can occur without binding of a phospholipid molecule and is likely a direct consequence of the absence of a signaling partner in the MD systems.

One of the most characteristic microswitches in CB1 is the Trp356$^{6.48}$/Phe200$^{3.36}$ double rotameric switch,[30,45,49,73] consisting of a χ_1 dihedral angle change in Trp356$^{6.48}$ from gauche(+) to trans and a χ_1 dihedral angle change in Phe200$^{3.36}$ from trans to gauche(+), which results in the breakage of the aromatic stacking interaction between these two residues upon

DOI: 10.1021/acs.jmedchem.9b00612
J. Med. Chem. 2019, 62, 5638−5654

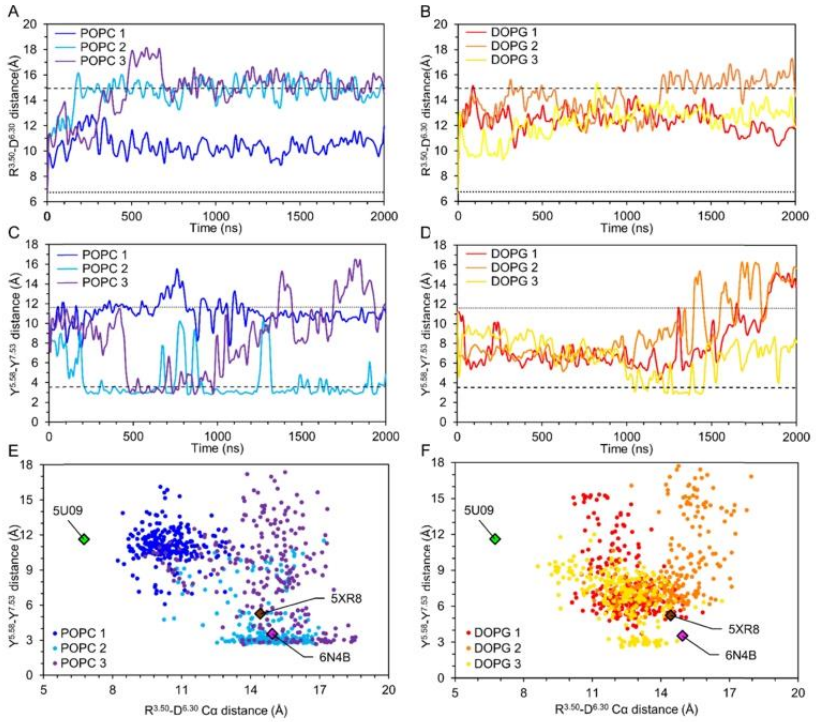

Figure 4. Intracellular features of CB1 activation during MD simulations with bound CP-55940 in a POPC (blue, cyan, purple) and DOPG (red, orange, yellow) membrane. (A, B) Distance between ionic lock residues in CB1 ($Arg214^{3.50}$ and $Asp338^{6.30}$). (C, D) Distance between side-chain oxygen atoms of residues $Tyr294^{5.58}$ and $Tyr397^{7.53}$ in CB1. Distances in the initial inactive crystal state (PDB entry 5U09) and the active crystal state (PDB entry 6N4B) are represented as dotted and dashed lines, respectively. (E, F) Distance between ionic lock residues against distance between $Tyr294^{5.58}$ and $Tyr397^{7.53}$ in CB1 conformations sampled every 8 ns of MD simulation time. Green, brown, and magenta diamonds represent inactive (PDB entry 5U09), agonist-bound (PDB entry 5XR8), and active (PDB entry 6N4B) crystal structures of CB1, respectively.

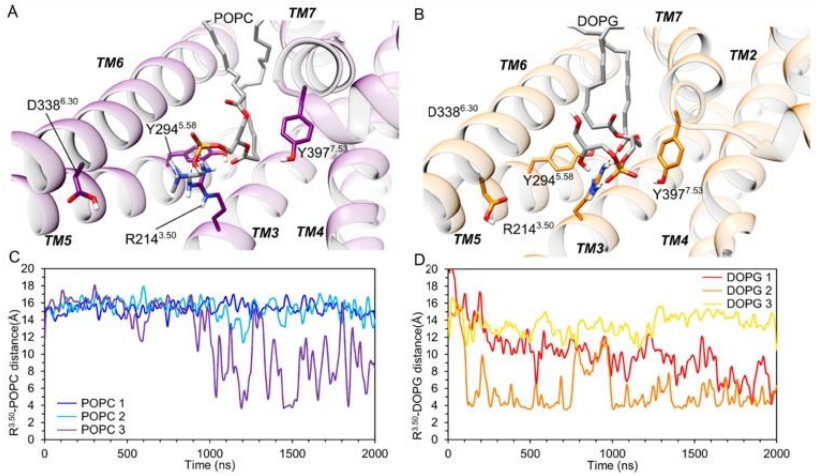

Figure 5. Intracellular point of view of the interaction between a single POPC or DOPG molecule with $Arg214^{3.50}$ at 1.0 μs of MD simulations of CB1 in replica #3 in POPC (A, purple) and replica #2 in DOPG (B, orange). (C, D) Distance between ionic lock residue $Arg214^{3.50}$ and phosphorus atom of the closest POPC or DOPG phospholipid headgroup.

receptor activation.[30,49,50] In the inactive CB1 crystal structure,[48] $Trp356^{6.48}$ forms aromatic stacking interactions with $Phe200^{3.36}$ (Figure 6A). As shown in Figure 6B, a conformational change from gauche(+) to trans is indeed observed in $Trp356^{6.48}$ in the CP-55940-bound receptor, and this residue either remains in trans conformation throughout the

DOI: 10.1021/acs.jmedchem.9b00612
J. Med. Chem. 2019, 62, 5638−5654

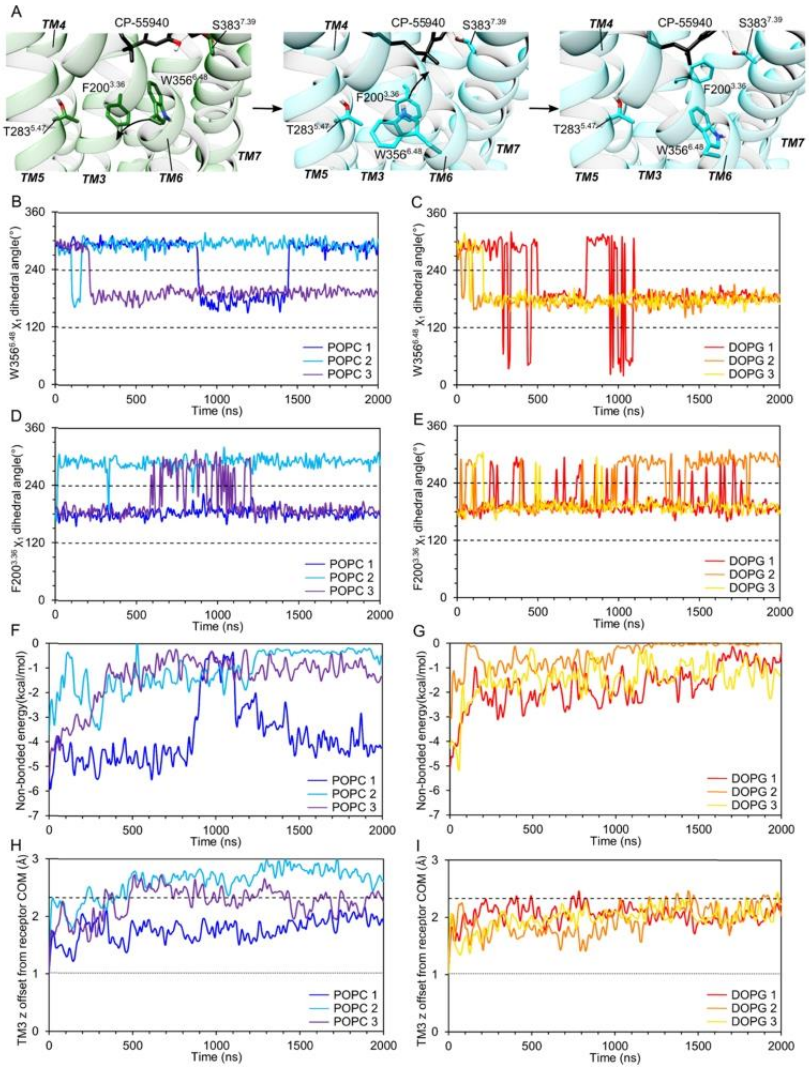

Figure 6. (A) Trp356$^{6.48}$/Phe200$^{3.36}$ double rotameric switch from the initial inactive CB1 crystal state (PDB entry 5U09, green) to active state via an intermediate (both cyan), during MD simulation #2 in POPC with bound CP-55940. χ_1 dihedral angle of residues Trp356$^{6.48}$ (B, C) and Phe200$^{3.36}$ (D, E) during MD simulations of CP-55940-bound CB1 in POPC and DOPG membranes. The dotted lines represent the angle intervals for gauche(−) (0−120°), trans (120−240°), and gauche(+) (240−360°). (F, G) Estimated nonbonded energy of interaction between Trp356$^{6.48}$ and Phe200$^{3.36}$ side chains. (H, I) Offset in the *Z* axis (perpendicular to the membrane) of the center of mass of TM3 with respect to the center of mass of TM helices of CB1 compared to the initial inactive crystal state (dotted line, PDB entry 5U09) and the active crystal state (dashed line, PDB entry 6N4B).

trajectory or later switches back to its gauche(+) conformation. In its trans conformation, the side-chain nitrogen atom of Trp356$^{6.48}$ points toward TM5 and forms either direct or water-mediated hydrogen bonds with Thr283$^{5.47}$ or Ser284$^{5.48}$, which is equivalent to the aromatic interaction observed between Trp$^{6.48}$ and Phe$^{5.47}$ in activated muscarinic M2 receptor.[59] Additionally, Phe200$^{3.36}$ may switch from trans to gauche(+) conformation either transiently or for the duration of the simulation time (Figure 6D). This rotameric switch results in the breakage of the aromatic stacking interaction between Trp356$^{6.48}$ and Phe200$^{3.36}$ (Figure 6F), which remains disrupted in replica #2 with bound CP-55940 in POPC even when Trp356$^{6.48}$ returns to its gauche(+) conformation due to the outward movement of TM6. However, in replica #1 in POPC, which does not yield active-like receptor conformations, no rotameric switch is observed in Phe200$^{3.36}$, which leads to the recovery of its aromatic interaction with Trp356$^{6.48}$ after the latter residue returns to its gauche(+) conformation. The rotameric switch of Trp356$^{6.48}$ most likely allows Phe200$^{3.36}$ to slide between Trp356$^{6.48}$ and Cys386$^{7.42}$ on TM7, resulting in an axial upward movement of TM3 (Figure 6H). This shift of Trp356$^{6.48}$ and Phe200$^{3.36}$ and the axial upward movement of

DOI: 10.1021/acs.jmedchem.9b00612
J. Med. Chem. 2019, 62, 5638−5654

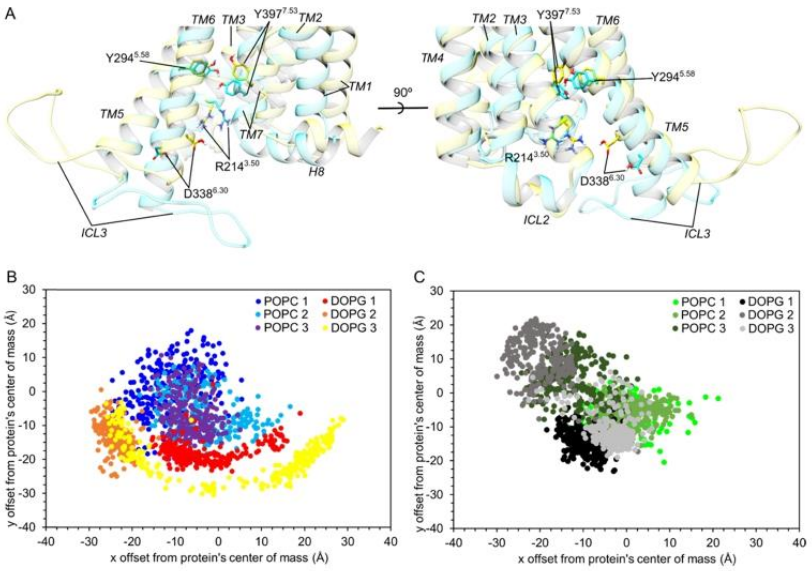

Figure 7. (A) Orientation of intracellular loop 3 (ICL3) at 1.0 μs of MD simulations of CB1 bound to CP-55940 in POPC (from replica #2, cyan) and DOPG membranes (from replica #3, yellow). Position of the center of mass of ICL3 along x–y coordinates (plane of the membrane) with respect to the center of mass of the receptor in MD simulations of CB1 bound to CP-55940 (B) and apo (C) in POPC and DOPG membranes, respectively.

TM3 is also observed in the agonist-bound and fully active crystal structures of CB1.[49,50] The importance of the aromatic interaction between Trp356$^{6.48}$ and Phe200$^{3.36}$ in the inactive state of the receptor is supported by mutational data, which show that Phe200$^{3.36}$Ala mutation results in higher constitutive activity compared to the WT receptor and Trp356$^{6.48}$Ala mutation results in increased agonist efficacy.[30] This could be due to alanine being a less bulky residue that reduces steric hindrance between positions 3.36 and 6.48 and thus facilitates easier TM3 upward movement.

Overall, the observed intracellular conformational changes in CB1 are consistent with receptor activation.[14,26,27,49,50] The approach between Tyr294$^{5.58}$ and Tyr397$^{7.53}$ side chains (Figure 4C) is seemingly triggered by the formation of the hydrogen bond between CP-55940 and Ser383$^{7.39}$ and by the upward axial movement of TM3 and outward movement of TM6 that follow the Trp356$^{6.48}$/Phe200$^{3.36}$ double rotameric switch. Similar conformational changes are also observed when performing MD simulations using the co-crystallized CB1 agonist AM-11542[49] (Figure S4, Supporting information). Although GPCR activation has been reported to occur at a millisecond timescale,[74] CB1 is a class A GPCR that exhibits a high level of constitutive activity,[72,75] which suggests that this receptor has a relatively low energy barrier of activation. This is possibly due to TM6 sequence divergence between CB1 and other class A GPCRs: for example, the presence of a leucine residue instead of the generally conserved Phe$^{6.44}$ might increase the flexibility of the receptor core and favor conformational changes required for activation,[28,76] while the presence of Gly357$^{6.49}$ immediately preceding the highly conserved proline kink residue Pro358$^{6.50}$ probably assists outward TM6 orientations.[77] Additionally, neutralization of key intracellular acidic residues (Asp213$^{3.49}$, Asp338$^{6.30}$, as well as Glu323^{ICL3} and Asp324^{ICL3} on intracellular loop 3 (ICL3)) seems to promote receptor activation as described for homologous GPCRs,[43,54,78] since simulations of the CP-55940–CB1 complex using the expected protonation state at pH 7.0 show less intracellular conformational change despite observed switching of Trp356$^{6.48}$/Phe200$^{3.36}$ and the presence of the CP-55940–Ser383$^{7.39}$ hydrogen bond (Figure S5, Supporting information).

Anionic DOPG Membrane Enhances Agonist-Mediated CB1 Activation. It has been proposed that DOPG (and other anionic phospholipids) may favor class A GPCR activation through protein–lipid allosteric interactions with ICL3 and TM6 of the receptor,[43] as well as with the "ionic lock" residue Arg$^{3.50}$ located at the intracellular side of TM3.[43,61] To assess if this type of receptor–phospholipid allosteric interaction is present in CB1, MD simulations were performed in homogeneous DOPG membranes. Receptor activation was observed in all replicas with bound CP-55940 in a DOPG membrane (Figures 3 and 4), suggesting enhanced mobility of TM6 compared to those in a POPC membrane. In general terms, features of receptor activation are similar to those observed in a POPC membrane using the same agonist, including outward movement of TM6 (Figure 3G), separation of ionic lock residues (Figure 4B) and changes in the Trp356$^{6.48}$/Phe200$^{3.36}$ double rotameric switch with consequent upward axial movement of TM3 (Figure 6). However, the insertion of a DOPG molecule into the intracellular side of the receptor is found to occur more consistently (in two out of three MD simulations; Figure 5D). This is most likely due to the net negative charge of the DOPG headgroup that interacts stronger with Arg214$^{3.50}$ than the zwitterionic headgroup of POPC and thus forms more stable protein–lipid allosteric interactions.[61] This has the effect of inducing earlier conformational change in TM6, with receptor activation initiated in just a few nanoseconds in DOPG replicas #1 and #2 compared to relevant MD simulations in POPC (Figure 3). However, this specific protein–lipid allosteric interaction is not strictly required for receptor activation, as it

DOI: 10.1021/acs.jmedchem.9b00612
J. Med. Chem. 2019, 62, 5638–5654

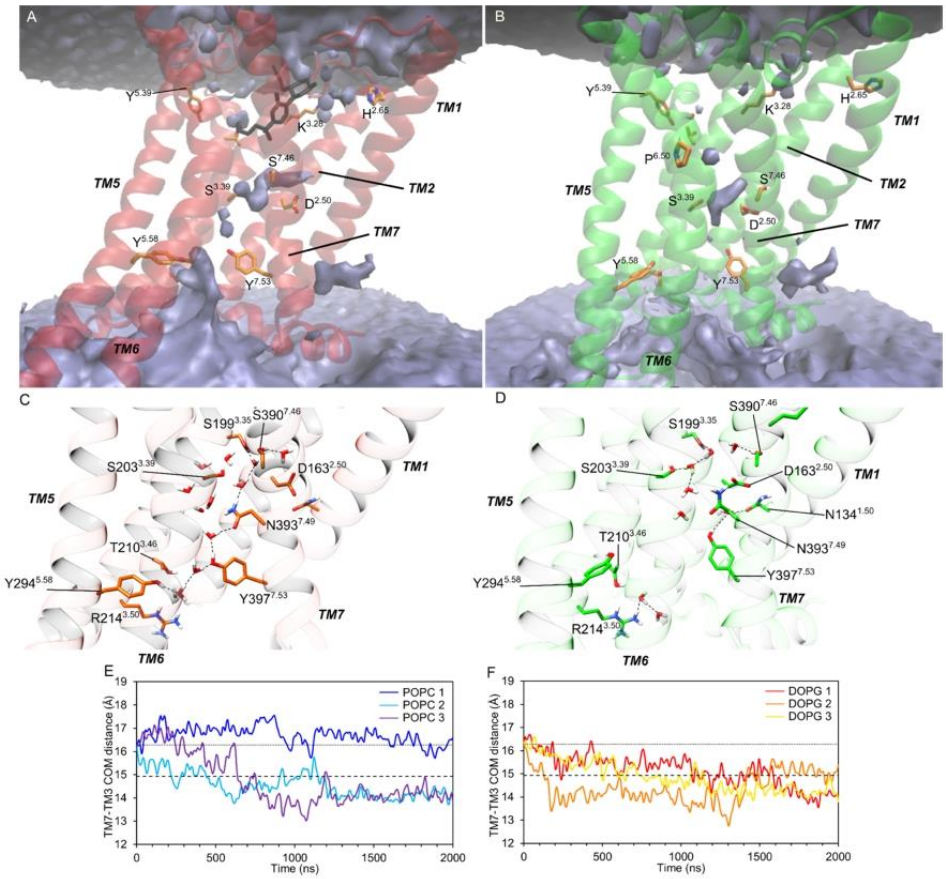

Figure 8. Average water density for MD simulations of CP-55940−CB1 complex (A, from replica #1 in DOPG) and apo receptor (B, from replica #1 in POPC). (C, D) Respective snapshots at 1.0 μs with water-mediated hydrogen bonds represented as dotted lines. (E, F) Distance between centers of mass of TM3 and TM7 during MD simulations of CB1 with bound CP-55940 in POPC and DOPG membranes, respectively.

is not observed in replica #3 in DOPG, which undergoes receptor activation nevertheless (Figure 3E,G).

In addition to the allosteric actions of a bound phospholipid molecule, external protein−lipid interactions can be formed with ICL3, which is connected to TM6. In an analysis of these interactions (Figure 7), it is observed that in CP-55940-bound CB1 in a DOPG membrane, ICL3 tends to adopt highly outward orientations (pointing away from ICL1 and ICL2), while in POPC, ICL3 can apparently switch between outward and inward conformations with more freedom. In addition, it is also observed that ICL3 associates closer with the anionic headgroups of DOPG molecules than respective zwitterionic headgroups of POPC (Figure S6, Supporting information), suggesting the presence of stronger electrostatic interactions between ICL3 (whose net charge is +4 in our simulations) and the DOPG membrane, including residues Lys315^{ICL3}, His320^{ICL3}, Lys326^{ICL3}, and Arg331^{ICL3} in ICL3, but also Arg336$^{6.28}$ at the intracellular end of TM6. As noted elsewhere,[43] an outward orientation of ICL3 favors an outward conformation of TM6 and provides an additional stabilizing factor in an active-like GPCR state. Interestingly, these observed CB1-phospholipid interactions in a DOPG membrane (both external and internal) act to increase stabilization of bound agonist CP-55940, showing higher binding mode convergence and interaction with TM7 compared to simulations in POPC (Figure 2A), as well as greater protein−ligand hydrogen-bond occupancy as mentioned above. This is evidence for a system of allosteric communication between the intracellular and extracellular sides of CB1, which has been previously observed in MD simulations of β_2 adrenergic receptor.[79]

Apoprotein State Reveals Partial Effects of Phospholipid-Mediated Allosterism. Phospholipid-mediated allosteric effects in CB1 were also considered in systems without a bound agonist as a control (apoprotein state). Although ionic lock residues Arg214$^{3.50}$ and Asp338$^{6.30}$ can separate in apoprotein state, suggesting the generation of an intermediate-like conformation, active receptor states are not observed, with conformational change of TM6 notably absent (Figure S7, Supporting information). Hence, Tyr294$^{5.58}$ and Tyr397$^{7.53}$ side chains do not approach in these simulations (Figure S8, Supporting information). A lower efficiency in the Trp356$^{6.48}$/Phe200$^{3.36}$ rotameric switch is also observed, which only occurs spontaneously in replica #3 in POPC (Figure S9, Supporting information). Despite this switch to an apparent intermediate-like state, there is no concomitant upward movement of TM3 relative to TM6 (Figure S9G, Supporting information),

DOI: 10.1021/acs.jmedchem.9b00612
J. Med. Chem. 2019, 62, 5638−5654

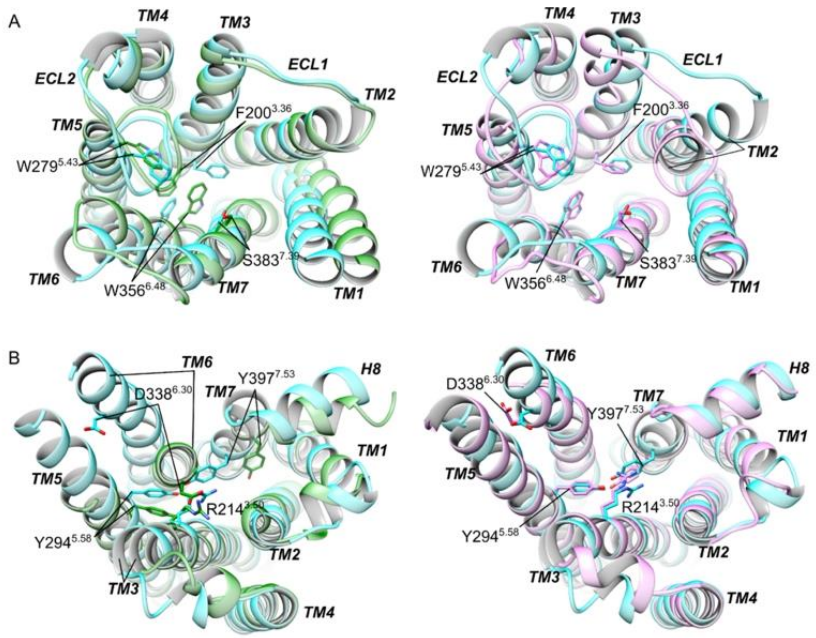

Figure 9. Structural comparison of fully active-like conformation of CB1 after 0.9 μs of MD simulation #2 with bound CP-55940 in a POPC membrane (cyan) against the initial CB1 inactive crystal state (in green, PDB entry 5U09) and fully active CB1 crystal structure (in pink, PDB entry 6N4B) from extracellular (A) and intracellular (B) points of view.

suggesting a lack of conformational change in the core of the protein. Consequently, the receptor fails to activate with little conformational change in TM6 (Figure S7, Supporting information). On the contrary, in replica #1 in DOPG, the intracellular end of TM6 develops an "L-shape" with conformational distortion at Ile339$^{6.31}$, resulting in one part of the helix attaining an outward orientation while the rest of TM6 remaining in an inactive-like conformation (Figure S10, Supporting information). This results in RMSD values >5.0 Å in TM6 and separation of the ionic lock (Figures S5D and S6B, Supporting information), but no other features of activation are observed in the receptor (Figure S8B,D, Supporting information). As far as we know, this unusual TM6 conformation does not correspond to any known GPCR crystal structure state and is likely a direct consequence of allosteric protein−lipid interactions with ICL3. This may offer some assistance in the outward movement of TM6 at its intracellular end but not enough to fully promote receptor activation by itself. Although insertion of a phospholipid molecule between TM6 and TM7 is not observed, transient protein−lipid interactions with ionic lock residue Arg214$^{3.50}$ were recorded in a DOPG membrane, in this case due to rotation of Arg214$^{3.50}$ toward the membrane, which is possible because of high flexibility in the apoprotein state (Figure S10, Supporting information).

Differences in the orientation of ICL3 between membranes (DOPG or POPC) in apoprotein state MD simulations are not as pronounced as in CP-55940-bound CB1 systems (Figure 7B,C). This supports the presence of cooperative allosteric communication between DOPG phospholipids and agonist when bound to CB1. On the other hand, in the apoprotein state of CB1, it is observed that ICL3 may adopt either inward or outward conformation regardless of the membrane phospholipid. However, direct interaction between ICL3 and the membrane is only observed with DOPG (Figure S6, Supporting information), which indicates its potential for positive allosteric modulation.

Receptor Activation Modifies an Internal Water Network. Internal water molecules can modulate the conformational properties of proteins and have a role in GPCR activation.[80−82] Together with the opening of the intracellular cavity of the receptor that is mainly due to the outward movement of TM6, conformational changes of TM3 and TM7 allow the penetration of water molecules into the receptor in CP-55940−CB1 complexes. Water density maps of our MD simulations reveal the presence of water molecules at several locations in the receptor (Figure 8). Active-like CP-55940-bound CB1 (replicas #2 and #3 in POPC and #1, #2, and #3 in DOPG) show a highly mobile water-mediated hydrogen bond network that connects residues Asp163$^{2.50}$, Ser203$^{3.39}$, and Ser390$^{7.46}$ at the core of the receptor with residues Thr210$^{3.46}$, Arg214$^{3.50}$, and Tyr294$^{5.58}$ through Tyr397$^{7.53}$ and Asn393$^{7.49}$ of the NPxxY motif on TM7. This occurs due to an inward movement of TM7 toward TM3 and the shift of Tyr397$^{7.53}$ toward Tyr294$^{5.58}$ (Figure 8). In contrast, receptors that remain in an inactive state show an interrupted water network where either Tyr397$^{7.53}$ interacts with Asp163$^{2.50}$ or Asn184$^{1.50}$ (CP-55940-bound CB1 replica #1 in POPC, and apo CB1 replicas #1 in POPC and all in DOPG) or Tyr397$^{7.53}$ points toward the cytoplasmic region instead (apo CB1 replicas #2 and #3 in POPC). These water networks are conserved in class A GPCRs and are in agreement with the activation state of the receptor.[82] Indeed, Asp163$^{2.50}$ is a highly conserved residue in class A GPCRs[83] that is described to participate in sodium-mediated negative allosteric modulation in CB1,[84] while Ser390$^{7.46}$ is located two helix turns after Ser383$^{7.39}$, a crucial binding residue for CP-55940.[69] In addition, Ser$^{7.46}$Ala and Asp$^{2.50}$Asn

DOI: 10.1021/acs.jmedchem.9b00612
J. Med. Chem. 2019, 62, 5638−5654

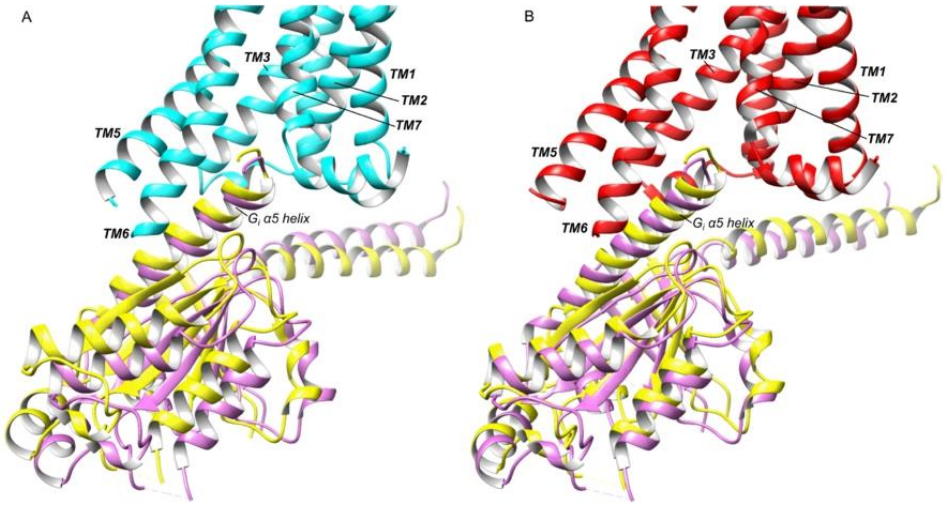

Figure 10. Docking of the co-crystallized G_i protein α subunit from the fully active CB1 crystal structure (PDB entry 6N4B) into MD-generated conformations of CB1. The best docking position of G_i protein (in yellow) is compared to its crystallized position (in pink) in the fully active CB1 crystal structure (with receptor structures superimposed). (A) At 0.9 μs of MD simulation #2 with CP-55940 in POPC (in cyan), corresponding to a G_i α5 helix RMSD of 0.9 Å. (B) At 0.6 μs of MD simulation #1 with CP-55940 in DOPG (in red), corresponding to a G_i α5 helix RMSD of 2.9 Å.

mutations have been reported to alter the intracellular conformation of TM7 toward a more inactive state near the NPxxY motif in adenosine A2A receptor.[85]

On the contrary, stable water molecules in the orthosteric site are not conserved within GPCRs.[82] The extracellular region of CB1 shows water molecules interacting with residues Tyr275$^{5.39}$–Thr197$^{3.33}$ and K192$^{3.28}$–Asp184^{ECL1}–Asp176$^{2.63}$ (Figure S3A, Supporting information). Additional water molecules interact with His178$^{2.65}$ and Gln116$^{1.32}$ in all replicas, which, in the case of apo receptors, forms a network that connects His178$^{2.65}$ to Ser383$^{7.39}$. In CP-55940–CB1 complexes, this water network connects His178$^{2.65}$ to the C-ring hydroxyl group of CP-55940 in replica #3 in POPC and in replica #1 in DOPG, which in turn possibly stabilizes further interaction with TM7 through the backbone of Ala380$^{7.36}$ (Figure S3, Supporting information). Finally, CP-55940-bound CB1 replicas #1 and #2 in POPC, #1 and #3 in DOPG, and apo CB1 replicas #1 in POPC and all in DOPG also show a water molecule interacting with the backbone of TM6 in close proximity to the proline kink residue Pro358$^{6.50}$ (Figure S3B, Supporting information). This water molecule has been co-crystallized in a crystal structure of μ-opioid receptor[86] and is independent of GPCR activation state.[82] The low level of hydration in the TM3–TM5–TM6 interface in CB1 can be attributed to the high hydrophobicity of this subpocket. In contrast, water molecules found in the TM1–TM2–TM3–TM7 interface, especially in apo receptors, suggest that internal water molecules have a role in agonist binding.

Fully Activated CB1 with Bound CP-55940 Can Dock G Protein. Active-like CB1 conformations generated in MD simulations were compared against the fully active, G_i protein-bound CB1 crystal structure with co-crystallized agonist MDMB-Fubinaca (PDB entry 6N4B).[50] At its extracellular region, this crystal structure shows an inward bend of TM1 and TM2 that approach the orthosteric binding site relative to the inactive crystal state. At the intracellular side, an outward bend of TM6 and an inward movement of TM7 allow G_i protein binding. Here, the extracellular TM1 inward bend is observed in replica #2 with bound CP-55940 in POPC only, while TM2 remains in its original state in all replicas (Figure 9A). However, different degrees of conformational change may occur depending on bound agonist as well as surrounding membrane composition. Indeed, this TM2 movement is not commonly associated with receptor activation in class A GPCRs,[26−28] which suggests that it is a result of the binding of different ligands.

In contrast, a higher degree of correlation is found in the core and intracellular region of CB1 between our MD conformations and the fully active crystal structure, specifically regarding TM6 outward movement and rearrangement of the NPxxY motif in TM7 (Figure 9B). Thus, the signaling capability of our MD-generated conformations was assessed by docking the co-crystallized G_i protein α-subunit from the active crystal structure of CB1[50] into our MD-generated conformations. Satisfactory protein–protein docking solutions for CP-55940-bound CB1 were obtained for the two replicas in POPC that yield active-like receptor conformations and for all three replicas within a DOPG membrane (criteria according to docking score and RMSD; see Table S1, Supporting information). The position of successfully docked G_i proteins is consistent with the fully active CB1 crystal structure (Figure 10), yielding G_i α5 helix RMSDs of 0.9 and 2.4 Å in POPC replicas (#2 and #3, respectively) and 2.9, 3.6, and 2.4 Å in DOPG replicas (#1, #2, and #3, respectively). However, MD-generated fully active states of CB1 are not stabilized for long and G_i protein can only be satisfactorily docked into selected conformations from our MD simulations. This is likely due to the absence of a permanently bound intracellular partner in our MD systems, as supported by the spontaneous deactivation of β_2 adrenergic receptor in previous MD simulation studies.[43,54] Thus, a G protein or other signaling partner is probably necessary to stabilize the fully active state of the receptor for longer than a few nanoseconds.

DOI: 10.1021/acs.jmedchem.9b00612
J. Med. Chem. 2019, 62, 5638−5654

DISCUSSION AND CONCLUSIONS

Agonist-Mediated CB1 Receptor Activation. In the inactive state of CB1, Trp356$^{6.48}$ forms $\pi-\pi$ aromatic interactions with Phe200$^{3.36}$, probably acting as an aromatic lock to prevent axial upward movement of TM3, which is a characteristic feature of class A GPCR activation.[28] Upon CP-55940 binding, the hydrophobic alkyl chain of the agonist induces the rotameric switch of Trp356$^{6.48}$ from gauche(+) to trans conformation, as proposed by McAllister et al.[30] and Shim et al.[45] This may occur through two coexisting activation pathways for CP-55940 depending on the orientation of the hydrophobic alkyl chain: (a) mediated by its dimethyl group, which has been reported to increase the potency of cannabinoids,[87] or (b) mediated by the rest of the alkyl chain. Thus, the absence of the dimethyl group in less potent agonists such as Δ^9-THC may result in only one optimal pathway for receptor activation, which might explain the lower potency and/or efficacy of Δ^9-THC compared to CP-55940.[63,87] The rotameric switch of Trp356$^{6.48}$ allows Phe200$^{3.36}$ to slide upward between Trp356$^{6.48}$ and TM7 and switch its conformation from trans to gauche(+). In addition, the breakage of the Trp356$^{6.48}$ and Phe200$^{3.36}$ aromatic interaction leads to the uncoupling of TM3 and TM6 at the core of the receptor, which favors an outward movement of TM6 that is later transmitted to the intracellular region and leads to the breakage of the ionic lock (Arg214$^{3.50}$–Asp338$^{6.30}$). In β_2 adrenergic receptor, TM3–TM6 uncoupling has been described to involve residues Leu$^{3.43}$, Ile$^{6.40}$, and Phe$^{6.44}$, which rearrange upon receptor activation to allow TM3 upward axial movement.[28] However, the semiconserved residue Leu352$^{6.44}$ in CB1 possibly confers higher flexibility to this region of the receptor and perhaps facilitates easier TM3–TM6 uncoupling, as shown by F$^{6.44}$L mutation in α_{1B} adrenergic receptor, which increases both constitutive and agonist-induced receptor activity.[76] After TM3 upward movement in CB1, Trp356$^{6.48}$ can change its conformation back to gauche(+), resulting in the positioning of Trp356$^{6.48}$ below Phe200$^{3.36}$, as observed in the agonist-bound crystal structures of CB1.[49,50]

In addition to the hydrophobic alkyl chain of CP-55940, the cyclic core of the agonist also seems to play an important role in receptor activation. The presence of a hydrogen bond between the agonist and Ser383$^{7.39}$ of the receptor can be considered essential for receptor activation, as Ser383$^{7.39}$Ala mutation completely abolishes CP-55940 function, possibly due to a destabilization of TM7 active-like conformations in the mutant receptor.[69] Moreover, the presence of hydrogen bonds between agonists and TM7 promotes TM3–TM7 interaction and receptor activation in class A GPCRs.[27] This appears to be the case in the CB1 receptor as well, where the agonist-Ser383$^{7.39}$ and agonist-Ala380$^{7.36}$ hydrogen bonds seem to stabilize the inward orientation of the core and intracellular end of TM7 toward TM3, starting from residue Ser390$^{7.46}$ and extending to the NPxxY$^{7.53}$ motif. In turn, this modifies a water-mediated hydrogen-bond network at the core of the receptor, ultimately leading to the rotation of Tyr397$^{7.53}$ toward Tyr294$^{5.58}$ on TM5, whose interaction has a role in G protein binding.[14]

It is likely that other well-known cannabinoid agonists share a similar activation mechanism to CP-55940, as AM-11542 also triggers the Trp356$^{6.48}$/F200$^{3.36}$ double rotameric switch through its alkyl chain and induces conformational change in TM7 by forming a hydrogen bond with Ser383$^{7.39}$ through its only hydroxyl group. Similarly, endogenous cannabinoids such as anandamide and 2-arachidonoylglycerol may trigger Trp356$^{6.48}$/F200$^{3.36}$ switching through their fatty acid chain while forming a hydrogen bond with Ser383$^{7.39}$ through their hydroxyl groups. The G_i protein-bound crystal structure of CB1[50] shows the co-crystallized agonist MDMB-Fubinaca stabilizing the active gauche(+) conformation of Phe200$^{3.36}$ through aromatic interactions instead, while suggesting the presence of a water-mediated hydrogen bond with Ser383$^{7.39}$ and His178$^{2.65}$. This idea is supported in our MD simulations by the observation of water molecules forming a network between residues Ser383$^{7.39}$ and His178$^{2.65}$ in the inactive apo receptor and between the C-ring hydroxyl group of CP-55940 and His178$^{2.65}$. We expect that aminoalkylindoles such as WIN55,212-2 share a similar set of interactions to MDMB-Fubinaca, as Trp356$^{6.48}$Ala and Phe200$^{3.36}$Ala mutations decrease the affinity of WIN55,212-2.[30,72]

The switch of Trp356$^{6.48}$/Phe200$^{3.36}$, the breakage of the ionic lock, TM3 axial upward movement, and inward movement of TM7, which are all observed in the agonist-bound crystal structures of CB1,[49,50] constitute an early-activated state of the receptor. From this, TM6 can move more outward and yield a fully active receptor state capable of binding a signaling protein.[50] We also expect that a bound signaling protein could confer extra stability to the fully active receptor state and possibly assist full activation by binding to an intermediate receptor state as proposed with β_2 adrenergic receptor.[54]

Phospholipid-Mediated CB1 Receptor Allosteric Modulation. DOPG is a net negatively charged lipid that has been shown to exert a positive allosteric effect on β_2 adrenergic receptor, a homologous class A GPCR,[42] stabilizing the active conformation of the receptor by forming electrostatic interactions with intracellular positively charged residues.[43,61] In particular, this involves interactions with ICL3, which plays a critical role in spontaneous GPCR activation.[88] For example, inward conformations of ICL3 have been reported to inactivate β_2 adrenergic receptor by favoring an inward conformation of TM6 and hindering G protein binding,[79,89] while outward conformations of ICL3 may provide an outward pull of TM6 that assists receptor activation, apparently favored by a DOPG membrane.[42,43] Interestingly, DOPG phospholipids do not seem to have an effect on the CB1 activation pathway itself, but rather on speed and consistency of receptor activation as well as agonist stability, especially in terms of protein–ligand interactions with TM7. Since only partial effects of DOPG were observed in the apoprotein state receptor, this suggests the presence of a cooperative allosteric interaction between DOPG and the agonist, in this case mediated through intracellular regions of TM5, TM6, and ICL3 of the receptor. This is consistent with a previous study[79] that showed how an expanded/narrowed orthosteric binding site hindered/facilitated an outward orientation of ICL3 in β_2 adrenergic receptor.

Residues involved in CB1-phospholipid allosteric modulation include positively charged residues in ICL3, as well as Arg336$^{6.28}$ and the semiconserved residue Arg340$^{6.32}$ at the intracellular end of TM6. In other class A GPCRs, even more positively charged residues are located at this region (Arg/Lys$^{6.29}$, Arg/Lys$^{6.31}$, and Lys$^{6.32}$ in 5-HT$_{1B}$ receptor,[90] muscarinic M$_{1-4}$ receptors,[22,23,91] β_2 adrenergic receptor,[17−19] and dopamine D$_{2-4}$ receptors;[92−94] Lys$^{6.28}$, Lys$^{6.29}$, Arg$^{6.30}$, His$^{6.31}$, and Arg$^{6.32}$ in chemokine receptors CCR2 and CCR5;[95,96] Arg/Lys$^{6.24}$, Lys$^{6.26}$, Arg$^{6.28}$, Arg$^{6.31}$, and Arg$^{6.32}$ in δ-, κ-, and μ-opioid receptors[97−101]). This suggests that negatively charged phospholipids may act as

DOI: 10.1021/acs.jmedchem.9b00612
J. Med. Chem. 2019, 62, 5638−5654

positive allosteric modulators of a broad range of class A GPCRs, likely with different sensitivity in a receptor-dependent manner.

Our study provides valuable knowledge regarding the mode of action of cannabinoid agonists in CB1. We expect that similar microswitches would also be present in other homologous GPCRs, especially those with conserved sequence motifs. This could be particularly useful for the design of novel cannabinoid agonists and for studying the mechanism of activation of GPCRs that have not yet been crystallized in an active state. For example, the residue pair Trp$^{6.48}$−Phe/Tyr$^{3.36}$ is present in chemokine receptors, as well as the Pro$^{5.50}$-Ile$^{3.43}$-Phe/Tyr$^{6.44}$ motif that is not conserved in cannabinoid receptors. Interestingly, allosteric modulation by net negatively charged phospholipids like DOPG does not seem to be β_2 adrenergic receptor-specific, and they may be positive allosteric modulators of a broad range of GPCRs, including CB1. Thus, the phospholipid composition of the membrane may be an important factor in GPCR activation in different cell types.

■ EXPERIMENTAL SECTION

Crystal Structure Preparation and Ligand Docking. To date, two human inactive CB1 receptor crystal structures are available, with PDB entries 5TGZ[47] and 5U09.[48] The crystal structure with the PDB entry 5U09 was selected for its higher resolution (2.6 Å), lower number of mutations, and the presence of two co-crystallized water molecules inside the protein core. The non-native fusion protein (glycogen synthase) from the GPCR structure was removed, the Thr210$^{3.46}$Ala mutation was restored to wild type (WT), and the missing regions of TM5, TM6, and ICL3 were modeled ab initio using MODELLER v9.14[102] to obtain a WT receptor structure. As part of this process, the end of TM5 was extended until Arg311$^{5.75}$ and the beginning of TM6 was extended until Pro332$^{6.24}$ according to the secondary structure prediction tools PSIPRED[103] and JPRED.[104] The obtained structure was energy-minimized using CHIMERA v1.11.2 software[105] in the AMBER14SB force field,[106] to improve contacts within modeled regions. Then, CB1 agonist CP-55940 was docked into this inactive structure, as well as into the agonist-bound crystal structure of CB1 (PDB entry 5XR8). For this purpose, respective co-crystallized ligands were first removed and CP-55940 was docked using AUTODOCK4.2.[68] Atomic coordinates for CP-55940 were obtained from the PubChem database (CID 104895). The highest scoring conformation that best fulfilled requirements described in the literature: formation of a hydrogen bond between the A-ring hydroxyl group of CP-55940 and Ser383$^{7.39}$,[45,49,69] aromatic interaction between the A-ring of CP-55940 and Phe268^{ECL2},[45,49] and orientation of the hydrophobic alkyl chain of CP-55940 toward TM5,[49] was selected. To further validate CP-55940-mediated receptor conformational changes, agonist AM-11542 was positioned into the inactive CB1 crystal structure with coordinates extracted from the agonist-bound crystal structure (PDB entry 5XRA)[49] by superimposing the transmembrane domains of both receptor structures.

Molecular Dynamics (MD) Simulations Setup. After a second short energy minimization to refine protein−ligand interactions as described above, MD simulation systems of the inactive receptor were built using CHARMM-GUI.[107] The disulfide bridge between Cys257^{ECL2} and Cys264^{ECL2} of the receptor was maintained,[108] and three residue side chains: Asp163$^{2.50}$, Asp213$^{3.49}$, and Asp338$^{6.30}$ were protonated to favor GPCR activation according to mutational data from CB1[29] and MD simulations of other homologous GPCRs.[54,78,109,110] Additionally, His302$^{5.66}$, His304$^{5.68}$, His320^{ICL3}, Glu323^{ICL3}, Asp324^{ICL3}, and Asp333$^{6.25}$, which are all located in intracellular regions of the receptor, were protonated to potentially assist interactions of ICL3 with the membrane, consistent with a previous study of β_2 adrenergic receptor.[43] Simulations at the expected protonation state of all residues at pH 7.0 as predicted by PROPKA[111,112] were also analyzed in POPC membranes. The receptor was oriented according to the Orientations of Proteins in Membranes (OPM) database[113] and embedded in 80 × 80 Å^2 homogeneous membranes composed of POPC in the AM-11542−CB1 complex, and POPC or DOPG[42,43] for the CP-55940−CB1 complex. All systems were solvated with TIP3P water molecules above and below the membrane, and a 0.3 M concentration of K^+ and Cl^- ions was used to neutralize system charge. K^+ ions were used instead of Na^+ to avoid sodium-mediated negative allosteric modulation.[84] Systems without agonist (apoprotein state) were also analyzed for control purposes.

All MD simulations were performed in the CHARMM36 force field[114] using ACEMD software[115] (simulation conditions: 300 K and 1 atm). Agonists were parametrized with the CHARMM General Force Field[116] using ParamChem service.[117,118] During equilibration, the protein and ligand were initially restrained, with these restraints progressively released over the first 8 ns, followed by a further 20 ns without restraints. Then, the systems were simulated (production run without restraints) for 2 μs. Three replicas were performed for each CP-55940−CB1 complex and apo receptor at the selected protonation state, two replicas were performed for the AM-11542 complex at the selected protonation state, and two replicas were performed for the CP-55940−CB1 complex at the expected protonation state at pH 7.0, constituting a total simulation time of 32 μs.

MD simulation trajectories were analyzed with Visual Molecular Dynamics 1.9.3 software and associated plugins.[119] Receptor conformational change was measured by calculating the root-mean-square deviation (RMSD) of Cα atoms of TM helices to the inactive CB1 crystal structure,[48] RMSD of Cα atoms of TM6 alone, distance of the "ionic lock" formed between Asp338$^{6.30}$ and Arg214$^{3.50}$ (measured between their Cα atoms), distance between Tyr294$^{5.58}$ and Tyr397$^{7.53}$ (measured between oxygen atoms of respective side chains), and χ_1 dihedral angles of Trp356$^{6.48}$ and Phe200$^{3.36}$. The upward movement of TM3 was measured as the distance offset in the Z axis (perpendicular to the membrane) from the center of mass of TM3 to the center of mass of other TM helices of the receptor and TM3−TM7 distance was measured between their centers of mass. The stability of the ligand was assessed by calculating its RMSD (with respect to initial docked position and excluding hydrogen atoms) and by measuring the distance of hydrogen bonds that the A-ring ligand hydroxyl group formed with the side-chain oxygen atom of Ser383$^{7.39}$ and, in the case of CP-55940, the hydrogen bonds that the C-ring hydroxyl groups formed with water molecules and with the backbone oxygen atoms of Ile267^{ECL2} and Ala380$^{7.36}$. The occupancy of hydrogen bonds was calculated as the fraction of simulation time where the oxygen atoms involved were within 3.5 Å of one another and the angle of the hydrogen bond was from 120 to 180°. Additionally, CP-55940 conformations were grouped into clusters using Clustering Tool plugin with a 2.0 Å RMSD cutoff. The interaction between membrane phospholipid(s) and ICL3 was measured in terms of the distance between the center of mass of His320^{ICL3}, a positively charged residue located at the center of ICL3, and the phosphorus atom of the closest lipid. Additionally, outward/inward orientations of ICL3 were assessed by calculating the offset in XY coordinates (plane of the membrane) of the center of mass of ICL3 with respect to the center of mass of receptor TM helices. Nonbonded energies of interaction between residue side chains were estimated using NAMD Energy plugin.[120] Water density maps were created using VolMap plugin by calculating the weighted atomic density of water molecules averaged over the total MD trajectory. In simulations where a phospholipid molecule bound to Arg214$^{3.50}$, only the first 1 μs of simulation was considered.

Protein−Protein Docking. In those MD simulations where characteristic features of receptor activation were collectively observed (see Introduction section), 10 conformations were selected for G_i protein−protein docking according to the highest ionic lock distance, the lowest Tyr294$^{5.58}$−Tyr397$^{7.53}$ distance, and the lowest TM6 RMSD to the G protein-bound active crystal structure of CB1 (PDB entry 6N4B). These MD-generated conformations were initially superimposed against the active crystal structure of CB1 according to their TM domains. Then, using CHIMERA software,[105] the co-crystallized α-subunit of the G_i protein from the active CB1 crystal structure was translated 5 Å in the Z axis away from the receptor (creating a clear gap between proteins) before performing protein−protein docking using

DOI: 10.1021/acs.jmedchem.9b00612
J. Med. Chem. 2019, 62, 5638−5654

the ROSIE web server.[121] ICL3 of MD-generated receptor conformations was removed to avoid clashes with G_i protein since protein−protein docking is performed with a rigid backbone. Docking solutions were evaluated by calculating the RMSD of Cα atoms of the G_i α5 helix to the original fully active CB1 crystal structure and by the interface docking score (I_sc) provided by ROSIE (0.0 to −10.0), where more negative values represent better interaction.

■ ASSOCIATED CONTENT

Supporting Information

The Supporting Information is available free of charge on the ACS Publications website at DOI: 10.1021/acs.jmedchem.9b00612.

Docking poses of CP-55940 in the inactive and in the agonist-bound crystal structures; two-dimensional ligand−receptor interaction diagrams of CP-55940 docking solutions and major clusters; MD snapshots of water molecules in the orthosteric site of CP-55940-bound and apo CB1; supplementary figures of Ile267^{ECL2} analysis, analysis of MD simulations with bound AM-11542 agonist, MD analysis of CP-55940-bound CB1 MD simulations at expected protonation state at pH 7.0, detailed ICL3−DOPG interactions, and analysis of apoprotein state receptors; and tabulated data for CB1-G_i protein−protein docking (Figures S1−S10 and Table S1) (PDF)

Molecular formula strings for CP-55940 and AM-11542 (CSV)

■ AUTHOR INFORMATION

Corresponding Authors

*E-mail: James.Dalton@uab.es (J.A.R.D.).
*E-mail: Jesus.Giraldo@uab.es. Phone: +34 93 581 3813 (J.G.).

ORCID

Jesús Giraldo: 0000-0001-7082-4695

Author Contributions

O.D. performed the MD simulations, analyzed results, and wrote the manuscript. J.A.R.D. supervised results and analyses and wrote the manuscript. J.G. supervised the whole study.

Notes

The authors declare no competing financial interest.

■ ACKNOWLEDGMENTS

This study was supported in part by Ministerio de Economía y Competitividad (SAF2014-58396-R) and Ministerio de Ciencia, Innovación y Universidades (SAF2017-87199-R), Spain.

■ ABBREVIATIONS

CB1, cannabinoid receptor 1; TM, transmembrane domain; ECL, extracellular loop; ICL, intracellular loop; PDB, Protein Data Bank; RMSD, root-mean-square deviation; MD, molecular dynamics; NMR, nuclear magnetic resonance

■ REFERENCES

(1) Mechoulam, R.; Parker, L. A. The Endocannabinoid System and the Brain. *Annu. Rev. Psychol.* **2013**, *64*, 21−47.
(2) Reggio, P. H. Endocannabinoid Binding to the Cannabinoid Receptors: What Is Known and What Remains Unknown. *Curr. Med. Chem.* **2010**, *17*, 1468−1486.
(3) Kendall, D. A.; Yudowski, G. A. Cannabinoid Receptors in the Central Nervous System: Their Signaling and Roles in Disease. *Front. Cell. Neurosci.* **2017**, *10*, No. 294.
(4) Martín-Couce, L.; Martín-Fontecha, M.; Palomares, Ó.; Mestre, L.; Cordomí, A.; Hernangomez, M.; Palma, S.; Pardo, L.; Guaza, C.; López-Rodríguez, M. L.; Ortega-Gutiérrez, S. Chemical Probes for the Recognition of Cannabinoid Receptors in Native Systems. *Angew. Chem., Int. Ed.* **2012**, *51*, 6896−6899.
(5) Houston, D. B.; Howlett, A. C. Differential Receptor-G-Protein Coupling Evoked by Dissimilar Cannabinoid Receptor Agonists. *Cell. Signal.* **1998**, *10*, 667−674.
(6) Howlett, A. C. International Union of Pharmacology. XXVII. Classification of Cannabinoid Receptors. *Pharmacol. Rev.* **2002**, *54*, 161−202.
(7) Howlett, A. C.; Blume, L. C.; Dalton, G. D. CB(1) Cannabinoid Receptors and Their Associated Proteins. *Curr. Med. Chem.* **2010**, *17*, 1382−1393.
(8) Thakur, Ga.; Tichkule, R.; Bajaj, S.; Makriyannis, A. Latest Advances in Cannabinoid Receptor Agonists. *Expert Opin. Ther. Pat.* **2009**, *19*, 1647−1673.
(9) Pertwee, R. G. Pharmacological Actions of Cannabinoids. In *Cannabinoids*; Pertwee, R. G., Ed.; Handbook of Experimental Pharmacology; Springer, 2005; Vol. *168*, pp 1−51.
(10) Janero, D. R.; Makriyannis, A. Cannabinoid Receptor Antagonists: Pharmacological Opportunities, Clinical Experience, and Translational Prognosis. *Expert Opin. Emerging Drugs* **2009**, *14*, 43−65.
(11) Blaazer, A. R.; Lange, J. H. M.; Van Der Neut, M. A. W.; Mulder, A.; Den Boon, F. S.; Werkman, T. R.; Kruse, C. G.; Wadman, W. J. Novel Indole and Azaindole (Pyrrolopyridine) Cannabinoid (CB) Receptor Agonists: Design, Synthesis, Structure-Activity Relationships, Physicochemical Properties and Biological Activity. *Eur. J. Med. Chem.* **2011**, *46*, 5086−5098.
(12) Seltzman, H. H.; Shiner, C.; Hirt, E. E.; Gilliam, A. F.; Thomas, B. F.; Maitra, R.; Snyder, R.; Black, S. L.; Patel, P. R.; Mulpuri, Y.; Spigelman, I. Peripherally Selective Cannabinoid 1 Receptor (CB1R) Agonists for the Treatment of Neuropathic Pain. *J. Med. Chem.* **2016**, *59*, 7525−7543.
(13) Di Marzo, V.; Stella, N.; Andreas, Z. Endocannabinoid Signalling and the Deteriorating Brain. *Nat. Rev. Neurosci.* **2015**, *16*, 30−42.
(14) Lee, Y.; Basith, S.; Choi, S. Recent Advances in Structure-Based Drug Design Targeting Class A G Protein-Coupled Receptors Utilizing Crystal Structures and Computational Simulations. *J. Med. Chem.* **2018**, *61*, 1−46.
(15) Palczewski, K.; Kumasaka, T.; Hori, T.; Behnke, C. A.; Motoshima, H.; Fox, B. A.; Trong, I. L.; Teller, D. C.; Okada, T.; Stenkamp, R. E.; Yamamoto, M.; Miyano, M. Crystal Structure of Rhodopsin: A G Protein − Coupled Receptor. *Science* **2000**, *289*, 739−745.
(16) Scheerer, P.; Park, J. H.; Hildebrand, P. W.; Kim, Y. J.; Krauß, N.; Choe, H. W.; Hofmann, K. P.; Ernst, O. P. Crystal Structure of Opsin in Its G-Protein-Interacting Conformation. *Nature* **2008**, *455*, 497−502.
(17) Cherezov, V.; Rosenbaum, D. M.; Hanson, M. A.; Rasmussen, S. G. F.; Thian, F. S.; Kobilka, T. S.; Choi, H.-J.; Kuhn, P.; Weis, W. I.; Kobilka, B. K.; Stevens, R. C. High-Resolution Crystal Structure of an Engineered Human 2-Adrenergic G Protein-Coupled Receptor. *Science* **2007**, *318*, 1258−1265.
(18) Rasmussen, S. G. F.; Choi, H.-J.; Fung, J. J.; Pardon, E.; Casarosa, P.; Chae, P. S.; DeVree, B. T.; Rosenbaum, D. M.; Thian, F. S.; Kobilka, T. S.; Schnapp, A.; Konetzki, I.; Sunahara, R. K.; Gellman, S. H.; Pautsch, A.; Steyaert, J.; Weis, W. I.; Kobilka, B. K. Structure of a Nanobody-Stabilized Active State of the β2 Adrenoceptor. *Nature* **2011**, *469*, 175−180.
(19) Rasmussen, S. G. F.; Devree, B. T.; Zou, Y.; Kruse, A. C.; Chung, K. Y.; Kobilka, T. S.; Thian, F. S.; Chae, P. S.; Pardon, E.; Calinski, D.; Mathiesen, J. M.; Shah, S. T. A.; Lyons, J. A.; Caffrey, M.; Gellman, S. H.; Steyaert, J.; Skiniotis, G.; Weis, W. I.; Sunahara, R. K.; Kobilka, B. K. Crystal Structure of the β2adrenergic Receptor-Gs Protein Complex. *Nature* **2011**, *477*, 549−557.
(20) Jaakola, V.-P.; Griffith, M. T.; Hanson, M. A.; Cherezov, V.; Chien, E. Y. T.; Lane, J. R.; Ijzerman, A. P.; Stevens, R. C. The 2.6 Angstrom Crystal Structure of a Human A2A Adenosine Receptor Bound to an Antagonist. *Science* **2008**, *322*, 1211−1217.

DOI: 10.1021/acs.jmedchem.9b00612
J. Med. Chem. 2019, 62, 5638−5654

(21) Carpenter, B.; Nehmé, R.; Warne, T.; Leslie, A. G. W.; Tate, C. G. Structure of the Adenosine A 2A Receptor Bound to an Engineered G Protein. *Nature* **2016**, *536*, 104−107.
(22) Haga, K.; Kruse, A. C.; Asada, H.; Yurugi-Kobayashi, T.; Shiroishi, M.; Zhang, C.; Weis, W. I.; Okada, T.; Kobilka, B. K.; Haga, T.; Kobayashi, T. Structure of the Human M2 Muscarinic Acetylcholine Receptor Bound to an Antagonist. *Nature* **2012**, *482*, 547−551.
(23) Kruse, A. C.; Ring, A. M.; Manglik, A.; Hu, J.; Hu, K.; Eitel, K.; Hübner, H.; Pardon, E.; Valant, C.; Sexton, P. M.; Christopoulos, A.; Felder, C. C.; Gmeiner, P.; Steyaert, J.; Weis, W. I.; Garcia, K. C.; Wess, J.; Kobilka, B. K. Activation and Allosteric Modulation of a Muscarinic Acetylcholine Receptor. *Nature* **2013**, *504*, 101−106.
(24) Choe, H.-W.; Park, J. H.; Kim, Y. J.; Ernst, O. P. Transmembrane Signaling by GPCRs: Insight from Rhodopsin and Opsin Structures. *Neuropharmacology* **2011**, *60*, 52−57.
(25) Ballesteros, J. A.; Weinstein, H. Integrated Methods for the Construction of Three-Dimensional Models and Computational Probing of Structure-Function Relations in G Protein-Coupled Receptors. *Methods Neurosci.* **1995**, *25*, 366−428.
(26) Katritch, V.; Cherezov, V.; Stevens, R. C. Structure-Function of the G-Protein-Coupled Receptor Superfamily. *Annu. Rev. Pharmacol. Toxicol.* **2013**, *53*, 531−556.
(27) Dalton, J. A. R.; Lans, I.; Giraldo, J. Quantifying Conformational Changes in GPCRs: Glimpse of a Common Functional Mechanism. *BMC Bioinf.* **2015**, *16*, 124.
(28) Tehan, B. G.; Bortolato, A.; Blaney, F. E.; Weir, M. P.; Mason, J. S. Unifying Family A GPCR Theories of Activation. *Pharmacol. Ther.* **2014**, *143*, 51−60.
(29) Scott, C. E.; Abrol, R.; Ahn, K. H.; Kendall, D. A.; Goddard, W. A. Molecular Basis for Dramatic Changes in Cannabinoid CB1 G Protein-Coupled Receptor Activation upon Single and Double Point Mutations. *Protein Sci.* **2013**, *22*, 101−113.
(30) McAllister, S. D.; Hurst, D. P.; Barnett-Norris, J.; Lynch, D.; Reggio, P. H.; Abood, M. E. Structural Mimicry in Class A G Protein-Coupled Receptor Rotamer Toggle Switches: The Importance of the F3.36(201)/W6.48(357) Interaction in Cannabinoid CB1 Receptor Activation. *J. Biol. Chem.* **2004**, *279*, 48024−48037.
(31) Glukhova, A.; Thal, D. M.; Nguyen, A. T.; Vecchio, E. A.; Jörg, M.; Scammells, P. J.; May, L. T.; Sexton, P. M.; Christopoulos, A. Structure of the Adenosine A1Receptor Reveals the Basis for Subtype Selectivity. *Cell* **2017**, *168*, 867−877.
(32) Laprairie, R. B.; Kulkarni, A. R.; Kulkarni, P. M.; Hurst, D. P.; Lynch, D.; Reggio, P. H.; Janero, D. R.; Pertwee, R. G.; Stevenson, L. A.; Kelly, M. E. M.; Denovan-Wright, E. M.; Thakur, G. A. Mapping Cannabinoid 1 Receptor Allosteric Site(s): Critical Molecular Determinant and Signaling Profile of GAT100, a Novel, Potent, and Irreversibly Binding Probe. *ACS Chem. Neurosci.* **2016**, *7*, 776−798.
(33) Immadi, S. S.; Dopart, R.; Wu, Z.; Fu, B.; Kendall, D. A.; Lu, D. Exploring 6-Azaindole and 7-Azaindole Rings for Developing Cannabinoid Receptor 1 Allosteric Modulators. *Cannabis Cannabinoid Res.* **2018**, *3*, 252−258.
(34) Bari, M.; Paradisi, A.; Pasquariello, N.; Maccarrone, M. Cholesterol-Dependent Modulation of Type 1 Cannabinoid Receptors in Nerve Cells. *J. Neurosci. Res.* **2005**, *81*, 275−283.
(35) Bari, M.; Battista, N.; Fezza, F.; Finazzi-Agrò, A.; Maccarrone, M. Lipid Rafts Control Signaling of Type-1 Cannabinoid Receptors in Neuronal Cells. *J. Biol. Chem.* **2005**, *280*, 12212−12220.
(36) Maccarrone, M.; Bernardi, G.; Agrò, A. F.; Centonze, D. Cannabinoid Receptor Signalling in Neurodegenerative Diseases: A Potential Role for Membrane Fluidity Disturbance. *Br. J. Pharmacol.* **2011**, *163*, 1379−1390.
(37) Stornaiuolo, M.; Bruno, A.; Botta, L.; Regina, G. L.; Cosconati, S.; Silvestri, R.; Marinelli, L.; Novellino, E. Endogenous vs Exogenous Allosteric Modulators in GPCRs: A Dispute for Shuttling CB1 among Different Membrane Microenvironments. *Sci. Rep.* **2015**, *5*, No. 15453.
(38) Oddi, S.; Dainese, E.; Fezza, F.; Lanuti, M.; Barcaroli, D.; De Laurenzi, V.; Centonze, D.; Maccarrone, M. Functional Characterization of Putative Cholesterol Binding Sequence (CRAC) in Human Type-1 Cannabinoid Receptor. *J. Neurochem.* **2011**, *116*, 858−865.
(39) McGraw, C.; Yang, L.; Levental, I.; Lyman, E.; Robinson, A. S. Membrane Cholesterol Depletion Reduces Downstream Signaling Activity of the Adenosine A2A Receptor. *Biochim. Biophys. Acta, Biomembr.* **2019**, *1861*, 760−767.
(40) Nguyen, D. H.; Taub, D. D. Inhibition of Chemokine Receptor Function by Membrane Cholesterol Oxidation. *Exp. Cell Res.* **2003**, *291*, 36−45.
(41) Hanson, M. A.; Cherezov, V.; Griffith, M. T.; Roth, C. B.; Jaakola, V. P.; Chien, E. Y. T.; Velasquez, J.; Kuhn, P.; Stevens, R. C. A Specific Cholesterol Binding Site Is Established by the 2.8 Å Structure of the Human β2-Adrenergic Receptor. *Structure* **2008**, *16*, 897−905.
(42) Dawaliby, R.; Trubbia, C.; Delporte, C.; Masureel, M.; Van Antwerpen, P.; Kobilka, B. K.; Govaerts, C. Allosteric Regulation of G Protein−coupled Receptor Activity by Phospholipids. *Nat. Chem. Biol.* **2016**, *12*, 35−39.
(43) Bruzzese, A.; Gil, C.; Dalton, J. A. R.; Giraldo, J. Structural Insights into Positive and Negative Allosteric Regulation of a G Protein-Coupled Receptor through Protein-Lipid Interactions. *Sci. Rep.* **2018**, *8*, No. 4456.
(44) Durdagi, S.; Papadopoulos, M. G.; Zoumpoulakis, P. G.; Koukoulitsa, C.; Mavromoustakos, T. A Computational Study on Cannabinoid Receptors and Potent Bioactive Cannabinoid Ligands: Homology Modeling, Docking, de Novo Drug Design and Molecular Dynamics Analysis. *Mol. Diversity* **2010**, *14*, 257−276.
(45) Shim, J. Y.; Bertalovitz, A. C.; Kendall, D. A. Identification of Essential Cannabinoid-Binding Domains: Structural Insights into Early Dynamic Events in Receptor Activation. *J. Biol. Chem.* **2011**, *286*, 33422−33435.
(46) Shim, J. Y.; Padgett, L. Functional Residues Essential for the Activation of the CB1 Cannabinoid Receptor. *Methods in Enzymology*; Elsevier Inc., 2013; Vol. *520*, pp 337−355.
(47) Hua, T.; Vemuri, K.; Pu, M.; Qu, L.; Han, G. W.; Wu, Y.; Zhao, S.; Shui, W.; Li, S.; Korde, A.; Laprairie, R. B.; Stahl, E. L.; Ho, J. H.; Zvonok, N.; Zhou, H.; Kufareva, I.; Wu, B.; Zhao, Q.; Hanson, M. A.; Bohn, L. M.; Makriyannis, A.; Stevens, R. C.; Liu, Z. J. Crystal Structure of the Human Cannabinoid Receptor CB1. *Cell* **2016**, *167*, 750−762.
(48) Shao, Z.; Yin, J.; Chapman, K.; Grzemska, M.; Clark, L.; Wang, J.; Rosenbaum, D. M. High-Resolution Crystal Structure of the Human CB1 Cannabinoid Receptor. *Nature* **2016**, *540*, 602−606.
(49) Hua, T.; Vemuri, K.; Nikas, S. P.; Laprairie, R. B.; Wu, Y.; Qu, L.; Pu, M.; Korde, A.; Jiang, S.; Ho, J.-H.; Han, G. W.; Ding, K.; Li, X.; Liu, H.; Hanson, M. A.; Zhao, S.; Bohn, L. M.; Makriyannis, A.; Stevens, R. C.; Liu, Z.-J. Crystal Structures of Agonist-Bound Human Cannabinoid Receptor CB1. *Nature* **2017**, *547*, 468−471.
(50) Krishna Kumar, K.; Shalev-Benami, M.; Robertson, M. J.; Hu, H.; Banister, S. D.; Hollingsworth, S. A.; Latorraca, N. R.; Kato, H. E.; Hilger, D.; Maeda, S.; Weis, W. I.; Farrens, D. L.; Dror, R. O.; Malhotra, S. V.; Kobilka, B. K.; Skiniotis, G. Structure of a Signaling Cannabinoid Receptor 1-G Protein Complex. *Cell* **2019**, *176*, No. 448.e12.
(51) Klepeis, J. L.; Lindorff-Larsen, K.; Dror, R. O.; Shaw, D. E. Long-Timescale Molecular Dynamics Simulations of Protein Structure and Function. *Curr. Opin. Struct. Biol.* **2009**, *19*, 120−127.
(52) Dror, R. O.; Pan, A. C.; Arlow, D. H.; Borhani, D. W.; Maragakis, P.; Shan, Y.; Xu, H.; Shaw, D. E. Pathway and Mechanism of Drug Binding to G-Protein-Coupled Receptors. *Proc. Natl. Acad. Sci. U.S.A.* **2011**, *108*, 13118−13123.
(53) Plazinska, A.; Plazinski, W.; Jozwiak, K. Agonist Binding by the β2-Adrenergic Receptor: An Effect of Receptor Conformation on Ligand Association−dissociation Characteristics. *Eur. Biophys. J.* **2015**, *44*, 149−163.
(54) Dror, R. O.; Arlow, D. H.; Maragakis, P.; Mildorf, T. J.; Pan, A. C.; Xu, H.; Borhani, D. W.; Shaw, D. E. Activation Mechanism of the β(2)-Adrenergic Receptor. *Proc. Natl. Acad. Sci. U.S.A.* **2011**, *108*, 18684−18689.
(55) Li, J.; Jonsson, A. L.; Beuming, T.; Shelley, J. C.; Voth, G. A. Ligand-Dependent Activation and Deactivation of the Human Adenosine A 2A Receptor. *J. Am. Chem. Soc.* **2013**, *135*, 8749−8759.
(56) Troupiotis-Tsaïlaki, A.; Zachmann, J.; González-Gil, I.; Gonzalez, A.; Ortega-Gutiérrez, S.; López-Rodríguez, M. L.; Pardo,

DOI: 10.1021/acs.jmedchem.9b00612
J. Med. Chem. 2019, 62, 5638−5654

L.; Govaerts, C. Ligand Chain Length Drives Activation of Lipid G Protein-Coupled Receptors. *Sci. Rep.* **2017**, *7*, No. 2020.
(57) Dror, R. O.; Green, H. F.; Valant, C.; Borhani, D. W.; Valcourt, J. R.; Pan, A. C.; Arlow, D. H.; Canals, M.; Lane, J. R.; Rahmani, R.; Baell, J. B.; Sexton, P. M.; Christopoulos, A.; Shaw, D. E. Structural Basis for Modulation of a G-Protein-Coupled Receptor by Allosteric Drugs. *Nature* **2013**, *503*, 295−299.
(58) Fu, T.; Zheng, G.; Tu, G.; Yang, F.; Chen, Y.; Yao, X.; Li, X.; Xue, W.; Zhu, F. Exploring the Binding Mechanism of Metabotropic Glutamate Receptor 5 Negative Allosteric Modulators in Clinical Trials by Molecular Dynamics Simulations. *ACS Chem. Neurosci.* **2018**, *9*, 1492−1502.
(59) Miao, Y.; Nichols, S.; Gasper, P.; Metger, V.; McCammon, J. Activation and Dynamic Network of the M2 Muscarinic Receptor. *Proc. Natl. Acad. Sci. U.S.A.* **2013**, *110*, 10982−10987.
(60) Caliman, A. D.; Miao, Y.; McCammon, J. A. Activation Mechanisms of the First Sphingosine-1-Phosphate Receptor. *Protein Sci.* **2017**, *26*, 1150−1160.
(61) Neale, C.; Herce, H. D.; Pomès, R.; García, A. E. Can Specific Protein-Lipid Interactions Stabilize an Active State of the Beta 2 Adrenergic Receptor? *Biophys. J.* **2015**, *109*, 1652−1662.
(62) Rosenbaum, D. M.; Zhang, C.; Lyons, J. A.; Holl, R.; Aragao, D.; Arlow, D. H.; Rasmussen, S. G. F.; Choi, H.-J.; DeVree, B. T.; Sunahara, R. K.; Chae, P. S.; Gellman, S. H.; Dror, R. O.; Shaw, D. E.; Weis, W. I.; Caffrey, M.; Gmeiner, P.; Kobilka, B. K. Structure and Function of an Irreversible Agonist-β2 Adrenoceptor Complex. *Nature* **2011**, *469*, 236−240.
(63) Felder, C. C.; Joyce, K. E.; Briley, E. M.; Mansouri, J.; Mackie, K.; Blond, O.; Lai, Y.; Ma, A. L.; Mitchell, R. L. Comparison of the Pharmacology and Signal Transduction of the Human Cannabinoid CB1 and CB2 Receptors. *Mol. Pharmacol.* **1995**, *48*, 443−450.
(64) Song, Z. H.; Bonner, T. I. A Lysine Residue of the Cannabinoid Receptor Is Critical for Receptor Recognition by Several Agonists but Not WIN55212-2. *Mol. Pharmacol.* **1996**, *49*, 891−896.
(65) Song, Z. H.; Slowey, C. A.; Hurst, D. P.; Reggio, P. H. The Difference between the CB(1) and CB(2) Cannabinoid Receptors at Position 5.46 Is Crucial for the Selectivity of WIN55212-2 for CB(2). *Mol. Pharmacol.* **1999**, *56*, 834−840.
(66) Hillard, C. J.; Manna, S.; Greenberg, M. J.; DiCamelli, R.; Ross, R. A.; Stevenson, L. A.; Murphy, V.; Pertwee, R. G.; Campbell, W. B. Synthesis and Characterization of Potent and Selective Agonists of the Neuronal Cannabinoid Receptor (CB1). *J. Pharmacol. Exp. Ther.* **1999**, *289*, 1427−1433.
(67) Xie, X. Q.; Melvin, L. S.; Makriyannis, A. The Conformational Properties of the Highly Selective Cannabinoid Receptor Ligand CP-55,940. *J. Biol. Chem.* **1996**, *271*, 10640−10647.
(68) Morris, G. M.; Huey, R.; Lindstrom, W.; Sanner, M. F.; Belew, R. K.; Goodsell, D. S.; Olson, A. J. AutoDock4 and AutoDockTools4: Automated Docking with Selective Receptor Flexibility. *J. Comput. Chem.* **2009**, *30*, 2785−2791.
(69) Kapur, A.; Hurst, D. P.; Fleischer, D.; Whitnell, R.; Thakur, G. A.; Makriyannis, A.; Reggio, P. H.; Abood, M. E. Mutation Studies on Ser7.39 and Ser2.60 in the Human CB1 Receptor: Evidence for a Serine-Induced Bend in CB1 Transmembrane Helix 7. *Mol. Pharmacol.* **2007**, *71*, 1512−1524.
(70) Ahn, K. H.; Bertalovitz, A. C.; Mierke, D. F.; Kendall, D. A. Dual Role of the Second Extracellular Loop of the Cannabinoid Receptor 1: Ligand Binding and Receptor Localization. *Mol. Pharmacol.* **2009**, *76*, 833−842.
(71) Murphy, J. W.; Kendall, D. A. Integrity of Extracellular Loop 1 of the Human Cannabinoid Receptor 1 Is Critical for High-Affinity Binding of the Ligand CP 55,940 but Not SR 141716A. *Biochem. Pharmacol.* **2003**, *65*, 1623−1631.
(72) Shen, C. P.; Xiao, J. C.; Armstrong, H.; Hagmann, W.; Fong, T. M. F200A Substitution in the Third Transmembrane Helix of Human Cannabinoid CB1 Receptor Converts AM2233 from Receptor Agonist to Inverse Agonist. *Eur. J. Pharmacol.* **2006**, *531*, 41−46.
(73) Shim, J.-Y.; Howlett, A. C. Steric Trigger as a Mechanism for CB1 Cannabinoid Receptor Activation. *J. Chem. Inf. Comput. Sci.* **2004**, *44*, 1466−1476.
(74) Vilardaga, J. P.; Bünemann, M.; Krasell, C.; Castro, M.; Lohse, M. J. Measurement of the Millisecond Activation Switch of G Protein-Coupled Receptors in Living Cells. *Nat. Biotechnol.* **2003**, *21*, 807−812.
(75) Mato, S.; Pazos, A.; Valdizán, E. M. Cannabinoid Receptor Antagonism and Inverse Agonism in Response to SR141716A on cAMP Production in Human and Rat Brain. *Eur. J. Pharmacol.* **2002**, *443*, 43−46.
(76) Greasley, P. J. Mutagenesis and Modelling of the Alpha 1b-Adrenergic Receptor Highlight the Role of the Helix 3/Helix 6 Interface in Receptor Activation. *Mol. Pharmacol.* **2002**, *61*, 1025−1032.
(77) Barnett-Norris, J.; Hurst, D. P.; Buehner, K.; Ballesteros, J. A.; Guarnieri, F.; Reggio, P. H. Agonist Alkyl Tail Interaction with Cannabinoid CB1 Receptor V6.43/I6.46 Groove Induces a Helix 6 Active Conformation. *Int. J. Quantum Chem.* **2002**, *88*, 76−86.
(78) Lans, I.; Dalton, J. A. R.; Giraldo, J. Selective Protonation of Acidic Residues Triggers Opsin Activation. *J. Phys. Chem. B* **2015**, *119*, 9510−9519.
(79) Ozgur, C.; Doruker, P.; Akten, E. D. Investigation of Allosteric Coupling in Human β 2-Adrenergic Receptor in the Presence of Intracellular Loop 3. *BMC Struct. Biol.* **2016**, *16*, No. 9.
(80) Filipek, S.; Palczewski, K.; Yuan, S.; Vogel, H. Activation of G Protein-Coupled Receptors Correlates with the Formation of a Continuous Internal Water Pathway. *Nat. Commun.* **2014**, *5*, No. 4733.
(81) Tomobe, K.; Yamamoto, E.; Kholmurodov, K.; Yasuoka, K. Water Permeation through the Internal Water Pathway in Activated GPCR Rhodopsin. *PLoS One* **2017**, *12*, No. e0176876.
(82) Venkatakrishnan, A. J.; Ma, A. K.; Fonseca, R.; Latorraca, N. R.; Kelly, B.; Betz, R. M.; Asawa, C.; Kobilka, B. K.; Dror, R. O. Diverse GPCRs Exhibit Conserved Water Networks for Stabilization and Activation. *Proc. Natl. Acad. Sci.* **2019**, *116*, 3288−3293.
(83) Katritch, V.; Fenalti, G.; Abola, E. E.; Roth, B. L.; Cherezov, V.; Stevens, R. C. Allosteric Sodium in Class A GPCR Signaling. *Trends Biochem. Sci.* **2014**, *39*, 233−244.
(84) Tao, Q.; Abood, M. E. Mutation of a Highly Conserved Aspartate Residue in the Second Transmembrane Domain of the Cannabinoid Receptors, CB1 and CB2, Disrupts G-Protein Coupling. *J. Pharmacol. Exp. Ther.* **1998**, *285*, 651−658.
(85) White, K. L.; Eddy, M. T.; Gao, Z. G.; Han, G. W.; Lian, T.; Deary, A.; Patel, N.; Jacobson, K. A.; Katritch, V.; Stevens, R. C. Structural Connection between Activation Microswitch and Allosteric Sodium Site in GPCR Signaling. *Structure* **2018**, *26*, No. 259.e5.
(86) Weis, W. I.; Sanborn, A. L.; Traynor, J. R.; Dror, R. O.; Manglik, A.; Kling, R. C.; Huang, W.; Granier, S.; Husbands, S. M.; Laeremans, T.; Thorsen, T. S.; Feinberg, E. N.; Kato, H. E.; Gmeiner, P.; Kobilka, B. K.; Livingston, K. E.; Steyaert, J.; Venkatakrishnan, A. J. Structural Insights into M-Opioid Receptor Activation. *Nature* **2015**, *524*, 315−321.
(87) Bow, E. W.; Rimoldi, J. M. The Structure−Function Relationships of Classical Cannabinoids: CB1/CB2 Modulation. *Perspect. Med. Chem.* **2016**, *8*, 17−39.
(88) Chakir, K.; Xiang, Y.; Yang, D.; Zhang, S.-J.; Cheng, H.; Kobilka, B. K.; Xiao, R.-P. The Third Intracellular Loop and the Carboxyl Terminus of b2 - Adrenergic Receptor Confer Spontaneous Activity of the Receptor. *Mol. Pharmacol.* **2003**, *64*, 1048−1058.
(89) Ozcan, O.; Uyar, A.; Doruker, P.; Akten, E. D. Effect of Intracellular Loop 3 on Intrinsic Dynamics of Human β 2-Adrenergic Receptor. *BMC Struct. Biol.* **2013**, *13*, No. 29.
(90) Wang, C.; Jiang, Y.; Ma, J.; Wu, H.; Wacker, D.; Katritch, V.; Han, G. W.; Liu, W.; Huang, X. P.; Vardy, E.; McCorvy, J. D.; Gao, X.; Zhou, X. E.; Melcher, K.; Zhang, C.; Bai, F.; Yang, H.; Yang, L.; Jiang, H.; Roth, B. L.; Cherezov, V.; Stevens, R. C.; Xu, H. E. Structural Basis for Molecular Recognition at Serotonin Receptors. *Science* **2013**, *340*, 610−614.
(91) Thal, D. M.; Sun, B.; Feng, D.; Nawaratne, V.; Leach, K.; Felder, C. C.; Bures, M. G.; Evans, D. A.; Weis, W. I.; Bachhawat, P.; Kobilka, T.

DOI: 10.1021/acs.jmedchem.9b00612
J. Med. Chem. 2019, 62, 5638−5654

S.; Sexton, P. M.; Kobilka, B. K.; Christopoulos, A. Crystal Structures of the M1 and M4 Muscarinic Acetylcholine Receptors. *Nature* **2016**, *531*, 335−340.
(92) Wang, S.; Che, T.; Levit, A.; Shoichet, B. K.; Wacker, D.; Roth, B. L. Structure of the D2 Dopamine Receptor Bound to the Atypical Antipsychotic Drug Risperidone. *Nature* **2018**, *555*, 269−273.
(93) Chien, E. Y. T.; Liu, W.; Zhao, Q.; Katritch, V.; Han, G. W.; Hanson, Ma.; Shi, L.; Newman, A. H.; Javitch, Ja.; Cherezov, V.; Stevens, R. C. Structure of the Human Dopamine D3 Receptor in Complex with a D2/D3 Selective Antagonist. *Science* **2010**, *330*, 1091−1095.
(94) Wang, S.; Wacker, D.; Levit, A.; Che, T.; Betz, R. M.; McCorvy, J. D.; Venkatakrishnan, A. J.; Huang, X.-P.; Dror, R. O.; Shoichet, B. K.; Roth, B. L. D(4) Dopamine Receptor High Resolution Structures Enable the Discovery of Selective Agonists. *Science* **2017**, *358*, 381−386.
(95) Zheng, Y.; Qin, L.; Zacarías, N. V. O.; De Vries, H.; Han, G. W.; Gustavsson, M.; Dabros, M.; Zhao, C.; Cherney, R. J.; Carter, P.; Stamos, D.; Abagyan, R.; Cherezov, V.; Stevens, R. C.; Ijzerman, A. P.; Heitman, L. H.; Tebben, A.; Kufareva, I.; Handel, T. M. Structure of CC Chemokine Receptor 2 with Orthosteric and Allosteric Antagonists. *Nature* **2016**, *540*, 458−461.
(96) Tan, Q.; Zhu, Y.; Li, J.; Chen, Z.; Han, G. W.; Kufareva, I.; Li, T.; Ma, L.; Fenalti, G.; Li, J.; Zhang, W.; Xie, X.; Yang, H.; Cherezov, V.; Liu, H.; Stevens, R. C.; Zhao, Q.; Wu, B. Structure of the CCR5 Chemokine Receptor−HIV Entry Inhibitor Maraviroc Complex. *Science* **2013**, *341*, 1387−1390.
(97) Fenalti, G.; Giguere, P. M.; Katritch, V.; Huang, X. P.; Thompson, A. A.; Cherezov, V.; Roth, B. L.; Stevens, R. C. Molecular Control of δ-Opioid Receptor Signalling. *Nature* **2014**, *506*, 191−196.
(98) Wu, H.; Wacker, D.; Mileni, M.; Katritch, V.; Han, G. W.; Vardy, E.; Liu, W.; Thompson, A. A.; Huang, X. P.; Carroll, F. I.; Mascarella, S. W.; Westkaemper, R. B.; Mosier, P. D.; Roth, B. L.; Cherezov, V.; Stevens, R. C. Structure of the Human κ-Opioid Receptor in Complex with JDTic. *Nature* **2012**, *485*, 327−332.
(99) Che, T.; Majumdar, S.; Zaidi, S. A.; Ondachi, P.; McCorvy, J. D.; Wang, S.; Mosier, P. D.; Uprety, R.; Vardy, E.; Krumm, B. E.; Han, G. W.; Lee, M. Y.; Pardon, E.; Steyaert, J.; Huang, X. P.; Strachan, R. T.; Tribo, A. R.; Pasternak, G. W.; Carroll, F. I.; Stevens, R. C.; Cherezov, V.; Katritch, V.; Wacker, D.; Roth, B. L. Structure of the Nanobody-Stabilized Active State of the Kappa Opioid Receptor. *Cell* **2018**, *172*, 55−67.
(100) Manglik, A.; Kruse, A. C.; Kobilka, T. S.; Thian, F. S.; Mathiesen, J. M.; Sunahara, R. K.; Pardo, L.; Weis, W. I.; Kobilka, B. K.; Granier, S. Crystal Structure of the μ-Opioid Receptor Bound to a Morphinan Antagonist. *Nature* **2012**, *485*, 321−326.
(101) Koehl, A.; Hu, H.; Maeda, S.; Zhang, Y.; Qu, Q.; Paggi, J. M.; Latorraca, N. R.; Hilger, D.; Dawson, R.; Matile, H.; Schertler, G. F. X.; Granier, S.; Weis, W. I.; Dror, R. O.; Manglik, A.; Skiniotis, G.; Kobilka, B. K. Structure of the μ-Opioid Receptor-Giprotein Complex. *Nature* **2018**, *558*, 547−552.
(102) Webb, B.; Sali, A. Comparative Protein Structure Modeling Using MODELLER. *Curr. Protoc. Bioinf.* **2014**, *47*, 5.6.1−5.6.32.
(103) Buchan, D. W. A.; Ward, S. M.; Lobley, A. E.; Nugent, T. C. O.; Bryson, K.; Jones, D. T. Protein Annotation and Modelling Servers at University College London. *Nucleic Acids Res.* **2010**, *38*, W563−W568.
(104) Drozdetskiy, A.; Cole, C.; Procter, J.; Barton, G. J. JPred4: A Protein Secondary Structure Prediction Server. *Nucleic Acids Res.* **2015**, *43*, W389−W394.
(105) Pettersen, E. F.; Goddard, T. D.; Huang, C. C.; Couch, G. S.; Greenblatt, D. M.; Meng, E. C.; Ferrin, T. E. UCSF Chimera—A Visualization System for Exploratory Research and Analysis. *J. Comput. Chem.* **2004**, *25*, 1605−1612.
(106) Case, D. A.; Cheatham, T. E.; Darden, T.; Gohlke, H.; Luo, R.; Merz, K. M.; Onufriev, A.; Simmerling, C.; Wang, B.; Woods, R. J. The Amber Biomolecular Simulation Programs. *J. Comput. Chem.* **2005**, *26*, 1668−1688.
(107) Jo, S.; Kim, T.; Iyer, V. G.; Im, W. CHARMM-GUI: A Web-Based Graphical User Interface for CHARMM. *J. Comput. Chem.* **2008**, *29*, 1859−1865.
(108) Fay, J. F.; Dunham, T. D.; Farrens, D. L. Cysteine Residues in the Human Cannabinoid Receptor: Only C257 and C264 Are Required for a Functional Receptor, and Steric Bulk at C386 Impairs Antagonist SR141716A Binding. *Biochemistry* **2005**, *44*, 8757−8769.
(109) Ranganathan, A.; Dror, R. O.; Carlsson, J. Insights into the Role of Asp79 2.50 in β 2 Adrenergic Receptor Activation from Molecular Dynamics Simulations. *Biochemistry* **2014**, *53*, 7283−7296.
(110) Mahalingam, M.; Martínez-Mayorga, K.; Brown, M. F.; Vogel, R. Two Protonation Switches Control Rhodopsin Activation in Membranes. *Proc. Natl. Acad. Sci. U.S.A.* **2008**, *105*, 17795−17800.
(111) Olsson, M. H. M.; Sondergaard, C. R.; Rostkowski, M.; Jensen, J. H. PROPKA3: Consistent Treatment of Internal and Surface Residues in Empirical pKa Predictions. *J. Chem. Theory Comput.* **2011**, *7*, 525−537.
(112) Søndergaard, C. R.; Olsson, M. H. M.; Rostkowski, M.; Jensen, J. H. Improved Treatment of Ligands and Coupling Effects in Empirical Calculation and Rationalization of pKa Values. *J. Chem. Theory Comput.* **2011**, *7*, 2284−2295.
(113) Lomize, M. A.; Lomize, A. L.; Pogozheva, I. D.; Mosberg, H. I. OPM: Orientations of Proteins in Membranes Database. *Bioinformatics* **2006**, *22*, 623−625.
(114) Huang, J.; MacKerell, A. D. CHARMM36 All-Atom Additive Protein Force Field: Validation Based on Comparison to NMR Data. *J. Comput. Chem.* **2013**, *34*, 2135−2145.
(115) Harvey, M. J.; Giupponi, G.; De Fabritiis, G. ACEMD: Accelerating Biomolecular Dynamics in the Microsecond Time Scale. *J. Chem. Theory Comput.* **2009**, *5*, 1632−1639.
(116) Vanommeslaeghe, K.; Hatcher, E.; Acharya, C.; Kundu, S.; Zhong, S.; Shim, J.; Darian, E.; Guvench, O.; Lopes, P.; Vorobyov, I.; MacKerell, A. D., Jr. CHARMM General Force Field (CGenFF): A Force Field for Drug-like Molecules Compatible with the CHARMM All-Atom Additive Biological Force Fields. *J. Comput. Chem.* **2010**, *31*, 671−690.
(117) Vanommeslaeghe, K.; MacKerell, A. D. J. Automation of the CHARMM General Force Field (CGenFF) I: Bond Perception and Atom Typing. *J. Chem. Inf. Model.* **2012**, *52*, 3144−3154.
(118) Vanommeslaeghe, K.; Raman, E. P.; MacKerell, A. D. J. Automation of the CHARMM General Force Field (CGenFF) II: Assignment of Bonded Parameters and Partial Atomic Charges. *J. Chem. Inf. Model.* **2012**, *52*, 3155−3168.
(119) Humphrey, W.; Dalke, A.; Schulten, K. VMD: Visual Molecular Dynamics. *J. Mol. Graphics* **1996**, *14*, 33−38.
(120) Phillips, J. C.; Braun, R.; Wang, W.; Gumbart, J.; Tajkhorshid, E.; Villa, E.; Chipot, C.; Skeel, R. D.; Kalé, L.; Schulten, K. Scalable Molecular Dynamics with NAMD. *J. Comput. Chem.* **2005**, *26*, 1781−1802.
(121) Lyskov, S.; Chou, F.-C.; Conchúir, S. Ó.; Der, B. S.; Drew, K.; Kuroda, D.; Xu, J.; Weitzner, B. D.; Renfrew, P. D.; Sripakdeevong, P.; Borgo, B.; Havranek, J. J.; Kuhlman, B.; Kortemme, T.; Bonneau, R.; Gray, J. J.; Das, R. Serverification of Molecular Modeling Applications: The Rosetta Online Server That Includes Everyone (ROSIE). *PLoS One* **2013**, *8*, No. e63906.

DOI: 10.1021/acs.jmedchem.9b00612
J. Med. Chem. 2019, 62, 5638−5654

5.2. Article 2: Evaluating Allosteric Perturbations in Cannabinoid Receptor 1 by *In Silico* Single-Point Mutation

ACS OMEGA

http://pubs.acs.org/journal/acsodf

Article

Evaluating Allosteric Perturbations in Cannabinoid Receptor 1 by *In Silico* Single-Point Mutation

Oscar Díaz, Pedro Renault,* and Jesús Giraldo*

Cite This: *ACS Omega* 2022, 7, 37873−37884

Read Online

ACCESS | Metrics & More | Article Recommendations | Supporting Information

ABSTRACT: Cannabinoid receptor 1 (CB1) is a promising drug target involved in many physiological processes. Using atomistic molecular dynamics (MD) simulations, we examined the structural effect of F237L mutation on CB1, a mutation that has qualitatively similar effects to allosteric ligand ORG27569 binding. This mutation showed a global effect on CB1 conformations. Among the observed effects, TM6 outward movement and the conformational change of the NPxxY motif upon receptor activation by CB1 agonist CP55940 were hindered compared to *wt* CB1. Within the orthosteric binding site, CP55940 interactions with CB1 were altered. Our results revealed that allosteric perturbations introduced by the mutation had a global impact on receptor conformations, suggesting that the mutation site is a key region for allosteric modulation in CB1.

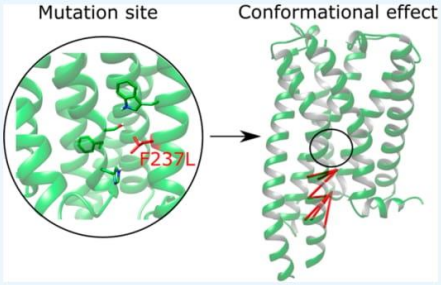

INTRODUCTION

Cannabinoid receptor 1 (CB1) is one of the key components of the endocannabinoid system. CB1 belongs to the class A G protein-coupled receptor (GPCR) family, is one of the most abundantly expressed GPCRs in the brain, and is involved in the modulation of pain, behavior, memory, and cognition.[1,2] CB1 is one of the targets of Δ^9-tetrahydrocannabinol (THC), the major psychoactive component of the cannabis plant, which has been consumed over millennia for recreational and medical uses.[3] Thus, the pharmacological properties of drugs that bind to cannabinoid receptors (cannabinoids) have been extensively studied over the years, including their endogenous ligands (endocannabinoids), cannabinoids present in the cannabis plant such as THC, and synthetic cannabinoids.[2,4,5] Although synthetic THC and a synthetic analogue (nabilone) are approved for medical use in the United States and in several countries in the EU (see ref 6 for a review on approved medications in the EU countries), the development of synthetic cannabinoid drugs with clinical use has been difficult. Specifically, inverse agonist SR141716A (rimonabant) was withdrawn from the market due to its apparent association to depression and suicidal ideation.[5,7] Given the difficulty of developing drugs that target the CB1 orthosteric site, allosteric modulation has emerged as an interesting approach to regulate the effects exhibited by orthosteric ligands. Importantly, allosteric compounds have known advantages over orthosteric ligands, such as a ceiling effect (in contrast to the effect of competition with a different orthosteric ligand, which can indefinitely shift the response of the endogenous ligand in a dose-dependent manner, the functional effects of allosteric modulators are "saturable", with a ceiling driven by the cooperativity between ligands and thus may offer an advantage to avoid overdose) and greater GPCR subtype-selectivity.[8,9] Allosteric modulators can increase (positive allosteric modulators, PAMs) and decrease (negative allosteric modulators, NAMs) the functional response exerted by orthosteric ligands or the receptor itself[10] or provide bias toward a particular signaling pathway (biased allosteric modulators, BAMs).[11] The first allosteric modulator targeting CB1 (ORG27569) was discovered in 2005,[12] but many others have since been discovered.[13−16]

Currently, a crystal structure of CB1 with bound ligands CP55940 (orthosteric agonist) and ORG27569 (allosteric modulator) is available.[17] In this structure, the orthosteric binding site is adapted for CP55940 binding but the intracellular region is in an inactive-like conformation. This structure confirmed the known pharmacologic behavior of ORG27569: positive allosterism for binding and negative allosterism for function,[12] known as a PAM-antagonist.[18] Moreover, this crystal structure shows ORG27569 bound to the intracellular region of transmembrane helix (TM) 2 and TM4, in an extrahelical cavity in contact with the membrane.[17] This binding site overlaps with a cholesterol binding site in CB1 as shown by agonist-bound crystal structures of CB1.[19] Consequently, ORG27569 competes with cholesterol binding, as described previously in rat brain membranes.[20] Interestingly,

Received: August 4, 2022
Accepted: September 28, 2022
Published: October 14, 2022

cholesterol enrichment reduces CP55940 binding,[21] while cholesterol depletion decreases inverse agonist binding,[20] suggesting cholesterol behaves as a NAM. This indicates this cavity contains key residues that affect orthosteric ligand binding and receptor activation, despite not being part of the orthosteric binding site or the G protein binding site.

Recently, parallel tempering metadynamics simulations indicated that a shift in F155$^{2.42}$ (Ballesteros-Weinstein numbering scheme included as a superscript[22]), a residue located in this cavity, is critical for receptor activation, and this rearrangement displayed a higher energy barrier than TM6 outward movement.[23] This shift of F155$^{2.42}$ can be observed by comparing inactive and active G protein-bound crystal structures of CB1, where F155$^{2.42}$ points toward the overlapping binding site of ORG27569 and cholesterol in the active receptor.[24−26] Another residue located at the overlapping binding pocket is F237$^{4.46}$. Mutation of this residue to leucine has been shown to increase CP55940 affinity and reduce inverse agonist SR141716A affinity.[17] As for its functional effect, it has been proposed that F237$^{4.46}$ has a role in the activation process.[17] In active crystal structures of CB1 with cocrystallized G protein,[25,26] F237$^{4.46}$ is displaced toward the extrahelical site and away from TM2 and TM3 (overlapping with the binding pose of ORG27569) and its space is replaced by F155$^{2.42}$, which shifts toward TM4 (Figure 1). This shift of

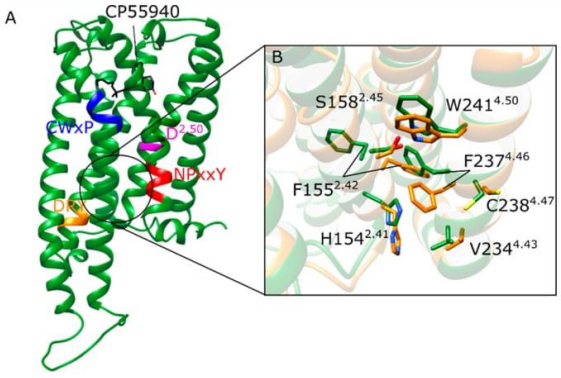

Figure 1. (A) View of the inactive *wt* CB1 model with bound CP55940 and with conserved sequence motifs in class A GPCRs highlighted. (B) Close up view of the extrahelical cavity in the inactive state (green, from PDB ID 5U09) and active state (orange, from PDB ID 6KPG) containing ORG27569 and cholesterol contact residues.

F155$^{2.42}$ and F237$^{4.46}$ is not tied to intracellular conformational changes in TM6 and TM7, which can be observed in active-like agonist-bound crystal structures of CB1 without bound G protein,[19] since F155$^{2.42}$ and F237$^{4.46}$ are in an "inactive-like" state in these structures. Interestingly, a cholesterol molecule is bound to the extrahelical cavity in these active-like crystal structures. Overall, this indicates CB1 activation is sensitive to perturbations in this region, which may be introduced by allosteric ligand binding, residue mutation or membrane lipid composition. Furthermore, F237$^{4.46}$ is not part of well-known sequence motifs or activation microswitches in class A GPCRs despite its capability to modulate ligand binding.

In this study, we investigate structural and dynamical effects of the F237L mutation. This work follows a previous study on the molecular mechanism of agonist-mediated CB1 activation.[27] In that study, starting from an inactive crystal structure of CB1,[24] we performed unbiased, microsecond-length molecular dynamics (MD) simulations in the apo state and also bound to the agonist CP55940, and observed spontaneous transitions to active-like states. This model included the protonation of some selected residues shown to favor active-like conformations (see Methods section). Thus, it provides a reference for comparison with subsequent studies on CB1. Here, we perform additional MD simulations to explore the perturbations on CB1 introduced by F237L mutation, as a model for allosteric perturbation at the allosteric site observed in crystal structures,[17,19] and evaluate their effects on CP55940-mediated CB1 activation. To do this, we employ the same CB1 model as presented in Díaz et al.[27] so as to compare the F237L mutant to *wt* CB1.

MATERIALS AND METHODS

The *wt* CB1 model employed was previously used in Díaz et al.[27] Briefly, the model was built from starting coordinates of the inactive crystal structure of CB1[24] obtained from the Protein Data Bank (PDB 5U09). After removal of the cocrystallized fusion protein, T210A mutation was restored to *wt* and the missing regions of TM5, TM6, and ICL3 were modeled using MODELER v9.14.[28] Then, the receptor was energy minimized, and CP55940 was docked into the orthosteric binding site using AUTODOCK4.2.[29] After our simulations with this model in Díaz et al.,[27] an inactive structure of CB1 with cocrystallized CP55940 was published.[17] Nevertheless, to allow direct comparisons with these earlier simulations, we kept the same protocol here and used the model built with docking. In the present study, the F237L mutant CB1 was generated from this previous model by replacing F237$^{4.46}$ with the leucine rotamer with highest probability in CHIMERA 1.14[30] according to the Dunbrack library.[31] Then, models of F237L CB1 and *wt* CB1 were minimized in CHIMERA 1.14 performing 1000 steps of steepest descent and 100 conjugate gradient steps in the AMBER14SB force field.

Molecular dynamics (MD) simulations of *wt* CB1 analyzed in this study at apo and CP55940-bound conditions were previously published in Díaz et al.[27] In two replicas of these simulations, starting from the inactive state, *wt* CB1 achieved active-like conformations when bound to CP55940. Therefore, they provide a good point of comparison to evaluate CB1 activation. The same MD simulation approach was employed for F237L CB1. The C257^{ECL2}-C264^{ECL2} disulfide bridge was maintained, and charges for D163$^{2.50}$, D213$^{3.49}$, E323^{ICL3}, D324^{ICL3}, D333$^{6.25}$, and D338$^{6.30}$ were neutralized, while H302$^{5.66}$, H304$^{5.68}$, and H320^{ICL3} were protonated.[27] Compared to the expected residue protonation state at pH 7, this alternative protonation state was shown to promote activation of CB1[27] and other class A GPCRs.[32−34] Systems were embedded in 80 × 80 Å 1-palmitoyl-2-oleoyl-*sn*-glycero-3-phosphocoline (POPC) homogeneous membranes, and the system charge was neutralized at 0.15 M concentration of KCl. Simulations were performed using ACEMD software[35] in the CHARMM36 force field[36] at 300 K and 1 atm, while CP55940 was parametrized in the CHARMM GenFF[37] using ParamChem.[38] Equilibration consisted in 8 ns of simulation time progressively releasing restraints on protein and ligand heavy atoms followed by 20 ns of simulation without restraints, and then each production run consisted of 2 μs of simulation time. MD simulation input files are provided in Supporting Information. Three replicas were performed for each

https://doi.org/10.1021/acsomega.2c04980
ACS Omega 2022, 7, 37873−37884

simulation condition (apo and agonist-bound *wt* CB1; apo and agonist-bound mutant), adding up to a total of 24 μs of simulation time analyzed in this study.

Trajectories were analyzed by examining MD-generated snapshots at an interval of 4 ns of simulation time. These MD-generated conformations were visually inspected and distances between Cα atoms of R214$^{3.50}$-D338$^{6.30}$ (residues implicated in the formation of the ionic lock), side chain hydroxyl atoms of Y294$^{5.58}$-Y397$^{7.53}$ and the χ_1 dihedral angles of W356$^{6.48}$, F200$^{3.36}$, F155$^{2.42}$, and F237$^{4.46}$ were measured using VMD 1.9.3.[39] Distances between aromatic moieties of F155$^{2.42}$, F237$^{4.46}$, and W241$^{4.50}$ were measured from the center of mass of the heavy atoms of aromatic rings in VMD, and the presence of aromatic interactions was considered when this distance was within a 7.0 Å distance cutoff.

Protein root-mean square deviation (RMSD) was also measured in VMD based on C_α atoms of transmembrane helices and taking the initial structure as reference. Ligand RMSD was based on its heavy atoms and measured against the initial docking pose. The initial CP55940 docking pose was compared to crystal structures with cocrystallized CP55940 (PDB 6KQI[17] and 7WV9[23]), and contact residues were defined as those within 4 Å of CP55940 heavy atoms.

Principal component analysis (PCA) was performed with GROMACS.[40] To do this, all replicas of agonist-bound *wt* and agonist-bound mutant CB1 were concatenated and aligned to the Cα atoms of the initial model. The N-terminal and the highly flexible ICL3 were excluded and not considered in the analysis. Therefore, only residues from A118$^{1.34}$ to R307$^{5.71}$ and from A335$^{6.27}$ to F412^{H8} were included in PC calculations. Then, we built and diagonalized the covariance matrix corresponding to this concatenated and aligned trajectory. The elements of this matrix were $C_{ij} = \langle (\mathbf{r}_i - \langle \mathbf{r}_i \rangle)(\mathbf{r}_j - \langle \mathbf{r}_j \rangle) \rangle$ where i and j denote the Cartesian coordinates of the Cα atoms of the receptor. The vector $\mathbf{r}_i$ indicates the instantaneous value of coordinate i and $\langle \mathbf{r}_i \rangle$ is the average value of this coordinate in the ensemble of conformations. Each individual trajectory was then projected on the space of the first two principal components.

The statistical analysis of pairwise residue distances was performed using the Ensemble Difference Distance Matrix, implemented in the Bio3D package in R.[41] Residue distances were compared between two groups, based on the results of PCA: (i) replicas 2 and 3 of agonist-bound *wt* CB1 and (ii) all replicas of agonist-bound F237L CB1. The distance between two residues was defined as the closest distance between any heavy atoms in the residues (side chains included). Residue pairs whose distances were greater than 10 Å across all frames of all trajectories were excluded from the analysis. In the same manner as PCA, the N-terminal and the ICL3 were also excluded (only residues from A118$^{1.34}$ to R307$^{5.71}$ and from A335$^{6.27}$ to F412^{H8} were considered). Matrices of the average distances between residues were built for the two groups and a difference distance matrix was obtained by subtracting the matrix of the mutant from that of the *wt* receptor; however, only statistically significant differences greater than 1 Å were retained. Statistical significance was determined by a two-sample Wilcoxon test, with p-value lower than 0.005. To identify close contacts that were present in one group but not in other, we selected a subset of the significant differences in which the average residue distance was lower than a 4 Å cutoff in one group and greater than this cutoff in the other.

In order to characterize differences in the interaction frequencies between agonist and contacting residues for both *wt* and F237L CB1, first the distance between the closest heavy atoms of CP55940 and the receptor for each trajectory frame was measured using *gmx pairdist* in GROMACS.[40] Then, contact frequencies for each residue were calculated considering that a contact is present if the distance is <4 Å. Finally, the frequencies for CP55940-F237L CB1 contacts were subtracted from the frequencies for *wt* CB1 for each respective residue to generate a frequency difference. As a second approach, ΔG_{bind} was estimated using gmx_MMPBSA,[42] including an implicit membrane with thickness determined by CHARMM-GUI initial setup. Solvent, membrane, and internal dielectric constants used were 80, 7, and 2, respectively. Residues within 4 Å of the starting CP55940 binding position and residues that showed average difference in contact frequency over 0.1 were considered for decomposition analysis. Average differences in free energy decomposition were evaluated by a two-sample, two-tailed Student's t test, with equal or unequal variances as assessed by an F-test.

Water occupancy was defined as the percentage of frames in which a given protein residue established a contact (distance within 4 Å) with a water molecule. Distances between protein and water were measured with the tool *gmx pairdist* in GROMACS.[40]

RESULTS

Overall, MD trajectories were stable, as indicated by the RMSD curves in Figure S1. Higher values were observed for two of the replicas of agonist-bound *wt* receptor (Figure S1A), and this is consistent with the conformational changes seen in these trajectories, where CB1 achieved active-like conformations,[27] characterized by a movement of TM6 (Figure S1E). In comparison to *wt* systems, the RMSD was higher in trajectories of the mutant, and this can be explained by the relaxation that followed the perturbation introduced by the mutation (Figure S1B, D, F). Plots of the root mean square fluctuation (RMSF) also point to a consistent pattern of CB1 fluctuations in all trajectories (Figure S2).

The RMSD of the agonist CP55940 was relatively high (Figure S3B, C), and probably reflected inaccuracies introduced by docking. As shown in Figure S3A, the docking pose differs from the crystal structure (PDB 6KQI) mainly in the position of the C ring and the orientation of its OH groups (Figure S4A). As a result, native contacts between the ligand and TM2 are missing from the docking pose. Overall, from 19 protein−ligand contacts present in the crystal structure, 12 were found in docking (63%). In addition, contacts with I267^{ECL2} and L276$^{5.40}$ were frequently formed during the simulations, raising the percentage of native contacts retained from the crystal structure to 74%. More details about the frequency of CB1-CP55940 contacts in the simulations can be found in Table S1. Nevertheless, CP55940 remained in its binding site throughout the MD trajectories (Figure S3B, C), despite fluctuations observed mostly due to movement of its alkyl chain and, to a lesser extent, its C-ring (Figure S4). Moreover, as active-like conformations were generated in CP55940-bound CB1 but not in apo,[27] this indicates that our model captures native contacts that are likely important for receptor activation. Taken together, these observations suggest that, despite inaccuracies introduced by docking, and considering that MD simulations of F237L CB1 started from

https://doi.org/10.1021/acsomega.2c04980
ACS Omega 2022, 7, 37873−37884

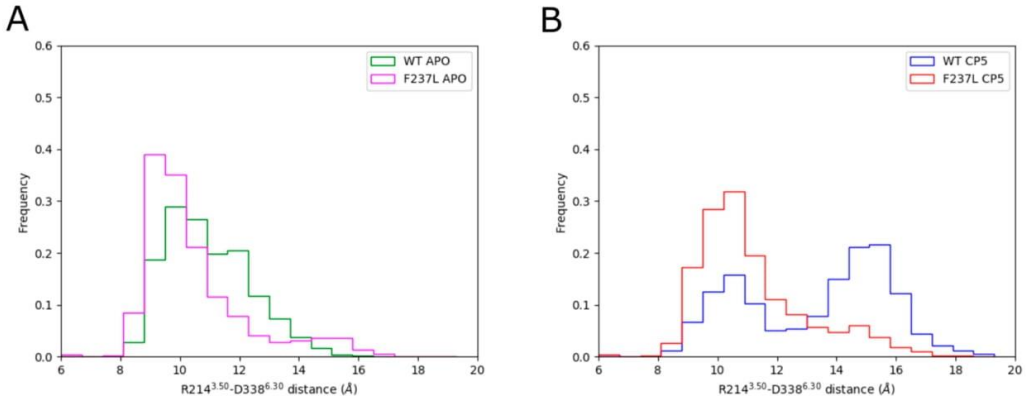

Figure 2. Distribution of the R214$^{3.50}$-D338$^{6.30}$ distance in MD simulations of (A) apo CB1 and (B) CP55940-bound CB1. Data from all replicas; MD snapshots were collected at a 4 ns time interval in each one of them. Histograms for *wt* CB1 were calculated from MD simulations published in Díaz et al. 2019.

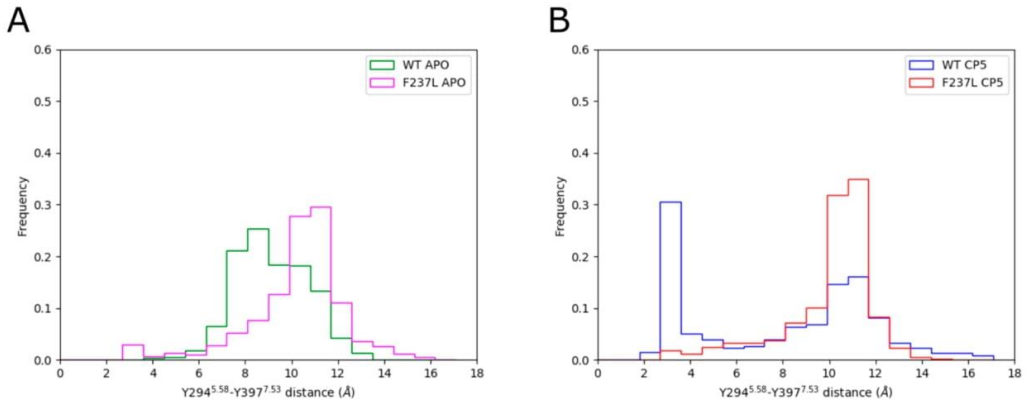

Figure 3. Distribution of the distance between side chain oxygen atoms of Y294$^{5.58}$ and Y397$^{7.53}$ in MD simulations of (A) apo CB1 and (B) CP55940-bound CB1. Data from all replicas; MD snapshots were collected at a 4 ns time interval in each one of them. Histograms for *wt* CB1 were calculated from MD simulations published in Díaz et al.[27]

the same initial model, it was still possible to discern the effect of the mutation on collective motions of the receptor.

F237L Mutation Hindered Outward Movement of TM6. The hallmark of class A GPCR activation is the breakage of the salt-bridge formed by residues 3.50 and 6.30 (ionic lock) and consequent outward movement of TM6 away from TM3,[43] which can be observed by comparing inactive and active CB1 crystal structures.[19,23−26,44] In our MD simulations of apo CB1, TM6 remained in inactive-like conformations both in *wt* and F237L CB1, as shown by the distance between residues R214$^{3.50}$-D338$^{6.30}$ (Figure 2A), which is expected because CB1 was in the inactive conformation at the start of MD simulations. In CP55940-bound *wt* CB1 MD simulations, TM6 moved outward, reaching active-like states in two of the three replicas performed.[27] Thus, two subpopulations of TM6 conformation can be observed: an inactive-like conformation that is represented by a closer R214$^{3.50}$-D338$^{6.30}$, and an active-like conformation represented by a larger TM3-TM6 distance, indicating a broken ionic lock (blue curve in Figure 2B). On the contrary, this did not occur in F237L mutant CB1 (red curve in Figure 2B) even when CP55940 was bound to the receptor. Here, TM6 remained mostly in an inactive-like conformation, similar to the observations in apo conditions. This indicates the outward movement of TM6 upon receptor activation by CP55940 was hindered by F237L mutation, and this is consistent with a role of F237$^{4.46}$ on receptor activation.[17,25]

F237L Mutation Blocked Y397$^{7.53}$ Conformational Change. At the receptor level, the binding of a signaling protein is the final consequence of receptor activation. In this regard, the NPxxY motif has been linked to G protein binding, as Y397$^{7.53}$ shifts toward Y294$^{5.58}$ in active receptor conformations to facilitate G protein binding and blocking TM6 inactivation.[25,43] In MD simulations of apo CB1, Y397$^{7.53}$ remained in an inactive-like conformation overall, as shown by the distance between Y397$^{7.53}$ and Y294$^{5.58}$ (Figure 3A), regardless of F237L mutation. In contrast, a new population was observed in *wt* CB1 bound to CP55940 centered at ∼3 Å, indicating the presence of active-like conformations[27] (blue curve in Figure 3B). However, this subpopulation was not clearly represented in CP55940-bound F237L CB1 (red curve in Figure 3B), where Y397$^{7.53}$ remained in inactive-like conformations such as in apo CB1. This suggests that F237L mutation blocks the conformational change in Y397$^{7.53}$ observed in active crystal structures of CB1.[25,26] Together with the hindrance of TM6 movement, our results indicate that

https://doi.org/10.1021/acsomega.2c04980
ACS Omega 2022, 7, 37873−37884

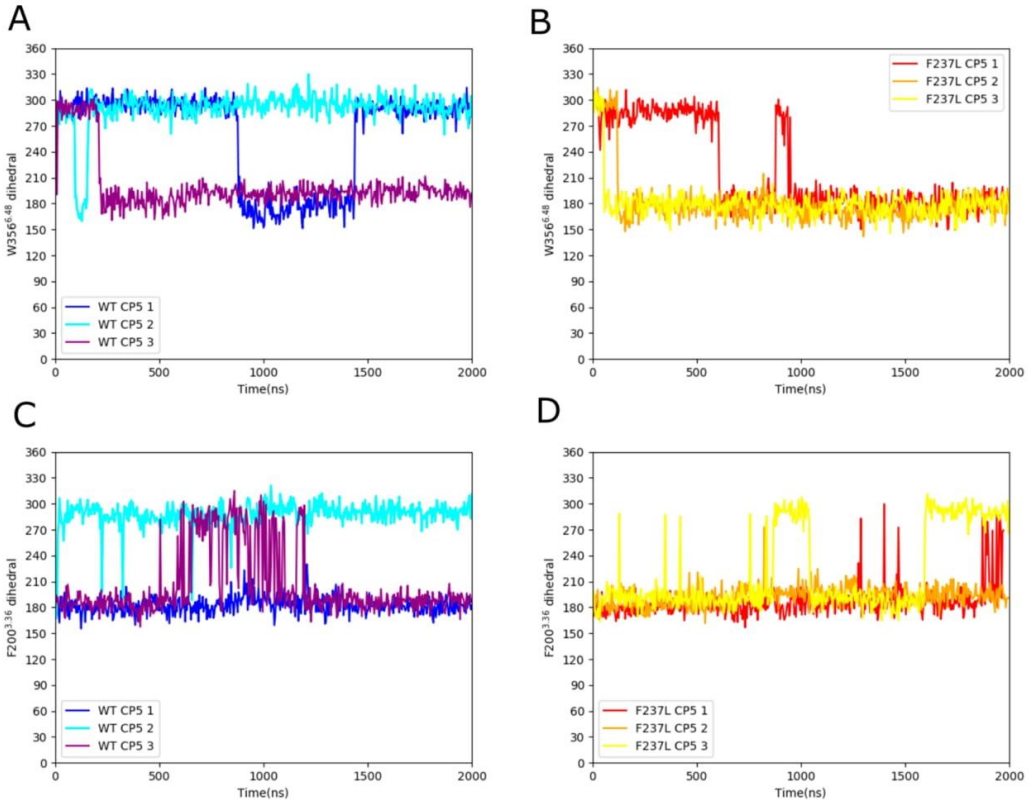

Figure 4. χ_1 dihedral angles of (A, B) W356$^{6.48}$ and (C, D) F200$^{3.36}$ along MD simulation time for three trajectories of (A, C) *wt* CB1* and (B, D) F237L CB1. *Data from MD simulations of *wt* CB1 taken from Díaz et al.[27]

F237L mutation interfered with receptor activation during the simulations.

W356$^{6.48}$/F200$^{3.36}$ Rotameric Switch Was Unaffected by F237L Mutation. The residue pair W356$^{6.48}$/F200$^{3.36}$ forms an additional microswitch for receptor activation in CB1, consisting of a double rotameric switch where W356$^{6.48}$ and F200$^{3.36}$ are rearranged upon receptor activation. This is accompanied by an upward movement of TM3.[27] This rearrangement has been proposed to be mediated by changes in the χ_1 dihedral angles of W356$^{6.48}$ and F200$^{3.36}$ that result in the breakage of aromatic stacking interactions between these two residues upon receptor activation.[25] McAllister et al., 2004 proposed W356$^{6.48}$ shifts its χ_1 dihedral angle from *gauche(+)* to *trans*, followed by a transition in the χ_1 dihedral angle of F200$^{3.36}$ from *trans* to *gauche(+)*.[45] This was observed in MD simulations of *wt* CB1 as described in Díaz et al., 2019 (Figure 4A, C), although W356$^{6.48}$ conformation may return to *gauche(+)* after TM3 upward movement while the receptor is in an active-like conformation, as shown by active CB1 crystal structures.[25,26] In MD simulations of CP55940-bound F237L CB1 (Figure 4B, D), the χ_1 dihedral angle from W356$^{6.48}$ transitioned from *gauche(+)* to *trans* and χ_1 dihedral angle from F200$^{3.36}$ transitioned from *trans* to *gauche(+)*, suggesting that the double rotameric switch was unaffected by F237L mutation.

Contacts between CP55940 and CB1 Were Affected by F237L Mutation. To evaluate the effect of F237L mutation on agonist binding, the frequencies of contact between CP55940 and CB1 were calculated for MD simulations of *wt* and mutant receptors. The difference in average frequencies between *wt* and mutant suggests there is a difference on how CP55940 interacts with CB1, with some interactions favored for *wt* and others for F237L (Figure 5). Moreover, interaction differences were consistent across simulation time (Figures S5 and S6).

Additionally, the affinity of CP55940 for *wt* and F237L CB1 was estimated using Molecular Mechanics Poisson−Boltzmann Surface Area (MMPBSA), decomposed for each residue within 4 Å of CP55940 starting conformation, in addition to residues identified by contact frequency difference analysis. Overall, the difference between global ΔG_{bind} for *wt* and F237L was not statistically significant as calculated by a two-sample Student's *t* test ($\Delta G_{bind}^{wt} = -12.22 \pm 0.52$ kcal/mol, $\Delta G_{bind}^{F237L} = -12.48 \pm 0.71$ kcal/mol (mean ± S.E.M.), $p = 0.583$, for $n = 3$ trajectories). From both contact frequency difference and MMPBSA decomposition, residues could be grouped according to whether their interaction with CP55940 was favored in *wt* or in F237L. According to frequency differences, residues favored by *wt* CB1 were most notably S123$^{1.39}$, F170$^{2.57}$, and M384$^{7.40}$, while residues favored by F237L CB1 were P269^{ECL2}, A380$^{7.36}$, C382$^{7.38}$, and C386$^{7.42}$. MMPBSA decomposition (Figure 5C) showed residues S123$^{1.39}$, F170$^{2.57}$, F200$^{3.36}$, L276$^{5.40}$, M384$^{7.40}$, and L387$^{7.43}$ were favored toward *wt* CB1, while residues L359$^{6.51}$, F379$^{7.35}$, A380$^{7.36}$, and C386$^{7.42}$ were favored toward F237L CB1. To a lesser extent, this analysis also indicated that interaction with residues

https://doi.org/10.1021/acsomega.2c04980
ACS Omega 2022, 7, 37873−37884

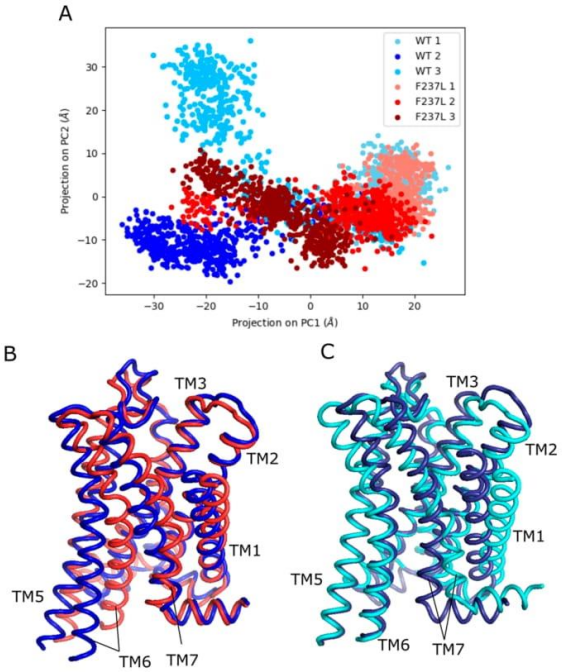

Figure 6. (A) Projection on the principal components PC1 and PC2 of the *wt* and F237L CB1 MD-generated conformations with bound CP55940. (B) Extreme conformations along the direction of PC1 (minimum value in blue, maximum value in red). A transition from the red to the blue conformation corresponds to a movement from positive to negative projections along the direction of PC1. (C) Extreme conformations along the direction of PC2 (minimum value in blue, maximum value in cyan). A transition from the blue to the cyan conformation corresponds to a movement from negative to positive projections along the direction of PC2.

correspond to PCs 1 and 2. Figure 6B shows that going from positive to negative values of the projection along PC1 (from right to left in the PC map in Figure 6A) corresponds to an outward motion of TM6. In the case of PC2, Figure 6C shows the motion from negative to positive values of the projection (from bottom to top in the PC map) corresponds to a bending of TM7 that contributes to open the intracellular cavity of the receptor (besides a collective rearrangement around the orthosteric site). Therefore, open and active-like conformations of CB1 are scarcely explored by the mutant. Taken together, these results indicate that the mutation had an impact on the dynamical behavior of CB1 and shifted the receptor population toward the inactive state.

As detailed in the Methods section, PCA was based on the Cα atoms of CB1, thus providing information on motions of the main chain. However, we also wanted to investigate how the mutation affected the side chains of the receptor. The residues analyzed in the previous sections are either microswitches of CB1 activation well established in the literature[25,26] or form the binding cavity of the orthosteric ligand, and thus were selected as a first indicator of the effect of F237L mutation. To characterize other residues that may be affected by F237L mutation, we calculated distance matrices of *wt* and mutant CB1, both in the presence of the agonist. PCA results allowed us to separate two groups for comparison in order to reduce noise and focus on differences between the two conditions: (i) replicas 2 and 3 of *wt* CB1 (where active-like conformations were observed); (ii) the three replicas of the mutant. We then determined statistically significant differences in average residue pairwise distances between these two groups. Residue pairs with distances always longer than 10 Å in all trajectories were excluded from the analysis. A list of the 1378 residue pairs whose variations in distance were significantly higher than 1 Å is available in the Supporting Information. Considering the magnitude of distance variations, the top 35 (variations in the range 4.6−6.7 Å) corresponded to distances that were larger in the *wt* receptor; interestingly, they involved residue pairs in TM6-TM2 and TM6-ICL2. It is necessary to descend to the 36th position in the ranking to find a residue pair with increased distance in the mutant, and it involved residues in TM7 and TM3. The 10 largest differences are listed in Table 1 and schematically depicted in Figure 7A,

Table 1. Top 10 Highest Differences in Average Residue Pairwise Distance between MD Simulations of *wt* (Replicas 2 and 3) and F237L CB1 (All Replicas) with Bound CP55940

residue 1	residue 2	avg. distance in *wt* (Å)	avg. distance in F237L (Å)	delta (Å)	*p* value
$P151^{2.38}$	$D338^{6.30}$	20.22	13.52	6.70	1.9×10^{-291}
$F155^{2.42}$	$L345^{6.37}$	11.98	6.00	5.98	1.9×10^{-254}
$S152^{2.45}$	$A342^{6.34}$	17.16	11.43	5.73	4.9×10^{-284}
$P151^{2.38}$	$L341^{6.33}$	15.88	10.19	5.69	2.9×10^{-275}
$F155^{2.42}$	$A342^{6.34}$	17.25	11.57	5.69	8.7×10^{-248}
$F155^{2.42}$	$V346^{6.38}$	16.15	10.45	5.69	9.6×10^{-244}
$P151^{2.38}$	$M337^{6.29}$	19.72	14.04	5.68	1.1×10^{-257}
$S152^{2.39}$	$L341^{6.33}$	12.68	7.04	5.64	7.5×10^{-277}
$S152^{2.39}$	$D338^{6.30}$	17.34	11.76	5.58	3.4×10^{-284}
$S152^{2.39}$	$I339^{6.31}$	19.59	14.06	5.53	3.7×10^{-276}

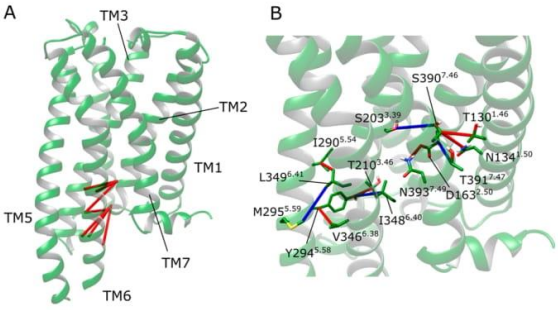

Figure 7. (A) Ten largest distance differences in MD simulations between *wt* CB1 (replicas 2 and 3) and F237L CB1 (all replicas) with bound CP55940. (B) Differences in contacts between *wt* CB1 (replicas 2 and 3) and F237L CB1 (all replicas) with bound CP55940. Contacts only present in *wt* CB1 are represented in blue and contacts only present in F237L are represented in red.

which shows that in *wt* CB1 there was a larger distance between TM6 and TM2 in comparison to the mutant. This increased distance was consistent across simulation time ($P151^{2.38}$-$D338^{6.30}$ distance shown in Figure S7). This is in agreement with our other results and indicates that an outward movement of TM6 was hindered by the mutation. It is also worth noting that the largest distance observed between TM7 and TM3 in the mutant is also consistent with the hypothesis

https://doi.org/10.1021/acsomega.2c04980
ACS Omega 2022, 7, 37873−37884

that the mutation suppresses collective motions that lead to activation, since the approach between these two helices is well described in the activation of class A GPCRs.[49]

Moreover, the hindrance of TM6 movement by the mutation was reflected by the higher frequency of water molecules in contact with residues A342$^{6.34}$ and I396$^{7.52}$ (close to the G protein binding cavity) in *wt* CB1 compared to F237L CB1 (Figure S8). The presence of these additional contacts with water molecules in this region suggests an entrance of water molecules as a consequence of the outward movement of TM6, and can be seen as an indicator of conformational change, which occurred in *wt* receptor and was hindered by the mutation.

In a complementary analysis, we also identified residues which formed close contacts (distance < 4 Å for at least 50% of the simulation time) in one group but not in the other (Table 2 and Figure 7B). In this category, we found residue pairs in TM6-TM3 and TM6-TM5; and also pairs between TM7 and TM1, and between and TM2 and TM3. Residues D163$^{2.50}$, Y294$^{5.58}$, S390$^{7.46}$, and L349$^{6.41}$ were each one of them involved in more than one of these contacts which were switched on or off, suggesting an important role for these residues in the collective dynamics of CB1. Notably, many of these changing contacts, as well as the large amplitude distance variations, occurred far from the site of the mutation, involving several other helices and distinct regions of the receptor, pointing to the global structural and dynamical effect of the mutation.

Table 2. Differences in Close Residue Contacts (Distance < 4 Å) between MD Simulations of *wt* (replicas 2 and 3) and F237L CB1 (All Replicas) with Bound CP55940

residue 1	residue 2	contact in *wt*	contact in F237L
S203$^{3.39}$	S390$^{7.46}$	yes	no
Y294$^{5.58}$	I348$^{6.40}$	yes	no
M295$^{5.59}$	L349$^{6.49}$	yes	no
D163$^{2.50}$	T391$^{7.47}$	yes	no
T130$^{1.46}$	S390$^{7.46}$	no	yes
N134$^{1.50}$	S390$^{7.46}$	no	yes
T210$^{3.46}$	Y294$^{5.58}$	no	yes
Y294$^{5.58}$	V346$^{6.38}$	no	yes
I290$^{5.54}$	L349$^{6.41}$	no	yes
D163$^{2.50}$	N393$^{7.49}$	no	yes

F237L Substitution Disrupted Aromatic Interactions in the Mutation Site. F237L mutation consists of a substitution of an aromatic residue with an aliphatic one. In crystal structures of CB1, F237$^{4.46}$ is in the vicinity of two aromatic residues, F155$^{2.42}$ and W241$^{4.50}$; the latter is a highly conserved residue in class A GPCRs[50] which participates in allosteric modulator ORG27569 binding.[17] In one of the MD simulation replicas of *wt* CB1 bound to CP55940,[27] a conformational change of F155$^{2.42}$ and F237$^{4.46}$ was observed. In this MD trajectory, active-like conformations were observed[27] and F155$^{2.42}$ shifted toward TM4 generating an intermediate state in which F155$^{2.42}$ and F237$^{4.46}$ briefly formed aromatic tilted T-shape interactions (Figure S9), after which F237$^{4.46}$ shifted away from TM3. This configuration of F155$^{2.42}$ and F237$^{4.46}$ (Figure S9C) can be seen in active crystal structures of CB1 with cocrystallized G protein,[25,26] but not in active-like crystal structures without the G protein.[19] Aromatic interactions between F237$^{4.46}$ and W241$^{4.50}$ are favored in this "displaced" configuration of F237$^{4.46}$ (Figure S10). Thus, substitution of phenylalanine by leucine would disrupt such aromatic interactions between F237$^{4.46}$ and W241$^{4.50}$ characteristic of states coupled to the G protein. Presumably, this modulation might extend to ligand binding to this region because of the fact that ORG27569 and cholesterol bind to CB1 with an inactive-like conformation of F155$^{2.42}$ and F237$^{4.46}$.[17,19,23]

DISCUSSION AND CONCLUSIONS

In this study, we have interrogated the effect of the F237L mutation upon CB1 activation through molecular dynamics simulations. Here, we performed MD simulations of apo and CP55940-bound F237L CB1, starting from the inactive state of the receptor. We compared our observations with results from our previous work, in which we performed simulations of *wt* CB1.[27] In that work, we observed that the agonist-bound *wt* receptor achieved active-like conformations during the trajectories; in contrast, in the simulations of the mutant performed here CB1 remained inactive, even in the presence of the agonist. Notably, the mutation was associated to a suppression of a large amplitude outward movement of TM6 in the simulations.

In both of our studies—our previous work with *wt* CB1 and the present one with the mutant—systems were setup in the same way, and we followed the same simulation protocol. This included the insertion of the receptor in a very simple model membrane, composed of POPC. Though it has been shown that cholesterol can play an important role as an allosteric modulator of GPCRs,[51] and particularly of CB1,[20,21,52] it was not included in our simulations. This allowed us to make direct comparisons with our previous work and also to decouple the effect of the mutation from allosteric effects exerted by cholesterol. Moreover, F237$^{4.46}$ is located in a cholesterol binding site of CB1,[19] and an investigation of the impact of the mutation on cholesterol binding or the combined effects of cholesterol and the mutation were beyond the scope of this paper. However, it should be important to consider the behavior of the mutant receptor in the presence of cholesterol, and we believe this topic deserves attention in the future.

Crystal structures show that the conformation of F237$^{4.46}$ changes upon receptor activation, and this conformational change is accompanied by a rearrangement of F155$^{2.42}$ (see Figure 1B). In the inactive state,[24] F155$^{2.42}$ points toward the G protein binding cavity, interacting with residues L207$^{3.43}$, T210$^{3.46}$, L345$^{6.37}$, I348$^{6.40}$, and Y397$^{7.53}$ in other TMs. Upon activation,[25,26] F155$^{2.42}$ shifts and points toward the extracellular cavity and interacts with residues L209$^{3.45}$, D213$^{3.49}$, A233$^{4.42}$, and L237$^{4.46}$. This shift therefore leads to a loss of contacts between TM2 and TM6 which possibly facilitates the uncoupling between these two helices. The important role of F155$^{2.42}$ in CB1 activation has been recently highlighted by metadynamics simulations,[23] which indicated that the rearrangement of this residue (and, more generally, a rearrangement of TM2) is a critical step in CB1 activation. Importantly, these simulations revealed that the free energy barrier to the conformational change of F155$^{2.42}$ is much higher than the one associated to the outward movement of TM6. Our results are consistent with this picture, since the outward movement of TM6 was more frequently observed in our simulations than the reorientation of F155$^{2.42}$. Importantly, we should note that in our trajectories the F237L mutation hindered this relatively easier movement of TM6, suggesting

https://doi.org/10.1021/acsomega.2c04980
ACS Omega 2022, 7, 37873−37884

that the mutation contributes to heighten the energy barrier to the displacement of this helix.

The active-like states observed in our simulations were then frequently characterized by TM6 and F155$^{2.42}$ in active and inactive conformations, respectively (this also characterizes conformational states explored in the metadynamics simulations referred to above, in which TM6 could switch between inward and outward states while F155$^{2.42}$ remained in its inactive conformation). The existence of such distinct intermediate states is consistent with models of GPCR dynamics that propose the existence of multiple conformational states in dynamical equilibrium.[53] Other molecules—for instance, orthosteric or allosteric ligands, membrane lipids or intracellular proteins such as G proteins—would be able to shift this equilibrium and stabilize certain conformations, thus modulating the receptor function. For example, recent NMR experiments with CB1 in the presence of different ligands (including the agonist CP55940 and the allosteric modulator ORG27569) detected a variety of conformational states, leading the authors to propose a model for activation and allosteric modulation including not only inactive and active states but also preactive and active-like conformations; each one of them would be favored by the interaction with distinct partners.[54] In the particular case of the conformations of TM6 and F155$^{2.42}$, it is possible that the stabilization of both in the fully active conformation requires coupling to the G protein. Our results suggest that the F237L mutation renders G protein coupling less probable, because it shifts the dynamical equilibrium toward the inactive state of the receptor.

Structural differences between *wt* and mutant CB1 in the simulations were accompanied by modifications in the hydration of the receptor. In particular, *wt* CB1 exhibited a higher occupancy of water molecules in specific residues close to the G-protein binding site. The entrance of these water molecules was possibly facilitated by the outward movement of TM6, that opened the intracellular cavity. It constituted another indicator of conformational changes observed in *wt* CB1 and suppressed by the mutation. However, the observed differences in the pattern of hydration between *wt* and mutant CB1 are complex (Figure S8), and it remains to be verified if water molecules play an active part in triggering CB1 conformational changes, as suggested for the activation of other GPCRs.[55,56]

It seems logical to attribute the behavior of F237L mutation to the loss of aromatic interactions in the mutated receptor due to the substitution of an aromatic residue for an aliphatic one. It should be noted that, although our simulations indicated that stacking or T-shape aromatic interactions between F155$^{2.42}$ and F237$^{4.46}$ may form transiently in a dynamic context (Figure S9), aromatic interactions between these residues are not present in CB1 crystal structures. Moreover, in mutagenesis experiments the replacement of F155$^{2.42}$ by V, an aliphatic but smaller side chain, was shown to increase G_i signaling; in contrast, mutation to the aromatic but larger W had the opposite effect.[23] These results suggest the aromaticity of F155$^{2.42}$ might not be the determinant factor for its role in the activation process, and also the possibility that the size of the side chain at this location might be important.

On the other hand, W241$^{4.50}$ is a highly conserved aromatic residue in GPCRs (conserved at 97% in class A GPCRs[50]) located one helix turn from F237$^{4.46}$ and is also a contact residue for ORG27569[17] and cholesterol.[19] In our trajectories, W241$^{4.50}$ could form stacking or T-shape aromatic interactions with F237$^{4.46}$ in its "displaced" conformation (Figures S9 and S10), and such interactions would be lost in the F237L mutant CB1. Though contacts between F237$^{4.46}$ and W241$^{4.50}$ are observed in crystal structures of the receptor coupled to the G protein,[25,26] suggesting aromatic interactions between F237$^{4.46}$ and W241$^{4.50}$ are characteristic of the active state, the disruption of such interactions is likely not the only factor involved in the effect of F237L mutation upon activation. Actually, one of the important results in this study is the global effect of the mutation. While the perturbation of local aromatic interactions is probably relevant, we observed that the effects are nonlocal and widespread, affecting pairwise residue distances and contacts across CB1 structure. The dynamical coupling between the local network of aromatic residues and the global state of the receptor deserves further investigation. F155$^{2.42}$, F237$^{4.46}$, and W241$^{4.50}$ may work as an "allosteric micro-switch" that could be modulated by mutations, allosteric ligands, or membrane lipids. We believe this hypothesis should be further explored through new simulations with mutations of these residues, and also through metadynamics simulations, to probe free energy barriers associated to their conformational changes.

Experimental results showed that F237L increases CP55940 binding and reduces inverse agonist SR141716A binding.[17] Our simulations indicated that the F237L mutation had an impact on residues on the CP55940 binding site, and therefore they are consistent with the experimental verification that perturbations in F237$^{4.46}$ can affect orthosteric ligand binding. However, we have not been able to capture significant differences between *wt* and mutant affinities for CP55940. This can be explained by the relatively low difference in the experimentally determined CP55940 affinity between *wt* and F237L CB1 (K_d in *wt* CB1:8.7 ± 0.7 nM; K_d F237L CB1:5.0 ± 0.2 nM; data from Shao et al.[17]) and also by limitations in MMPBSA methodology, such as considering an implicit solvent and membrane. Also, the entropic component was not considered, which might be an important factor contributing to the free energy of binding, or perhaps altered by F237L mutation. Despite these limitations and inaccuracies introduced by docking, our results suggest that multiple residues in the CP55940 binding site are affected by F237L mutation, as shown by contact analysis and MMPBSA free energy decomposition (Figure 5). These results indicate a complex effect, with some protein−ligand interactions being more probable in *wt* CB1 and others favored in the mutant. Among the residues that display different contact frequencies with the agonist, I267^{ECL2}, P269^{ECL2}, and D272^{ECL2} are located in the ECL2; notably, contacts between the agonist and I267^{ECL2} and P269^{ECL2} are favored in the mutant. This is an interesting result, since it has been shown that ECL2 is a critical region for CP55940 binding.[46] One hypothesis is that the F237L mutation, by favoring these contacts, leads to a stronger interaction with ECL2 and facilitate agonist binding into a higher affinity state. The small difference in experimental affinities for CP55940 between *wt* and F237L CB1 poses a challenge to the corroboration of this hypothesis through simulations. Nevertheless, it could be interesting to use more sophisticated free energy estimation methods (e.g., funnel metadynamics[57]) to interrogate more closely the role of these ECL2 residues in the process of agonist binding. Mutations at these ECL2 sites could be tested both theoretically and experimentally to test the validity of our observations.

https://doi.org/10.1021/acsomega.2c04980
ACS Omega 2022, 7, 37873−37884

The F237L mutation exhibits a qualitatively similar effect to allosteric ligand binding. Mutations whose effect is similar to allosteric ligand binding have been reported before for other GPCRs. For example, in the metabotropic glutamate receptor 2 (mGluR2), it has been observed that Q679V and C770A mutations converted a partial agonist into a full agonist, therefore acting in a similar way as a positive allosteric modulator (PAM).[58] ORG27569 is one of the most studied CB1 allosteric modulators and has intriguing pharmacological properties in that it displays positive binding cooperativity and negative functional cooperativity with CB1 agonists such as CP55940. Allosteric modulators with this behavior have been previously denominated PAM-antagonists.[18] However, the mechanism by which ORG27569 exerts this effect is still unknown. In the CP55940 and ORG27569-bound crystal structure of CB1,[17] ORG27569 can be observed bound to the intracellular side of the receptor, in an extrahelical binding site formed by TM2 and TM4 that partially overlaps with a cholesterol binding site.[17,19] $F237^{4.46}$ is a contact residue for both ORG27569 and cholesterol binding as shown in these crystal structures. Moreover, F237L mutation causes an increase in the affinity of CP55940 for CB1[17] and, as examined in this study, impairs receptor activation. Furthermore, it has been shown that ORG27569 promotes receptor internalization,[20,S9] an effect that is also observed in homologous F238L mutation in rat CB1.[60] When considered together, all these data and the shared effects between ORG27569 binding and F237L mutation, combined with the fact that $F237^{4.46}$ is a contact residue for ORG27569, suggest that $F237^{4.46}$ contributes to mediate its allosteric effects.

This study was limited to the analysis of F237L mutation. Since this mutation has a global effect on the receptor conformational properties, this indicates that this region is a potential hotspot for allosteric modulation in CB1. It would be expected that other perturbations in this region such as those resulting from ligand binding would affect distant regions of the receptor, thus suggesting a chemical space where a variety of allosteric ligands may be developed. Finally, we conclude that MD simulations on mutant receptor models, despite their inherent limitations and taken with the necessary caution,[61] can be used as an exploratory tool to provide clues for subsequent structure-based drug design of allosteric compounds.

■ ASSOCIATED CONTENT

Data Availability Statement

Atomic coordinates for the initial MD systems for *wt* and F237L CB1, both apo and bound to CP55940, as well as input files for MD simulations with ACEMD and MMPBSA calculations are provided in the Supporting Information. The following software was used: CHARMM-GUI (https://www.charmm-gui.org/), ACEMD2 (https://www.acellera.com/acemd/), MODELER 9.14 (https://salilab.org/modeller/), AUTODOCK 4.2 (https://autodock.scripps.edu/), CHIMERA 1.14 (https://www.cgl.ucsf.edu/chimera/), VMD 1.9.4 (https://www.ks.uiuc.edu/Research/vmd/), Bio3D 2.4.1 (http://thegrantlab.org/bio3d/), gmx_MMPBSA 1.4.3 (https://pypi.org/project/gmx-MMPBSA/) and GROMACS2020.4 (https://www.gromacs.org/). Graphs were generated with Matplotlib 2.2.5 (https://matplotlib.org/).

Supporting Information

The Supporting Information is available free of charge at https://pubs.acs.org/doi/10.1021/acsomega.2c04980.

Statistically significant differences in average pairwise residue distance between MD simulations of *wt* and F237L CB1 bound to CP55940 (ODS), protein and CP55940 RMSD over time for each replica, RMSF of all residues for each replica, structural comparison of docked CP55940 to cocrystallized CP55940, distance between CP55940 and $P269^{ECL2}$, CP55940 and $M384^{7.40}$, and $P151^{2.38}$ and $D338^{6.30}$ in MD simulations of *wt* and F237L CB1 bound to CP55940, differences in occupancy of water molecules for each residue in MD simulations of *wt* and F237L CB1 bound to CP55940, distances between residues $F155^{2.42}$, $F237^{4.46}$, and $W241^{4.50}$ and their configurations during MD simulations, contact frequencies of CP55940 with the receptor in MD simulations of *wt* and F237L CB1, *p*-values of performed statistical tests for the difference in CP55940 binding residue energy decomposition between *wt* and F237L CB1 (PDF)

Atomic coordinates for all models and input files for MD simulations and MMPBSA calculations (ZIP)

Differences in average residue pairwise distances between agonist-bound *wt* and agonist-bound mutant receptor (TXT)

■ AUTHOR INFORMATION

Corresponding Authors

Jesús Giraldo − *Laboratory of Molecular Neuropharmacology and Bioinformatics, Unitat de Bioestadística and Institut de Neurociències and Unitat de Neurociència Traslacional, Parc Taulí Hospital Universitari, Institut d'Investigació i Innovació Parc Taulí (I3PT), Institut de Neurociències, Universitat Autònoma de Barcelona, Bellaterra 08193, Spain; Instituto de Salud Carlos III, Centro de Investigación Biomédica en Red de Salud Mental (CIBERSAM), Madrid 28029, Spain;* orcid.org/0000-0001-7082-4695; Email: Jesus.Giraldo@uab.es

Pedro Renault − *Laboratory of Molecular Neuropharmacology and Bioinformatics, Unitat de Bioestadística and Institut de Neurociències and Unitat de Neurociència Traslacional, Parc Taulí Hospital Universitari, Institut d'Investigació i Innovació Parc Taulí (I3PT), Institut de Neurociències, Universitat Autònoma de Barcelona, Bellaterra 08193, Spain; Instituto de Salud Carlos III, Centro de Investigación Biomédica en Red de Salud Mental (CIBERSAM), Madrid 28029, Spain;* orcid.org/0000-0002-5649-3057; Email: Pedro.Renault@uab.cat

Author

Oscar Díaz − *Laboratory of Molecular Neuropharmacology and Bioinformatics, Unitat de Bioestadística and Institut de Neurociències and Unitat de Neurociència Traslacional, Parc Taulí Hospital Universitari, Institut d'Investigació i Innovació Parc Taulí (I3PT), Institut de Neurociències, Universitat Autònoma de Barcelona, Bellaterra 08193, Spain; Instituto de Salud Carlos III, Centro de Investigación Biomédica en Red de Salud Mental (CIBERSAM), Madrid 28029, Spain*

Complete contact information is available at: https://pubs.acs.org/10.1021/acsomega.2c04980

Author Contributions

MD simulations were performed and analyzed by Ó.D. P.R. and J.G. designed and supervised the study. The manuscript

was written through contributions of all authors. All authors have given approval to the final version of the manuscript.

Notes

The authors declare no competing financial interest.

■ ACKNOWLEDGMENTS

This project has received funding from the European Union's Horizon2020 research and innovation programme under grant agreement 848068 and from Ministerio de Ciencia e Innovación (Spain) under grant agreement PID2020-119136RB-I00. This publication reflects only the authors' view and the European Commission is not responsible for any use that may be made of the information it contains. We thank Xin Yang for providing the MD-generated receptor structures[23] at the end of this project.

■ ABBREVIATIONS

CB1, cannabinoid receptor 1; GPCR, G protein-coupled receptor; THC, Δ9-tetrahydrocannabinol; TM, transmembrane helix; ICL, intracellular loop; ECL, extracellular loop; PDB, Protein Data Bank; NAM, negative allosteric modulator; PAM, positive allosteric modulator; POPC, 1-palmitoyl-2-oleoyl-sn-glycero-3-phosphocoline; MMPBSA, molecular mechanics Poisson−Boltzmann surface area

■ REFERENCES

(1) Marsicano, G.; Lutz, B. Expression of the Cannabinoid Receptor CB1 in Distinct Neuronal Subpopulations in the Adult Mouse Forebrain. *Eur. J. Neurosci.* **1999**, *11* (12), 4213−4225.
(2) Reggio, P. H. Endocannabinoid Binding to the Cannabinoid Receptors: What Is Known and What Remains Unknown. *Curr. Med. Chem.* **2010**, *17* (14), 1468−1486.
(3) Mechoulam, R.; Parker, L. A. The Endocannabinoid System and the Brain. *Annu. Rev. Psychol.* **2013**, *64*, 21−47.
(4) Pertwee, R. Pharmacological Actions of Cannabinoids. In *Cannabinoids*; Pertwee, R., Ed.; Springer, 2005; pp 1−51.
(5) Janero, D. R.; Makriyannis, A. Cannabinoid Receptor Antagonists: Pharmacological Opportunities, Clinical Experience, and Translational Prognosis. *Expert Opin. Emerg. Drugs* **2009**, *14* (1), 43−65.
(6) Lipnik-Štangelj, M.; Razinger, B. A Regulatory Take on Cannabis and Cannabinoids for Medicinal Use in the European Union. *Arh. Hig. Rada Toksikol.* **2020**, *71* (1), 12−18.
(7) Giraldo, J. How Inverse Can a Neutral Antagonist Be? Strategic Questions after the Rimonabant Issue. *Drug Discovery Today* **2010**, *15* (11−12), 411−415.
(8) Melancon, B. J.; Hopkins, C. R.; Wood, M. R.; Emmitte, K. A.; Niswender, C. M.; Christopoulos, A.; Conn, P. J.; Lindsley, C. W. Allosteric Modulation of Seven Transmembrane Spanning Receptors: Theory, Practice, and Opportunities for Central Nervous System Drug Discovery. *J. Med. Chem.* **2012**, *55* (4), 1445−1464.
(9) Fasciani, I.; Petragnano, F.; Aloisi, G.; Marampon, F.; Carli, M.; Scarselli, M.; Maggio, R.; Rossi, M. Allosteric Modulators of g Protein-Coupled Dopamine and Serotonin Receptors: A New Class of Atypical Antipsychotics. *Pharmaceuticals* **2020**, *13* (11), 388.
(10) Christopoulos, A.; Kenakin, T. G Protein-Coupled Receptor Allosterism and Complexing. *Pharmacol. Rev.* **2002**, *54* (2), 323−374.
(11) Foster, D. J.; Conn, P. J. Allosteric Modlation of GPCRs: New Insights and Potential Utility for Treatment of Schizophrenia and Other CNS Disorders. *Neuron* **2017**, *94* (3), 431−446.
(12) Price, M. R.; Baillie, G. L.; Thomas, A.; Stevenson, L. a; Easson, M.; Goodwin, R.; Mclean, A.; Mcintosh, L.; Goodwin, G.; Walker, G.; Westwood, P.; Marrs, J.; Thomson, F.; Cowley, P.; Christopoulos, A.; Pertwee, R. G.; Ross, R. A. Allosteric Modulation of the Cannabinoid CB1 Receptor. *Mol. Pharmacol.* **2005**, *68* (5), 1484−1495.
(13) Horswill, J. G.; Bali, U.; Shaaban, S.; Keily, J. F.; Jeevaratnam, P.; Babbs, A. J.; Reynet, C.; Wong Kai In, P. PSNCBAM-1, a Novel Allosteric Antagonist at Cannabinoid CB 1 Receptors with Hypophagic Effects in Rats. *Br. J. Pharmacol.* **2007**, *152* (5), 805−814.
(14) Immadi, S. S.; Dopart, R.; Wu, Z.; Fu, B.; Kendall, D. A.; Lu, D. Exploring 6-Azaindole and 7-Azaindole Rings for Developing Cannabinoid Receptor 1 Allosteric Modulators. *Cannabis Cannabinoid Res.* **2018**, *3* (1), 252−258.
(15) Laprairie, R. B.; Kulkarni, P. M.; Deschamps, J. R.; Kelly, M. E. M.; Janero, D. R.; Cascio, M. G.; Stevenson, L. A.; Pertwee, R. G.; Kenakin, T. P.; Denovan-Wright, E. M.; Thakur, G. A. Enantiospecific Allosteric Modulation of Cannabinoid 1 Receptor. *ACS Chem. Neurosci.* **2017**, *8* (6), 1188−1203.
(16) Nguyen, T.; Li, J.-X.; Thomas, B. F.; Wiley, J. L.; Kenakin, T. P.; Zhang, Y. Allosteric Modulation: An Alternate Approach Targeting the Cannabinoid CB1 Receptor. *Med. Res. Rev.* **2017**, *37* (3), 441−474.
(17) Shao, Z.; Yan, W.; Chapman, K.; Ramesh, K.; Ferrell, A. J.; Yin, J.; Wang, X.; Xu, Q.; Rosenbaum, D. M. Structure of an Allosteric Modulator Bound to the CB1 Cannabinoid Receptor. *Nat. Chem. Biol.* **2019**, *15*, 1199−1205.
(18) Kenakin, T.; Strachan, R. T. PAM-Antagonists: A Better Way to Block Pathological Receptor Signaling? *Trends Pharmacol. Sci.* **2018**, *39* (8), 748−765.
(19) Hua, T.; Vemuri, K.; Nikas, S. P.; Laprairie, R. B.; Wu, Y.; Qu, L.; Pu, M.; Korde, A.; Jiang, S.; Ho, J.-H.; Han, G. W.; Ding, K.; Li, X.; Liu, H.; Hanson, M. A.; Zhao, S.; Bohn, L. M.; Makriyannis, A.; Stevens, R. C.; Liu, Z.-J. Crystal Structures of Agonist-Bound Human Cannabinoid Receptor CB1. *Nature* **2017**, *547* (7664), 468−471.
(20) Stornaiuolo, M.; Bruno, A.; Botta, L.; Regina, G. La; Cosconati, S.; Silvestri, R.; Marinelli, L.; Novellino, E. Endogenous vs Exogenous Allosteric Modulators in GPCRs: A Dispute for Shuttling CB1 among Different Membrane Microenvironments. *Sci. Rep.* **2015**, *5* (1), 1−13.
(21) Bari, M.; Paradisi, A.; Pasquariello, N.; Maccarrone, M. Cholesterol-Dependent Modulation of Type 1 Cannabinoid Receptors in Nerve Cells. *J. Neurosci. Res.* **2005**, *81* (2), 275−283.
(22) Ballesteros, J. A.; Weinstein, H. Integrated Methods for the Construction of Three-Dimensional Models and Computational Probing of Structure-Function Relations in G Protein-Coupled Receptors. *Methods Neurosci.* **1995**, *25*, 366−428.
(23) Yang, X.; Wang, X.; Xu, Z.; Wu, C.; Zhou, Y.; Wang, Y.; Lin, G.; Li, K.; Wu, M.; Xia, A. Molecular Mechanism of Allosteric Modulation for the Cannabinoid Receptor CB1. *Nat. Chem. Biol.* **2022**, *18*, 831.
(24) Shao, Z.; Yin, J.; Chapman, K.; Grzemska, M.; Clark, L.; Wang, J.; Rosenbaum, D. M. High-Resolution Crystal Structure of the Human CB1 Cannabinoid Receptor. *Nature* **2016**, *540* (7634), 602−606.
(25) Krishna Kumar, K.; Shalev-Benami, M.; Robertson, M. J.; Hu, H.; Banister, S. D.; Hollingsworth, S. A.; Latorraca, N. R.; Kato, H. E.; Hilger, D.; Maeda, S.; Weis, W. I.; Farrens, D. L.; Dror, R. O.; Malhotra, S. V.; Kobilka, B. K.; Skiniotis, G. Structure of a Signaling Cannabinoid Receptor 1-G Protein Complex. *Cell* **2019**, *176* (3), 448−458 e12.
(26) Hua, T.; Li, X.; Wu, L.; Iliopoulos-Tsoutsouvas, C.; Wang, Y.; Wu, M.; Shen, L.; Brust, C. A.; Nikas, S. P.; Song, F.; Song, X.; Yuan, S.; Sun, Q.; Wu, Y.; Jiang, S.; Grim, T. W.; Benchama, O.; Stahl, E. L.; Zvonok, N.; Zhao, S.; Bohn, L. M.; Makriyannis, A.; Liu, Z. J. Activation and Signaling Mechanism Revealed by Cannabinoid Receptor-Gi Complex Structures. *Cell* **2020**, *180* (4), 655−665.
(27) Díaz, Ó.; Dalton, J. A. R.; Giraldo, J. Revealing the Mechanism of Agonist-Mediated Cannabinoid Receptor 1 (CB1) Activation and Phospholipid-Mediated Allosteric Modulation. *J. Med. Chem.* **2019**, *62* (11), 5638−5654.
(28) Webb, B.; Sali, A. Comparative Protein Structure Modeling Using MODELLER. *Curr. Protoc. Bioinforma.* **2014**, *47*, 5.6.1−5.6.32.
(29) Morris, G. M.; Huey, R.; Lindstrom, W.; Sanner, M. F.; Belew, R. K.; Goodsell, D. S.; Olson, A. J. AutoDock4 and AutoDockTools4:

https://doi.org/10.1021/acsomega.2c04980
ACS Omega 2022, 7, 37873−37884

Automated Docking with Selective Receptor Flexibility. *J. Comput. Chem.* **2009**, *30* (16), 2785−2791.
(30) Pettersen, E. F.; Goddard, T. D.; Huang, C. C.; Couch, G. S.; Greenblatt, D. M.; Meng, E. C.; Ferrin, T. E. UCSF Chimera—A Visualization System for Exploratory Research and Analysis. *J. Comput. Chem.* **2004**, *25* (13), 1605−1612.
(31) Shapovalov, M. V.; Dunbrack, R. L. A Smoothed Backbone-Dependent Rotamer Library for Proteins Derived from Adaptive Kernel Density Estimates and Regressions. *Structure* **2011**, *19* (6), 844−858.
(32) Lans, I.; Dalton, J. A. R.; Giraldo, J. Selective Protonation of Acidic Residues Triggers Opsin Activation. *J. Phys. Chem. B* **2015**, *119* (30), 9510−9519.
(33) Bruzzese, A.; Gil, C.; Dalton, J. A. R.; Giraldo, J. Structural Insights into Positive and Negative Allosteric Regulation of a G Protein-Coupled Receptor through Protein-Lipid Interactions. *Sci. Rep.* **2018**, *8* (1), 4456.
(34) Bruzzese, A.; Dalton, J. A. R.; Giraldo, J. Insights into Adenosine A2A Receptor Activation through Cooperative Modulation of Agonist and Allosteric Lipid Interactions. *PLoS Computat. Biol.* **2020**, *16*, e1007818.
(35) Harvey, M. J.; Giupponi, G.; De Fabritiis, G. ACEMD: Accelerating Biomolecular Dynamics in the Microsecond Time Scale. *J. Chem. Theory Comput.* **2009**, *5* (6), 1632−1639.
(36) Huang, J.; MacKerell, A. D. CHARMM36 All-Atom Additive Protein Force Field: Validation Based on Comparison to NMR Data. *J. Comput. Chem.* **2013**, *34* (25), 2135−2145.
(37) Vanommeslaeghe, K.; Hatcher, E.; Acharya, C.; Kundu, S.; Zhong, S.; Shim, J.; Darian, E.; Guvench, O.; Lopes, P.; Vorobyov, I.; MacKerell Jr, A. D. CHARMM General Force Field (CGenFF): A Force Field for Drug-like Molecules Compatible with the CHARMM All-Atom Additive Biological Force Fields. *J. Comput. Chem.* **2010**, *31* (4), 671−690.
(38) Vanommeslaeghe, K.; MacKerell, A. D. J. Automation of the CHARMM General Force Field (CGenFF) I: Bond Perception and Atom Typing. *J. Chem. Inf. Model.* **2012**, *52* (12), 3144−3154.
(39) Humphrey, W.; Dalke, A.; Schulten, K. VMD: Visual Molecular Dynamics. *J. Mol. Graph.* **1996**, *14* (1), 33−38.
(40) Lindahl, E.; Hess, B.; van der Spoel, D. GROMACS 3.0: A Package for Molecular Simulation and Trajectory Analysis. *Mol. Model. Annu.* **2001**, *7* (8), 306−317.
(41) Grant, B. J.; Rodrigues, A. P. C.; ElSawy, K. M.; McCammon, J. A.; Caves, L. S. D. Bio3d: An R Package for the Comparative Analysis of Protein Structures. *Bioinformatics* **2006**, *22* (21), 2695−2696.
(42) Miller, B. R.; McGee, T. D.; Swails, J. M.; Homeyer, N.; Gohlke, H.; Roitberg, A. E. MMPBSA.py: An E Ffi Cient Program for End-State Free Energy Calculations. *J. Chem. Theory Comput.* **2012**, *8*, 3314−3321.
(43) Katritch, V.; Cherezov, V.; Stevens, R. C. Structure-Function of the G-Protein-Coupled Receptor Superfamily. *Annu. Rev. Pharmacol. Toxicol.* **2013**, *53*, 531−556.
(44) Hua, T.; Vemuri, K.; Pu, M.; Qu, L.; Han, G. W.; Wu, Y.; Zhao, S.; Shui, W.; Li, S.; Korde, A.; Laprairie, R. B.; Stahl, E. L.; Ho, J. H.; Zvonok, N.; Zhou, H.; Kufareva, I.; Wu, B.; Zhao, Q.; Hanson, M. A.; Bohn, L. M.; Makriyannis, A.; Stevens, R. C.; Liu, Z. J. Crystal Structure of the Human Cannabinoid Receptor CB1. *Cell* **2016**, *167* (3), 750−762.
(45) McAllister, S. D.; Hurst, D. P.; Barnett-Norris, J.; Lynch, D.; Reggio, P. H.; Abood, M. E. Structural Mimicry in Class A G Protein-Coupled Receptor Rotamer Toggle Switches: The Importance of the F3.36(201)/W6.48(357) Interaction in Cannabinoid CB1 Receptor Activation. *J. Biol. Chem.* **2004**, *279* (46), 48024−48037.
(46) Ahn, K. H.; Bertalovitz, A. C.; Mierke, D. F.; Kendall, D. A. Dual Role of the Second Extracellular Loop of the Cannabinoid Receptor 1 : Ligand Binding and Receptor Localization. *Mol. Pharmacol.* **2009**, *76* (4), 833−842.
(47) Shim, J. Y.; Bertalovitz, A. C.; Kendall, D. A. Identification of Essential Cannabinoid-Binding Domains: Structural Insights into Early Dynamic Events in Receptor Activation. *J. Biol. Chem.* **2011**, *286* (38), 33422−33435.
(48) Kapur, A.; Hurst, D. P.; Fleischer, D.; Whitnell, R.; Thakur, G. A.; Makriyannis, A.; Reggio, P. H.; Abood, M. E. Mutation Studies on Ser7.39 and Ser2.60 in the Human CB1 Receptor: Evidence for a Serine-Induced Bend in CB1 Transmembrane Helix 7. *Mol. Pharmacol.* **2007**, *71* (6), 1512−1524.
(49) Dalton, J. A. R.; Lans, I.; Giraldo, J. Quantifying Conformational Changes in GPCRs: Glimpse of a Common Functional Mechanism. *BMC Bioinformatics* **2015**, *16*, 124.
(50) Isberg, V.; de Graaf, C.; Bortolato, A.; Cherezov, V.; Katritch, V.; Marshall, F. H.; Mordalski, S.; Pin, J.-P.; Stevens, R. C.; Vriend, G.; Gloriam, D. E. Generic GPCR Residue Numbers - Aligning Topology Maps While Minding the Gaps. *Trends Pharmacol. Sci.* **2015**, *36* (1), 22−31.
(51) Guixà-González, R.; Albasanz, J. L.; Rodriguez-Espigares, I.; Pastor, M.; Sanz, F.; Martí-Solano, M.; Manna, M.; Martinez-Seara, H.; Hildebrand, P. W.; Martín, M.; Selent, J. Membrane Cholesterol Access into a G-Protein-Coupled Receptor. *Nat. Commun.* **2017**, *8*, 14505.
(52) Oddi, S.; Dainese, E.; Fezza, F.; Lanuti, M.; Barcaroli, D.; De Laurenzi, V.; Centonze, D.; Maccarrone, M. Functional Characterization of Putative Cholesterol Binding Sequence (CRAC) in Human Type-1 Cannabinoid Receptor. *J. Neurochem.* **2011**, *116* (5), 858−865.
(53) Niesen, M. J. M.; Bhattacharya, S.; Vaidehi, N. The Role of Conformational Ensembles in Ligand Recognition in G-Protein Coupled Receptors. *J. Am. Chem. Soc.* **2011**, *133* (33), 13197−13204.
(54) Wang, X.; Liu, D.; Shen, L.; Li, F.; Li, Y.; Yang, L.; Xu, T.; Tao, H.; Yao, D.; Wu, L.; Hirata, K.; Bohn, L. M.; Makriyannis, A.; Liu, X.; Hua, T.; Liu, Z.; Wang, J. A Genetically Encoded F - 19 NMR Probe Reveals the Allosteric Modulation Mechanism of Cannabinoid Receptor 1. *J. Am. Chem. Soc.* **2021**, *143* (40), 16320−16325.
(55) Yuan, S.; Vogel, H.; Filipek, S. The Role of Water and Sodium Ions in the Activation of the μ-Opioid Receptor. *Angew. Chem., Int. Ed. Engl.* **2013**, *52* (38), 10112−10115.
(56) Yuan, S.; Hu, Z.; Filipek, S.; Vogel, H. W246(6.48) Opens a Gate for a Continuous Intrinsic Water Pathway during Activation of the Adenosine A2A Receptor. *Angew. Chem., Int. Ed. Engl.* **2015**, *54* (2), 556−559.
(57) Limongelli, V.; Bonomi, M.; Parrinello, M. Funnel Metadynamics as Accurate Binding Free-Energy Method. *Proc. Natl. Acad. Sci. U. S. A.* **2013**, *110* (16), 6358−6363.
(58) Doumazane, E.; Scholler, P.; Fabre, L.; Zwier, J. M.; Trinquet, E.; Pin, J. P.; Rondard, P. Illuminating the Activation Mechanisms and Allosteric Properties of Metabotropic Glutamate Receptors. *Proc. Natl. Acad. Sci. U. S. A.* **2013**, *110* (15), E1416.
(59) Ahn, K. H.; Mahmoud, M. M.; Kendall, D. A. Allosteric Modulator ORG27569 Induces CB1 Cannabinoid Receptor High Affinity Agonist Binding State, Receptor Internalization, and Gi Protein-Independent ERK1/2 Kinase Activation. *J. Biol. Chem.* **2012**, *287* (15), 12070−12082.
(60) Wickert, M.; Hildick, K. L.; Baillie, G. L.; Jelinek, R.; Aparisi Rey, A.; Monory, K.; Schneider, M.; Ross, R. A.; Henley, J. M.; Lutz, B. The F238L Point Mutation in the Cannabinoid Type 1 Receptor Enhances Basal Endocytosis via Lipid Rafts. *Front. Mol. Neurosci.* **2018**, *11* (July), 1−11.
(61) Giraldo, J. Agonist Induction, Conformational Selection, and Mutant Receptors. *FEBS Lett.* **2004**, *556* (1−3), 13−18.

https://doi.org/10.1021/acsomega.2c04980
ACS Omega 2022, 7, 37873−37884

5.3. Article 3: Allosteric binding cooperativity in a kinetic context

ELSEVIER

Feature

Allosteric binding cooperativity in a kinetic context

Óscar Díaz [1,2,3], Victor Martín [1,4], Pedro Renault [1,2,3], David Romero [5], Antoni Guillamon [4,5], Jesús Giraldo [1,2,3,*]

Allosteric modulators are of prime interest in drug discovery. These drugs regulate the binding and function of endogenous ligands, with some advantages over orthosteric ligands. A typical pharmacological parameter in allosteric modulation is binding cooperativity. This property can yield unexpected but illuminating results when decomposed into its kinetic parameters. Using two reference models (the allosteric ternary complex receptor model and a heterodimer receptor model), a relationship has been derived for the cooperativity rate constant parameters. This relationship allows many combinations of the cooperativity kinetic parameters for a single binding cooperativity value obtained under equilibrium conditions. This assessment may help understand striking experimental results involving allosteric modulation and suggest further investigations in the field.

Keywords: allosteric modulation; binding kinetics; binding cooperativity; rate constant; cooperativity rate constant; residence time; GPCRs; heterodimer receptor

Allosteric modulation at equilibrium conditions

Allostery, in particular in G-protein-coupled receptors (GPCRs), is a research area of special interest to both academia and the pharmaceutical industry because of the known advantages (a ceiling effect level and greater GPCR subtype selectivity, among others) that allosteric modulators have with respect to orthosteric ligands.[1] In this study, we consider first the allosteric ternary complex receptor model, in which a receptor R bears two binding sites to which the orthosteric ligand A and the allosteric ligand B bind.[2,3] In the first instance, we do not consider how ligand binding translates into receptor function and we limit the analysis to a pure binding scenario in which either equilibrium or rate constants are used.

At equilibrium, the concentrations of the four receptor species present in the system are regulated by the corresponding K_1 to K_4 equilibrium dissociation constants (Fig. 1a).[2,3] We can change the notation and introduce the α and β binding cooperativity parameters (Fig. 1b). α measures the binding affinity of A to RB with respect to the free receptor R, whereas β measures the binding affinity of B to AR with respect to R. Only three of the four equilibrium constants are independent or, in other words, α is equal to β. From now on, we use α to denote the binding cooperativity parameter between the two ligands. α can be greater, lower, or equal to one, indicating, respectively, an increase, decrease or no effect on the affinity of each of the ligands for the receptor because of the presence of the other bound ligand. Binding cooperativities can be experimentally measured by different methods and allosteric modulators can be classified as positive, negative, or neutral depending on $\alpha > 1$, $\alpha < 1$, or $\alpha = 1$, respectively.[2] However, the mutual influence between the two ligands can be further examined when time is considered. For example, we can

https://doi.org/10.1016/j.drudis.2022.103441

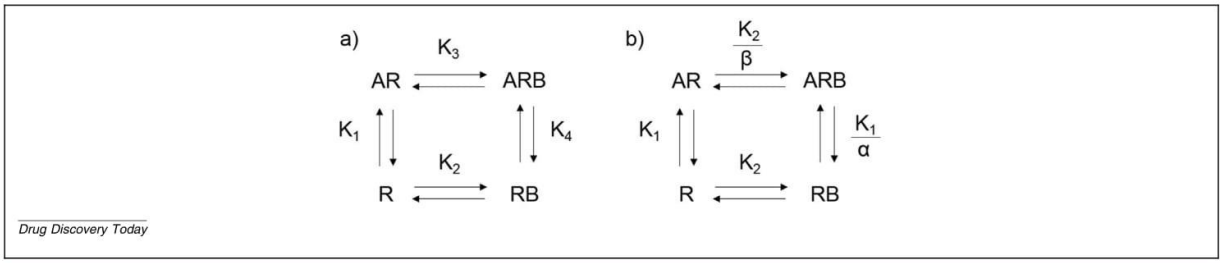

Drug Discovery Today

FIG. 1

Allosteric ternary complex model. It is assumed that A is the agonist and B is the allosteric modulator. **(a)** K_1 to K_4 equilibrium dissociation constants are used: K_1 = [A][R]/[AR]; K_2 = [B][R]/[RB]; K_3 = [B][AR]/[ARB]; K_4 = [A][RB]/[ARB]. **(b)** K_3 and K_4 have been removed by including α and β binding cooperativity parameters, with $\alpha = K_1/K_4$ and $\beta = K_2/K_3$. It can be shown that only three of the four K_1 to K_4 constants are independent: if we substitute each equilibrium dissociation constant by its expression in terms of concentrations of receptor species, then $K_1/K_4 = K_2/K_3$ = [R][ARB]/([AR][RB]) (one equilibrium constant depends on the other three), or, in other words, $\alpha = \beta$. Adapted from [2].

FEATURE

ask whether it is possible to find a positive allosteric modulator (PAM) B that is more kinetically unstable in its binding site when A is present than when it is bound to the free receptor. If $\alpha > 1$, one would expect an increase in the affinity of each of the two ligands when the other is present, but this conclusion does not explain the behavior of the ligands and the mutual influence between them when they are already at the receptor binding site and only the processes of ligand–receptor dissociation are considered.

From equilibrium constants to rate constants: including the kinetic context

Equilibrium constants are the ratio between rate constants (Fig. 2a). The inclusion of rate constants in the analysis opens the discussion to binding kinetics, a pharmacological research area of major application in clinical and drug discovery research.[4,5] We follow the same rationale as in Fig. 1 but using rate constants (association: k_{+1} to k_{+4} and dissociation: k_{-1} to k_{-4}) (Fig. 2a) and their corresponding α_+, α_-, β_+, and β_- cooperativity rate constant parameters, with $\alpha_+ = k_{+4}/k_{+1}$, $\alpha_- = k_{-4}/k_{-1}$, $\beta_+ = k_{+3}/k_{+2}$, and $\beta_- = k_{-3}/k_{-2}$ (Fig. 2b). It can be shown that only seven of the eight rate constants are independent: $(k_{-1}\ k_{+4})/(k_{+1}\ k_{-4}) = (k_{-2}\ k_{+3})/(k_{+2}\ k_{-3})$, or, in other words, $\alpha_+/\alpha_- = \beta_+/\beta_-$.

In the same way as equilibrium constants are the ratio between rate constants, the binding cooperativity parameters (α and β) are the ratio between the corresponding cooperativity rate constant parameters ($\alpha = \alpha_+/\alpha_-$ and $\beta = \beta_+/\beta_-$). Given $\alpha = \beta$, this does not necessarily mean that $\alpha_+ = \beta_+$ and $\alpha_- = \beta_-$. The latter is a sufficient but not a necessary condition and, thus, the kinetic reciprocity between orthosteric and allosteric ligands occurs at the level of their cooperativity rate constant ratios and not their absolute values.

Let us consider the following example: $\alpha = \beta = 4$, with $\alpha_+ = 2$, $\alpha_- = 0.5$, $\beta_+ = 8$ and $\beta_- = 2$ for an orthosteric ligand A and an allosteric ligand B. These values imply a PAM in binding terms ($\alpha > 1$) and, thus, the equilibrium dissociation constants of both the orthosteric and the allosteric ligands decrease in the presence of the other bound ligand or, in other words, their affinities for the receptor increase in the presence of the other

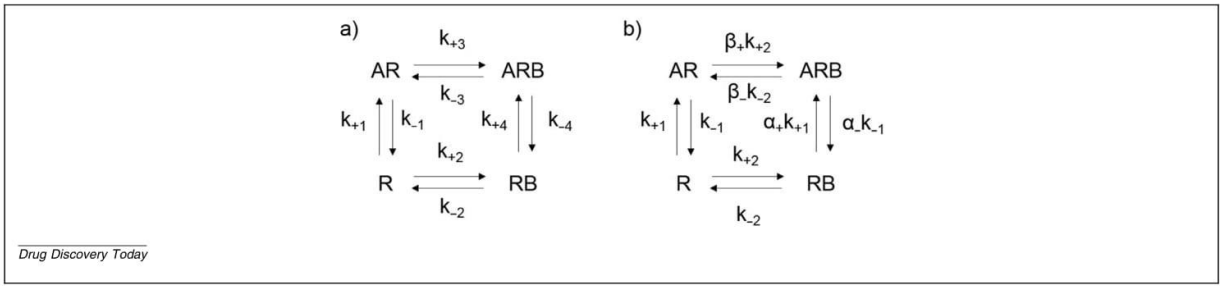

Drug Discovery Today

FIG. 2

Allosteric ternary complex model. It is assumed that A is the agonist and B is the allosteric modulator. **(a)** The equilibrium dissociation constants in Fig. 1 in the main text are substituted by the corresponding association (k_{+1} to k_{+4}) and dissociation (k_{-1} to k_{-4}) rate constants: $K_1 = k_{-1}/k_{+1}$, $K_2 = k_{-2}/k_{+2}$, $K_3 = k_{-3}/k_{+3}$, $K_4 = k_{-4}/k_{+4}$. **(b)** k_{+3}, k_{-3}, k_{+4}, and k_{-4} have been removed by including α_+, α_-, β_+, and β_- cooperativity rate constant parameters, with $\alpha_+ = k_{+4}/k_{+1}$, $\alpha_- = k_{-4}/k_{-1}$, $\beta_+ = k_{+3}/k_{+2}$, and $\beta_- = k_{-3}/k_{-2}$. It can be shown that only seven of the eight k_{+1} to k_{+4} and k_{-1} to k_{-4} rate constants are independent: if we express each equilibrium dissociation constant in terms of concentrations of receptor species, then $K_1/K_4 = K_2/K_3$ = [R][ARB]/([AR][RB]) (Fig. 1 in the main text) and, by putting equilibrium constants in terms of rate constants, it can be seen that $(k_{-1}\ k_{+4})/(k_{+1}\ k_{-4}) = (k_{-2}\ k_{+3})/(k_{+2}\ k_{-3})$ (one rate constant depends on the other seven), or, in other words, $\alpha_+/\alpha_- = \beta_+/\beta_-$. Adapted from [3].

bound ligand. However, if we look at the α_- and β_- parameter values, we see opposite effects. Whereas the dissociation rate constant of the orthosteric ligand decreases when the allosteric ligand is bound ($\alpha_- = 0.5$), that of the allosteric ligand increases when the orthosteric ligand is bound ($\beta_- = 2$). Moreover, if we look at the α_+ and β_+ parameter values, we see that both are > 1 although the effect of the orthosteric ligand on the association rate constant of the allosteric modulator ($\beta_+ = 8$) is greater than that of the allosteric modulator on the association rate constant of the orthosteric ligand ($\alpha_+ = 2$).

Interestingly, for this particular $\alpha = \beta = 4$ value, many other combinations of values of the cooperativity rate constant parameters are possible, which indicates that different mechanistic hypothesis concerning microscopic events are compatible with a macroscopic outcome. For instance, the $\alpha = \beta = 4$ binding cooperativity value can also result from $\alpha_+ = 8$, $\alpha_- = 2$, $\beta_+ = 0.8$ and $\beta_- = 0.2$. Now, the effects that the allosteric modulator and the orthosteric ligand exert on each other are opposite in both the association and the dissociation rate constants ($\alpha_+>1$ and $\beta_+<1$; $\alpha_->1$ and $\beta_-<1$). See the discussion below on the relationship between residence time and agonist efficacy and [6] for an insightful review on the influence of allosteric modulators on the binding kinetics of the orthosteric ligand.

In this report[6], adenosine receptors were selected for analysis and, among others, adenosine A_3 allosteric modulators were examined. For purposes of illustration, two compounds are now taken. The first, VUF5455, behaved as an A_3 PAM by significantly retarding the dissociation rate of the agonist radioligand [^{125}I]-I-AB-MECA, from the adenosine A_3 receptor in a concentration-dependent manner.[7] Interestingly, its effect on the dissociation rate of the antagonist [^{3}H]-PSB-11 was insignificant.[6,7] These data illustrate the known dependence of allosteric modulation on the orthosteric ligand used, which is reflected in both equilibrium and kinetic assays.[1,8] The second compound, LUF6096, which bears a different chemical scaffold, also behaved as a PAM of the adenosine A_3 receptor.[9] Noteworthy, the compound was able to change the biphasic dissociation of [^{125}I]-I-AB-MECA from the receptor into a monophasic process, by slowing the kinetics of the agonist in the fast dissociating phase (k_{off_fast} = 0.089 to 0.035 min^{-1}). This effect was attributed to the stabilization of the receptor active conformation. This proposal was corroborated by a functional assay, in which LUF6096 significantly enhanced the intrinsic activity of Cl-IBMECA agonist.[6,9] These are two examples showing the effects of allosteric modulators on the dissociation rate constants of orthosteric ligands.

As recognized in [6], the influence of allosteric modulators on association rate constants of orthosteric compounds has been less investigated, which indicates that further work is needed to cover the entire kinetic space. However, the occurrence of receptor–receptor interactions in GPCRs adds a layer of complexity to the concept of allosterism.

Allostery in a heteromeric context

Allostery can arise not only from the interaction between an orthosteric and an allosteric ligand within a single receptor protein, but also from the interaction between two or more orthosteric ligands in an oligomeric receptor. Given its analogy with the previous case, at least at the mathematical level, we consider the model of receptor heterodimerization. Previously,[10] we proposed a mathematical model for receptor heterodimerization. Fig. 3a shows an adaptation of the binding part of the model in which kinetic constants for the binding of ligands A and B to the corresponding R_1 and R_2 receptor protomers in the heterodimer are included. Figs. 2 and 3 depict two models describing allostery between two ligands. Although the models are different in terms of protein structure (one or two proteins, respectively), they are equivalent to each other from the point of view of the kinetic parameters involved. This means that, in the absence of structural information about the allosteric interactions between the two bound receptor–ligands, binding experimental data are compatible with both a monomeric and a heterodimeric receptor. Therefore, the discussion above on the variability of cooperativity kinetic parameter values within a common $\alpha_+/\alpha_- = \beta_+/\beta_-$ ratio is also valid.

At this point, it is worth comparing heterodimeric receptors with homodimeric receptors. We see that a homodimeric receptor is a particular case of a heterodimeric receptor with $R_1 = R_2 = R$ or, in other words, a homodimeric receptor is a limit-

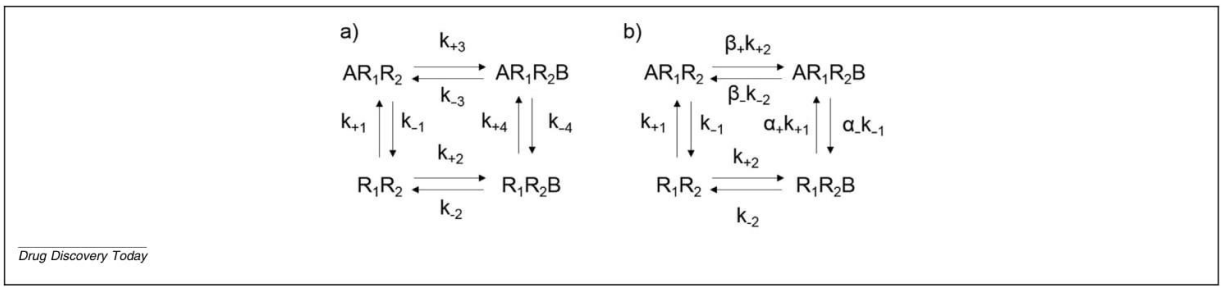

FIG. 3

Heterodimer receptor model considering only the binding part. A is a ligand selective for R_1 and B is a ligand selective for R_2. **(a)** k_{+1} to k_{+4} association and k_{-1} to k_{-4} dissociation rate constants are used. **(b)** k_{+3}, k_{-3}, k_{+4} and k_{-4} have been removed by including α_+, α_-, β_+, and β_- cooperativity rate constant parameters, with $\alpha_+ = k_{+4}/k_{+1}$, $\alpha_- = k_{-4}/k_{-1}$, $\beta_+ = k_{+3}/k_{+2}$, and $\beta_- = k_{-3}/k_{-2}$. Proceeding analogously as in Fig. 2 in the main text, it can be shown that only seven of the eight k_{+1} to k_{+4} and k_{-1} to k_{-4} rate constants are independent, $(k_{-1}\,k_{+4})/(k_{+1}\,k_{-4}) = (k_{-2}\,k_{+3})/(k_{+2}\,k_{-3})$, or, in other words, $\alpha_+/\alpha_- = \beta_+/\beta_-$. Adapted from [10].

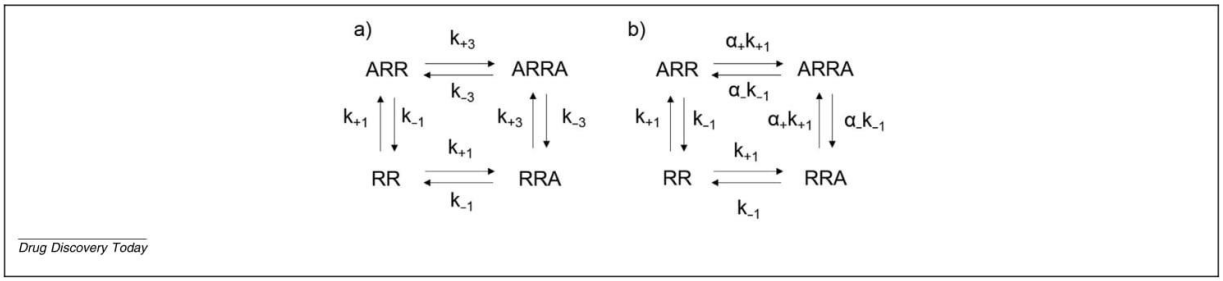

FIG. 4

Homodimer receptor model constructed from the heterodimer model shown in Fig. 3 in the main text by considering $R_1 = R_2 = R$ and $A = B$. **(a)** The set of rate constants present in Fig. 3a in the main text is reduced because $k_{+2} = k_{+1}$, $k_{-2} = k_{-1}$, $k_{+4} = k_{+3}$ and $k_{-4} = k_{-3}$. **(b)** k_{+3} and k_{-3} have been removed by including α_+ and α_- cooperativity rate constant parameters, with $\alpha_+ = k_{+3}/k_{+1}$ and $\alpha_- = k_{-3}/k_{-1}$. Comparing Fig. 3b in the main text with **(b)**, it can be seen that $k_{+2} = k_{+1}$, $k_{-2} = k_{-1}$, $\alpha_+ = \beta_+$ and $\alpha_- = \beta_-$.

FEATURE

ing case of a heterodimeric receptor in which the two protomers progressively resemble each other until finally they are the same.[11] If, in addition, only one ligand species (say A) is included, then the previous relationship between cooperativity rate constants is simplified ($\alpha_+ = \beta_+$ and $\alpha_- = \beta_-$) and only two cooperativity rate constants (α_+ and α_-) contribute to the homodimer receptor system[12] (Fig. 4).

In functional terms, a heterodimer receptor with two orthosteric sites is more complex than a monomeric receptor with an orthosteric site and an allosteric site. In the heterodimer, at least two signaling pathways are present, one for each protomer, leading to a more complex functional scenario. The present study is mainly aimed at binding. However, it appears clear that the mutual influence in binding kinetics that ligands can have on each other could affect their respective functional responses. The potential variability in cooperativity kinetic parameter values might be obscured under equilibrium conditions but can be determinant when equilibrium is not present. In this regard, it can be interesting to consider whether complex pharmacological problems, such as that described in [13] can be reanalyzed through binding kinetics.

In [13], the potential relationship of the 5HT2A-mGlu2 heteromer with schizophrenia was postulated. For this heteromer, a Gq signaling pathway is linked to the 5HT2A protomer, whereas a Gi signaling pathway is linked to the mGlu2 protomer. In healthy circumstances, a determined Gi-Gq balance is present, which is disrupted by a decrease in Gi and an increase in Gq signaling under schizophrenia conditions. The authors found that, in general, dominant (strong) agonists enhance signaling through the protomer they target as part of the heteromer but inhibit signaling of the heteromeric receptor partner. By contrast, inverse agonists inhibit signaling through the protomer they target as part of the heteromer but enhance signaling of the heteromeric receptor partner.[13] Thus, to restore normal balance in patients with schizophrenia, an mGlu2 dominant agonist would be appropriate to increase Gi signaling and additionally decrease Gq signaling. In the same way, a serotonin 5HT2A inverse agonist would be appropriate to decrease Gq signaling and additionally increase Gi signaling. Furthermore, a combination of the two ligands would synergistically favor the desired effect.[13] This behavior was modeled in [14] by using a heterodimer model under equilibrium conditions.[10] To do so, proper values for the parameters describing receptor function under equilibrium conditions were chosen; in particular, values either greater than one or lower than one for the functional cooperativities in their respective Gi or Gq signaling pathways were chosen.[14] A second layer of complexity comes from considering the mutual influence between the receptors through ligand binding. Thus, if we are including a combination of two ligands, that is, a strong agonist A for mGlu2 and an inverse agonist B for 5HT2A, a binding cooperativity $\alpha > 1$ would favor the binding of the two ligands. Interestingly, and as discussed above, a single α value can be obtained from different (α_+, α_-) and (β_+, β_-) combinations. This variability in association and dissociation cooperativity rate constants can yield striking and unexpected results for those cases not restricted to equilibrium conditions, which could provide new insights into the biological problem. Furthermore, this mechanistic knowledge can help design the appropriate protocol for combination drug therapy in neurologic and psychiatric diseases.[15]

Residence time, agonist efficacy, and allosteric interactions

Binding kinetics and, consequently, the time factor are conceptual pieces in the mechanism of drug action that should not be neglected in pharmacological research and pharmaceutical development. The time factor is present in an explicit way through the concept of residence time.[16] If we define residence time as the time a ligand spends at the receptor-binding site, many different combinations of cooperativity rate constant values can be obtained from different ligands with similar equilibrium dissociation constants. In the above proposed case ($\alpha = \beta = 4$, with $\alpha_+ = 2$, $\alpha_- = 0.5$, $\beta_+ = 8$, and $\beta_- = 2$), if no other factors are considered, there would be expected an increase in the residence time of ligand A because of the presence of ligand B ($\alpha_- < 1$) and a decrease in the residence time of ligand B because of the presence of ligand A ($\beta_- > 1$).

There are studies in the literature showing the effect of allosteric modulators on the binding kinetics of orthosteric ligands. As examples, we can mention values included in Table 7 of [6] showing the

decrease in the dissociation rate constant of the adenosine A_3 [^{125}I]-I-AB-MECA agonist exerted by some allosteric modulators, namely, 43% (VUF5455),[7] 46% (DU124183),[17] 58% (2-AG),[18] and 47% (HMA).[19] Interestingly, the HMA allosteric modulator increased 1.6-fold the dissociation rate constant of the [^{3}H]-PSB-11 antagonist.[19]

Residence time is expected to be positively correlated with agonist efficacy because the longer an agonist remains bound to the receptor, the more cycles of G-protein activation it can catalyze.[8] This proposal has been proven in some receptor systems, such as the M_3 muscarinic acetylcholine,[20] the adenosine A_{2A},[21] the adenosine A_3,[9] and the β_2 adrenergic[22] receptors, but not in others, such as the adenosine A_1[23] and dopamine D_2 [24] receptors (see [8] for a discussion). These discrepancies can be a consequence of the intrinsic complexity of the relationship between efficacy and residence time when, for example, allosteric effects coming from lipid–receptor[25,26] or receptor–receptor [11,27] interactions might be present (reviewed in [8]). These interactions might differently modulate agonist-binding kinetics, yielding a functional result that is the product of a combination of association and dissociation rate constants. In this regard, dissociation rate constants determine the time ligands spend in the receptor binding site. Yet, before dissociating from the receptor, the ligand must bind to it. Thus, dissociation and association rate constants influence drug action and should be considered together.[28,29] On the one hand, high association rate constants can be useful in pharmacological therapy to allow fast association of the drug to its target.[30,31] On the other hand, although dissociation rate constants might be fundamental for drug action, this is not always the case because, as found in [32], the prolongation of binding owing to a long drug–target residence time can only occur when the binding dissociation is slower than the pharmacokinetics (PK) elimination. PK is beyond the scope of the present report, which is limited to the study of cooperativity from a binding kinetics perspective and applied to two receptor models: a ternary complex receptor model and a heterodimer model.

Moreover and to make the picture more complex, when relating residence time with efficacy, the former should include only the time the ligand spends bound to active receptor conformations, such as, for instance, the results in [9] and reviewed in [6], in which the adenosine A_3 receptor allosteric compound LUF6096 specifically stabilized the active conformation of the receptor with a concomitant increase in the intrinsic efficacy of orthosteric agonist Cl-IBMECA. In this regard, we have to take into account that the receptor species included in Figs. 1–4 represent macroscopic terms, including populations of different receptor conformations and states. Thus, inactive and active receptor species, either free or ligand bound, are present in the system. Moreover, if we attribute the observed receptor effect to receptor–G protein interactions, G protein-bound receptors are also implicitly included in the receptor terminology.

The question arises on how the schemes in Figs. 1–4 represent this molecular variety. For the sake of simplicity, we denote R as the free receptor and LR as the ligand-bound receptor in the figures. When using mathematical models of receptor function, it is said that a stimulus is provided by each of the receptor species through the product of the concentration of the considered receptor species and the corresponding intrinsic efficacy ε ($S_R = \varepsilon_R[R]$ and $S_{LR} = \varepsilon_{LR}[LR]$); where, if L is an agonist then $\varepsilon_{LR} > \varepsilon_R$; if L is an inverse agonist then $\varepsilon_{LR} < \varepsilon_R$; and if L is a neutral antagonist $\varepsilon_{LR} = \varepsilon_R$. Then, these stimuli are summed up ($S = S_R + S_{LR}$) and converted into effect through the transducer function $E = E_m S/(S + K_E)$, with E_m the maximum possible effect and K_E the transducer parameter.[33] Yet, and speaking in molecular terms, for the receptor to generate a stimulus, it is necessary that an active conformation is formed. If R and LR now denote inactive receptor conformations, R* and LR* are the corresponding active ones. If, in addition, the G protein is the transducer protein involved in the signaling pathway, we can accept that R*G and LR*G represent the receptor species responsible for the produced stimuli and, subsequently, for the observed effect. We can consider the binding kinetics concept through the association and dissociation rate constants of the different species of the system and, most importantly, of those related with the generated stimuli. Thus, we can consider that a low LR* dissociation rate constant (high residence time of the ligand in the active receptor complex) would be beneficial to allow the binding of the G protein. By contrast, if we focus our attention on the free receptor, initial receptor stimulus through R*G precoupling would be increased by an agonist with a high association rate constant for this receptor–G protein complex, because the intrinsic efficacy of an agonist–receptor complex (ε_{LR}) is higher than that of the free receptor (ε_R) (see [34,35] for detailed descriptions of GPCR kinetics). These are two examples of microscopic events showing how either decreasing or increasing dissociation or association ligand–receptor rate constants, respectively, can both increase the efficacy of the system. These changes in ligand–receptor rate constants both will lead to a decrease in the ligand–receptor equilibrium dissociation constant. The increase in efficacy will result only if a concomitant increase in the efficiency of G protein activation is part of the process.

To quantitatively illustrate these concepts, a simulation of the biological response under the heterodimer receptor model depicted in Fig. 3 was performed.[10] To this end, the transducer function $E/E_m = S/(K_E + S)$ proposed above was used, with the total stimulus S defined as $S = \varepsilon[R_1R_2] + \varepsilon_A[AR_1R_2] + \varepsilon_B[R_1R_2B] + \varepsilon_{AB}[AR_1R_2B]$. The model has the complexity of including two ligands, A and B, which are selective for protomers R_1 and R_2, respectively. We assume that both ligands are in excess with respect to the total receptor concentration. The model includes constitutive receptor activity through the ε parameter and ligands A and B are agonists, neutral antagonists, or inverse agonists depending on the values of their intrinsic efficacies, ε_A and ε_B, compared with ε. The doubly bound receptor has an intrinsic efficacy, ε_{AB}, defined as $\varepsilon_A\varepsilon_B\delta$. In a similar way to the binding cooperativity α, δ can be greater than, lower than, or equal to one, thus reflecting the mutual allosteric interaction between the two ligands at the functional level (see [10] for a detailed description of the heterodimer model).

For the sake of simplicity, we examined the biological effect of changing the concentration of various agonists in the presence of a constant concentration of allosteric modulators (Fig. 5). To analyze the effect of binding kinetics on the transducer function, some parameters were

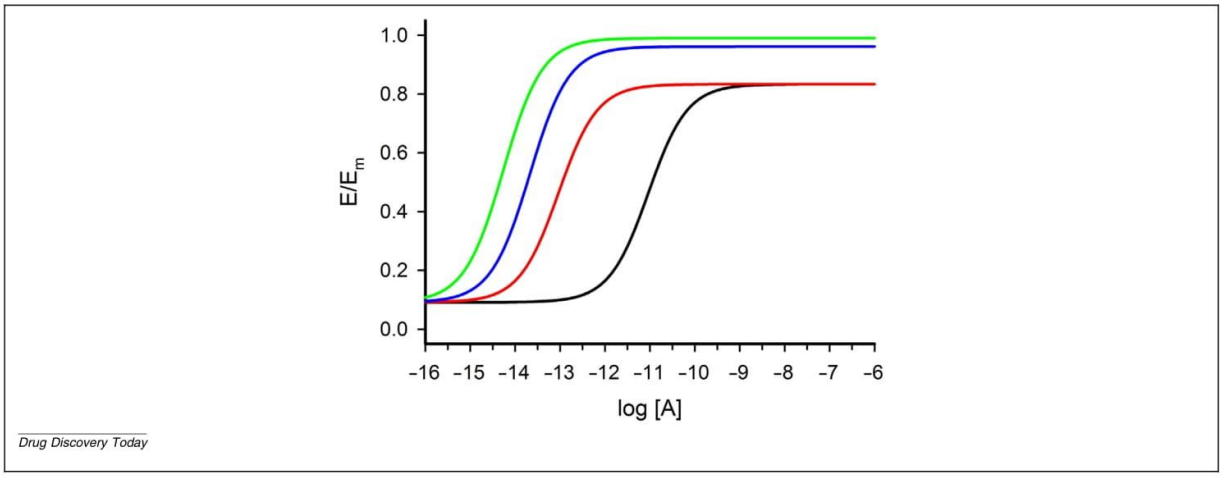

FIG. 5

Simulation of the E/E_m fractional effect resulting from the heterodimer binding kinetics model depicted in Fig. 3 in the main text. The translation of binding into function is made through the relationship $E/E_m = S/(K_E + S)$, with the total stimulus S defined as $S = \varepsilon[R_1R_2] + \varepsilon_A[AR_1R_2] + \varepsilon_B[R_1R_2B] + \varepsilon_{AB}[AR_1R_2B]$, where ε, ε_A, ε_B, and $\varepsilon_{AB} = \delta\varepsilon_A\varepsilon_B$ are the intrinsic efficacies of the free receptor, the singly bound A and B receptors, and the doubly bound receptor, respectively; δ measures the functional interaction between A and B, and K_E is the transduction factor of stimulus into effect.[10] The reference curve is the black curve, which includes the following functional parameter values: $\chi = [R_T]/K_E = 1$, $\varepsilon = 1$, $\varepsilon_A = 10$, $\varepsilon_B = 10^{-1}$, and $\delta = 5$ and the following binding kinetics parameter values: $k_{+1} = 10^7$, $k_{-1} = 10^{-1}$, $k_{+2} = 10^7$, $k_{-2} = 10^{-2}$, $k_{+4} = 2*10^7$, $k_{-4} = 10^{-3}$, $k_{+3} = 4*10^7$, $k_{-3} = 2*10^{-4}$, with M^{-1} s^{-1} and s^{-1} units for association and dissociation rate constants, respectively. Ligands A and B are an agonist and an inverse agonist, respectively, because their intrinsic efficacies are greater and lower than that of the free receptor, ε, respectively. Using cooperativity rate constant parameters, it can be seen that $\alpha_+ = k_{+4}/k_{+1} = 2$, $\alpha_- = k_{-4}/k_{-1} = 10^{-2}$, $\beta_+ = k_{+3}/k_{+2} = 4$ and $\beta_- = k_{-3}/k_{-2} = 2*10^{-2}$. Moreover, it is found that $\alpha_+/\alpha_- = \beta_+/\beta_- = 200$. The allosteric compound B is present at 10^{-6} M fixed concentration. Red curve: the dissociation rate constants k_{-4} and k_{-1} are decreased with respect to the black curve, that is, $k_{-4} = 10^{-5}$ and $k_{-1} = 10^{-3}$. The values for the cooperativity rate constant parameters are the same. The decrease in the k_{-4} and k_{-1} dissociation rate constants translates into a decrease in the dissociation equilibrium constant of A for R_1 and, consequently, into an increase in the potency of A, which is reflected in the displacement of the red curve to the left with respect to the black one. Note: the red curve can be equally obtained by an increase in the association rate constants k_{+4} and k_{+1}, with respect to the black curve, that is, $k_{+4} = 2*10^9$ and $k_{+1} = 10^9$. Blue curve: taking the black curve as a reference, k_{-4} and k_{-1} are changed in the same way as for the red curve, that is, $k_{-4} = 10^{-5}$ and $k_{-1} = 10^{-3}$, but, in addition, there is an increase in the intrinsic efficacy associated with ligand A, $\varepsilon_A = 50$. As a result, there is an increase in the potency and efficacy of the system with a displacement of the black curve both left and upwards (the maximum response is increased). Green curve: taking the black curve as a reference, k_{-4} and k_{-1} are changed in the same way as in the red curve, that is, $k_{-4} = 10^{-5}$ and $k_{-1} = 10^{-3}$, but, in addition, δ is changed from 5 to 100. As a result, there is an increase in the potency and efficacy of the system with a displacement of the black curve both left and upwards (the maximum response is increased). Note: mathematical expressions of the maximum response (the limiting value of E/E_m as [A] or [B] increase) can be found in [14].

changed with respect to a reference condition (Fig. 5, black curve). First, we considered the effects of either decreasing the dissociation rate constant of ligand A through k_{-1} and k_{-4} rate constants or increasing the association rate constant of ligand A through k_{+1} and k_{+4} rate constants (Fig. 5, red curve). The values used were chosen so that the $(k_{-1}\ k_{+4})/(k_{+1}\ k_{-4}) = (k_{-2}\ k_{+3})/(k_{+2}\ k_{-3})$, or, in other words, $\alpha_+/\alpha_- = \beta_+/\beta_-$ condition was satisfied. We can see that a change in binding kinetics has an effect only on the observed potency of ligand A (shift to the left with respect to the reference curve) with no change in efficacy (maximum response). However, as discussed above, a change in the asymptotic maximum effect can be observed if the change in binding involves a change in intrinsic efficacy. To illustrate this, the blue curve in Fig. 5 was obtained from the red curve by assuming an increase in ε_A that might result from either a decrease of the dissociation rate constants or an increase of the association rate constants of ligand A. Both changes might increase the biological response: in the former case, by assuming active AR_1R_2 and AR_1R_2B receptor states in which a low dissociation rate constant of ligand A favors the binding of the G protein; in the latter case, by assuming active R_1R_2 and R_1R_2B receptors coupled to G proteins in which ligand A presents a high association rate constant for the complexes. The maximum response displayed by the agonist A can also be increased through the mutual allosteric effect between ligands A and B. To show this point, the green curve in Fig. 5 was obtained from the red curve by assuming an increase in the δ parameter from 5 to 100. This increase in δ leads to an increase in ε_{AB} and, as a result, an increase in the concentrations of active AR_1R_2B receptor states. To generalize the concept of allosterism, we draw attention again to the conceptual similarities between the allosteric ternary complex receptor model and the heterodimer receptor model, where δ is present in both (see [36] for a discussion on operational models of allosterism).

As mentioned above, some, but not all, experimental studies have found a correlation between residence time and efficacy. In particular, we can recall on a study on the adenosine A_{2A} receptor,[21] in which the authors found a correlation between the residence time of an agonist and its functional efficacy in two assays; they also found that, compared with the equilibrium affinity, the receptor residence time of the A_2 receptor agonist had a much bet-

ter correlation to its intrinsic efficacy. Similarly, in a study of the M_3 muscarinic acetylcholine receptor involving seven agonists,[20] the authors did not find a relationship between agonist efficacy and the equilibrium binding affinity. However, when efficacy was compared with the dissociation rate constant, a high correlation was found, suggesting a relationship between the duration of agonist binding at the receptor and the intrinsic efficacy.[20]

Apart from experimental studies, a typical field in which the discussion on residence time makes particular sense is molecular dynamics (MD) simulations. In the case of a PAM in the context of binding to the receptor ($\alpha > 1$), one would expect that, in those MD simulations including both the orthosteric and the allosteric ligands, the stability of ligand–receptor interactions of both ligands in their binding sites would increase compared with their simulations in the absence of the partner ligand. However, if this were not the case, we can now understand, based on the above discussion on α_{-} and β_{-} values, that a variety of results can be obtained from the dynamic interactions between orthosteric and allosteric ligands that can be compatible with a single cooperativity binding parameter obtained at equilibrium conditions.

Concluding remarks

Inclusion of cooperativity in a binding kinetic model of allosterism has enabled us to find a mathematical expression ($\alpha_{+}/\alpha_{-} = \beta_{+}/\beta_{-}$) that links the cooperativity rate constants of the orthosteric and allosteric ligands. The expression shows that many different combinations of kinetic allosteric effects are possible for a particular value of the α binding cooperativity parameter obtained under equilibrium conditions. This assessment could help understand striking experimental results involving allosteric modulation and suggest further investigations in the field. Furthermore, the fact that allosteric modulators can exert pathway-specific effects leads to the concept of biased allosteric modulation,[37] a chemical space in which kinetically oriented drug discovery programs can help in the search for new pharmacological therapies.

Data availability

Data will be made available on request.

Acknowledgments

This project received funding from the European Union's Horizon2020 research and innovation programme under grant agreement No 848068 and by the grant PID2020-119136RB-I00 funded by MCIN/AEI/10.13039/501100011033. This publication reflects only the authors' view and the European Commission is not responsible for any use that may be made of the information it contains. A.G. has been funded by grant PID-2021-122954NB-100 funded by MCIN/AEI/10.13039/50110001 1033 and by ERDF 'A way of making Europe'.

Declaration of interests

The authors declare no competing interests.

References

1 A. Christopoulos, T. Kenakin, G protein-coupled receptor allosterism and complexing, Pharmacol Rev 54 (2002) 323–374.
2 F.J. Ehlert, Estimation of the affinities of allosteric ligands using radioligand binding and pharmacological null methods, Mol Pharmacol 33 (1988) 187–194.
3 S. Tucek, J. Proska, Allosteric modulation of muscarinic acetylcholine receptors, Trends Pharmacol Sci 16 (1995) 205–212.
4 D.A. Sykes, L.A. Stoddart, L.E. Kilpatrick, S.J. Hill, Binding kinetics of ligands acting at GPCRs, Mol Cell Endocrinol 485 (2019) 9–19.
5 D. Guo, L.H. Heitman, A.P. Ijzerman, The role of target binding kinetics in drug discovery, ChemMedChem 10 (2015) 1793–1796.
6 D. Guo, L.H. Heitman, A.P. IJzerman, Kinetic aspects of the interaction between ligand and G protein-coupled Receptor: the case of the adenosine receptors, Chem Rev 117 (2017) 38–66.
7 Z.G. Gao, J.E. Van Muijlwijk-Koezen, A. Chen, C.E. Müller, A.P. Ijzerman, K.A. Jacobson, Allosteric modulation of A(3) adenosine receptors by a series of 3-(2-pyridinyl)isoquinoline derivatives, Mol Pharmacol 60 (2001) 1057–1063.
8 J.R. Lane, L.T. May, R.G. Parton, P.M. Sexton, A. Christopoulos, A kinetic view of GPCR allostery and biased agonism, Nat Chem Biol 13 (2017) 929–937.
9 L.H. Heitman, A. Göblyös, A.M. Zweemer, R. Bakker, T. Mulder-Krieger, J.P. van Veldhoven, et al., A series of 2,4-disubstituted quinolines as a new class of allosteric enhancers of the adenosine A3 receptor, J Med Chem 52 (2009) 926–931.
10 B. Zhou, J. Giraldo, Quantifying the allosteric interactions within a G-protein-coupled receptor heterodimer, Drug Discov Today 23 (2018) 7–11.
11 B. Zhou, J. Giraldo, An operational model for GPCR homodimers and its application in the analysis of biased signaling, Drug Discovery Today 23 (2018) 1591–1595.
12 C. White, L.J. Bridge, Ligand binding dynamics for pre-dimerised G protein-coupled receptor homodimers: linear models and analytical solutions, Bull Math Biol 81 (2019) 3542–3574.
13 M. Fribourg, J.L. Moreno, T. Holloway, D. Provasi, L. Baki, R. Mahajan, et al., Decoding the signaling of a GPCR heteromeric complex reveals a unifying mechanism of action of antipsychotic drugs, Cell 147 (2011) 1011–1023.
14 J. Giraldo, B. Zhou, D. Roche, C. Gil, J. Ortiz, I. Lans, et al., Analysis of the function of receptor oligomers by operational models of agonism, in: T.E. Kenakin (Ed.), Comprehensive Pharmacology, Elsevier, Amsterdam, 2022, pp. 337–359.
15 I. Gilron, T.S. Jensen, A.H. Dickenson, Combination pharmacotherapy for management of chronic pain: from bench to bedside, Lancet Neurol 12 (2013) 1084–1095.
16 R.A. Copeland, D.L. Pompliano, T.D. Meek, Drug-target residence time and its implications for lead optimization, Nat Rev Drug Discov 5 (2006) 730–739.
17 Z.G. Gao, S.G. Kim, K.A. Soltysiak, N. Melman, A.P. IJzerman, K.A. Jacobson, Selective allosteric enhancement of agonist binding and function at human A3 adenosine receptors by a series of imidazoquinoline derivatives, Mol Pharmacol 62 (2002) 81–89.
18 J.R. Lane, M.W. Beukers, T. Mulder-Krieger, A.P. Ijzerman, The endocannabinoid 2-arachidonylglycerol is a negative allosteric modulator of the human A3 adenosine receptor, Biochem Pharmacol 79 (2010) 48–56.
19 Z.G. Gao, N. Melman, A. Erdmann, S.G. Kim, C.E. Müller, A.P. Ijzerman, et al., Differential allosteric modulation by amiloride analogues of agonist and antagonist binding at A(1) and A(3) adenosine receptors, Biochem Pharmacol 65 (2003) 525–534.
20 D.A. Sykes, M.R. Dowling, S.J. Charlton, Exploring the mechanism of agonist efficacy: a relationship between efficacy and agonist dissociation rate at the muscarinic M3 receptor, Mol Pharmacol 76 (2009) 543–551.
21 D. Guo, T. Mulder-Krieger, A.P. Ijzerman, L.H. Heitman, Functional efficacy of adenosine A_2A receptor agonists is positively correlated to their receptor residence time, British J Pharmacol 166 (2012) 1846–1859.
22 E.M. Rosethorne, M.E. Bradley, K. Gherbi, D.A. Sykes, A. Sattikar, J.D. Wright, et al., Long receptor residence time of C26 contributes to super agonist activity at the human beta2 adrenoceptor, Mol Pharmacol 89 (2016) 467–475.
23 J. Louvel, D. Guo, M. Soethoudt, T.A. Mocking, E.B. Lenselink, T. Mulder-Krieger, et al., Structure-kinetics relationships of Capadenoson derivatives as adenosine A1 receptor agonists, Eur J Med Chem 101 (2015) 681–691.
24 C.K. Herenbrink, D.A. Sykes, P. Donthamsetti, M. Canals, T. Coudrat, J. Shonberg, et al., The role of kinetic context in apparent biased agonism at GPCRs, Nat Commun 7 (2016) 10842.
25 A. Bruzzese, C. Gil, J.A.R. Dalton, J. Giraldo, Structural insights into positive and negative allosteric regulation of a G protein-coupled receptor through protein-lipid interactions, Sci Rep 8 (2018) 4456.
26 Ó. Díaz, J.A.R. Dalton, J. Giraldo, Revealing the mechanism of agonist-mediated cannabinoid receptor 1 (CB1) activation and phospholipid-mediated allosteric modulation, J Med Chem 62 (2019) 5638–5654.
27 K.J. Gregory, J. Giraldo, J. Diao, A. Christopoulos, K. Leach, Evaluation of operational models of agonism and allosterism at receptors with multiple orthosteric binding sites, Mol Pharmacol 97 (2020) 35–45.
28 G. Vauquelin, Link between a high k (on) for drug binding and a fast clinical action: to be or not to be?, MedChemComm 9 (2018) 1426–1438
29 G. Vauquelin, Effects of target binding kinetics on in vivo drug efficacy: koff, kon and rebinding, British J Pharmacol 173 (2016) 2319–2334.

30 N. Yin, J. Pei, L. Lai, A comprehensive analysis of the influence of drug binding kinetics on drug action at molecular and systems levels, Mol Biosyst 9 (2013) 1381–1389.
31 A. Schoop, F. Dey, On-rate based optimization of structure-kinetic relationship–surfing the kinetic map, Drug Discovery Today Technol 17 (2015) 9–15.
32 G. Dahl, T. Akerud, Pharmacokinetics and the drug-target residence time concept, Drug Discov Today 18 (2013) 697–707.
33 D. Roche, D. Gil, J. Giraldo, Mechanistic analysis of the function of agonists and allosteric modulators: reconciling two-state and operational models, Br J Pharmacol 169 (2013) 1189–1202.
34 R.S. Stein, F.J. Ehlert, A kinetic model of GPCRs: analysis of G protein activity, occupancy, coupling and receptor-state affinity constants, J Recept Signal Transduct Res 1–15 (2014).
35 L.D. Shea, R.R. Neubig, J.J. Linderman, Timing is everything the role of kinetics in G protein activation, Life Sci 68 (2000) 647–658.
36 J. Giraldo, Operational models of allosteric modulation: caution is needed, Trends Pharmacol Sci 36 (2015) 1–2.
37 L.M. Slosky, M.G. Caron, L.S. Barak, Biased allosteric modulators: new frontiers in GPCR drug discovery, Trends Pharmacol Sci 42 (2021) 283–299.

Óscar Díaz [1,2,3], Victor Martín [1,4], Pedro Renault [1,2,3], David Romero [5], Antoni Guillamon [4,5], Jesús Giraldo [1,2,3,*]

[1] Laboratory of Molecular Neuropharmacology and Bioinformatics, Unitat de Bioestadística and Institut de Neurociències, Universitat Autònoma de Barcelona, 08193 Bellaterra, Spain
[2] Instituto de Salud Carlos III, Centro de Investigación Biomédica en Red de Salud Mental, CIBERSAM, Spain
[3] Unitat de Neurociència Traslacional, Parc Taulí Hospital Universitari, Institut d'Investigació i Innovació Parc Taulí (I3PT), Institut de Neurociències, Universitat Autònoma de Barcelona, Spain
[4] Departament de Matemàtiques, Universitat Politècnica de Catalunya, Barcelona, Spain
[5] Centre de Recerca Matemàtica, Universitat Autònoma de Barcelona, 08193 Bellaterra, Spain

* *Corresponding author:*

5.4. Article 4: Artificial Intelligence: A Novel Approach for Drug Discovery

Trends in Pharmacological Sciences

CellPress REVIEWS

Special Issue: Rise of Machines in Medicine

Spotlight

Artificial Intelligence: A Novel Approach for Drug Discovery

Óscar Díaz, [1,2,3] James A.R. Dalton, [1,2,3] and Jesús Giraldo [1,2,3,*]

Molecular dynamics (MD) simulations can mechanistically explain receptor function. However, the enormous data sets that they may imply can be a hurdle. Plante and colleagues (*Molecules*, 2019) recently described a machine learning approach to the analysis of MD simulations. The approach successfully classified ligands and identified functional receptor motifs and thus it seems promising for mechanism-based drug discovery.

G protein-coupled receptors (GPCRs) are one of the most targeted protein families in current pharmaceutical research [1]. There can be various explanations: one is that these proteins are involved in many physiological functions and, therefore, their malfunctioning can be the cause of disease. Another is their structural and functional complexity, which is on the one hand a hurdle for drug discovery, but, on the other hand, it poses an extra level of richness to ligand space. The more subtle the desired functional effect, the more extensive and varied the molecular space for drug design will be. Different types of ligands can be found depending on the pharmacological effect sought: full and partial agonists, neutral antagonists, and full and partial inverse agonists. In addition, allosteric modulators and biased ligands are now attracting much attention because of their particular properties: the former, modulating the effects of endogenous ligands without replacing them from their binding sites [2] and the latter, differentially selecting one signaling pathway with respect to others [3].

Crystallography has contributed enormously to GPCR knowledge by determining the structures of receptors, either free or bound to agonists, antagonists, inverse agonists, and allosteric modulators, thereby helping to establish the general characteristics associated with GPCR active and inactive states (i.e., the structural motifs of receptor function) [4]. Nevertheless, crystal structures are snapshots, static views, of very flexible molecules. GPCRs, as proteins, can adopt multiple 3D forms (molecular conformations) and these forms will determine their ultimate physiological response.

Molecular dynamics (MD) simulations is a computational technique that can effectively explore the conformational space of GPCRs [5] (Figure 1). However, this technique inherently presents a 'Big Data' problem. To satisfactorily explore the GPCR conformational space, long-timescale MD simulations are needed and this implies the involvement of a large collection of molecular structures of the system. How can we manage such a large set? How can we extract relevant information from it? Although current state-of-the-art GPCR-ligand MD simulations can be analyzed effectively with conventional methods in the field of multivariate statistics, it can be assumed that if advances in computational power and force-field accuracy continue to be made as expected [6], MD simulations of GPCRs will become exclusively high throughput, as well as robustly predictive, in the near future. This means the functional effect of perhaps hundreds (or even thousands) of ligands could theoretically be characterized over microsecond (or millisecond) time-lengths in a single receptor and readily achieved in a manageable time-frame. The concomitant explosion of such simulation data will likely necessitate the implementation of automated analytical methods, such as that provided by machine learning (ML) or other artificial intelligence (AI) techniques [6,7].

In a recent article [8], Harel Weinstein's group describes a new ML approach to the analysis of MD simulations that is based on transforming MD simulation trajectories into a representation recognizable by deep learning object recognition technology. Two Class A GPCRs were chosen as targets: serotonin 5-HT2A and dopamine D2 receptors, which were studied bound to a collection of eight ligands: either full, partial, or inverse agonists. After MD simulations of each receptor–ligand complex, the atomic coordinates (XYZ) for each MD-generated conformation (or frame) were transformed into the colors of an image (RGB) that was easily recognizable by the ML algorithm. After training, the ML algorithm was able to classify the MD-generated GPCR conformations according to the pharmacological effect of the bound ligand (full, partial, inverse agonist) with high accuracy for the tested ligands (>98%). Furthermore, the contribution of each atom to the classification could be calculated, allowing the identification of the molecular determinants of receptor function (i.e., those atoms/residues of the receptor that are most important for classification according to ligand pharmacological effect). Remarkably, it was found that the most important regions responsible for receptor activation were common to both 5-HT2A and D2 receptors. In particular, the extracellular ends of transmembrane (TM) helices 4 and 5, extracellular loop 2, the intracellular ends of TM helices 5 and 6, and intracellular loops ICL2 and ICL3

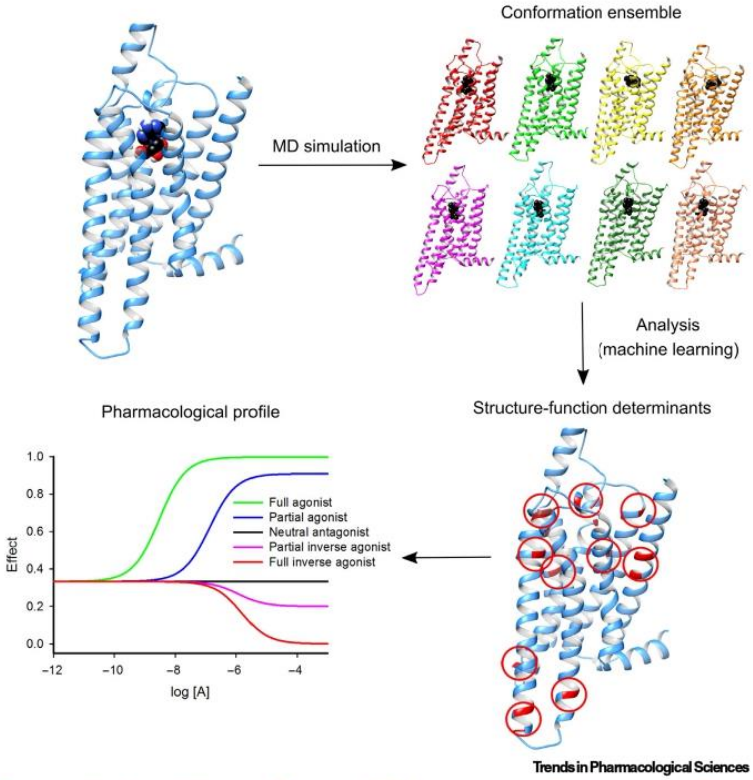

Figure 1. Workflow of Molecular Dynamics (MD) Simulations and Machine Learning-Based Approach for Ligand Classification. MD simulations of a ligand-bound G protein-coupled receptor generate multiple ligand–receptor conformations (conformational ensemble). Machine learning can be used as a powerful analysis tool to differentiate between ligand-induced receptor conformational changes, which allows the identification of residues involved in the pharmacological action of the ligand. When a large collection of ligands are studied, machine learning approaches could potentially classify the pharmacological profile of new drugs.

were identified as important for discrimination between different ligand types.

With this work, the authors added to ongoing work in the area of ligand bias, which is a pharmacological concept of fundamental importance, the appropriate quantification of which [9,10] in drug discovery programs can be key to finding drugs with the desired efficacy in the selected signaling pathway. It is expected that the coupling of MD simulations with AI approaches integrated in a general pharmacological model of drug action will be a promising tool in the design of more efficacious and safer medicines. Moreover, advances in computational capability can make this conceptual progress accessible to the simultaneous analysis of large data sets of ligands, thus making dynamic virtual screening a systematic tool for novel drug discovery.

Acknowledgments

This study was supported in part by Ministerio de Economía, Industria y Competitividad (SAF2017-87199-R).

[1]Laboratory of Molecular Neuropharmacology and Bioinformatics, Unitat de Bioestadística and Institut de Neurociències, Universitat Autònoma de Barcelona, 08193 Bellaterra, Spain
[2]Instituto de Salud Carlos III, Centro de Investigación Biomédica en Red de Salud Mental, CIBERSAM, 08193, Bellaterra, Spain
[3]Unitat de Neurociència Traslacional, Parc Taulí Hospital Universitari, Institut d'Investigació i Innovació Parc Taulí (I3PT), Institut de Neurociències, Universitat Autònoma de Barcelona, 08193 Bellaterra, Spain

*Correspondence:
Jesus.Giraldo@uab.es (J. Giraldo).

https://doi.org/10.1016/j.tips.2019.06.005

References

1. Santos, R. *et al.* (2017) A comprehensive map of molecular drug targets. *Nat. Rev. Drug Discov.* 16, 19–34
2. Thal, D.M. *et al.* (2018) Structural insights into G-protein-coupled receptor allostery. *Nature* 559, 45–53
3. Kenakin, T. (2019) Biased receptor signaling in drug discovery. *Pharmacol. Rev.* 71, 267–315
4. Weis, W.I. and Kobilka, B.K. (2018) The molecular basis of G protein-coupled receptor activation. *Annu. Rev. Biochem.* 87, 897–919
5. Hollingsworth, S.A. and Dror, R.O. (2018) Molecular dynamics simulation for all. *Neuron* 99, 1129–1143
6. Perez, A. *et al.* (2018) Simulations meet machine learning in structural biology. *Curr. Opin. Struct. Biol.* 49, 139–144
7. Degiacomi, M.T. (2019) Coupling molecular dynamics and deep learning to mine protein conformational space. *Structure* 27, 1034–1040
8. Plante, A. *et al.* (2019) A machine learning approach for the discovery of ligand-specific functional mechanisms of GPCRs. *Molecules* 24, E2097
9. Kenakin, T. *et al.* (2012) A simple method for quantifying functional selectivity and agonist bias. *ACS Chem. Neurosci.* 3, 193–203
10. Zhou, B. *et al.* (2019) Can adding constitutive receptor activity redefine biased signaling quantification? *Trends Pharmacol. Sci.* 40, 156–160

Special Issue: Rise of Machines in Medicine

Forum

Deep Learning to Therapeutically Target Unreported Complexes

Ariel Fernández [1,2,3,4,*]

The disruption of large protein–protein (PP) interfaces remains a challenge in targeted therapy. Designing drugs that compete with binding partners is daunting, especially when the structure of the protein complex is unknown.

CHAPTER 6. SUMMARY OF RESULTS AND GLOBAL DISCUSSION

In this thesis we have examined mechanisms of allosteric communication in GPCRs involving allosteric perturbations in order to provide a conceptual framework that includes structural and mathematical pieces potentially useful for drug design. The nature of allosteric perturbations is varied and can be exerted by ligand binding, receptor mutation, ion concentration, membrane lipids and protein-protein interactions. We have focused our study on cannabinoid receptor 1 (CB1).

We first started by identifying key residues involved in the activation mechanism of CB1 (Article 1). To do this, a model of the inactive state of CB1 was generated from an available crystal structure (Shao et al. 2016). To examine the dynamics of the activation process, MD simulations of inactive CB1 bound to full agonists CP-55940 and AM-11542 were performed. Active-like structures were generated during MD simulations, as shown by the outward movement of TM6, conformational change of the intracellular region of TM7 and upward axial movement of TM3. The degree of receptor activation was validated by comparing those conformations to active crystal structures and by G protein docking. We found active-like states at particular MD snapshots, but they were not stable for more than a few nanoseconds, possibly due to the absence of G protein in the MD system. Nevertheless, this allowed to identify intermediate states and thus propose the role of residues involved in the activation process. In general, the residues involved in the activation process can be classified into three groups according to their position in the receptor:

I. **Ligand contact residues**. These include the W356$^{6.48}$/F200$^{3.36}$ double-rotameric switch and S383$^{7.39}$. W356$^{6.48}$ (from the CWxP motif) and F200$^{3.36}$ form aromatic stacking interactions in the inactive state that are broken in active states. The conformational shifts of W356$^{6.48}$ (from the CWxP motif) and F200$^{3.36}$ upon activation were described before in CB1 (McAllister et al. 2004). However, by examining intermediate states in our MD simulations we proposed that W356$^{6.48}$ and F200$^{3.36}$ form a microswitch in CB1 that acts as a lock for the upward movement of TM3. Although the conformational change of W356$^{6.48}$ might be facilitated by clashes between flexible regions of the ligand bound to the inactive state of the receptor (in this case, CP-55940 and AM-11542 have a flexible alkyl chain), the shift of W356$^{6.48}$ was also observed in the free receptor. In addition to the W356$^{6.48}$/F200$^{3.36}$ double rotameric switch, CP-55940 forms a hydrogen bond with S383$^{7.39}$ in TM7. Hydrogen bonds with TM7 residues have been associated with agonism in GPCRs (Dalton, Lans, and Giraldo 2015) and S383$^{7.39}$ is critical for CP-55940 binding and function (Kapur et al. 2007). We proposed that the stability of this hydrogen bond mediates conformational changes in TM7 that lead to the approach between residues at the core of TM7 and TM3 with consequent outward movement of TM6 and rearrangement of an internal water network at the receptor core.

II. **Core residues**. At the receptor core, we observed the uncoupling of hydrophobic residues of TM3 and TM6, together with the approach of TM7 towards TM3. This involves the rearrangement of an internal water network that connects polar core residues D163$^{2.50}$, S390$^{7.46}$, S203$^{3.39}$ to intracellular residues such as N393$^{7.49}$ and Y397$^{7.53}$ from the NPxxY motif. This suggests that the hydrogen bond between CP-55940 and S383$^{7.39}$ mediates TM7 conformational change through a network of interactions that communicates TM2, TM3 and TM7.

III. **Intracellular residues**. Conformational changes observed in the intracellular side of the receptor are consistent with the opening of the G protein binding cavity, which includes outward movement of TM6 with consequent separation of ionic lock residues R214$^{3.50}$ (from the DRY motif) and D338$^{6.30}$, and shift of Y397$^{7.53}$ from the NPxxY motif towards Y294$^{5.58}$.

The large-scale conformational changes observed upon activation of CB1 are in agreement with the known mechanism of activation of class A GPCRs (Weis and Kobilka 2018; Katritch, Cherezov, and Stevens 2013; Tehan et al. 2014). However, the PIF residues of the "transmission switch", which have been proposed to play the role of transmitting conformational changes between orthosteric site and core of the receptor in other class A GPCRs, are not conserved in CB1. It should be noticed that these described conformational changes have been widely studied for class A GPCRs, but they are not universal across all GPCR classes. For example, work published in our laboratory found differences in the activation mechanism between class A and class C GPCRs (Dalton, Pin, and Giraldo 2017; Lans et al. 2020) where outward movement of TM6 was not necessary to achieve active-like states. This proposal was later validated by the crystallization of metabotropic glutamate receptor 2 and 4 (class C GPCRs) in their active conformation bound to G protein (Lin et al. 2021; Seven et al. 2021).

Interestingly, conformational changes in the microswitches did not always proceed towards receptor activation. As an example, shifts in the W356$^{6.48}$/F200$^{3.36}$ double rotameric switch were observed in the free receptor despite not leading towards active-like conformations. This is likely due to the intrinsic conformational flexibility of the receptor, and is a key concept of conformational selection (Van Eps et al. 2018; Schafer and Farrens 2015; Niesen, Bhattacharya, and Vaidehi 2011), a widely studied category of mechanisms of protein function. Conformational selection implies the presence of different receptor conformations in the ensemble that the agonist binds selectively and thus redistributes the population of conformations at the equilibrium. On the contrary, the fact that transition from the inactive to active-like states was only observed when the agonist was bound to the receptor would support an induced fit mechanism, by which the agonist binds to the inactive state of the receptor and triggers receptor activation. In the two-state model of agonism (**Equation 1**), conformational selection is represented by an agonist-mediated shift in the vertical chemical equilibria (agonist A stabilizes active

AR* by binding selectively to active R*), while induced fit is represented by the agonist-mediated shift in the horizontal chemical equilibria (agonist A increases the propensity of forming active AR* relative to inactive AR) (Giraldo 2004). Our MD simulations suggest that both mechanisms may coexist. Further studies are needed to evaluate the importance of one mechanism over the other, which has been a subject of debate (Redhair and Atkins 2021), but we hypothesize that GPCR mechanism of activation is promiscuous, and the propensity of one over the other may depend on the specific ligand and receptor. Despite agreement in the observed conformational changes in the microswitches and large-scale motion of TM6, attributing a unique time-sequence of structural changes was not possible from the MD trajectories. Instead, we interpret the conformational changes that lead towards activation of the receptor as a collective rearrangement that may follow a multitude of pathways with variable probabilities depending on the receptor and the bound ligand. This is consistent with the notion that allosteric communication has been selected in evolution in such a way to confer robustness to the signaling process of proteins (Buchenberg, Sittel, and Stock 2017), and is further supported by NMR experiments that show many intermediate conformations exist in the ensemble of conformations of CB1, described as an equilibrium between at least four states (apo, pre-active, active-like and active) that can be modulated by ligands (X. Wang et al. 2021).

Observing the transition from inactive to active-like states of CB1 allowed to perform further studies on this receptor by introducing additional perturbations. First, we evaluated the effect of a different membrane phospholipid on the activation process, in this case DOPG. DOPG is a net-negatively charged phospholipid that has been previously described to promote receptor activation in homologous class A GPCRs (Dawaliby et al. 2015; Neale et al. 2015) through charge-charge interaction with positively charged residues can be found in other class A GPCRs such as CB1. In our MD simulations, interactions with ICL3 were stably present in MD simulations of CB1 in membranes composed of DOPG, but not in membranes composed of net neutral phospholipid POPC, and have been proposed to provide an additional “pull” that favors outward movement of TM6 (Bruzzese et al. 2018). This effect was reflected in the higher frequency of outward conformations of TM6 and in the increased stability of full agonist CP-55940 bound to CB1, which indicates higher stabilization of active-like states. Thus, membrane composition can alter CB1 conformational space and as such, its function might be differentially modulated in different cell types or in regions of the membrane with different membrane composition. One of such regions of the membrane is lipid rafts, where cholesterol is a highly abundant lipid. There is evidence that suggests cholesterol behaves as a NAM for CB1 (Bari et al. 2005), and that cholesterol can bind to CB1 in an allosteric pocket that partially overlaps the binding site of CB1 allosteric modulator ORG27569 (Hua et al. 2017; Shao et al. 2019). Thus, this site in CB1 appears to be sensitive to allosteric perturbations.

We studied the effect of allosteric perturbations in this site by introducing single point F237L mutation (Article 2). This mutation has been shown to increase CP-55940 binding and it has been proposed that $F237^{4.46}$ has a role in the activation process (Shao et al. 2019). Moreover, $F237^{4.46}$ is located far from the orthosteric site and the G protein binding site, in a cavity formed by TM2, TM3 and TM4, where it is a contact residue for CB1 allosteric modulator ORG27569. Consequently, it is likely that $F237^{4.46}$ is involved in the mechanism of ORG27569 allosteric modulation. Thus, we examined the effect of F237L mutation in the context of an allosteric perturbation using the same approach as we did when observing the CP-55940-mediated activation mechanism of CB1. We observed impaired outward movement of TM6 and TM7 conformational change in MD simulations of F237L CB1 compared to *wt* CB1 with bound CP-55940, which supported the concept that allosteric perturbations have a global effect on the conformational properties of the receptor. Indeed, many residues located in distant regions were affected by F237L mutation. Moreover, we highlighted residues $D163^{2.50}$, $Y294^{5.58}$, $S390^{7.46}$ and $L349^{6.41}$ as key residues that have a role in the collective dynamics of CB1 and are affected by F237L mutation. This is in agreement with the core and intracellular residues identified in Article 1 as key residues for CB1 activation.

Among the methods employed in SBDD, MD simulations stand out as they can describe the dynamical behavior that is intrinsic in the field of allosteric modulation. Many efforts have been directed towards the characterization of the pharmacological profiles of ligands from MD trajectories, including their affinity (Lagarias et al. 2018; Y. Lee, Basith, and Choi 2018; Miller et al. 2012) and efficacy (Jung, Cho, and Yu 2018; Ricarte, Dalton, and Giraldo 2021). Given the technological advances in the last few decades in the field of computation, more sophisticated simulation methods are being developed (Limongelli, Bonomi, and Parrinello 2013). These methods would allow more precise estimations of pharmacological parameters such as ligand affinity, and thus optimize virtual screening techniques or *de novo* drug design. Unsurprisingly, because their capability of observing mechanistic aspects of physiological and pharmacological processes, as shown in Articles 1 and 2, MD simulation methods have also been applied to the estimation of kinetic parameters of drugs (S. Huang et al. 2020). In this context, we highlight the importance of the kinetics of allosteric modulation when studying MD simulations starting from a receptor bound to both an orthosteric and an allosteric ligand.

In Article 3, we show that an allosteric ligand may increase or decrease the residence time of the orthosteric ligand and vice versa, regardless of positive or negative binding cooperativity. For example, a PAM may increase the dissociation rate constant of an orthosteric agonist (decreasing residence time) while still exerting positive binding cooperativity. In other words, two ligands A (orthosteric) and B (allosteric) can have opposite effects on the binding kinetics of the other for a single binding cooperativity. This is due to the found equation $\alpha_+/\alpha_- = \beta_+/\beta_-$, where α_+ and β_+ are the cooperativity rate

constant parameters of association and α_{-} and β_{-} are the cooperativity rate constant parameters of dissociation for ligands A and B, which is derived from the relationship between rate constants of the equilibrium $(k_{-1}k_{+4})/(k_{+1}k_{-4}) = (k_{-2}k_{+3})/(k_{+2}k_{-3})$. This is in contrast with the binding cooperativity parameter $\alpha = \beta$, which is mutual, and derived from the relationship between equilibrium binding constants $K_1/K_4 = K_2/K_3$. Furthermore, the found equations are equivalent for a receptor heterodimer, where ligands A and B are both orthosteric ligands of a receptor heterodimer R_1R_2. Consequently, the effects of allosteric communication on the binding rate constants can alter the efficacy and potency of a ligand, which may be exerted through increasing or decreasing residence time. As such, careful interpretation of equilibrium parameters derived from MD simulations is required, especially when the timescale of the simulation is smaller than that required to obtain equilibrium conditions, which is common in current state of the art atomistic MD simulations of GPCRs.

In recent years, the field of GPCRs has experimented a series of breakthroughs due to the growth of publicly available databases, ranging from static crystal structures deposited in databases such as the Protein Data Bank (Berman et al. 2000) and structural alignment, drug and signaling protein binding databases such as GPCRdb (Isberg et al. 2016) and, more recently, databases for MD trajectories of GPCRs such as GPCRmd (Rodríguez-Espigares et al. 2020). The large amount of data opens the door for the use of machine learning (ML) and artificial intelligence (AI) methods for drug discovery, a field that has grown exponentially in recent years. Currently, this field includes promising applications such as accurate prediction of protein structure (Jumper et al. 2021; C. Lee, Su, and Tseng 2022), drug binding sites (Kandel, Tayara, and Chong 2021; Kozlovskii and Popov 2020) and exploration of the chemical space for novel drug discovery (Maragakis et al. 2020). ML methods have also been applied with the aim of analyzing MD trajectories (Plante et al. 2019; Noé 2018; Noé et al. 2020), but also for the development of force fields with faster algorithms (Doerr et al. 2021), which allows to increase the accuracy and/or achievable timescales of MD simulations. A perspective on the use of ML methods for the analysis was discussed in Article 4, and we expect these methods to grow with the availability of public databases and computational resources.

CHAPTER 7.

CONCLUSIONS AND FUTURE PERSPECTIVES

In this thesis, we have identified key residues that affect the structural dynamics of CB1. As such, it is important to examine the behavior of those residues when applying structure-based drug design methods. We have limited our approach to the classical cannabinoid AM-11542 and non-classical cannabinoid analog CP-55940, which are both agonists that share a similar structural scaffold. It would be interesting to evaluate the dynamical behavior of these residues in presence of an inverse agonist or a chemically different agonist to examine how these residues are affected and/or identifying common residues involved in the signaling process. Indeed, crystal structures of CB1 bound to diverse ligands are available, which provide accurate coordinates to facilitate this endeavor. These include crystal structures of CB1 bound to agonists CP-55940 (X. Wang et al. 2021), MDMB-Fubinaca (Krishna Kumar et al. 2019) and THC analogues AM841 (Hua et al. 2020; 2017) and AM11542 (Hua et al. 2017); antagonist AM6538 (Hua et al. 2016) and inverse agonist taranabant (Shao et al. 2016). Moreover, there are crystal structures of homologous CB2 available bound to antagonist AM10257 (X. Li et al. 2019), THC-like agonist AM12033 (Hua et al. 2020) and CB1/CB2 agonist WIN55,212-2 (Xing et al. 2020). In a similar manner, it would be interesting to examine how allosteric modulators affect the behavior of key residues for the dynamics of CB1. In this regard, there is a crystal structure of CB1 bound to ago-PAM ORG27569 (Shao et al. 2019) and a more recent crystal structure of CB1 bound to PAM ZCZ-011 published (Yang et al. 2022), which may provide insights into the allosteric modulation of CB1.

The structural determinants of efficacy and subtype receptor selectivity remain to be well understood. For this thesis it is relevant to consider ligand selectivity towards CB1 or CB2, as selective CB2 drug targets have been facing challenges in their development due to their lack of efficacy and/or CB1-mediated effects resulting from low CB2 selectivity (Bow and Rimoldi 2016). In this regard, ligands with intriguing pharmacology in that they are CB1 antagonists but CB2 agonist (Dhopeshwarkar et al. 2016) may be helpful for the identification of determinant chemical features of efficacy and selectivity. On the other hand, allosteric modulators may present a more practical solution to receptor subtype selectivity, as allosteric sites are generally less conserved. Among allosteric modulators of CB1, ORG27569 has an interesting pharmacological profile in that of a PAM-antagonist (Ahn, Mahmoud, and Kendall 2012; Shao et al. 2019), but insights into the allosteric modulation of CB1 may be gained from studying others (see Kulkarni et al. 2017 for a review of different CB1 allosteric modulators). As an example, cannabidiol is a non-psychoactive compound that is currently marketed as a blend of Δ^9-tetrahydrocannabinol/cannabidiol (Sativex® (Keating 2017)) and is a NAM with estimated affinity of 302 nM for CB1 (R B Laprairie et al. 2015). The new crystal structures of CB1 bound to allosteric modulators (Shao et al. 2019; Yang et al. 2022) and the crystallization of CB2 (X. Li et al. 2019; Hua et al. 2020; Xing et al. 2020) may assist in the design of further studies directed on improving the pharmacology of CB1 and CB2 allosteric modulators. As an example, understanding the molecular

determinants for efficacy and selectivity is critical for the curation of large libraries of compounds by structure-based virtual screening, which is a typical computational method employed to select potential candidates for biological assays (Ripphausen, Nisius, and Bajorath 2011; Ferreira et al. 2015).

In addition to performing MD simulations to understand CB1 allosterism under different conditions, we have developed a mathematical modeling approach under a kinetic perspective. Our aim was to set the basis of a mathematical framework in which relevant data from MD simulations could be later included. This mathematical approach is being further developed in our laboratory by solving the ordinary differential equations associated to the time-dependent models. Moreover, to connect MD simulations with time-dependent mathematical modeling, reliable parameter estimation is needed. To this end, we expect that the next future MD simulations will deliver more accurate estimates of the energy barriers associated to ligand-receptor interactions. These energies could be used to simulate the effects on the variation of the values of the rate constants included in the mathematical models. It is worth noting, that the mathematical models shown in (Ó. Díaz et al. 2023) can give a mechanistic explanation to the widely applied drug combination therapy. The fact that the combination of drugs A and B, with particular concentrations, may result in a better treatment than that coming from doubling the concentration of A or doubling the concentration of B can be explained by the synergistic effects resulting from the crosstalk between the physically interacting protomers in a heterodimer or by those resulting from the crosstalk between downstream signaling pathways. The former explanation was developed in (Zhou and Giraldo 2018; Ó. Díaz et al. 2023), the latter is currently being developed in our group.

In the longer term, our binding kinetics models might be integrated within the pharmacodynamics part of a pharmacodynamics/pharmacokinetics (PK/PD) generalized model aimed to provide a mechanistic framework for different medical treatments, in particular, drug combination therapy. For example, in an attempt to understand GPCR biology by complementary mathematical and biophysical methods, our mathematical modeling for receptor heteromerization is performed in parallel with coarse-grained MD simulations of the self-assembly of two different protomers. These studies are expected to identify the optimal interfaces between the two protomers in the heterodimer and, thus, provide the right model for subsequent all-atom MD simulations of heterodimers including different combinations of drugs (none, A, B, or A and B, in which A binds protomer 1 and B binds protomer B) for which allosterism can be studied at the atomic level.

We expect that these molecular and mathematical studies may help a better understanding of GPCR complexity and, consequently, be useful for a mechanism-based drug discovery and mechanistically explained drug therapies.

APPENDIX 1. SUPPORTING INFORMATION FOR ARTICLE 1 (5.1)

Supporting information

Revealing the mechanism of agonist-mediated cannabinoid receptor 1 (CB1) activation and phospholipid-mediated allosteric modulation

Óscar Díaz[1,2,3], James A. R. Dalton[1,2,3*] and Jesús Giraldo[1,2,3*]

[1]Laboratory of Molecular Neuropharmacology and Bioinformatics, Unitat de Bioestadística and Institut de Neurociències, Universitat Autònoma de Barcelona, 08193 Bellaterra, Spain

[2]Instituto de Salud Carlos III, Centro de Investigación Biomédica en Red de Salud Mental, CIBERSAM, 08193 Bellaterra, Spain

[3]Unitat de Neurociència Traslacional, Parc Taulí Hospital Universitari, Institut d'Investigació i Innovació Parc Taulí (I3PT), Institut de Neurociències, Universitat Autònoma de Barcelona, 08193 Bellaterra, Spain

*Corresponding authors:

James A. R. Dalton, E-mail: James.Dalton@uab.es

Jesús Giraldo, E-mail: Jesus.Giraldo@uab.es

Laboratory of Molecular Neuropharmacology and Bioinformatics, Unitat de Bioestadística and Institut de Neurociències, Universitat Autònoma de Barcelona, 08193 Bellaterra, Spain

Phone: +34 93 581 3813

Table of contents

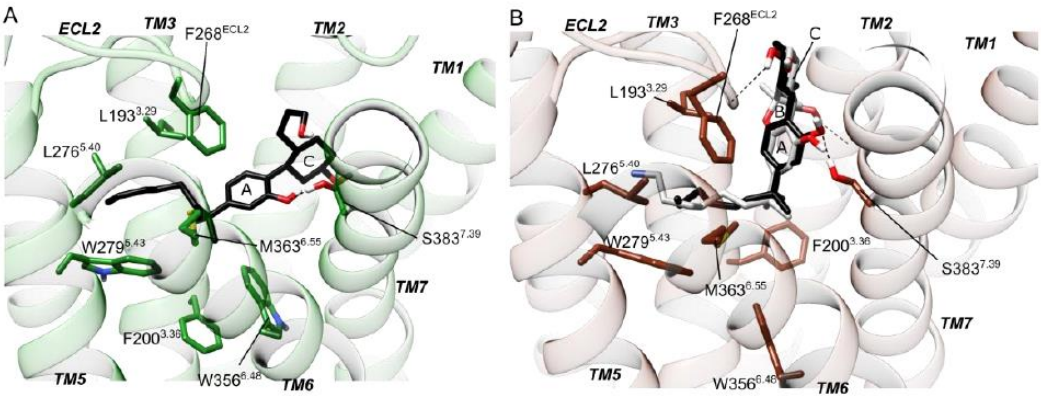

Figure S 1. Docking of CP-55940 (black sticks) into the inactive crystal structure of CB1 (A, PDB entry 5U09, green) and agonist-bound crystal structure of CB1 (B, PDB entry 5XR8, brown) compared to the co-crystallized agonist AM-841 (white sticks) with labelled A(B)C rings.

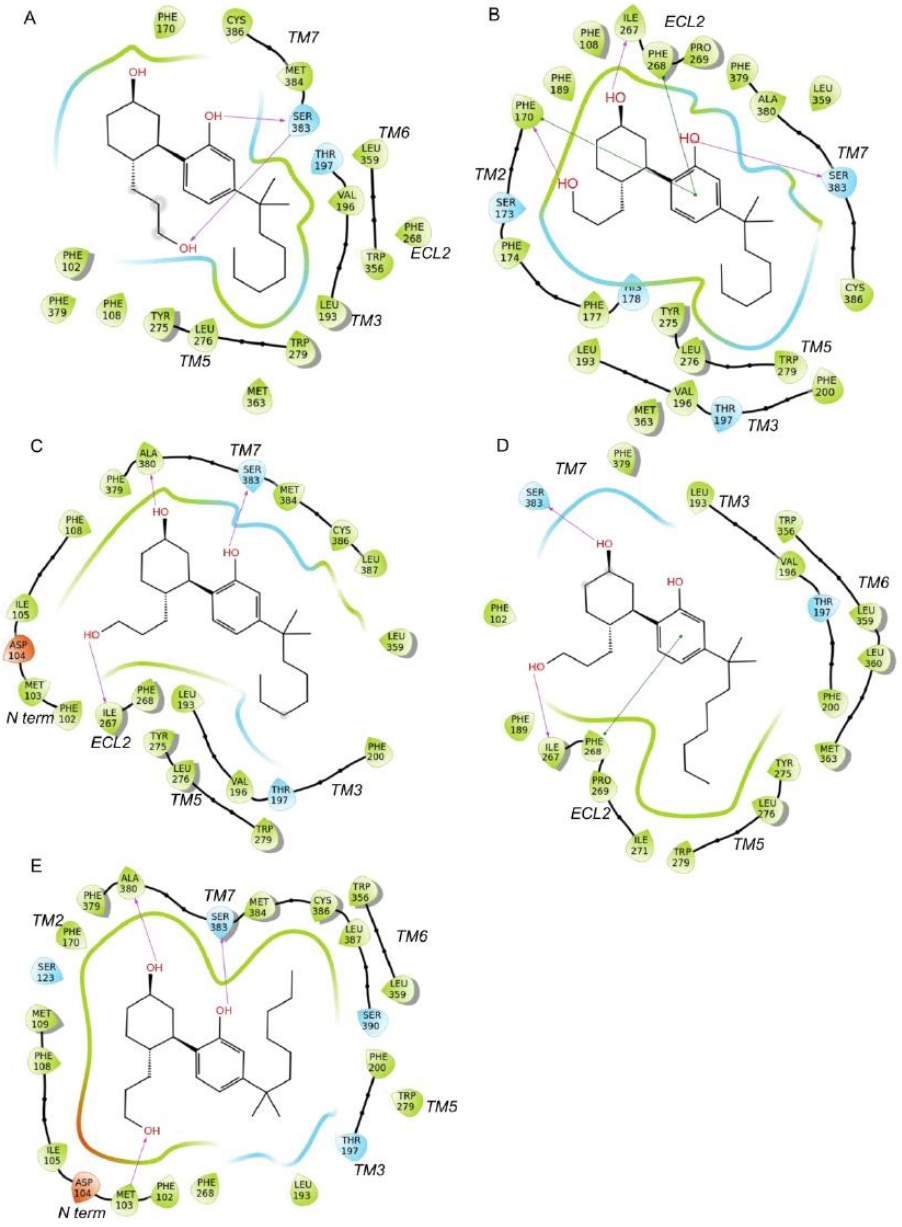

Figure S 2. Ligand-receptor interaction diagrams for CP-55940 docking solutions in the inactive CB1 crystal state (A, PDB entry 5U09) and in the agonist-bound CB1 crystal state (B, PDB entry 5XR8) and for representative conformations of cluster 1 (C), cluster 2 (D) and cluster 3 (E).

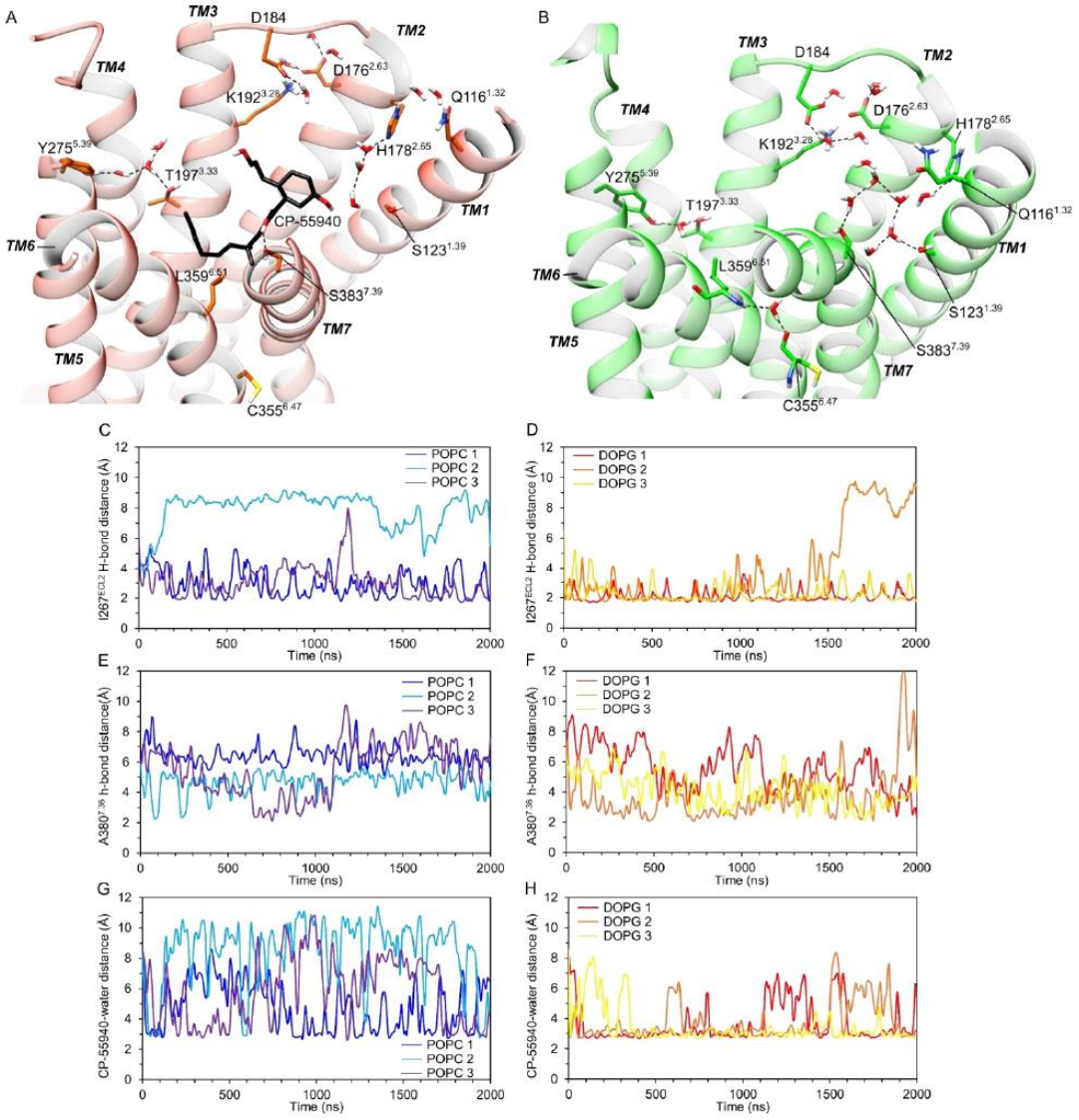

Figure S 3. Water hydration of the orthosteric pocket in CP-55940-CB1 complex (A, from simulation #1 in DOPG) and in apo CB1 (B, from simulation #2 in POPC). Hydrogen bonds represented as black dotted lines. C, D) Distance of the protein-ligand hydrogen bond between the C-ring hydroxypropyl group of CP-55940 and backbone oxygen atom of Ile267^{ECL2}, E, F) between C-ring hydroxyl group of CP-55940 and backbone oxygen atom of Ala380$^{7.36}$ and G, H) between C-ring hydroxyl group of CP-55940 and oxygen atom of the closest water molecule in MD simulations of CB1 bound to CP-55940 in POPC and DOPG membranes.

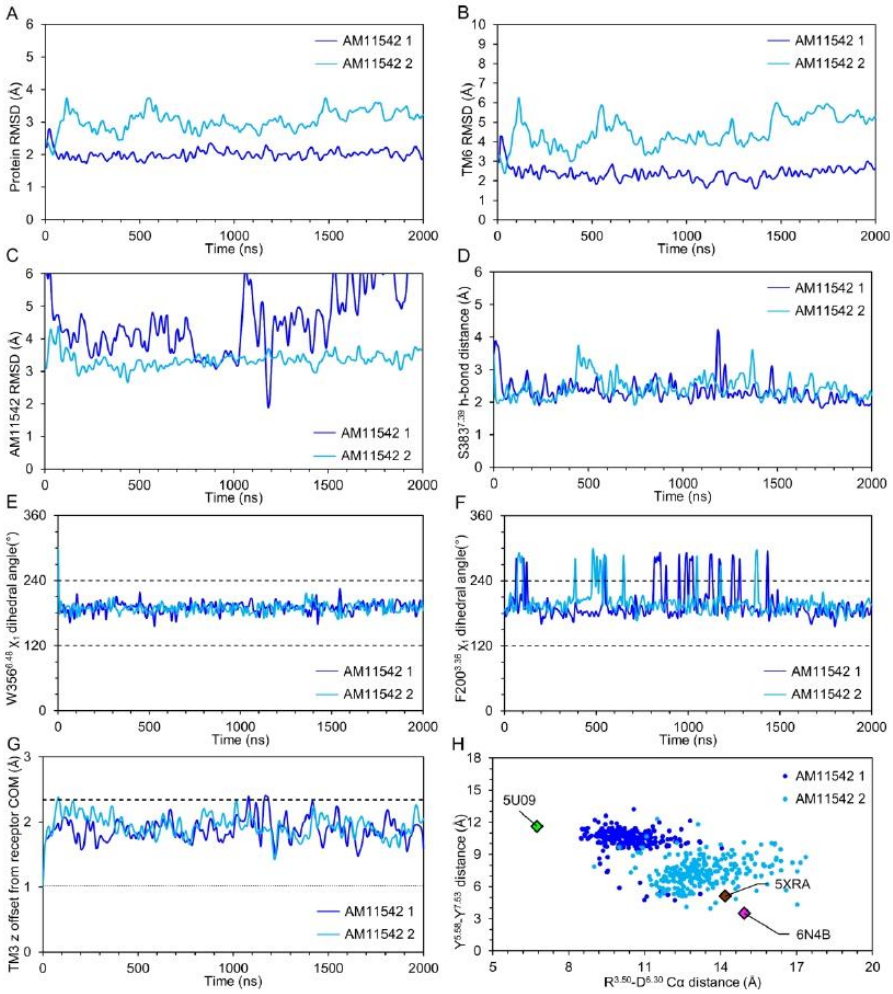

Figure S 4. Conformational change of AM-11542-CB1 complex in POPC membrane. A, B) RMSD of Cα atoms of TM helices and TM6 alone, relative to initial inactive CB1 crystal state, respectively. C) RMSD of AM-11542 excluding hydrogen atoms. D) Distance of hydrogen bond between A-ring hydroxyl group of AM-11542 and Ser383$^{7.39}$. E, F) χ_1 dihedral angle of rotameric switch residues Trp356$^{6.48}$ and Phe200$^{3.36}$. G) Offset in the Z axis (perpendicular to membrane) of center of mass of TM3 with respect to TM domain center of mass, compared to inactive crystal state (PDB entry 5U09, dotted line) and AM-11542-bound crystal (PDB entry 5XRA, dashed line). H) Distance between Tyr294$^{5.58}$ and Tyr397$^{7.53}$ with respect to ionic lock distance in conformations sampled each 8 ns of simulation time compared to relevant CB1 crystal structures (PDB entries indicated).

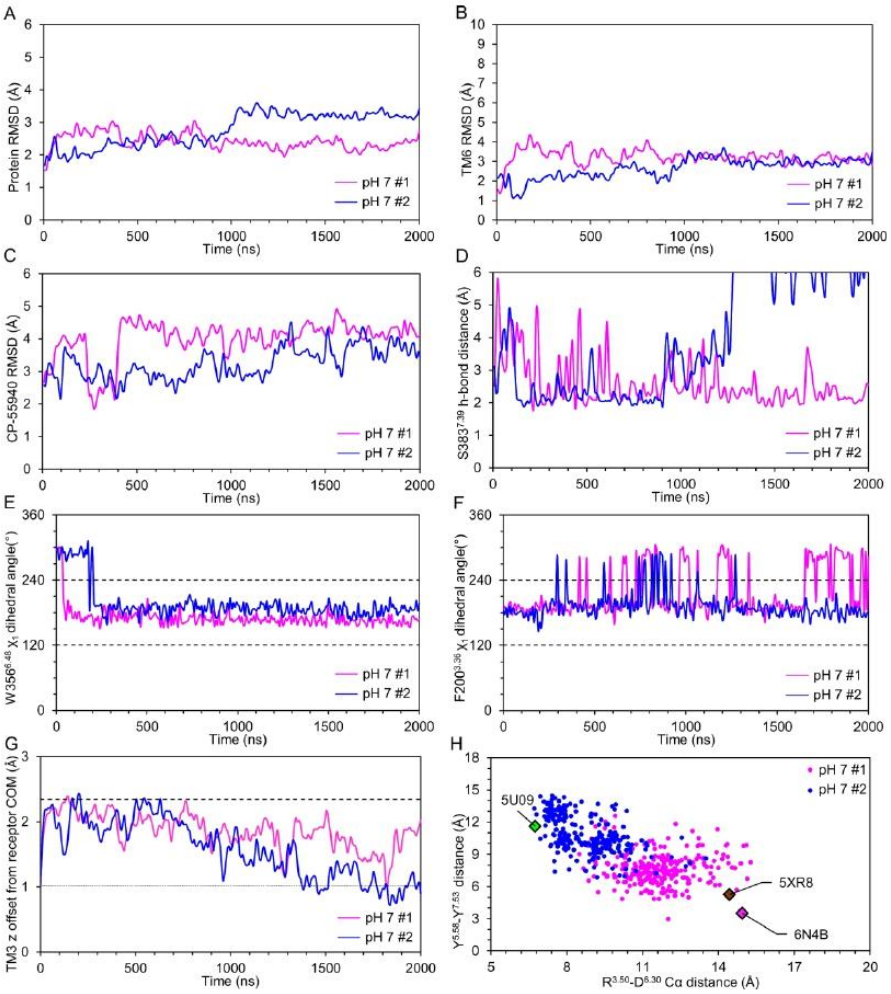

Figure S 5. Conformational change of CP-55940-CB1 complex in POPC membrane at expected major residue protonation states at pH 7.0. A, B) RMSD of Cα atoms of TM helices and TM6 alone, relative to initial inactive CB1 crystal state, respectively. C) RMSD of CP-55940 excluding hydrogen atoms. D) Distance of hydrogen bond between A-ring hydroxyl group of CP-55940 and Ser383$^{7.39}$. E, F) χ_1 dihedral angle of rotameric switch residues Trp356$^{6.48}$ and Phe200$^{3.36}$. G) Offset in Z axis (perpendicular to membrane) of the center of mass of TM3 with respect to TM domain center of mass compared to inactive (PDB entry 5U09) and active (PDB entry 6N4B) CB1 crystal states. H) Distance between Tyr294$^{5.58}$ and Tyr397$^{7.53}$ with respect to ionic lock distance in conformations sampled each 8 ns of simulation time compared to relevant crystal structures of CB1 (PDB entries indicated).

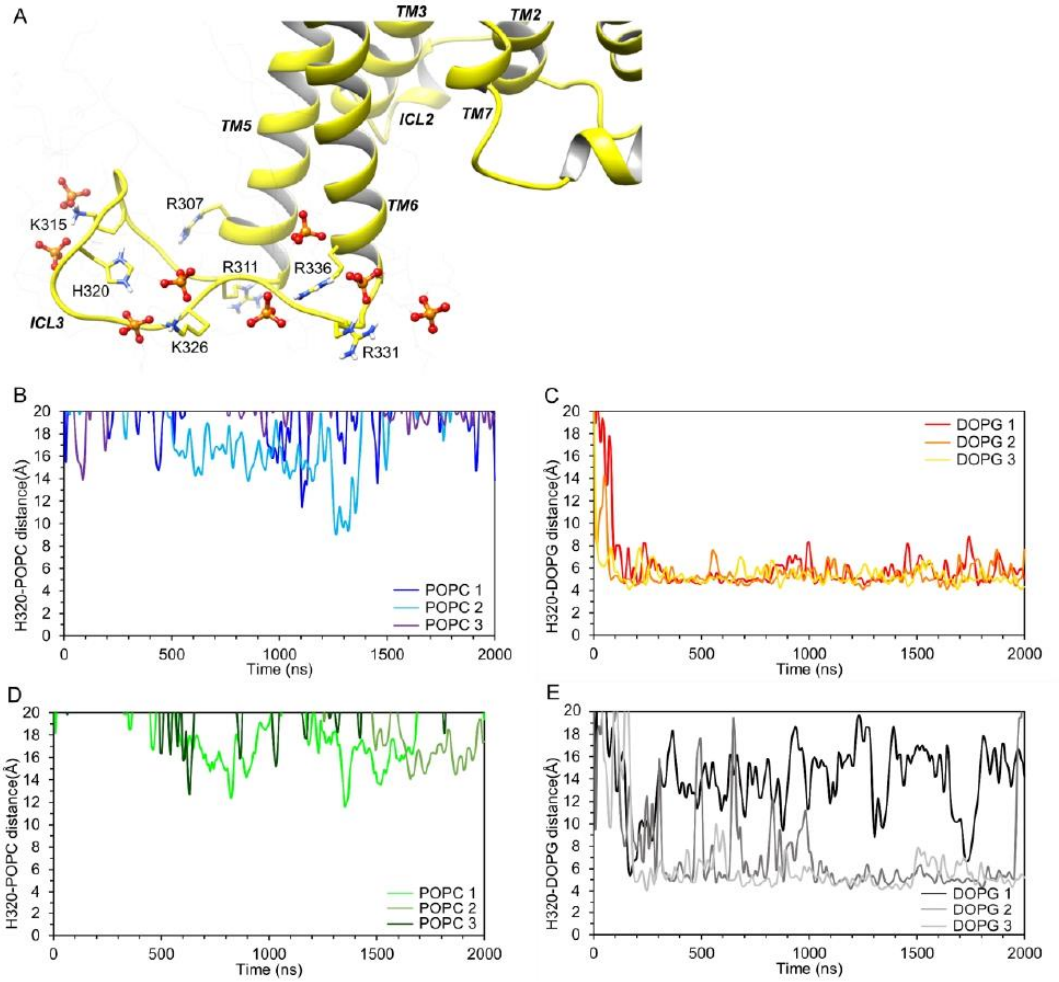

Figure S 6. A) Electrostatic interaction between DOPG phosphate groups (balls and sticks) and positively charged residues on intracellular loop 3 (ICL3) and intracellular regions of TM5 and TM6 of CB1 at 1.0 μs of MD in replica #3 in DOPG with bound CP-55940 (yellow). Distance between the center of mass of residue $His320^{ICL3}$ on ICL3 and the closest lipid phosphorus atom in MD simulations of CB1, bound to CP-55940 (B, C) or apo (D, E), in POPC (B,D) or DOPG (C,E) homogenous membranes.

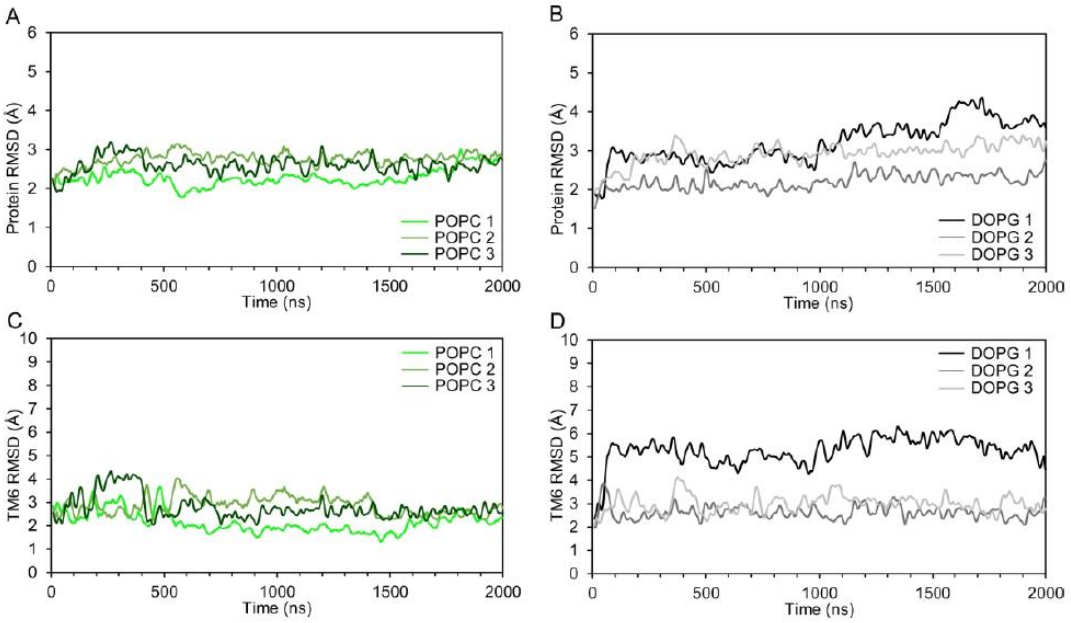

Figure S 7. Receptor conformational change during MD simulations of CB1 in the apo state in POPC (light green, olive green, dark green) and DOPG (black, grey, light grey) membranes. RMSD of Cα atoms of CB1 TM helices (A, B) and RMSD of Cα atoms of CB1 TM6 (C, D) to the initial inactive CB1 crystal state (PDB entry 5U09).

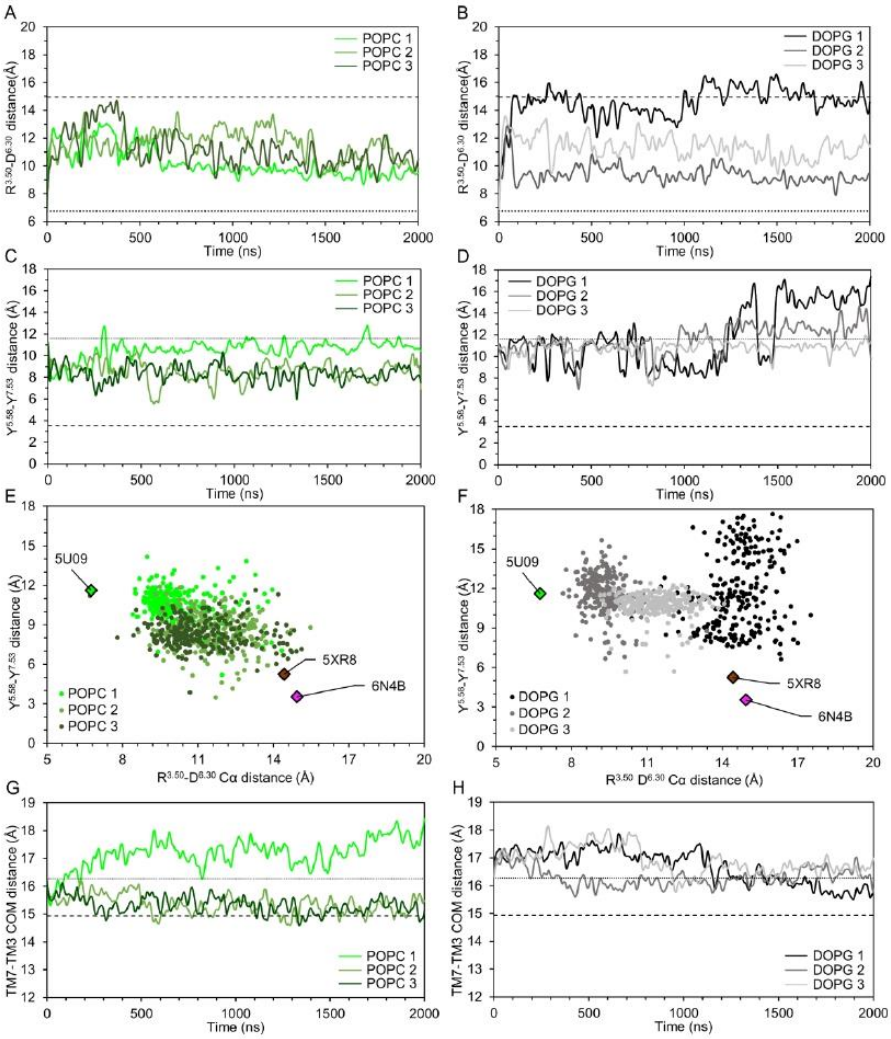

Figure S 8. Intracellular features of CB1 activation during MD simulations in the apo state in POPC (light green, olive green, dark green) and DOPG (black, grey, light grey) membranes. A, B) Distance between Cα atoms of ionic lock residues in CB1 (Arg214$^{3.50}$ and Asp338$^{6.30}$). C, D) Distance between sidechain oxygen atoms of residues Tyr294$^{5.58}$ and Tyr397$^{7.53}$. Distances in the initial inactive (PDB entry 5U09) and active (PDB entry 6N4B) CB1 crystal structures are represented as dotted and dashed lines, respectively. E, F) Distance between ionic lock residues against distance between Tyr294$^{5.58}$ and Tyr397$^{7.53}$ in CB1 conformations sampled every 8 ns of MD simulation time. Green, brown and magenta diamonds represent inactive (PDB entry 5U09), agonist-bound (PDB entry 5XR8), and active (PDB entry 6N4B) crystal structures of CB1, respectively. G, H) Distance between centers of mass of TM3 and TM7 in CB1.

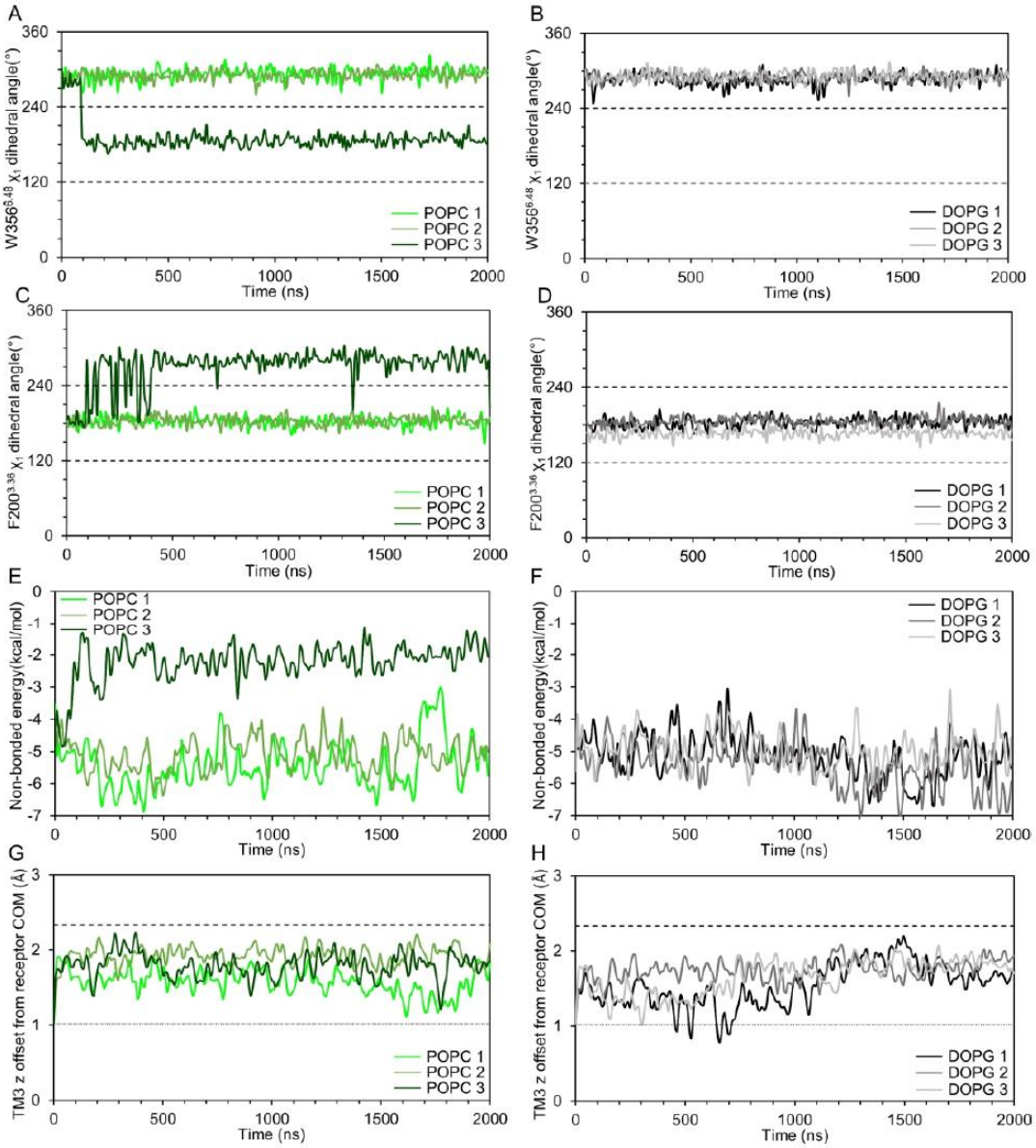

Figure S 9. χ1 dihedral angle of residues Trp356$^{6.48}$ (A, B) and Phe200$^{3.36}$ (C, D) during MD simulations of apo state CB1 in POPC and DOPG membranes. Dotted lines represent the angle intervals for *gauche*(-) (0°-120°), *trans* (120°-240°) and *gauche*(+) (240°-360°). E, F) Estimated non-bonded energy of interaction between Trp356$^{6.48}$ and Phe200$^{3.36}$ sidechains. G, H) Offset in Z-axis (perpendicular to membrane) of the center of mass of TM3 with respect to center of mass of TM helices of CB1 compared to initial inactive crystal state (dotted line, PDB entry 5U09) and active crystal state (dashed line, PDB entry 6N4B).

Table S1. Receptor-G_i protein-protein docking scores of selected MD-generated CB1 conformations compared to original crystal structures of CB1.

System	MD time (ns)	$R^{3.50}$-$D^{6.30}$ ionic-lock distance (Å)	$Y^{5.58}$-$Y^{7.53}$ distance (Å)	Receptor TM RMSD to active CB1 (Å)	G_i docking interface score (I_sc)	G_i α5 helix RMSD to active CB1 (Å)
CB1 Crystal structures						
Active CB1 (6N4B)	-	14.9	3.5	-	-9.3	1.1
Agonist-bound CB1 (5XRA) [a]	-	14.2	5.1	1.8	-6.4	8.8
Agonist-bound CB1 (5XR8) [a]	-	14.4	5.2	1.9	-6.5	4.8
Inactive CB1 (5U09)	-	6.7	11.6	3.0	-2.4	11.7
Selected CB1 MD-generated conformations						
CP-55940 and POPC #1	204	13.8	7.8	2.8	-4.5	7.3
CP-55940 and POPC #2	946	15.5	2.4	2.1	-6.4	0.9
CP-55940 and POPC #3	488	17.1	2.6	2.5	-6.5	2.4
CP-55940 and DOPG #1	608	13.8	4.1	2.8	-6.8	2.9
CP-55940 and DOPG #2	626	14.0	4.1	3.0	-8.0	3.6
CP-55940 and DOPG #3	141	12.2	9.4	2.6	-6.2	2.4
APO and POPC #1	463	12.8	10.3	2.4	-5.5	7.5
APO and POPC #2	1040	11.5	6.4	2.7	-5.5	4.1
APO and POPC #3	670	13.6	9.1	2.4	-5.6	4.4
APO and DOPG #1	1231	15.5	9.0	2.9	-4.9	4.8
APO and DOPG #2	1512	12.7	10.1	3.0	-5.3	6.9
APO and DOPG #3	1216	12.5	13.2	3.1	-5.2	10.2

[a] Crystal structures with incomplete TM5 and TM6, both missing one helix turn compared to active CB1 crystal (PDB entry 6N4B).

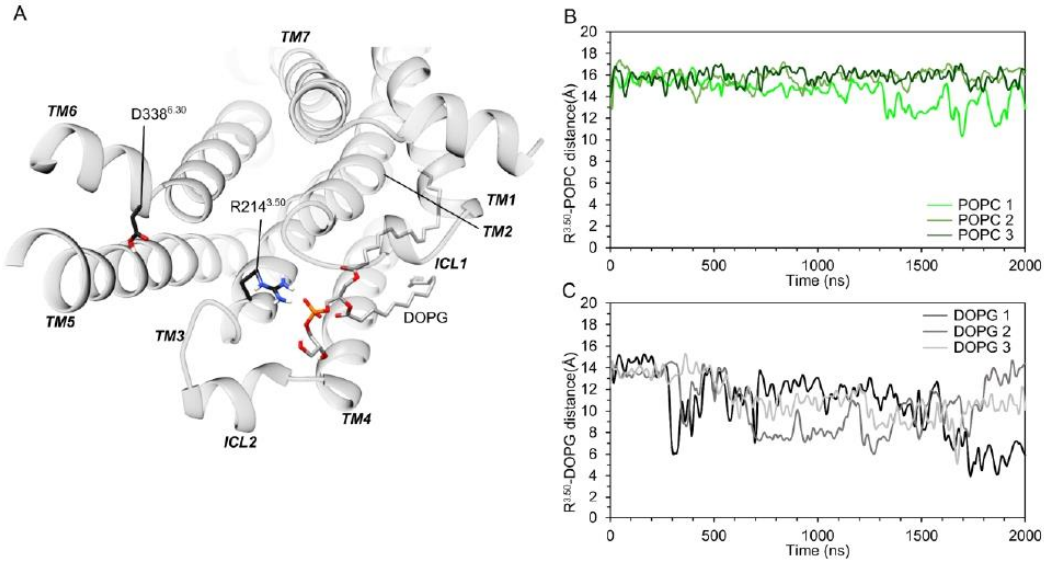

Figure S 10. A) Intracellular point of view of apo CB1 (ICL3 hidden) with conformational distortion of TM6 at 1.8 μs of MD simulation #1 in a DOPG membrane and interaction between a single DOPG molecule with residue Arg214$^{3.50}$. B, C) Distance between ionic lock residue Arg214$^{3.50}$ and phosphorus atom of the closest POPC or DOPG phospholipid headgroup.

APPENDIX 2. SUPPORTING INFORMATION FOR ARTICLE 2 (5.2)

Supporting Information

Evaluating allosteric perturbations in cannabinoid receptor 1 by *in silico* single-point mutation

Oscar Díaz[1,2,3], *Pedro Renault*[1,2,3]*, *Jesús Giraldo*[1,2,3]*

[1]Laboratory of Molecular Neuropharmacology and Bioinformatics, Unitat de Bioestadística and Institut de Neurociències, Universitat Autònoma de Barcelona, 08193 Bellaterra, Spain

[2]Instituto de Salud Carlos III, Centro de Investigación Biomédica en Red de Salud Mental, CIBERSAM, Spain

[3]Unitat de Neurociència Traslacional, Parc Taulí Hospital Universitari, Institut d'Investigació i Innovació Parc Taulí (I3PT), Institut de Neurociències, Universitat Autònoma de Barcelona, Spain

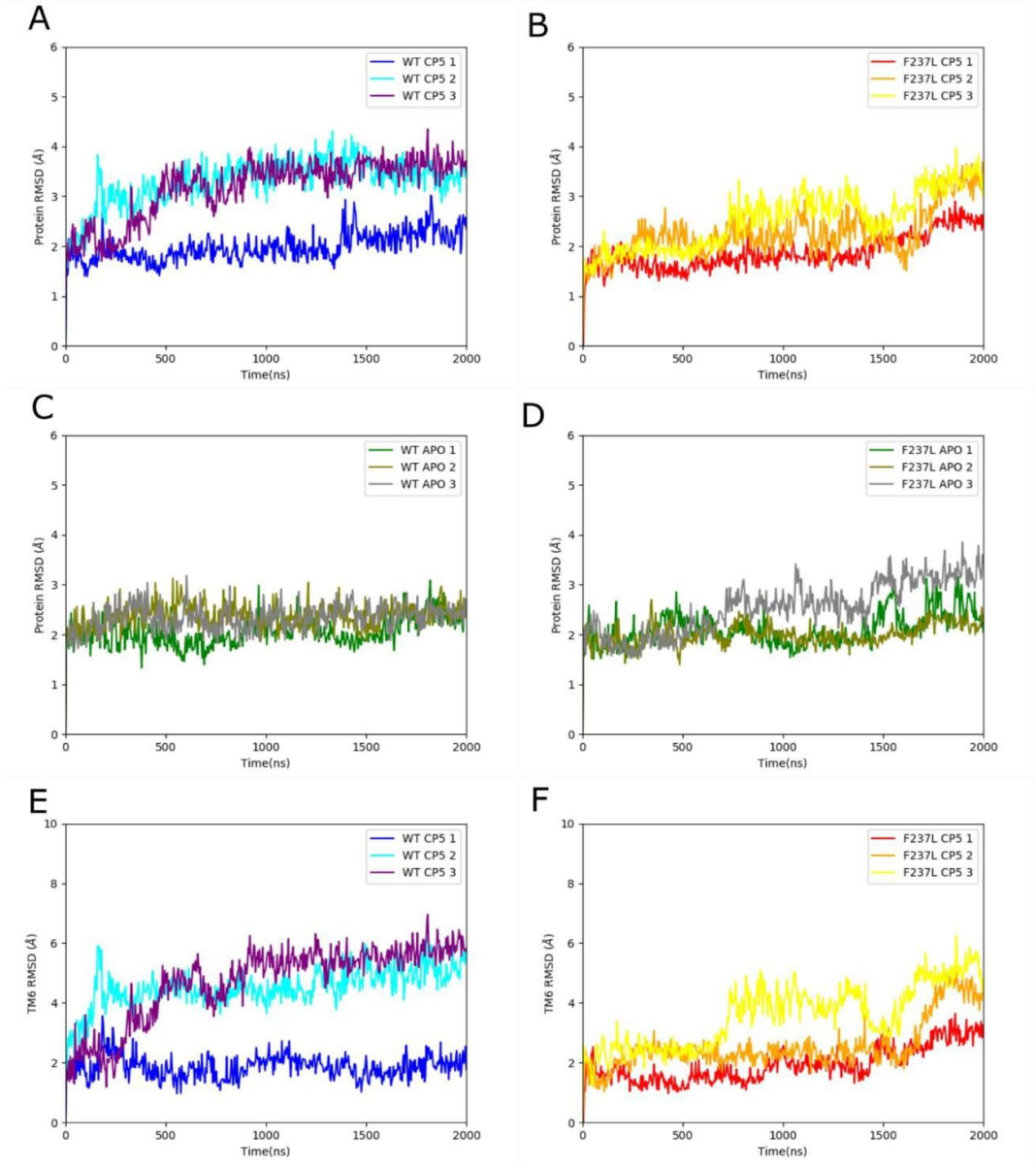

Figure S 1. Protein RMSD along the three MD trajectories for each condition: *wt* CB1 bound to CP55940* (A), F237L CB1 bound to CP55940 (B), *wt* apo CB1* (C) and F237L apo CB1 (D). TM6 RMSD for *wt** and F237L CB1 bound to CP55940 (E, F, respectively). *Data from MD simulations of *wt* CB1 taken from Díaz et al., 2019.

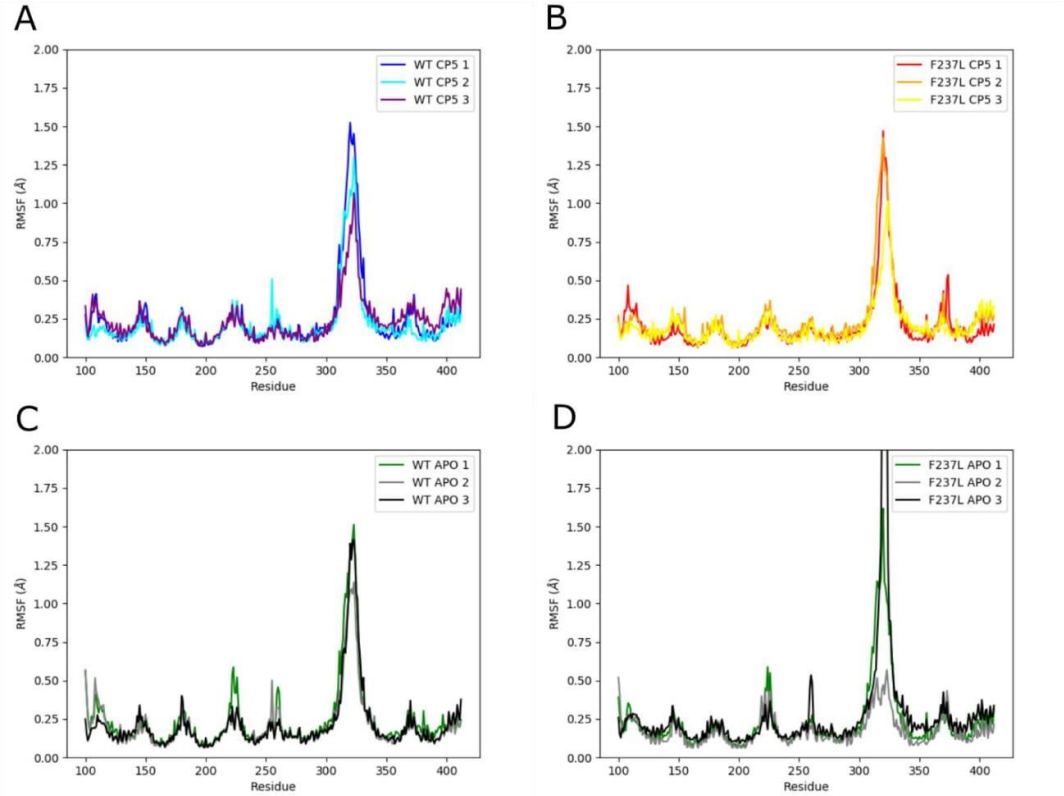

Figure S 2. Root mean square fluctuations (RMSF) in MD trajectories for each condition: *wt* CB1 bound to CP55940 * (A), F237L CB1 bound to CP55940 (B), *wt* apo CB1* (C) and F237L apo CB1 (D). *Data from MD simulations of *wt* CB1 taken from Díaz et al., 2019.

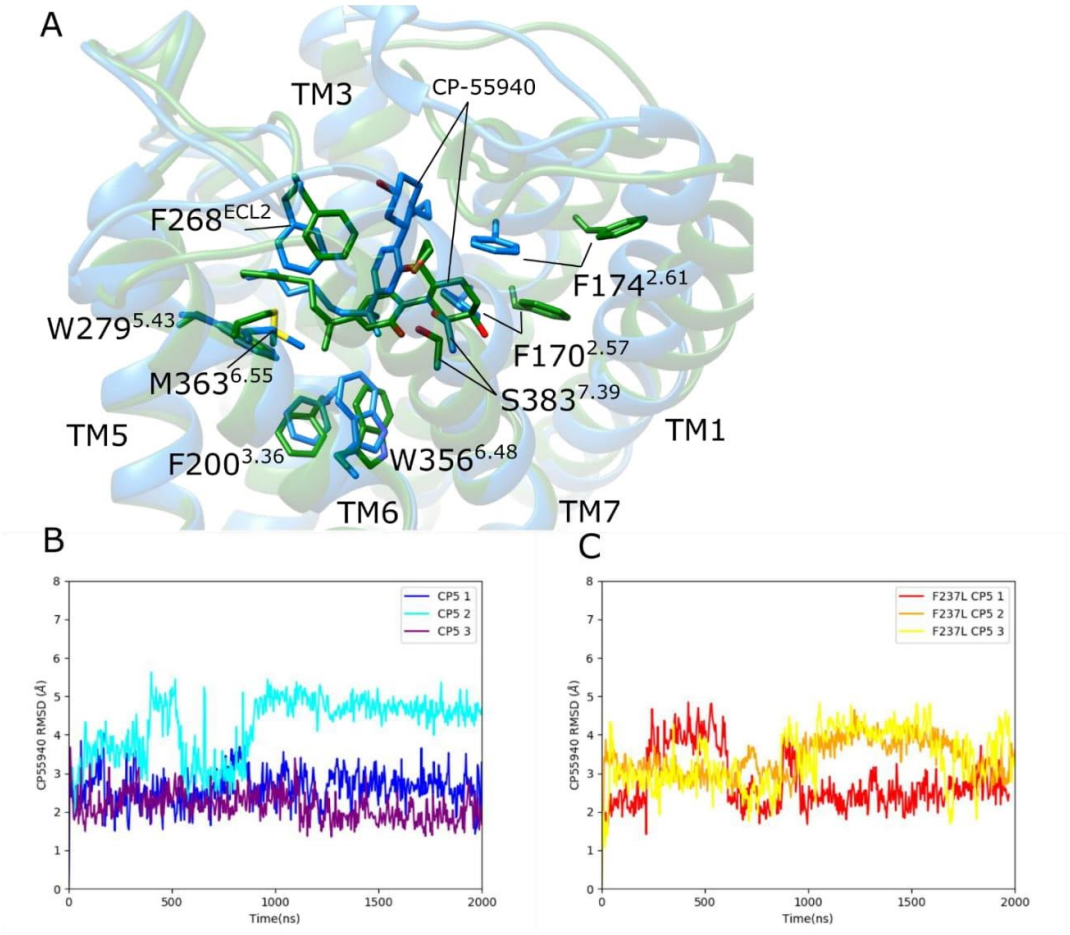

Figure S 3. A) Docking pose of CP55940 into the inactive crystal structure (PDB 5U09, green), compared to CP55940-bound crystal structure of CB1 (PDB 6KQI, blue). RMSD of CP55940 heavy atoms compared to the initial docking pose along MD trajectories of *wt* CB1* (B) and F237L CB1 (C). *Data from MD simulations of *wt* CB1 taken from Díaz et al., 2019.

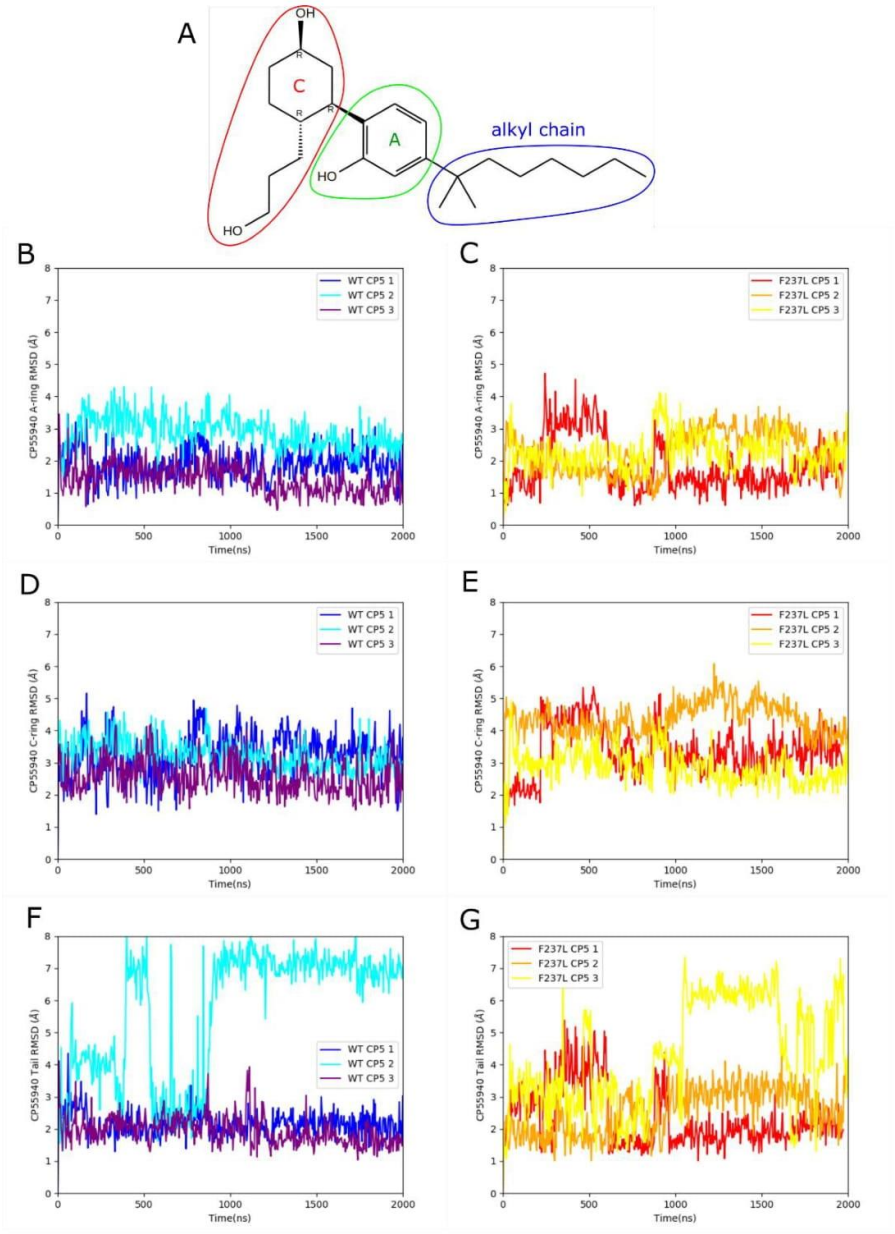

Figure S 4. Chemical structure of CP55940 with labeled A (green) and C (red) rings and alkyl chain (blue) (A). RMSD along MD trajectories of *wt** and F237L CB1 of CP55940 heavy atoms of its A ring (B,C), C ring (D, E) and alkyl chain (F, G). *Data from MD simulations from Díaz et.al 2019.

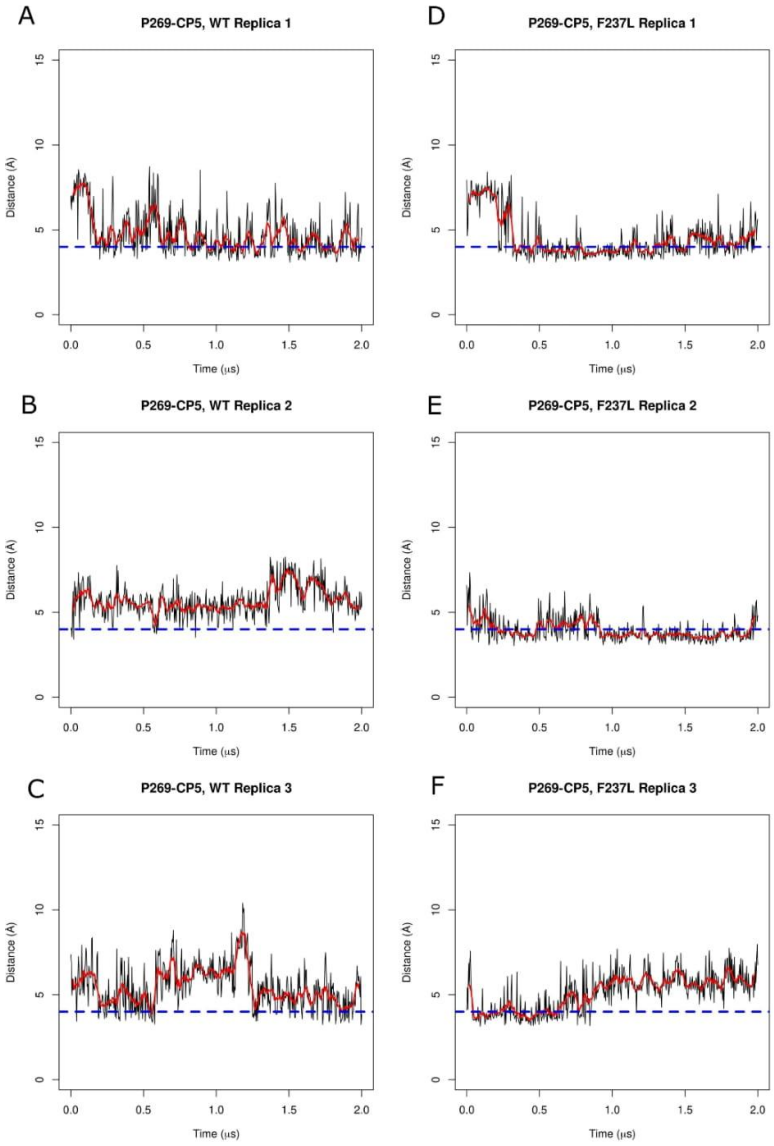

Figure S 5. Distance between CP55940 and P269^{ECL2} along MD trajectories of *wt* CB1* (A, B, C) and F237L CB1 (D, E, F). Running average represented in red. Dotted line represents the cutoff distance for contact (4 Å). *Data from MD simulations from Díaz et.al. 2019.

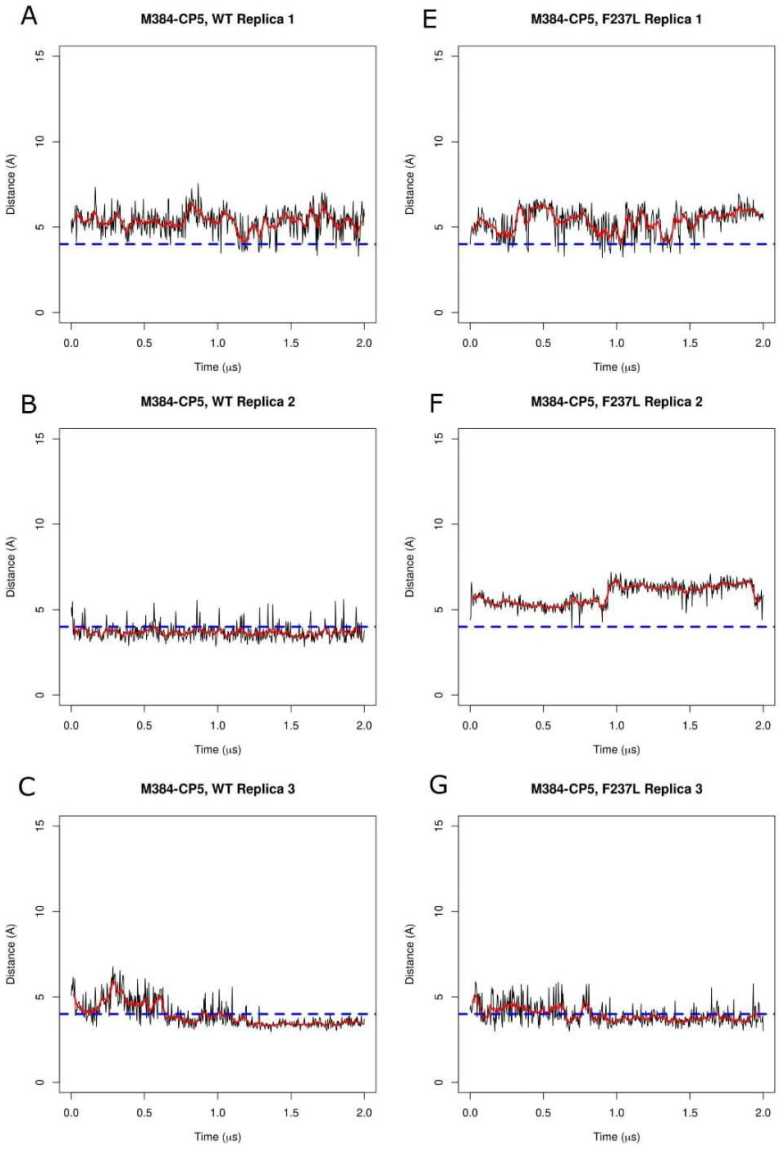

Figure S 6. Distance between CP55940 and M384$^{7.40}$ along MD trajectories of *wt* CB1* (A, B, C) and F237L CB1 (D,E,F). Running average represented in red. Dotted line represents the cutoff distance for contact (4 Å). *Data from MD simulations from Díaz et. al 2019.

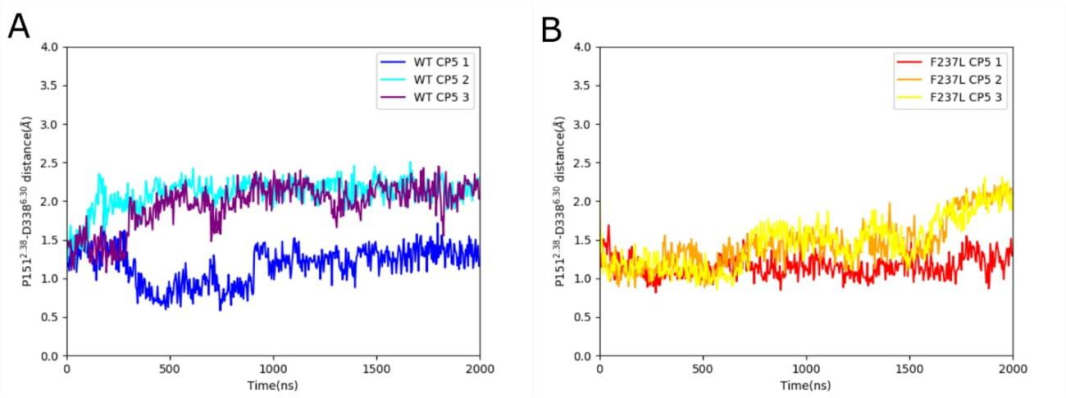

Figure S 7. Distance between P151$^{2.38}$ and D338$^{6.30}$ during MD simulations of *wt* CB1* (A) and F237L CB1 (B) bound to CP55940. *Data from MD simulations from Díaz et. al. 2019.

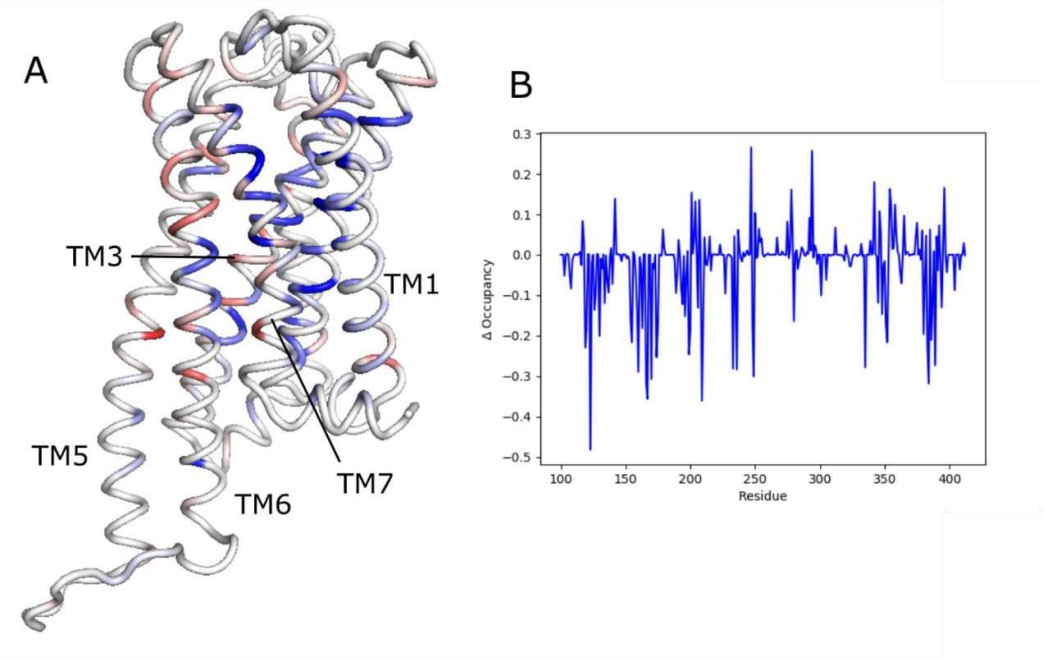

Figure S 8. Difference in per residue occupancy of water molecules between *wt** and F237L CB1 in MD simulations of CB1 bound to CP55940, represented in the initial structure (A, higher occupancy in wt CB1 in red, higher occupancy in F237L CB1 in blue). Differences are also plotted in (B), where positive values indicate higher water occupancy in the *wt* receptor. *Data from MD simulations from Díaz et. al. 2019.

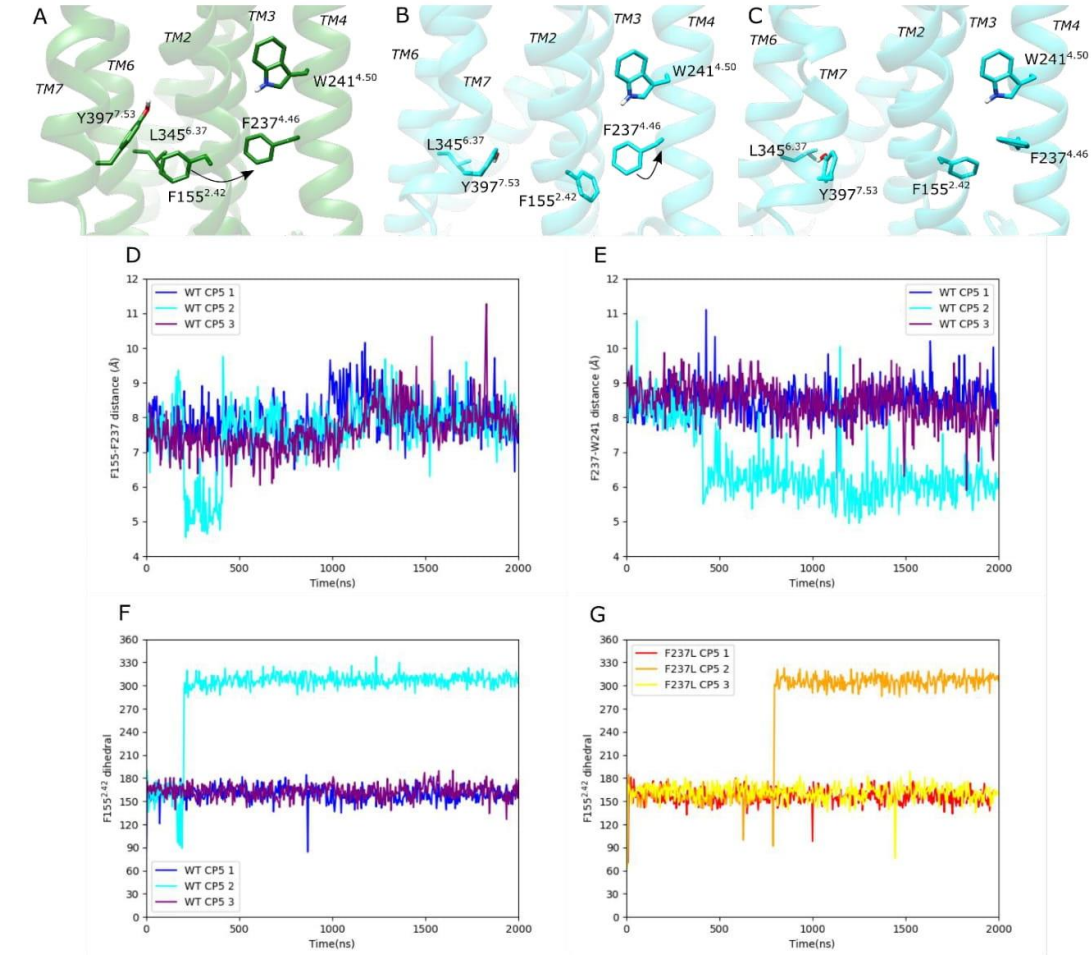

Figure S 9. A) Inactive crystal structure of CB1 (PDB ID 5U09). B, C) MD-generated conformations from replica #2 of *wt* CB1 bound to CP55940 at 280 ns and 2 µs of simulation time*, respectively. D, E) Distance between center of mass of sidechain aromatic moieties (hydrogens excluded) of $F155^{2.42}$ and $F237^{4.46}$, and $F237^{4.46}$ and $W214^{4.50}$, respectively, in MD simulations of *wt* CB1 bound to CP55940*. F, G) χ_1 dihedral angle of $F155^{2.42}$ along MD trajectories of *wt* *and F237L CB1 bound to CP55940. *MD trajectories of *wt* CB1 are taken from Díaz et al. 2019.

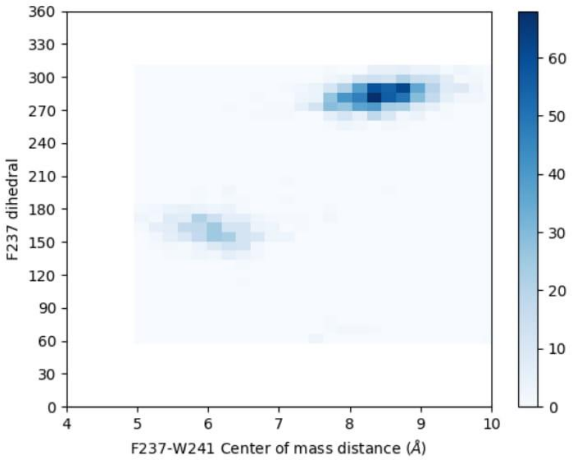

Figure S 10. Distribution of distances between the centers of mass of aromatic rings of F237$^{4.46}$ and W241$^{4.50}$ according to the χ_1 dihedral angle of F237$^{4.46}$ across 3 MD simulation replicas of CP55940-bound *wt* CB1 from Díaz et al. 2019.

Table S1. Contact frequencies of CP55940 with the receptor (residue heavy atoms within 4 Å of CP55940 heavy atoms) in MD simulations of *wt** and F237L CB1 bound to CP55940. *Data from MD simulations of *wt* CB1 taken from Díaz et. al. 2019.

Residue	***wt* 1**	***wt* 2**	***wt* 3**	**F237L 1**	**F237L 2**	**F237L 3**
F170$^{2.57}$	0.68	0.96	0.65	0.49	0.56	0.79
S173$^{2.60}$	0	0	0	0	0	0
F174$^{2.61}$	0	0.52	0	0	0	0.11
F177$^{2.64}$	0	0	0	0	0	0
H178$^{2.65\ a}$	0	0	0	0	0	0
K192$^{3.28\ a}$	0	0	0	0	0	0
L193$^{3.29}$	1	0.88	0.96	0.98	0.97	0.95
V196$^{3.32}$	1	0.93	1	1	1	0.97
T197$^{3.33}$	1	0.86	1	1	1	0.91
I267^{ECL2}	0.88	0.16	0.87	0.79	0.96	0.39
F268^{ECL2}	1	1	1	1	1	1
Y275$^{5.39\ a}$	0.99	0.19	0.9	0.79	0.55	0.4
L276$^{5.40}$	0.99	0.52	0.99	0.88	0.97	0.81

Table S1 (cont.)

Residue	*wt* 1	*wt* 2	*wt* 3	F237L 1	F237L 2	F237L 3
W279$^{5.43\ a}$	1	0.94	1	0.99	1	0.97
W356$^{6.48\ a}$	0.82	0.45	0.16	0.76	0.1	0.09
L359$^{3.51\ a}$	0.99	0.58	0.34	0.99	0.99	0.78
M363$^{6.55\ a}$	0.69	0.22	0.18	0.49	0.14	0.35
F379$^{7.35}$	0.92	1	0.55	0.86	1	0.99
S383$^{7.39\ a}$	1	1	1	1	1	1

[a] Contact absent in active crystal structure of CB1 bound to CP55940 and G protein (PDB 7WV9)

Table S*2*. Statistical analysis of differences in estimated ΔG_{bind} residue decomposition between *wt* and F237L CB1. Residues ordered by the *p*-value in a two-sample Student's t-test with unequal variance.

Residue	*p-value*
W356$^{6.48}$	0.129
T197$^{3.33}$	0.161
C382$^{7.38}$	0.221[a]
L387$^{7.43}$	0.291
Y275$^{5.39}$	0.298
F379$^{7.35}$	0.309
L359$^{6.51}$	0.328
M384$^{7.40}$	0.347
A380$^{7.36}$	0.349
S123$^{1.39}$	0.400[b]
W279$^{5.43}$	0.468
F268^{ECL2}	0.483
C386$^{7.42}$	0.522
D272^{ECL2}	0.524

Residue	*p-value*
F108$^{N\text{-}term}$	0.538
F170$^{2.57}$	0.608
I280$^{5.44}$	0.620
F102$^{N\text{-}term}$	0.682
M363$^{6.55}$	0.722
F200$^{3.36}$	0.722
I271^{ECL2}	0.723
P269^{ECL2}	0.730
L360$^{6.52}$	0.767[c]
L276$^{5.40}$	0.800
I267^{ECL2}	0.810
S383$^{7.39}$	0.846
M103$^{N\text{-}term}$	0.950
L193$^{3.29}$	0.997

[a, b, c] *p-values* correspond to two-sample Student's t-test with equal variance. Equal variance observed by a F-test with *p-values*: a: 0.006; b: 0.005; c: 0.001)

CHAPTER 8.

REFERENCES

Ahn, Kwang H., Mariam M. Mahmoud, and Debra A. Kendall. 2012. "Allosteric Modulator ORG27569 Induces CB1 Cannabinoid Receptor High Affinity Agonist Binding State, Receptor Internalization, and Gi Protein-Independent ERK1/2 Kinase Activation." *Journal of Biological Chemistry* 287 (15): 12070–82.

Alhadeff, Raphael, Igor Vorobyov, Han Wool Yoon, and Arieh Warshel. 2018. "Exploring the Free-Energy Landscape of GPCR Activation." *Proceedings of the National Academy of Sciences*, 201810316.

Altwaijry, Nojood A, Michael Baron, David W Wright, Peter V Coveney, and Andrea Townsend-Nicholson. 2017. "An Ensemble-Based Protocol for the Computational Prediction of Helix-Helix Interactions in G Protein-Coupled Receptors Using Coarse-Grained Molecular Dynamics." *Journal of Chemical Theory and Computation* 13 (5): 2254–70.

Anderson, Amy C. 2003. "The Process of Structure-Based Drug Design." *Chemistry & Biology* 10 (9): 787–97.

Ballesteros, Juan A, and Harel Weinstein. 1995. "Integrated Methods for the Construction of Three-Dimensional Models and Computational Probing of Structure-Function Relations in G Protein-Coupled Receptors." *Methods in Neurosciences* 25: 366–428.

Bari, Monica, Andrea Paradisi, Nicoletta Pasquariello, and Mauro Maccarrone. 2005. "Cholesterol-Dependent Modulation of Type 1 Cannabinoid Receptors in Nerve Cells." *Journal of Neuroscience Research* 81 (2): 275–83.

Batool, Maria, Bilal Ahmad, and Sangdun Choi. 2019. "A Structure-Based Drug Discovery Paradigm." *International Journal of Molecular Sciences* 20 (11).

Berman, Helen M, John Westbrook, Zukang Feng, Gary Gilliland, T N Bhat, Helge Weissig, Ilya N Shindyalov, and Philip E Bourne. 2000. "The Protein Data Bank." *Nucleic Acids Research* 28 (1): 235–42.

Bouvier, Michel, and Terence E. Hébert. 2014. "CrossTalk Proposal: Weighing the Evidence for Class A GPCR Dimers, the Evidence Favours Dimers." *Journal of Physiology* 592 (12): 2439–41.

Bow, Eric W, and John M Rimoldi. 2016. "The Structure – Function Relationships of Classical Cannabinoids : CB1 / CB2 Modulation." *Perspectives in Medicinal Chemistry* 8: 17–39.

Bruzzese, Agustín, Carles Gil, James A. R. Dalton, and Jesús Giraldo. 2018. "Structural Insights into

Positive and Negative Allosteric Regulation of a G Protein-Coupled Receptor through Protein-Lipid Interactions." *Scientific Reports* 8 (1): 4456.

Buchan, D W A, S M Ward, A E Lobley, T C O Nugent, K Bryson, and D T Jones. 2010. "Protein Annotation and Modelling Servers at University College London." *Nucleic Acids Research* 38 (Web Server issue): W563–68.

Buchenberg, Sebastian, Florian Sittel, and Gerhard Stock. 2017. "Time-Resolved Observation of Protein Allosteric Communication." *Proceedings of the National Academy of Sciences of the United States of America* 114 (33): E6804–11.

Carpenter, Byron, Rony Nehmé, Tony Warne, Andrew G W Leslie, and Christopher G Tate. 2017. "Structure of the Adenosine A 2A Receptor Bound to an Engineered G Protein." *Nature* 536 (7614): 104–7.

Case, David A, Thomas E Cheatham, Tom Darden, Holger Gohlke, Ray Luo, Kenneth M Merz, Alexey Onufriev, Carlos Simmerling, Bing Wang, and Robert J Woods. 2005. "The Amber Biomolecular Simulation Programs." *Journal of Computational Chemistry* 26 (16): 1668–88.

Castillo, J del, and B Katz. 1957. "Interaction at End-Plate Receptors between Different Choline Derivatives." *Proceedings of the Royal Society of London. Series B, Biological Sciences* 146 (924): 369–81.

Che, Tao, Susruta Majumdar, Saheem A. Zaidi, Pauline Ondachi, John D. McCorvy, Sheng Wang, Philip D. Mosier, et al. 2018. "Structure of the Nanobody-Stabilized Active State of the Kappa Opioid Receptor." *Cell* 172 (1–2): 55-67.e15.

Chen, Yu Chian. 2015. "Beware of Docking!" *Trends in Pharmacological Sciences* 36 (2): 78–95.

Christopoulos, Arthur, and Terry Kenakin. 2002. "G Protein-Coupled Receptor Allosterism and Complexing." *Pharmacological Reviews* 54 (2): 323–74.

Dalton, James A. R., Jean-Philippe Pin, and Jesús Giraldo. 2017. "Analysis of Positive and Negative Allosteric Modulation in Metabotropic Glutamate Receptors 4 and 5 with a Dual Ligand." *Scientific Reports* 7 (1): 4944.

Dalton, James A R, Isaias Lans, and Jesús Giraldo. 2015. "Quantifying Conformational Changes in GPCRs: Glimpse of a Common Functional Mechanism." *BMC Bioinformatics* 16: 124.

Dawaliby, Rosie, Cataldo Trubbia, Cédric Delporte, Matthieu Masureel, Pierre Van Antwerpen, Brian K Kobilka, and Cédric Govaerts. 2015. "Allosteric Regulation of G Protein–Coupled Receptor Activity by Phospholipids." *Nat. Chem. Biol.* 12 (1): 35–39.

Dhopeshwarkar, A., N. Murataeva, A. Makriyannis, A. Straiker, and K. P. Mackie. 2016. "Two Janus Cannabinoids That Are Both CB2 Agonists and CB1 Antagonists." *Journal of Pharmacology and Experimental Therapeutics* 4 (February): 300–311.

Díaz, Óscar, James A.R. Dalton, and Jesús Giraldo. 2019a. "Artificial Intelligence: A Novel Approach for Drug Discovery." *Trends in Pharmacological Sciences* 40 (8): 550–51.

———. 2019b. "Revealing the Mechanism of Agonist-Mediated Cannabinoid Receptor 1 (CB1) Activation and Phospholipid-Mediated Allosteric Modulation." *Journal of Medicinal Chemistry* 62 (11): 5638–54.

Díaz, Óscar, Victor Martín, Pedro Renault, David Romero, Antoni Guillamon, and Jesús Giraldo. 2023. "Allosteric Binding Cooperativity in a Kinetic Context." *Drug Discovery Today* 28 (2).

Díaz, Oscar, Pedro Renault, and Jesús Giraldo. 2022. "Evaluating Allosteric Perturbations in Cannabinoid Receptor 1 by in Silico Single-Point Mutation." *ACS Omega* 7 (42): 37873–84.

Doerr, Stefan, Maciej Majewski, Adrià Pérez, Andreas Krämer, Cecilia Clementi, Frank Noe, Toni Giorgino, and Gianni De Fabritiis. 2021. "TorchMD: A Deep Learning Framework for Molecular Simulations." *Journal of Chemical Theory and Computation* 17 (4): 2355–63.

Draper-Joyce, Christopher J., Maryam Khoshouei, David M. Thal, Yi-Lynn Liang, Anh T. N. Nguyen, Sebastian G. B. Furness, Hariprasad Venugopal, et al. 2018. "Structure of the Adenosine-Bound Human Adenosine A1 Receptor-Gi Complex." *Nature* 558 (7711): 559–63.

Drozdetskiy, Alexey, Christian Cole, James Procter, and Geoffrey J Barton. 2015. "JPred4: A Protein Secondary Structure Prediction Server." *Nucleic Acids Research* 43 (W1): W389–94.

Emmitte, K A. 2017. "MGlu5 Negative Allosteric Modulators: A Patent Review (2013-2016)." *Expert Opin Ther Pat* 27 (6): 691–706.

Eps, Ned Van, Christian Altenbach, Lydia N. Caro, Naomi R. Latorraca, Scott A. Hollingsworth, Ron O. Dror, Oliver P. Ernst, and Wayne L. Hubbell. 2018. "Gi- and Gs-Coupled GPCRs Show Different Modes of G-Protein Binding." *Proceedings of the National Academy of Sciences of the United States of America* 115 (10): 2383–88.

Ferreira, Leonardo G., Ricardo N. Dos Santos, Glaucius Oliva, and Adriano D. Andricopulo. 2015. *Molecular Docking and Structure-Based Drug Design Strategies*. *Molecules*. Vol. 20.

Filipek, Slawomir, Krzysztof Palczewski, Shuguang Yuan, and Horst Vogel. 2014. "Activation of G Protein-Coupled Receptors Correlates with the Formation of a Continuous Internal Water Pathway." *Nature Communications* 5 (4733): 1–10.

Foster, Daniel J, and P Jeffrey Conn. 2017. "Allosteric Modlation of GPCRs: New Insights and Potential Utility for Treatment of Schizophrenia and Other CNS Disorders." *Neuron* 94 (3): 431–46.

Friesner, Richard A, Robert B Murphy, Matthew P Repasky, Leah L Frye, Jeremy R Greenwood, Thomas A Halgren, Paul C Sanschagrin, and Daniel T Mainz. 2006. "Extra Precision Glide: Docking and Scoring Incorporating a Model of Hydrophobic Enclosure for Protein-Ligand Complexes." *Journal of Medicinal Chemistry* 49 (21): 6177–96.

Gaitonde, Supriya A, and Javier Gonza. 2017. "Contribution of Heteromerization to G Protein-Coupled Receptor Function." *Current Opinion in Pharmacology* 32: 23–31.

Ghosh, Eshan, Punita Kumari, Deepika Jaiman, and Arun K. Shukla. 2015. "Methodological Advances: The Unsung Heroes of the GPCR Structural Revolution." *Nature Reviews Molecular Cell Biology* 16 (2): 69–81.

Giraldo, Jesús. 2004. "Agonist Induction, Conformational Selection, and Mutant Receptors." *FEBS Letters* 556 (1–3): 13–18.

———. 2010. "How Inverse Can a Neutral Antagonist Be? Strategic Questions after the Rimonabant Issue." *Drug Discovery Today* 15 (11–12): 411–15.

Grant, Barry J, Ana P C Rodrigues, Karim M ElSawy, J Andrew McCammon, and Leo S D Caves. 2006. "Bio3d: An R Package for the Comparative Analysis of Protein Structures." *Bioinformatics (Oxford, England)* 22 (21): 2695–96.

Gregorio, G. Glenn, Matthieu Masureel, Daniel Hilger, Daniel S. Terry, Manuel Juette, Hong Zhao, Zhou Zhou, et al. 2017. "Single-Molecule Analysis of Ligand Efficacy in B2AR-G-Protein Activation." *Nature* 547 (7661): 68–73.

Hanson, Michael A., Vadim Cherezov, Mark T. Griffith, Christopher B. Roth, Veli Pekka Jaakola, Ellen Y.T. Chien, Jeffrey Velasquez, Peter Kuhn, and Raymond C. Stevens. 2008. "A Specific Cholesterol Binding Site Is Established by the 2.8 Å Structure of the Human B2-Adrenergic

Receptor." *Structure* 16 (6): 897–905.

Harvey, M. J., G. Giupponi, and G. De Fabritiis. 2009. "ACEMD: Accelerating Biomolecular Dynamics in the Microsecond Time Scale." *Journal of Chemical Theory and Computation* 5 (6): 1632–39.

Hiller, Christine, Julia Kühhorn, and Peter Gmeiner. 2013. "Class A G-Protein-Coupled Receptor (GPCR) Dimers and Bivalent Ligands." *Journal of Medicinal Chemistry* 56 (17): 6542–59.

Hu, Jianping, Zhiwei Feng, Shifan Ma, Yu Zhang, Qin Tong, Mohammed Hamed Alqarni, Xiaojun Gou, and Xiang Qun Xie. 2016. "Difference and Influence of Inactive and Active States of Cannabinoid Receptor Subtype CB2: From Conformation to Drug Discovery." *Journal of Chemical Information and Modeling* 56 (6): 1152–63.

Hua, Tian, Xiaoting Li, Lijie Wu, Christos Iliopoulos-Tsoutsouvas, Yuxia Wang, Meng Wu, Ling Shen, et al. 2020. "Activation and Signaling Mechanism Revealed by Cannabinoid Receptor-Gi Complex Structures." *Cell* 180 (4): 655-665.e18.

Hua, Tian, Kiran Vemuri, Spyros P. Nikas, Robert B. Laprairie, Yiran Wu, Lu Qu, Mengchen Pu, et al. 2017. "Crystal Structures of Agonist-Bound Human Cannabinoid Receptor CB1." *Nature* 547 (7664): 468–71.

Hua, Tian, Kiran Vemuri, Mengchen Pu, Lu Qu, Gye Won Han, Yiran Wu, Suwen Zhao, et al. 2016. "Crystal Structure of the Human Cannabinoid Receptor CB1." *Cell* 167 (3): 750–62.

Huang, Jing, and Alexander D MacKerell. 2013. "CHARMM36 All-Atom Additive Protein Force Field: Validation Based on Comparison to NMR Data." *Journal of Computational Chemistry* 34 (25): 2135–45.

Huang, Shuheng, Linxin Chen, Hu Mei, Duo Zhang, Tingting Shi, Zuyin Kuang, Yu Heng, Lei Xu, and Xianchao Pan. 2020. "In Silico Prediction of the Dissociation Rate Constants of Small Chemical Ligands by 3D-Grid-Based Volsurf Method." *International Journal of Molecular Sciences* 21 (7).

Humphrey, W, A Dalke, and K Schulten. 1996. "VMD: Visual Molecular Dynamics." *Journal of Molecular Graphics* 14 (1): 33–38.

Isberg, Vignir, Chris de Graaf, Andrea Bortolato, Vadim Cherezov, Vsevolod Katritch, Fiona H Marshall, Stefan Mordalski, et al. 2015. "Generic GPCR Residue Numbers - Aligning Topology Maps While Minding the Gaps." *Trends in Pharmacological Sciences* 36 (1): 22–31.

Isberg, Vignir, Stefan Mordalski, Christian Munk, Krzysztof Rataj, Kasper Harpsøe, Alexander S Hauser, Bas Vroling, Andrzej J Bojarski, Gert Vriend, and David E Gloriam. 2016. "GPCRdb: An Information System for G Protein-Coupled Receptors." *Nucleic Acids Research* 44 (Database issue): D356–64.

Jaiteh, Mariama, Ismael Rodríguez-Espigares, Jana Selent, and Jens Carlsson. 2020. "Performance of Virtual Screening against GPCR Homology Models: Impact of Template Selection and Treatment of Binding Site Plasticity." *PLoS Computational Biology* 16 (3): 1–25.

Janero, David R, and Alexandros Makriyannis. 2009. "Cannabinoid Receptor Antagonists: Pharmacological Opportunities, Clinical Experience, and Translational Prognosis." *Expert Opinion on Emerging Drugs* 14 (1): 43–65.

Jo, Sunhwan, Taehoon Kim, Vidyashankara G Iyer, and Wonpil Im. 2008. "CHARMM-GUI: A Web-Based Graphical User Interface for CHARMM." *Journal of Computational Chemistry* 29 (11): 1859–65.

Jones, K A, B Borowsky, J A Tamm, D A Craig, M M Durkin, M Dai, W J Yao, et al. 1998. "GABA(B) Receptors Function as a Heteromeric Assembly of the Subunits GABA(B)R1 and GABA(B)R2." *Nature* 396 (6712): 674–79.

Jumper, John, Richard Evans, Alexander Pritzel, Tim Green, Michael Figurnov, Olaf Ronneberger, Kathryn Tunyasuvunakool, et al. 2021. "Highly Accurate Protein Structure Prediction with AlphaFold." *Nature* 596 (7873): 583–89.

Jung, Sang Won, Art E. Cho, and Wookyung Yu. 2018. "Exploring the Ligand Efficacy of Cannabinoid Receptor 1 (CB1) Using Molecular Dynamics Simulations." *Scientific Reports* 8 (1): 1–11.

Kandel, Jeevan, Hilal Tayara, and Kil To Chong. 2021. "PUResNet: Prediction of Protein-Ligand Binding Sites Using Deep Residual Neural Network." *Journal of Cheminformatics* 13 (1): 1–14.

Kapur, Ankur, Dow P Hurst, Daniel Fleischer, Rob Whitnell, Ganesh A Thakur, Alexandros Makriyannis, Patricia H Reggio, and Mary E Abood. 2007. "Mutation Studies on Ser7.39 and Ser2.60 in the Human CB1 Receptor: Evidence for a Serine-Induced Bend in CB1 Transmembrane Helix 7." *Molecular Pharmacology* 71 (6): 1512–24.

Katritch, Vsevolod, Vadim Cherezov, and Raymond C Stevens. 2013. "Structure-Function of the G-Protein-Coupled Receptor Superfamily." *Annual Review of Pharmacology and Toxicology* 53

(January): 531–56.

Katritch, Vsevolod, Gustavo Fenalti, Enrique E. Abola, Bryan L. Roth, Vadim Cherezov, and Raymond C. Stevens. 2014. "Allosteric Sodium in Class A GPCR Signaling." *Trends in Biochemical Sciences* 39 (5): 233–44.

Kaupmann, K, B Malitschek, V Schuler, J Heid, W Froestl, P Beck, J Mosbacher, et al. 1998. "GABA(B)-Receptor Subtypes Assemble into Functional Heteromeric Complexes." *Nature* 396 (6712): 683–87.

Keating, Gillian M. 2017. "Delta-9-Tetrahydrocannabinol/Cannabidiol Oromucosal Spray (Sativex®): A Review in Multiple Sclerosis-Related Spasticity." *Drugs* 77 (5): 563–74.

Kenakin, Terry, and Ryan T. Strachan. 2018. "PAM-Antagonists: A Better Way to Block Pathological Receptor Signaling?" *Trends in Pharmacological Sciences* 39 (8): 748–65.

Khan, Shahriar M, Jennifer Y Sung, and Terence E Hébert. 2016. "Gβγ Subunits-Different Spaces, Different Faces." *Pharmacological Research* 111 (September): 434–41.

Kniazeff, Julie, Laurent Prézeau, Philippe Rondard, Jean-Philippe Pin, and Cyril Goudet. 2011. "Dimers and beyond: The Functional Puzzles of Class C GPCRs." *Pharmacology & Therapeutics* 130 (1): 9–25.

Kobilka, Brian. 2013. "The Structural Basis of G-Protein-Coupled Receptor Signaling (Nobel Lecture)." *Angewandte Chemie - International Edition* 52 (25): 6380–88.

Koehl, Antoine, Hongli Hu, Shoji Maeda, Yan Zhang, Qianhui Qu, Joseph M. Paggi, Naomi R. Latorraca, et al. 2018. "Structure of the μ-Opioid Receptor-Giprotein Complex." *Nature* 558 (7711): 547–52.

Kozlovskii, Igor, and Petr Popov. 2020. "Spatiotemporal Identification of Druggable Binding Sites Using Deep Learning." *Communications Biology* 3 (1): 1–12.

Krishna Kumar, Kaavya, Moran Shalev-Benami, Michael J. Robertson, Hongli Hu, Samuel D. Banister, Scott A. Hollingsworth, Naomi R. Latorraca, et al. 2019. "Structure of a Signaling Cannabinoid Receptor 1-G Protein Complex." *Cell* 176 (3): 448-458.e12.

Kulkarni, Abhijit R., Sumanta Garai, David R. Janero, and Ganesh A. Thakur. 2017. *Design and Synthesis of Cannabinoid 1 Receptor (CB1R) Allosteric Modulators: Drug Discovery Applications*.

Methods in Enzymology. 1st ed. Vol. 593. Elsevier Inc.

Lagarias, Panagiotis, Eleni Vrontaki, George Lambrinidis, Dimitrios Stamatis, Marino Convertino, Gabriella Ortore, Thomas Mavromoustakos, Karl-Norbert Klotz, and Antonios Kolocouris. 2018. "Discovery of Novel Adenosine Receptor Antagonists through a Combined Structure- and Ligand-Based Approach Followed by Molecular Dynamics Investigation of Ligand Binding Mode." *Journal of Chemical Information and Modeling*, acs.jcim.7b00455.

Lagerström, Malin C., and Helgi B. Schiöth. 2008. "Structural Diversity of G Protein-Coupled Receptors and Significance for Drug Discovery." *Nature Reviews Drug Discovery* 7 (4): 339–57.

Lambert, Nevin A., and Jonathan A. Javitch. 2014. "CrossTalk Opposing View: Weighing the Evidence for Class A GPCR Dimers, the Jury Is Still Out." *Journal of Physiology* 592 (12): 2443–45.

Lans, Isaias, James A R Dalton, and Jes??s Giraldo. 2015. "Selective Protonation of Acidic Residues Triggers Opsin Activation." *Journal of Physical Chemistry B* 119 (30): 9510–19.

Lans, Isaias, Óscar Díaz, James A.R. Dalton, and Jesús Giraldo. 2020. "Exploring the Activation Mechanism of the MGlu5 Transmembrane Domain." *Frontiers in Molecular Biosciences* 7 (March): 1–11.

Laprairie, R B, A. M. Bagher, M. E.M. Kelly, and E. M. Denovan-Wright. 2015. "Cannabidiol Is a Negative Allosteric Modulator of the Cannabinoid CB1 Receptor." *British Journal of Pharmacology* 172 (20): 4790–4805.

Laprairie, Robert B., Abhijit R. Kulkarni, Pushkar M. Kulkarni, Dow P. Hurst, Diane Lynch, Patricia H. Reggio, David R. Janero, et al. 2016. "Mapping Cannabinoid 1 Receptor Allosteric Site(s): Critical Molecular Determinant and Signaling Profile of GAT100, a Novel, Potent, and Irreversibly Binding Probe." *ACS Chemical Neuroscience* 7 (6): 776–98.

Latorraca, Naomi R., Jason K. Wang, Brian Bauer, Raphael J. L. Townshend, Scott A. Hollingsworth, Julia E. Olivieri, H. Eric Xu, Martha E. Sommer, and Ron O. Dror. 2018. "Molecular Mechanism of GPCR-Mediated Arrestin Activation." *Nature*, 1.

Lee, Chien, Bo-han Su, and Yufeng Jane Tseng. 2022. "Comparative Studies of AlphaFold , RoseTTAFold and Modeller : A Case Study Involving the Use of G-Protein-Coupled Receptors," 1–7.

Lee, Yoonji, Shaherin Basith, and Sun Choi. 2018. "Recent Advances in Structure-Based Drug Design

Targeting Class A G Protein-Coupled Receptors Utilizing Crystal Structures and Computational Simulations." *Journal of Medicinal Chemistry* 61 (1): 1–46.

Leff, P. 1995. "The Two-State Model of Receptor Activation." *Trends in Pharmacological Sciences* 16 (3): 89–97.

Li, Bian, Wei Li, Peng Du, Kun Qian Yu, and Wei Fu. 2012. "Molecular Insights into the D1R Agonist and D2R/D3R Antagonist Effects of the Natural Product (-)-Stepholidine: Molecular Modeling and Dynamics Simulations." *Journal of Physical Chemistry B* 116 (28): 8121–30.

Li, Jin, Ailing Fu, and Le Zhang. 2019. "An Overview of Scoring Functions Used for Protein-Ligand Interactions in Molecular Docking." *Interdisciplinary Sciences, Computational Life Sciences* 11 (2): 320–28.

Li, Xiaoting, Tian Hua, Kiran Vemuri, Jo-Hao Ho, Yiran Wu, Lijie Wu, Petr Popov, et al. 2019. "Crystal Structure of the Human Cannabinoid Receptor CB2." *Cell* 176 (3): 1–9.

Limongelli, Vittorio, Massimiliano Bonomi, and Michele Parrinello. 2013. "Funnel Metadynamics as Accurate Binding Free-Energy Method." *Proceedings of the National Academy of Sciences of the United States of America* 110 (16): 6358–63.

Lin, Shuling, Shuo Han, Xiaoqing Cai, Qiuxiang Tan, Kexiu Zhou, Dejian Wang, Xinwei Wang, et al. 2021. "Structures of Gi-Bound Metabotropic Glutamate Receptors MGlu2 and MGlu4." *Nature* 594 (7864): 583–88.

Lindahl, Erik, Berk Hess, and David van der Spoel. 2001. "GROMACS 3.0: A Package for Molecular Simulation and Trajectory Analysis." *Molecular Modeling Annual* 7 (8): 306–17.

Lindsley, Craig W., Kyle A. Emmitte, Corey R. Hopkins, Thomas M. Bridges, Karen J. Gregory, Colleen M. Niswender, and P. Jeffrey Conn. 2016. "Practical Strategies and Concepts in GPCR Allosteric Modulator Discovery: Recent Advances with Metabotropic Glutamate Receptors." *Chemical Reviews* 116 (11): 6707–41.

Lipnik-Štangelj, Metoda, and Barbara Razinger. 2020. "A Regulatory Take on Cannabis and Cannabinoids for Medicinal Use in the European Union." *Arhiv Za Higijenu Rada i Toksikologiju* 71 (1): 12–18.

Liu, Wei, Eugene Chun, Aaron A Thompson, Pavel Chubukov, Fei Xu, Gye Won Han, Christopher B Roth, et al. 2013. "Structural Basis for Allosteric Regulation of GPCRs by Sodium Ions." *Science*

337 (6091): 232–36.

Liu, Xiangyu, Seungkirl Ahn, Alem W. Kahsai, Kai Cheng Meng, Naomi R. Latorraca, Biswaranjan Pani, A. J. Venkatakrishnan, et al. 2017. “Mechanism of Intracellular Allosteric β 2 AR Antagonist Revealed by X-Ray Crystal Structure.” *Nature* 548 (7668): 480–84.

Lohse, Martin J, Isabella Maiellaro, and Davide Calebiro. 2014. “Kinetics and Mechanism of G Protein-Coupled Receptor Activation.” *Current Opinion in Cell Biology* 27: 87–93.

Lomize, Mikhail A, Andrei L Lomize, Irina D Pogozheva, and Henry I Mosberg. 2006. “OPM: Orientations of Proteins in Membranes Database.” *Bioinformatics* 22 (5): 623–25.

Lucchesi, Valentina, Dow P Hurst, Derek M Shore, Simone Bertini, Brandie M. Ehrmann, Marco Allarà, Lyle Lawrence, et al. 2014. “CB2-Selective Cannabinoid Receptor Ligands: Synthesis, Pharmacological Evaluation, and Molecular Modeling Investigation of 1,8-Naphthyridin-2(1 H)-One-3-Carboxamides.” *Journal of Medicinal Chemistry* 57 (21): 8777–91.

Lyskov, Sergey, Fang-Chieh Chou, Shane Ó Conchúir, Bryan S Der, Kevin Drew, Daisuke Kuroda, Jianqing Xu, et al. 2013. “Serverification of Molecular Modeling Applications: The Rosetta Online Server That Includes Everyone (ROSIE).” *PLOS ONE* 8 (5): e63906.

MacArron, Ricardo, Martyn N. Banks, Dejan Bojanic, David J. Burns, Dragan A. Cirovic, Tina Garyantes, Darren V.S. Green, et al. 2011. “Impact of High-Throughput Screening in Biomedical Research.” *Nature Reviews Drug Discovery* 10 (3): 188–95.

Mafi, Amirhossein, Soo-kyung Kim, and William A. Goddard. 2022. “The Mechanism for Ligand Activation of the GPCR – G Protein Complex.” *Proc Natl Acad Sci U S A* 119 (18).

Maragakis, Paul, Hunter Nisonoff, Brian Cole, and David E. Shaw. 2020. “A Deep-Learning View of Chemical Space Designed to Facilitate Drug Discovery.” *Journal of Chemical Information and Modeling* 60 (10): 4487–96.

McAllister, Sean D., Dow P. Hurst, Judy Barnett-Norris, Diane Lynch, Patricia H. Reggio, and Mary E. Abood. 2004. “Structural Mimicry in Class A G Protein-Coupled Receptor Rotamer Toggle Switches: The Importance of the F3.36(201)/W6.48(357) Interaction in Cannabinoid CB1 Receptor Activation.” *Journal of Biological Chemistry* 279 (46): 48024–37.

McGraw, Claire, Lewen Yang, Ilya Levental, Edward Lyman, and Anne Skaja Robinson. 2019. “Membrane Cholesterol Depletion Reduces Downstream Signaling Activity of the Adenosine A2A

Receptor." *Biochimica et Biophysica Acta - Biomembranes* 1861 (4): 760–67.

Melancon, Bruce J, Corey R Hopkins, Michael R Wood, Kyle A Emmitte, Colleen M Niswender, Arthur Christopoulos, P Jeffrey Conn, and Craig W Lindsley. 2012. "Allosteric Modulation of Seven Transmembrane Spanning Receptors: Theory, Practice, and Opportunities for Central Nervous System Drug Discovery." *Journal of Medicinal Chemistry* 55 (4): 1445–64.

Miao, Yinglong, Apurba Bhattarai, Anh T. N. Nguyen, Arthur Christopoulos, and Lauren T. May. 2018. "Structural Basis for Binding of Allosteric Drug Leads in the Adenosine A1 Receptor." *Scientific Reports* 8 (1): 16836.

Miller, Bill R, T Dwight Mcgee, Jason M Swails, Nadine Homeyer, Holger Gohlke, and Adrian E Roitberg. 2012. "MMPBSA . Py : An Efficient Program for End-State Free Energy Calculations." *Journal of Chemical Theory and Computation* 8: 3314–21.

Morris, Garrett M, Ruth Huey, William Lindstrom, Michel F Sanner, Richard K Belew, David S Goodsell, and Arthur J Olson. 2009. "AutoDock4 and AutoDockTools4: Automated Docking with Selective Receptor Flexibility." *Journal of Computational Chemistry* 30 (16): 2785–91.

Motlagh, Hesam N., James O. Wrabl, Jing Li, and Vincent J. Hilser. 2014. "The Ensemble Nature of Allostery." *Nature* 508 (7496): 331–39.

Neale, Chris, Henry D Herce, Régis Pomès, and Angel E García. 2015. "Can Specific Protein-Lipid Interactions Stabilize an Active State of the Beta 2 Adrenergic Receptor?" *Biophysical Journal* 109 (8): 1652–62.

Nguyen, Dzung H., and Dennis D. Taub. 2003. "Inhibition of Chemokine Receptor Function by Membrane Cholesterol Oxidation." *Experimental Cell Research* 291 (1): 36–45.

Niesen, Michiel J M, Supriyo Bhattacharya, and Nagarajan Vaidehi. 2011. "The Role of Conformational Ensembles in Ligand Recognition in G-Protein Coupled Receptors." *Journal of the American Chemical Society* 133 (33): 13197–204.

Noé, Frank. 2018. "Machine Learning for Molecular Dynamics on Long Timescales," 1–27.

Noé, Frank, Alexandre Tkatchenko, Klaus Robert Müller, and Cecilia Clementi. 2020. "Machine Learning for Molecular Simulation." *Annual Review of Physical Chemistry* 71: 361–90.

Olsson, Mats H M, Chresten R Sondergaard, Michal Rostkowski, and Jan H Jensen. 2011. "PROPKA3:

Consistent Treatment of Internal and Surface Residues in Empirical PKa Predictions." *Journal of Chemical Theory and Computation* 7 (2): 525–37.

Pereira, D A, and J A Williams. 2007. "Origin and Evolution of High Throughput Screening." *British Journal of Pharmacology* 152 (1): 53–61.

Pérez-Benito, Laura, Maarten L. J. Doornbos, Arnau Cordomí, Luc Peeters, Hilde Lavreysen, Leonardo Pardo, and Gary Tresadern. 2017. "Molecular Switches of Allosteric Modulation of the Metabotropic Glutamate 2 Receptor." *Structure* 25: 1153–62.

Pertwee, R. 2005. "Pharmacological Actions of Cannabinoids." In *Cannabinoids*, edited by R. Pertwee, 1–51. Springer.

Pettersen, Eric F, Thomas D Goddard, Conrad C Huang, Gregory S Couch, Daniel M Greenblatt, Elaine C Meng, and Thomas E Ferrin. 2004. "UCSF Chimera—A Visualization System for Exploratory Research and Analysis." *Journal of Computational Chemistry* 25 (13): 1605–12.

Plante, Ambrose, Derek M Shore, Giulia Morra, George Khelashvili, and Harel Weinstein. 2019. "A Machine Learning Approach for the Discovery of Ligand-Specific Functional Mechanisms of GPCRs." *Molecules* 24: 1–23.

Plazinska, Anita, Wojciech Plazinski, and Krzysztof Jozwiak. 2015. "Agonist Binding by the B2-Adrenergic Receptor: An Effect of Receptor Conformation on Ligand Association–Dissociation Characteristics." *European Biophysics Journal* 44 (3): 149–63.

Rasmussen, Sŏren G.F., Brian T. Devree, Yaozhong Zou, Andrew C. Kruse, Ka Young Chung, Tong Sun Kobilka, Foon Sun Thian, et al. 2011. "Crystal Structure of the B2adrenergic Receptor-Gs Protein Complex." *Nature* 477 (7366): 549–57.

Redhair, Michelle, and William M. Atkins. 2021. "Analytical and Functional Aspects of Protein-Ligand Interactions: Beyond Induced Fit and Conformational Selection." *Archives of Biochemistry and Biophysics* 714 (October): 109064.

Renault, Pedro, Maxime Louet, Jacky Marie, Gilles Labesse, and Nicolas Floquet. 2019. "Molecular Dynamics Simulations of the Allosteric Modulation of the Adenosine A2a Receptor by a Mini-G Protein." *Scientific Reports* 9 (1): 5495.

Ricarte, Adrián, James A.R. Dalton, and Jesús Giraldo. 2021. "Structural Assessment of Agonist Efficacy in the μ-Opioid Receptor: Morphine and Fentanyl Elicit Different Activation Patterns."

Journal of Chemical Information and Modeling 61 (3): 1251–74.

Ripphausen, Peter, Britta Nisius, and Jürgen Bajorath. 2011. "State-of-the-Art in Ligand-Based Virtual Screening." *Drug Discovery Today* 16 (9–10): 372–76.

Roche, David, Debora Gil, and Jesús Giraldo. 2013. "Mechanistic Analysis of the Function of Agonists and Allosteric Modulators: Reconciling Two-State and Operational Models." *British Journal of Pharmacology* 169 (6): 1189–1202.

Rodríguez-Espigares, Ismael, Mariona Torrens-Fontanals, Johanna K.S. Tiemann, David Aranda-García, Juan Manuel Ramírez-Anguita, Tomasz Maciej Stepniewski, Nathalie Worp, et al. 2020. "GPCRmd Uncovers the Dynamics of the 3D-GPCRome." *Nature Methods* 17 (8): 777–87.

Romero-Parra, Javier, Jaime Mella-Raipán, Vittoria Palmieri, Marco Allarà, Maria Jose Torres, Hernán Pessoa-Mahana, Patricio Iturriaga-Vásquez, et al. 2016. "Synthesis, Binding Assays, Cytotoxic Activity and Docking Studies of Benzimidazole and Benzothiophene Derivatives with Selective Affinity for the CB2 Cannabinoid Receptor." *European Journal of Medicinal Chemistry* 124: 17–35.

Rose, Alexander S., Matthias Elgeti, Ulrich Zachariae, Helmut Grubmüller, Klaus Peter Hofmann, Patrick Scheerer, and Peter W. Hildebrand. 2014. "Position of Transmembrane Helix 6 Determines Receptor G Protein Coupling Specificity." *Journal of the American Chemical Society* 136 (32): 11244–47.

Rutenber, E E, and R M Stroud. 1996. "Binding of the Anticancer Drug ZD1694 to E. Coli Thymidylate Synthase: Assessing Specificity and Affinity." *Structure (London, England : 1993)* 4 (11): 1317–24.

Santos, Rita, Oleg Ursu, Anna Gaulton, A Patrícia Bento, Ramesh S Donadi, Cristian G Bologa, Anneli Karlsson, et al. 2017. "A Comprehensive Map of Molecular Drug Targets." *Nature Publishing Group* 16 (1): 19–34.

Schafer, Christopher T., and David L. Farrens. 2015. "Conformational Selection and Equilibrium Governs the Ability of Retinals to Bind Opsin." *Journal of Biological Chemistry* 290 (7): 4304–18.

Schuler, Lukas, Xavier Daura, and Wilfred van Gunsteren. 2001. "An Improved GROMOS96 Force Field for Aliphatic Hydrocarbons in the Condensed Phase." *Journal of Computational Chemistry*

22 (August): 1205–18.

Schwartz, Thue W., and Birgitte Holst. 2006. “Ago-Allosteric Modulation and Other Types of Allostery in Dimeric 7TM Receptors.” *Journal of Receptors and Signal Transduction* 26 (1–2): 107–28.

Seltzman, Herbert H., Craig Shiner, Erin E. Hirt, Anne F. Gilliam, Brian F. Thomas, Rangan Maitra, Rod Snyder, et al. 2016. “Peripherally Selective Cannabinoid 1 Receptor (CB1R) Agonists for the Treatment of Neuropathic Pain.” *Journal of Medicinal Chemistry* 59 (16): 7525–43.

Sengupta, Durba, Manali Joshi, Chaitanya A Athale, and Amitabha Chattopadhyay. 2016. “What Can Simulations Tell Us about GPCRs: Integrating the Scales.” *Methods in Cell Biology* 132: 429–52.

Sengupta, Durba, Xavier Prasanna, Madhura Mohole, and Amitabha Chattopadhyay. 2018. “Exploring GPCR-Lipid Interactions by Molecular Dynamics Simulations: Excitements, Challenges, and the Way Forward.” *Journal of Physical Chemistry B* 122 (22): 5727–37.

Seven, Alpay B., Ximena Barros-Álvarez, Marine de Lapeyrière, Makaía M. Papasergi-Scott, Michael J. Robertson, Chensong Zhang, Robert M. Nwokonko, et al. 2021. “G-Protein Activation by a Metabotropic Glutamate Receptor.” *Nature* 595 (7867): 450–54.

Shao, Zhenhua, Wei Yan, Karen Chapman, Karthik Ramesh, Aaron J Ferrell, Jie Yin, Xuehui Wang, Qingping Xu, and Daniel M Rosenbaum. 2019. “Structure of an Allosteric Modulator Bound to the CB1 Cannabinoid Receptor.” *Nat. Chem. Biol.* 15: 1199–1205.

Shao, Zhenhua, Jie Yin, Karen Chapman, Magdalena Grzemska, Lindsay Clark, Junmei Wang, and Daniel M. Rosenbaum. 2016. “High-Resolution Crystal Structure of the Human CB1 Cannabinoid Receptor.” *Nature* 540 (7634): 602–6.

Shapovalov, Maxim V., and Roland L. Dunbrack. 2011. “A Smoothed Backbone-Dependent Rotamer Library for Proteins Derived from Adaptive Kernel Density Estimates and Regressions.” *Structure* 19 (6): 844–58.

Shim, Joong Youn, Alexander C. Bertalovitz, and Debra A. Kendall. 2011. “Identification of Essential Cannabinoid-Binding Domains: Structural Insights into Early Dynamic Events in Receptor Activation.” *Journal of Biological Chemistry* 286 (38): 33422–35.

Shim, Joong Youn, Leepakshi Khurana, and Debra A. Kendall. 2016. “Computational Analysis of the CB1 Carboxyl-Terminus in the Receptor-G Protein Complex.” *Proteins: Structure, Function and Bioinformatics* 84 (4): 532–43.

Song, Gaojie, Dehua Yang, Yuxia Wang, Chris De Graaf, Qingtong Zhou, Shanshan Jiang, Kaiwen Liu, et al. 2017. "Human GLP-1 Receptor Transmembrane Domain Structure in Complex with Allosteric Modulators." *Nature* 546 (7657): 312–15.

Tao, Q, and M E Abood. 1998. "Mutation of a Highly Conserved Aspartate Residue in the Second Transmembrane Domain of the Cannabinoid Receptors, CB1 and CB2, Disrupts G-Protein Coupling." *The Journal of Pharmacology and Experimental Therapeutics* 285 (2): 651–58.

Tehan, Benjamin G., Andrea Bortolato, Frank E. Blaney, Malcolm P. Weir, and Jonathan S. Mason. 2014. "Unifying Family A GPCR Theories of Activation." *Pharmacology and Therapeutics* 143 (1): 51–60.

Thakur, Ganesh a, Ritesh Tichkule, Shama Bajaj, and Alexandros Makriyannis. 2009. "Latest Advances in Cannabinoid Receptor Agonists." *Expert Opinion on Therapeutic Patents* 19 (12): 1647–73.

The UniProt Consortium. 2021. "UniProt: The Universal Protein Knowledgebase in 2021." *Nucleic Acids Research* 49 (D1): D480–89.

Torrens-Fontanals, Mariona, Tomasz Maciej Stepniewski, David Aranda-García, Adrián Morales-Pastor, Brian Medel-Lacruz, and Jana Selent. 2020. "How Do Molecular Dynamics Data Complement Static Structural Data of GPCRs." *International Journal of Molecular Sciences* 21 (16): 1–26.

Tzeng, Shiou Ru, and Charalampos G. Kalodimos. 2012. "Protein Activity Regulation by Conformational Entropy." *Nature* 488 (7410): 236–40.

Vanommeslaeghe, K, and A D Jr MacKerell. 2012. "Automation of the CHARMM General Force Field (CGenFF) I: Bond Perception and Atom Typing." *Journal of Chemical Information and Modeling* 52 (12): 3144–54.

Verdonk, Marcel L, Jason C Cole, Michael J Hartshorn, Christopher W Murray, and Richard D Taylor. 2003. "Improved Protein-Ligand Docking Using GOLD." *Proteins* 52 (4): 609–23.

Vilardaga, Jean Pierre, Moritz Bünemann, Cornelius Krasell, Mariàn Castro, and Martin J. Lohse. 2003. "Measurement of the Millisecond Activation Switch of G Protein-Coupled Receptors in Living Cells." *Nature Biotechnology* 21 (7): 807–12.

Wang, Xiaoyan, Dongsheng Liu, Ling Shen, Fahui Li, Yongze Li, Lingyun Yang, Tiandan Xu, et al. 2021. "A Genetically Encoded F - 19 NMR Probe Reveals the Allosteric Modulation Mechanism

of Cannabinoid Receptor 1." *Journal of the American Chemical Society* 143 (40): 16320–25.

Wang, Yong, Katrine Bugge, Birthe B. Kragelund, and Kresten Lindorff-Larsen. 2018. "Role of Protein Dynamics in Transmembrane Receptor Signalling." *Current Opinion in Structural Biology* 48 (November 2017): 74–82.

Webb, Benjamin, and Andrej Sali. 2014. "Comparative Protein Structure Modeling Using MODELLER." *Current Protocols in Bioinformatics* 47: 5.6.1-5.6.32.

Weis, William I, and Brian K Kobilka. 2018. "The Molecular Basis of G Protein–Coupled Receptor Activation." *Annual Review of Biochemistry*.

White, Kate L., Matthew T. Eddy, Zhan Guo Gao, Gye Won Han, Tiffany Lian, Alexander Deary, Nilkanth Patel, Kenneth A. Jacobson, Vsevolod Katritch, and Raymond C. Stevens. 2018. "Structural Connection between Activation Microswitch and Allosteric Sodium Site in GPCR Signaling." *Structure* 26 (2): 259-269.e5.

Wlodawer, A, and J Vondrasek. 1998. "Inhibitors of HIV-1 Protease: A Major Success of Structure-Assisted Drug Design." *Annual Review of Biophysics and Biomolecular Structure* 27: 249–84.

Wootten, Denise, Arthur Christopoulos, Maria Marti-Solano, M. Madan Babu, and Patrick M. Sexton. 2018. "Mechanisms of Signalling and Biased Agonism in G Protein-Coupled Receptors." *Nature Reviews Molecular Cell Biology* 19 (10): 638–53.

Xing, Changrui, Youwen Zhuang, Ting Hai Xu, Zhiwei Feng, X. Edward Zhou, Maozi Chen, Lei Wang, et al. 2020. "Cryo-EM Structure of the Human Cannabinoid Receptor CB2-Gi Signaling Complex." *Cell* 180 (4): 645-654.e13.

Yang, Xin, Xuehui Wang, Zheng Xu, Chao Wu, Yangli Zhou, Yifei Wang, Guifeng Lin, et al. 2022. "Molecular Mechanism of Allosteric Modulation for the Cannabinoid Receptor CB1." *Nat. Chem. Biol.*

Zhou, Bin, and Jesús Giraldo. 2018. "Quantifying the Allosteric Interactions within a G-Protein-Coupled Receptor Heterodimer." *Drug Discovery Today* 23 (1): 7–11.